JUSTUS-LIEBIG-
UNIVERSITÄT
GIESSEN

Disulfide-dithiol exchange in thioredoxin-dependent reactions of *Plasmodium falciparum* and its human host cells

A thesis submitted in fulfillment of the German degree
doctor rerum naturalium (Dr. rer. nat.)
to the
Faculty of Biology and Chemistry (FB 08)
of
Justus Liebig University, Giessen, Germany

by
Christina Brandstädter
born in Stralsund, Germany
- 2018 -

The work reported in this thesis was carried out during the period of February 2013 to September 2017 at the Institute for Nutritional Sciences, Chair of Biochemistry and Molecular Biology, Interdisciplinary Research Centre, Justus Liebig University, Giessen, Germany. The thesis was supervised by Prof. Dr. med. Katja Becker and Prof. Dr. rer. nat. Peter Friedhoff.

The thesis defense examination committee was composed of:

Prof. Dr. med. Katja Becker
Biochemistry and Molecular Biology
Interdisciplinary Research Centre (IFZ)
Justus Liebig University Giessen
Heinrich-Buff-Ring 26-32
35392 Giessen

Prof. Dr. rer. nat. Peter Friedhoff
Institute for Biochemistry
Faculty of Biology and Chemistry
Justus Liebig University Giessen
Heinrich-Buff-Ring 58
35392 Giessen

Prof. Dr. med. Eveline Baumgart-Vogt
Institute for Anatomy and Cell Biology
Justus Liebig University Giessen
Aulweg 123
35392 Giessen

Prof. Dr. rer. nat. Lienhard Schmitz
Department of Biochemistry
Faculty of Medicine
Justus Liebig University Giessen
Friedrichstrasse 24
35392 Giessen

DECLARATION

I declare that this thesis is my original work and sources of information have been properly quoted. This work has not been previously presented to obtain any other degree from any other university.

EIDESSTATTLICHE ERKLÄRUNG

Ich erkläre: Ich habe die vorgelegte Dissertation selbständig und ohne unerlaubte fremde Hilfe und nur mit den Hilfen angefertigt, die ich in der Dissertation angegeben habe. Alle Textstellen, die wörtlich oder sinngemäß aus veröffentlichten Schriften entnommen sind, und alle Angaben, die auf mündlichen Auskünften beruhen, sind als solche kenntlich gemacht. Bei den von mir durchgeführten und in der Dissertation erwähnten Untersuchungen habe ich die Grundsätze guter wissenschaftlicher Praxis, wie sie in der „Satzung der Justus-Liebig-Universität Gießen zur Sicherung guter wissenschaftlicher Praxis“ niedergelegt sind, eingehalten.

Gießen, Mai, 2018

_____

Christina Brandstädter

ACKNOWLEDGEMENTS

I wish to express my sincere gratitude to **Prof. Dr. Katja Becker**. I never met a person who inspired me in so many ways. Thank you for giving me the opportunity to prepare this dissertation in your group, for your support, motivation, patience, and professional guidance. Thank you for your trust, for helping me grow, and being a role model for young female scientists.
I would like to thank my second supervisor, **Prof. Dr. Peter Friedhoff**, for his interest in the topic of my thesis and his helpful hints and discussions.
I thank **Dr. Stefan Rahlfs** for his scientific ideas and helpful discussions during my Master's degree and this thesis. Thank you for your profound input in molecular biological issues and your open mind. I am thankful to **Dr. Julia Dzieciolowski** (Dr. Hahn) for her scientific enthusiasm and tremendous biochemical input into my own scientific thinking. Thank you for your open mind, patience, advice, and our uncountable brainstorming sessions. Furthermore, thank you for being such a good friend. I wish to thank **Dr. Esther Jortzik** and **Dr. Jochen Bathke** for their company and support, especially during my first years in the group. It was a pleasure and an honor to learn from you. I am grateful to **Dr. Jette Pretzel** for our scientific and personal discussions, your positive nature, your trust in me, and most of all, thank you for our ongoing friendship.

I would like to thank **Beate Hecker**, who introduced me to the lab and shared her scientific experience with me. I wish to thank **Michaela Stumpf** for her patience and positive mind, her great support, and trouble shooting. Many thanks to **Marina Fischer** for her support in enzyme kinetics and laboratory work as well as for her creative thinking. A big thank goes to Stine Weder, Christina Hailu, Anke Werner, and most of all to **Melissa Schmidt**, who supported my thesis in so many ways. Thank you for being extremely reliable and flexible and for the positive working atmosphere you created. I wish to thank **Siegrid Franke** and **Elisabeth Fischer** for their excellent work in cell culture and for providing the parasite cell pellets for my experiments. I like to thank **Dr. Karin Fritz-Wolf** for her helpful and critical comments and support in terms of protein structures and interactions. I wish to thank **Timothy Bostick** for his careful proof reading of this thesis and my manuscripts.

Furthermore, I wish to thank **Prof. Dr. Claire Delahunty** from The Scripps Research Institute in California for performing the mass spectrometry analyses for this thesis. I would like to thank **Prof. Dr. Karl-Josef Dietz** and **Michael Liebthal** for introducing me to isothermal titration calorimetry at the Faculty of Biology/Biochemistry and Physiology of Plants, Bielefeld, for performing the dissociation experiments and for our fruitful collaboration and discussions. I also wish to thank **Prof. Dr. Roland Lill** and **Dr. Sven-Andreas Freibert** from the Institute for Cytobiology and Cytopathology, Marburg, for their guidance in microscale thermophoresis and our intense exchange of views.

I thank my Master students **Kathrin Pauli**, **Laura Wittich**, **Katharina Leu**, **Eva König**, and **Norma Schultz** for their excellent enthusiasm in the lab (and at the desk) and their contribution of scientific results to support a number of experiments. I want to thank **Kristina Häussler**, **Susanne Schipper**, **Katharina Schuh**, and **Dr. Kathrin Buchholz** for being such good company in the lab, for the academic discussions, and for the good time we had.

Finally, I like to thank **my beloved parents and my partner** for their patience, support, and understanding during the last years.

SUMMARY

Specific protein cysteine residues can serve as structural components, catalysts, or redox switches. In peroxiredoxins (Prx), cysteines facilitate the enzymes' ability to reduce peroxides by forming intra- or intermolecular disulfide bridges and transient mixed disulfides in a downstream recycling process enabled by redoxins. Within the framework of my thesis, I aimed to further understand the underlying molecular processes. To characterize the role of specific, catalytically active cysteines during the recycling step of the catalytic cycle of Prxs, a surface plasmon resonance-based method was developed. With this new approach, which shows particular advantages over other methods investigating protein-protein interactions (PPIs), the regioselectivity of *Plasmodium falciparum* (*Pf*) thioredoxin (Trx) to recycle disulfides at active site cysteines of *Pf*Prxs was characterized in molecular detail. The data generated were confirmed with electrophoretic mobility shift assays on a selected, representative interaction couple. To compare the SPR-based approach with other methods currently used for studying PPI, isothermal titration calorimetry (ITC) and microscale thermophoresis (MST) were conducted with selected PPI partners. Comparing these three methods revealed the SPR-based approach as clearly preferable to ITC and MST in answering the leading question. Additionally, within this thesis the thiol-dependent interactomes of *Pf*Prx1a and *Pf*Prx1m were revealed using a pull-down assay. In the applied assay, 2-Cys Prxs and their mutants lacking the resolving or peroxidatic cysteines were used as bait to identify potential interacting partners. With this, 127 proteins were found to interact with *Pf*Prx1a and 20 proteins with *Pf*Prx1m via a mechanism involving disulfide bound formation. Based on bioinformatic and bibliographic analyses, the proteins identified components of various metabolic pathways such as carbohydrate metabolism, protein folding, the translational machinery, *S*-adenosylmethionine metabolism, signal transduction, and others. These results provide new insights into the regulatory mechanism of Prx-mediated redox biology in *Plasmodium falciparum* and many new candidate targets for oxidation signal transduction by *Pf*Prxs. Furthermore, proteins caught with resolving cysteine mutants may allow the innovative pronouncement of an additional function of Prxs as proteins that are capable of reducing oxidized proteins. This follows a catalytic process similar to peroxide reduction using the second active site cysteine to resolve the transient mixed disulfide between Prx and the targeted protein. To determine the pK_a of the peroxidatic cysteines of *Pf*Prxs, an HRP competition assay was used. The pK_a of *Pf*Prx1a, *Pf*Prx5, and *Pf*PrxQ$^{1\text{-}164}$ could be determined to be 6.16 ± 0.1, 6.01 ± 0.18, and 6.57 ± 0.2, respectively, and the determined second order rate constant was 1.6×10^8 M^{-1} sec^{-1} for *Pf*Prx1a, 2.8×10^8 M^{-1} sec^{-1} for *Pf*Prx5, and 2.2×10^7 M^{-1} sec^{-1} for *Pf*PrxQ$^{1\text{-}164}$.

In most cells, the thioredoxin (Trx) and glutathione systems are essentially involved in maintaining redox homeostasis in a thiol-dependent mechanism. The selenoprotein thioredoxin glutathione reductase (TGR) is a hybrid enzyme in which a glutaredoxin (Grx) domain is linked to a thioredoxin reductase (TrxR) and which is also capable of reducing glutathione disulfide (GSSG), thus representing an important link between the two redox systems. In this thesis, human TGR (hTGR wild type) was recombinantly produced by fusing its open reading frame with a bacterial SECIS element and co-expressing the construct in *E. coli* together with the *selA, selB,* and *selC* genes. Additionally, the Sec→Cys mutant (hTGR^{U642C}) of the full-length protein as well as the isolated TrxR domain (hTGR$^{151\text{-}642}$) and the Grx domain containing a monothiol active site (hTGR$^{1\text{-}150}$) were produced and purified. All four proteins were kinetically characterized in direct comparison using Trx, DTNB, HEDS, or GSSG as oxidizing substrates. Interestingly, the HEDS reduction activity was Sec

independent and comparable in the full-length protein and the isolated Grx domain, whereas the TrxR and the glutathione reductase (GR) reactions were clearly selenocysteine dependent, with the GR reaction requiring the Grx domain. Site-directed mutagenesis studies revealed novel insights into the mechanism of GSSG reduction. Furthermore, several glutathionylation sites in hTGR, including Cys93, Cys133, and Cys619, were identified with an inhibitory effect of these modifications on enzyme activity. In contrast to other TGRs, e.g. from platyhelminth parasites, hTGR did not exhibit hysteretic behavior. These findings provide new insights into the reaction mechanism and regulation of monothiol Grx containing TGRs.

ZUSAMMENFASSUNG

In Proteinen können spezifische Cysteinreste als strukturelle Komponenten, Katalysatoren oder Redoxschalter fungieren. In Peroxiredoxinen (Prx) vermitteln Cysteine die Peroxidasefunktion des Enzyms, was zur Entstehung von intra- oder intermolekularen Disulfidbrücken aber auch zu transienten, gemischten Disulfiden im Rahmen des nachgeschalteten Recyclingprozesses durch Redoxine führt. Im Rahmen meiner vorliegenden Arbeit galt das Ziel diese zugrundeliegenden Prozesse tiefer zu verstehen. Um die Rolle von spezifischen, katalytisch-aktiven Cysteinen in dem Prx-Recyclingschritt zu charakterisieren, wurde eine Oberflächenplasmonresonanz (SPR)-basierte Methode entwickelt. Mit dieser Methode, welche explizite Vorteile gegenüber anderen Methoden zur Protein-Protein-Interaktions (PPI)-Bestimmung aufzeigt, konnte die Regioselektivität von *Plasmodium falciparum* (*Pf*) Thioredoxin (Trx) im Recyclingprozess gegenüber Disulfiden des aktiven Zentrums von *Pf*Prx auf molekularer Ebene aufgezeigt werden. Zudem konnten die generierten Daten an einem ausgewählten, repräsentativen Beispiel durch *Electrophoretic Mobility Shift Assays* bestätigt werden. Um die SPR-basierte Methode mit bereits bestehenden Methoden der PPI-Bestimmung zu vergleichen, wurde mit ausgewählten PPI-Partnern ebenfalls die isothermale Titrationskalorimetrie (ITC) und Microscale Thermophorese (MST) durchgeführt. Der Vergleich dieser drei Methoden zeigt dabei eindeutig, dass die SPR-basierte Methode für die zugrundeliegende Fragestellung zu bevorzugen ist. Des Weiteren konnte in dieser Thesis mittels eines Pull-down Verfahrens das Thiol-abhängige Interaktom von *Pf*Prx1a sowie *Pf*Prx1m dargestellt werden. In dem verwendeten Verfahren wurden 2-Cys Prxs sowie deren *resolving* Cystein- und *peroxidatic* Cystein-Mutanten als Fänger genutzt, um potentielle Interaktionspartner zu identifizieren. Hierbei konnten 127 Proteine gefunden werden, die über einen Disulfid-involvierten Mechanismus mit *Pf*Prx1a interagieren und 20 Proteine, welche mit *Pf*Prx1m wechselwirken. Durch bioinformatische und bibliographische Analysen konnten diese Proteine verschiedenen metabolischen Stoffwechselwegen, wie dem Kohlenhydratstoffwechsel, der Proteinfaltung, der Translationsmaschinerie, dem *S*-Adenosylmethioninmetabolismus, der Signaltransduktion und anderen, zugeordnet werden. Diese Ergebnisse liefern neue Einblicke in den regulatorischen Mechanismus der Prx-vermittelten Redoxbiologie in *Plasmodium falciparum* sowie viele neue Kandidatenproteine für eine Oxidationssignalübertragung durch *Pf*Prxs. Weiterhin könnten Proteine, welche mit den *resolving*-Mutanten gefangen wurden, die Hypothese stützen, dass Prxs eine zusätzliche Funktion inne tragen. Demnach könnten Prxs in der Lage sein, oxidierte Proteine zu reduzieren, indem sie einem katalytischen Prozess ähnlich der Peroxidreduktion folgen, wobei das zweites Cystein im aktivem Zentrum genutzt wird, um das transiente, gemischte Disulfid zwischen dem Prx und seinem Zielprotein zu lösen. Um den pK_a der peroxidativen Cysteine von *Pf*Prx zu bestimmen, wurde ein HRP-Kompetitionsassay verwendet. Für *Pf*Prx1a, *Pf*Prx5 und *Pf*PrxQ$^{1\text{-}164}$ konnten hierbei ein pK_a von 6,16 ± 0,1, 6,01 ± 0,18, beziehungsweise 6,57 ± 0,2 gemessen und eine Geschwindigkeitskonstante 2. Ordnung von $1{,}6 \times 10^8$ M^{-1} sec^{-1} für *Pf*Prx1a, $2{,}8 \times 10^8$ M^{-1} sec^{-1} für *Pf*Prx5 und $2{,}2 \times 10^7$ M^{-1} sec^{-1} für *Pf*PrxQ$^{1\text{-}164}$ bestimmt werden.

In den meisten Zellen sind das Thioredoxin- (Trx) und das Glutathion-System essenziell in die Aufrechterhaltung der Redoxhomöostase in einem Thiol-abhängigen Mechanismus involviert. Das Selenoprotein Thioredoxin-Glutathion-Reduktase (TGR) ist ein Hybrid-enzym, in welchem eine Glutaredoxin (Grx)-Domäne mit einer Thioredoxinreduktase (TrxR) verknüpft ist, und das zudem in der Lage ist, Glutathiondisulfid (GSSG) zu

reduzieren, womit es eine bedeutende Verbindung zwischen zwei Redoxsystemen darstellt. In dieser Thesis wurde die humane TGR (hTGR Wildtyp) rekombinant hergestellt, indem sein offener Leserahmen mit einem bakteriellen SECIS-Element fusioniert wurde und das Konstrukt in *E. coli* zusammen mit *selA*, *selB* und *selC* Genen koexpremiert wurde. Zudem wurden die Sec→Cys Mutante ($hTGR^{U642C}$) des Proteins sowie die isolierte TrxR-Domäne ($hTGR^{151-642}$) und die Grx-Domäne ($hTGR^{1-150}$), welche ein Monothiol im aktiven Zentrum beinhaltet, hergestellt und gereinigt. Alle vier Proteine wurden im direkten Vergleich durch die Verwendung von Trx, DTNB, HEDS oder GSSG als oxidierende Substrate kinetisch charakterisiert. Interessanterweise war die HEDS-Reduktions-Aktivität Sec-unabhängig und zeigte sich vergleichbar in dem Volllängenprotein und der isolierten Grx-Domäne, wobei die TrxR- und die Glutathionreduktase(GR)-Reaktion eindeutig eine Selenocysteinabhängigkeit zeigten und die GR-Reaktion die Anwesenheit der Grx-Domäne benötigte. Ortsgerichtete Mutagenesestudien lieferten hierbei neuartige Einblicke in den Mechanismus der GSSG-Reduktion. Weiterhin konnten mehrere Glutathionylierungsstellen in der hTGR identifiziert (Cys93, Cys133 und Cys619) und ein inhibierender Effekt durch diese Modifikationen festgestellt werden. Im Gegensatz zu anderen TGRs, z.B. aus Platyhelminthen, weist die hTGR kein hysteretisches Verhalten auf. Diese Ergebnisse ermöglichen neue Einblicke in den Reaktionsmechanismus und die Regulation von Monothiol-Grx-beinhaltenden TGRs.

PUBLICATIONS

Peer-reviewed research articles

Bathke J, Fritz-Wolf K, **Brandstädter C**, Burkhardt A, Jortzik E, Rahlfs S, Becker K (**2016**) Structural and functional characterization of *Plasmodium falciparum* nicotinic acid mononucleotide adenylyltransferase, ***J Mol Biol***, 428: 4946–61.

Brandstaedter C, Fritz-Wolf K, Weder S, Fischer M, Hecker B, Rahlfs S, Becker K (**2017**) Kinetic characterization of wild type and mutant human thioredoxin glutathione reductase defines its reaction and regulatory mechanisms, ***FEBS J***, doi:10.1111/febs.14357.

Pauli K, Dzieciolowski J, Fritz-Wolf K, **Brandstaedter C**, Parsonage D, Poole LB, Rahlfs S, Becker K. Redox-regulation of peroxiredoxins, in preparation

Brandstaedter C, Delahunty C, Schipper S, Rahlfs S, Yates JR, Becker K. Identification of interacting proteins with 2-Cys peroxiredoxins from *Plasmodium falciparum*, in preparation

Brandstaedter C, Dzieciolowski J, Schulz N, Rahlfs S, Becker K. Surface plasmon resonance spectroscopy can provide insights into regioselective recognition processes, in preparation

CONFERENCE CONTRIBUTIONS

Brandstädter C., Jortzik E., Rahlfs S., Becker K.: Peroxiredoxin networks in malaria parasites. 6th Annual Conference of the Giessen Graduate School for the Life Sciences. Giessen, 2013, Poster

Brandstädter C., Jortzik E., Rahlfs S., Becker K.: Peroxiredoxin networks in the malaria parasite *Plasmodium falciparum*. 7th Annual Conference of the Giessen Graduate School for the Life Sciences. Giessen, 2014, Poster

Brandstädter C., Delahunty C., Yates J., Rahlfs S., Jortzik E., Becker K.: Peroxiredoxin networks in malaria parasites. Gordon Research Conference on Thiol-based Redox Regulation and Signaling, Stowe, 2016, Poster

Brandstädter C., Dzieciolowski J., Schulz N., Rahlfs S., Becker K.: Insights into the catalytic mechanism of peroxiredoxins using SPR-spectroscopy. Gordon Research Conference on Thiol-based Redox Regulation and Signaling, Stowe, 2016, Poster

Brandstädter C., Dzieciolowski J., Delahunty C., Yates J.R., Rahlfs S., Becker K.: Interactome and recycling of peroxiredoxins from *Plasmodium falciparum*. BioMalPar XIII: Biology and Pathology of the Malaria Parasite, Heidelberg, 2017, Poster

Bathke J., Fritz-Wolf K., **Brandstädter C.**, Burkhardt A., Jortzik E., Rahlfs S. and Becker K.: Structural and functional characterization of *P. falciparum* nicotinic acid mononucleotide Adenylyltransferase. BioMalPar XIII: Biology and Pathology of the Malaria Parasite, Heidelberg, 2017, Poster

Brandstädter C., Dzieciolowski J., Fritz-Wolf K., Fischer M., Hecker B., Rahlfs S., Becker K.: Characterization of human thioredoxin glutathione reductase. EMBO Conference on Redox Biology, Moscow - Saint Petersburg, 2017, Poster (Best Poster Prize)

Brandstädter C.: Characterization of the human thioredoxin glutathione reductase – a multifunctional thiol switch protein. 7th Meeting of the DFG Priority Program 1710 "Dynamics of Thiol-based Redox Switches in Cellular Physiology", Rauischholzhausen, 2018, Talk

“If I have seen further, it is by standing on the shoulders of giants.”

Isaac Newton 1676

CONTENT

DECLARATION III
EIDESSTATTLICHE ERKLÄRUNG III
ACKNOWLEDGEMENTS IV
SUMMARY V
ZUSAMMENFASSUNG VII
PUBLICATIONS IX
CONFERENCE CONTRIBUTIONS IX
CONTENT XII
TABLES XVI
FIGURES XVII
ABBREVIATIONS XX
1 INTRODUCTION 1
1.1 Oxidative stress 1
1.2 Thiol switches of cysteines 2
1.3 Peroxiredoxins 3
1.3.1 Classification of peroxiredoxins 3
1.3.1.1 Structural features of peroxiredoxins 4
1.3.2 Catalytic cycle of peroxiredoxins 6
1.4 Malaria and Plasmodium falciparum 7
1.4.1 Life cycle of *P. falciparum* 8
1.4.2 Maintenance of the intracellular redox balance in *P. falciparum* 9
1.4.2.1 Thioredoxin system of *P. falciparum* 9
1.4.2.2 Glutathione system of *P. falciparum* 10
1.4.3 Peroxiredoxins of *P. falciparum* 11
1.5 Thioredoxin glutathione reductase 13
1.5.1 Thioredoxin reductase 14
1.5.2 Glutathione reductase 15
1.5.3 Glutaredoxin 15
1.5.4 Mammalian thioredoxin glutathione reductase 16
1.6 Objectives of the study 18
2 MATERIAL 20
2.1 Instruments 20
2.2 Chemicals 22
2.3 Consumables 24
2.4 Kits 25

2.5 Enzymes ... 25
2.5.1 Restriction enzymes ... 25
2.5.2 Enzymes for molecular biology ... 26
2.5.3 Recombinant enzymes ... 26
2.6 Antibodies ... 26
2.7 *E. coli* cells ... 27
2.8 Cloning and expression vectors ... 27
2.9 Solutions and buffers ... 27
2.9.1 Buffer for Ni-NTA-affinity chromatography ... 27
2.9.2 Buffers for electrophoresis ... 28
2.9.3 Buffers for semi-dry Western blot ... 28
2.9.4 Gels for electrophoresis ... 29
2.9.5 Assay buffers and solutions ... 29
2.9.6 Stock solutions ... 31
2.10 Media for bacterial culture ... 32
2.11 Protein crystallization screens ... 32
2.12 Oligonucleotides ... 32
3 METHODS ... 34
3.1 Molecular biological methods ... 34
3.1.1 Plasmid preparation ... 34
3.1.2 Determination of DNA concentration ... 34
3.1.3 Site-directed mutagenesis for *Pf*Prxs ... 34
3.1.4 Site-directed mutagenesis for hTGR ... 35
3.1.5 Molecular cloning ... 35
3.2 Microbiological methods ... 36
3.2.1 Transformation ... 36
3.2.2 Heterologous overexpression in *E. coli* ... 36
3.2.2.1 Heterologous overexpression of *Pf*Prxs in *E. coli* ... 36
3.2.2.2 Heterologous overexpression of hTGR and mutants in *E. coli* ... 37
3.2.3 Cell harvest ... 37
3.3 Protein biochemical methods ... 38
3.3.1 Cell disruption ... 38
3.3.2 Purification with Ni-NTA affinity chromatography ... 38
3.3.2.1 Purification of *Pf*Prxs ... 38
3.3.2.2 Purification of hTGR ... 39
3.3.3 SDS polyacrylamide gel electrophoresis ... 39
3.3.4 Size exclusion chromatography ... 39

3.3.5 Determination of protein concentration ... 40
3.3.6 Western blot ... 40
3.3.6.1 Western blot analysis for hTGR ... 40
3.3.7 Protein-protein interaction analysis ... 41
3.3.7.1 Pull-down assay ... 41
3.3.7.2 Surface plasmon resonance spectroscopy ... 44
3.3.7.3 Electrophoretic mobility shift assay ... 47
3.3.7.4 Microscale thermophoresis ... 47
3.3.7.5 Isothermal titration calorimetry ... 49
3.3.8 Absorption titration spectrum ... 50
3.3.9 Measurement of the catalytic cysteine pK_a ... 50
3.4 Determination of kinetic parameters ... 52
3.4.1 Thioredoxin reductase activity assays ... 52
3.4.2 Grx activity assay ... 53
3.4.3 Glutathione reductase activity assay ... 53
3.4.4 Hysteretic effect ... 53
3.4.5 Protein-*S*-glutathionylation ... 53
3.5 *P. falciparum* cell culture methods ... 54
3.6 Protein crystallization ... 54
4 RESULTS ... 55
4.1 The interactome of *Plasmodium falciparum* 2-Cys peroxiredoxins ... 55
4.1.1 Site-directed mutagenesis of *Pf*Prxs ... 55
4.1.2 Heterologous overexpression and purification of *Pf*Prxs and mutants ... 55
4.1.3 Pull-down assay with 2-Cys *Pf*Prxs ... 57
4.1.4 Measurement of the catalytic cysteine pK_a of *Pf*Prxs ... 65
4.1.5 Crystallization of the truncated *Pf*PrxQ$^{1\text{-}164}$ ... 65
4.2 Protein-protein interaction analysis of *Pf*Prxs and their redoxins ... 66
4.3 Kinetic characterization of the human thioredoxin glutathione reductase ... 76
4.3.1 Heterologous overexpression and purification of hTGR and hTGR^{U642C} ... 76
4.3.2 Absorption titration spectrum for hTGR ... 77
4.3.3 Kinetic parameters of hTGR and hTGR^{U642C} ... 78
4.3.3.1 Thioredoxin reductase activity ... 78
4.3.3.2 Grx activity assay ... 81
4.3.3.3 Glutathione reductase activity ... 83
4.3.3.4 Hysteretic behavior of the GR activity of hTGR ... 84
4.3.4 Protein-*S*-glutathionylation of hTGR ... 85
5 DISCUSSION ... 87

5.1 Plasmodium falciparum peroxiredoxins 87
5.1.1 Pull-down assay with 2-Cys *Pf*Prxs 87
5.1.1.1 Identification of proteins interacting with *Pf*Prx1a 90
5.1.1.2 Identification of proteins interacting with *Pf*Prx1m 95
5.1.2 pK_a determination of the active site cysteine of *Pf*Prxs 99
5.1.3 Protein-protein interaction analysis of *Pf*Prxs using SPR spectroscopy 100
5.1.3.1 Protein interaction analysis with 2-Cys *Pf*Prxs 102
5.1.3.2 Protein interaction analysis with 1-Cys *Pf*Prxs 103
5.2 Human thioredoxin glutathione reductase 106
5.2.1 Heterologous overexpression and purification of hTGR 106
5.2.2 Kinetic characterization of hTGR and hTGR^{U642C} 107
5.2.3 Proposed catalytic reaction mechanism of hTGR 110
5.2.4 *S*-glutathionylation of hTGR 113
5.2.5 Hysteretic behavior of hTGR 113
REFERENCES 115
SUPPLEMENTS 137

TABLES

Table 1: General purification procedure for different Prxs. 38

Table 2: Peroxiredoxins and the respective pH used for immobilization..... 46

Table 3: Interaction partners of *Pf*Prx1a..... 59

Table 4: Interaction partners of *Pf*Prx1m. 63

Table 5: Interaction of *Pf*Prx1a with *Pf*Trx and *Pf*Grx. 68

Table 6: Interaction of *Pf*Prx1m with *Pf*Trx and *Pf*Grx. 69

Table 7: Interaction of *Pf*Prx5 with *Pf*Trx and *Pf*Grx. 69

Table 8: Interaction of *Pf*Prx6 with *Pf*Trx and *Pf*Grx. 70

Table 9: Interaction of *Pf*PrxQ$^{1\text{-}164}$ with *Pf*Trx and *Pf*Grx. 71

Table 10: Kinetic parameters of hTGR wild type and hTGR^{U642C} in the TrxR assay. 79

Table 11: Kinetic parameters of hTGR wild type and hTGR^{U642C} in the DTNB assay..... 80

Table 12: Kinetic parameters of hTGR wild type and hTGR^{U642C} in the HEDS reduction assay. 82

Table 13: Specific activity of hTrxR wt, hTrxR^{U498S}, hTGR$^{151\text{-}643}$, and hTGR in the mod. HEDS reduction assay. 83

Table 14: Kinetic parameters of hTGR wild type and hTGR^{U642C} in the GR assay. 83

Table 15: Specific activity of hTrxR wt, hTrxR^{U498S}, hTGR$^{151\text{-}643}$, and hTGR in the GR assay. 84

Table 16: Specific activities of hTGR and glutathionylated hTGR. 86

Table 17: Functional clustering of the proteins interacting with *Pf*Prx1a. 79

Table 18: Proteins interacting with *Pf*Prx1m. 96

Table 19: Comparison of kinetic activities of TGRs from different species. 101

FIGURES

Figure 1: Reaction mechanism of peroxiredoxin enzymes. 4

Figure 2: Characteristic structure of Prxs. 4

Figure 3: Quaternary structures of Prx. 5

Figure 4: Catalytic cycle of peroxiredoxins. 6

Figure 5: Mechanisms of H_2O_2 sensing. 7

Figure 6: Life cycle of *P. falciparum* with different targets of malaria vaccines. 8

Figure 7: Redox metabolism in *P. falciparum*. 9

Figure 8: The thioredoxin system in *P. falciparum*. 10

Figure 9: Compartmentation of the redox system in *P. falciparum*. 12

Figure 10: Postulated mechanism for Trx reduction by mammalian TrxR. 14

Figure 11: The glutaredoxin dithiol oxidoreductase mechanism. 15

Figure 12: The monothiol mechanism of glutaredoxins. 16

Figure 13: Proposed reaction mechanism for TGR. 17

Figure 14: Partial sequence comparison of TGR from different species. 18

Figure 15: Scheme of pull-down assay implementation. 42

Figure 16: Simplified depiction of surface plasmon polariton formation 44

Figure 17: General setup for an SPR biosensor 45

Figure 18: Activation of carboxymethyl dextran. 45

Figure 19: MST setup and thermophoresis assay. 48

Figure 20: Schematic representation of the isothermal titration calorimeter. 49

Figure 21: Basic principle of Prx activity determination by the HRP competition assay. .. 50

Figure 22: Determination of k_{Prx} with the HRP competition assay. 51

Figure 23: Purification of *Pf*Prxs via Ni-NTA affinity chromatography. 56

Figure 24: Size-exclusion chromatogram of *Pf*PrxQ$^{1\text{-}164}$ under reducing and oxidizing conditions. 56

Figure 25: Size-exclusion chromatography profile of *Pf*Prx1a wt and *Pf*Prx1m wt. 57

Figure 26: Elution profile of 2-Cys *Pf*Prxs during pull-down assays. 58

Figure 27: pH-dependent activity curves of *Pf*Prx1a, *Pf*PrxQ$^{1\text{-}164}$, and *Pf*Prx5 65

Figure 28: Protein crystals of *Pf*PrxQ$^{1-164}$. 66

Figure 29: Interaction profile of *Pf*Prx1a^{C50S} with *Pf*Trx wild type and its Cys mutants.... 67

Figure 30: Western blot confirmation of covalent binding in *Pf*Prx1a and *Pf*Trx1. 72

Figure 31: Western blot confirmation of cysteine-dependent regioselectivity of *Pf*Prx1a interacting with *Pf*Trx1..... 73

Figure 32: Quantitative determination of the interactions between *Pf*Prx1a and *Pf*Trx Cys mutants. 74

Figure 33: Dissociative calorimetric titration of *Pf*Prx1a wt coupled with *Pf*Trx^{CSC} and *Pf*Trx^{SSS}. 75

Figure 34: Purification of hTGR wild type. 76

Figure 35: Protein profile of purified recombinant hTGRs and their isolated domains..... 77

Figure 36: Oligomerization behavior of hTGR wild type. 77

Figure 37: NADPH titration of hTGR wild type. 78

Figure 38: K_M for hTrx and NADPH in hTGR wild type and hTGR^{U642C}. 79

Figure 39: K_M for DTNB and NADPH in hTGR wild type and hTGR^{U642C}. 80

Figure 40: Substrate inhibition at hTGR with GSH and HEDS. 81

Figure 41: K_M for GSH and HEDS for the enzymes hTGR wild type and hTGR^{U642C}..... 82

Figure 42: K_M for GSSG and NADPH for hTGR wild type. 83

Figure 43: Full time courses of NADPH oxidation by 2 µM of hTGR in the GR assay. ... 85

Figure 44: Western blot confirmation of *S*-glutathionylation of hTGR. 86

Figure 45: Proposed mechanisms of reduction and oxidation of targeted proteins via 2-Cys Prxs mutants. 90

Figure 46: Venn diagrams of the number of proteins found in pull-down assay with *Pf*Prx1a. 91

Figure 47: Venn diagrams of number of proteins found in pull-down assay with *Pf*Prx1m. 95

Figure 48: Proposed mechanisms of reduction and oxidation of targeted proteins via 2-Cys Prx wild type..... 98

Figure 49: Comparison of FF and LU states from *Ec*AhpC$^{1-186}$-YFSKHN crystal structures. 102

Figure 50: Cysteine preference in the recycling process of 2-Cys *Pf*Prxs with Trx. 103

Figure 51: Cysteine preference in the recycling process of 1-Cys *Pf*Prxs with Trx..... 104

Figure 52: Model of the hTGR dimer in complex with bound Trx and GSSG. 111

Figure 53: Structural model of GSH (A) and GSSG (B) binding to the monothiol Grx domain of hTGR 112

ABBREVIATIONS

Å	Ångström
A_x	Absorption at x nm
APS	Ammonium persulfate
ATP	Adenosine triphosphate
bp	Base pair
BSA	Bovine serum albumin
CHP	Cumene hydroperoxide
CNBr	Cyanogen bromide
C_P	Peroxidatic cysteine
C_R	Resolving cysteine
DMSO	Dimethyl sulfoxide
DNA	Deoxyribonucleic acid
DNase	Deoxyribonuclease
dNTP	Deoxyribonucleotide triphosphate
DTNB	5,5‘-dithio-bis-(-2-nitrobenzoeic acid)
DTT	1,4-dithiothreitol
ε	Molar extinction coefficient
ECL	Electrogenerated chemiluminescence
E. coli	*Escherichia coli*
EDC	1-ethyl-3-(3-dimethylaminopropyl)-carbodiimide
EDTA	Ethylenediaminetetraacetic acid
EH_4	Fully reduced enzyme
E_{ox}	Fully oxidized enzyme
FAD	Flavin adenine dinucleotide
FF	Fully folded
FPLC	Fast protein liquid chromatography
GLP	Glutaredoxin like protein
GR	Glutathione reductase
Grx	Glutaredoxin
GSH	Glutathione
GSNO	Nitrosoglutathione
GSSG	Glutathione disulfide
HEDS	Bis(2-hydroxyethyl)disulfide
H_2O	Water
H_2O_2	Hydrogen peroxide
HOCl	Hypochlorous acid
HRP	Horse radish peroxidase
IPTG	Isopropyl-β-D-thiogalactopyranoside
kDa	Kilodalton
K_M	Michaelis constant
LB	Lysogeny broth
LU	Locally unfolded
NHS	*N*-hydroxysuccinimide
Ni-NTA	Nickel nitrilotriacetic acid
NO	Nitric oxide
NOO^-	Peroxinitrite
NOS	Nitric oxide synthase

$\bullet O_2^-$	Superoxide anion
$^1O_2$	Singlet oxygen
O_3	Ozone
•OH	Hydroxyl radical
OD	Optical density
PCR	Polymerase chain reaction
PEG	Polyethylene glycol
Pf	*Plasmodium falciparum*
pK_a	Logarithmic acid dissociation constant
Plrx	Plasmoredoxin
Prx	Peroxiredoxin
PMSF	Phenylmethylsulfonylfluoride
PTM	Post-translational modifications
PVDF	Polyvinylidene difluoride
RNS	Reactive nitrogen species
RO•	Alkoxy radical
ROO•	Peroxy radical
ROOH	Organic hydroperoxide
ROS	Reactive oxygen species
RU	Response units
SDS	Sodium dodecyl sulfate
SDS-PAGE	Sodium dodecyl sulfate-polyacrylamide gel electrophoresis
Sm	*Schistosoma mansoni*
SP	Signaling protein
SPR	Surface plasmon resonance
tBuOOH	*Tert*-butyl hydroperoxide
TB	Terrific broth
TCEP	Tris(2-carboxyethyl)phosphine
TEMED	N,N,N',N'-tetramethylethylenediamine
TGR	Thioredoxin glutathione reductase
Tris	Tris-(hydroxymethyl)-aminomethane
Trx	Thioredoxin
TrxR	Thioredoxin reductase
U	International unit (µmol*min^{-1})
V_{max}	Maximum reaction rate
(v/v)	Volume per volume
(w/v)	Weight per volume

Abbreviations of nucleotides

nucleotide	abbreviation
adenine	A
thymine	T
cytosine	C
guanine	G
uracil	U

Abbreviations of amino acids

amino acid	3 letter code	1 letter code
alanine	Ala	A
arginine	Arg	R
asparagine	Asn	N
aspartic acid	Asp	D
cysteine	Cys	C
glutamic acid	Glu	E
glutamine	Gln	Q
glycine	Gly	G
histidine	His	H
isoleucine	Ile	I
leucine	Leu	L
lysine	Lys	K
methionine	Met	M
phenylalanine	Phe	F
proline	Pro	P
selenocysteine	Sec	U
serine	Ser	S
threonine	Thr	T
tryptophan	Trp	W
tyrosine	Tyr	Y
valine	Val	V

1 INTRODUCTION

1.1 Oxidative stress

An exposure to reactive oxygen species (ROS) is unavoidable for organisms living in an aerobic environment. Oxidative stress occurs when the cellular antioxidant capacity is decreased or when ROS are at high and/or sustained levels. ROS are generated intracellularly by a variety of physiological processes or can be provoked by exogenous sources where ROS can be taken up directly by the cell from the extracellular milieu or can be produced as a consequence of exposure to an environmental insult [1]. Endogenous sources of reactive oxygen are derived from leakages of activated oxygen from the respiratory chain during oxidative phosphorylation (complexes I and III), other enzymes such as xanthine oxidase or cytochrome P450, or autoxidation reactions or are deployed by the immune system to combat microorganisms. Xenobiotics [2], pollutants, heavy metal ions [3] (Haber-Weiss reaction or Fenton reaction), or ionizing radiation (radiolysis) [4] are exogenous sources of ROS. The term ROS encompasses superoxide anions ($\bullet O_2^-$), ozone (O_3), singlet oxygen ($^1O_2$), hydrogen peroxides (H_2O_2), hydroxyl radicals (•OH), organic hydroperoxides (ROOH), alkoxy and peroxy radicals (RO•, ROO•), hypochlorous acid (HOCl), and peroxinitrite (NOO^-). Since an excess of ROS can cause severe damage to DNA, RNA, proteins, or lipids, the human body is equipped with antioxidant systems to counterbalance these toxic effects. Antioxidants are composed of non-enzymatic and enzymatic antioxidants. Non-enzymatic molecules include α-tocopherol, ascorbic acid, β-carotene, and glutathione (GSH). α-Tocopherol is the principal defense against oxidant-induced membrane injury since it is able to donate electrons to the peroxyl radical, which is generated during the autoxidation of unsaturated lipids, turning itself to an α-tocopherol radical [5]. It triggers apoptosis of cancer cells and inhibits free radical formations [6], and ascorbic acid converts the α-tocopherol radical back to the non-radical form. GSH is highly abundant and serves as a nucleophile and as a reductant. It is ubiquitously present in all cell types at millimolar concentrations [7] and can exist either in a reduced (GSH) or oxidized (GSSG) form, where the reduced form represents the major portion inside the cell [8]. GSH mediates its redox capacity via reversible oxidation of an active thiol and can covalently bind to proteins (glutathionylation) in the context of post-translational modification in order to activate or inhibit enzyme activity. Due to this, GSH serves as a coenzyme of many enzymes involved in cell defense [9]. The most important enzymatic antioxidants are superoxide dismutase, which catalyzes the dismutation of superoxide radicals to molecular oxygen or hydrogen peroxide, catalase, which decomposes hydrogen peroxide to H_2O and oxygen, but also thiol-containing redox proteins like thioredoxin (Trx), glutaredoxin (Grx) and peroxiredoxins (Prxs). An imbalance of redox-homeostasis can lead to DNA modifications such as degradation of bases, DNA breaks, mutations, deletions, or translocation and cross-linking with proteins and therefore is highly relevant for carcinogenesis, aging, and neurodegenerative, cardiovascular, and autoimmune diseases [10]. ROS can also induce lipid peroxidation and can lead to membrane lipid bilayer derangement, inactivation of membrane-bound receptors, and an increase in tissue permeability [11]. Furthermore, ROS can regulate cellular signaling pathways such as mitogen-activated protein kinase (MAPK) cascades and the phosphoinositide 3-kinase (PI3K) pathway [2]. Moreover, cysteine and methionine residues are very prone to oxidation inside a protein, which can cause conformational changes, protein unfolding, and degradation [12]. Cysteines can undergo a broad range of redox modifications beyond classical thiol-disulfide redox equilibria, including *S*-sulfenylation (-SOH), *S*-sulfinylation ($-SO_2H$), *S*-sulfonylation ($-SO_3H$), *S*-nitrosylation (-SNO), *S*-sulfhydration (-SSH), *S*-glutathionylation (-SSG), and others [13], where some are reversible and others are not. Therefore, cysteines play a key role in the redox code, which

provides central principals of redox biology and genome-exposure interaction, contributing to the spatiotemporal organization of differentiation, development, and adaptation to the environment [14]. It should be mentioned at this point that the term ‘nitrosylation’ is often used mistakenly for the formation of a covalent bond between NO and a cysteine residue [15], which should correctly be termed as ‘nitrosation’. Since the incorrect term ‘nitrosylation’ is widespread in the redox community for this kind of modification, an amendment of this was not implemented in the text at hand.

1.2 Thiol switches of cysteines

Post-translational modifications (PTM) are required to mediate cellular signal transductions in order to change biological functions of proteins. PTMs can extend chemical features of amino acids and allow a specified response to external and internal stimuli. Moreover, selected cysteinyl side chains are targets of PTM and can influence the redox state of the thiol group and thereby protein structure and function. Regulatory cysteines are called ‘thiol switches’, and it was shown that the number of cysteines and thiol switches correlate positively with the complexity of an organism [16]. For categorizing a cysteine, parameters such as the redox state, molecular geometry of the cysteinyl residue, accessibility and environment of the residue inside the protein, and its properties as an acid/base or as a nucleophile/electrophile have to be taken into account. All of these parameters affect the role of the specific cysteine as a structurally important cysteine, as a catalyst, or as a redox switch [17]. The sulfur atoms of cysteinyl residues arise as thiolates ($-S^-$), thiols (-SH), sulfenic acids (-SOH), sulfinic acids ($-SO_2H$), sulfonic acids ($-SO_3H$), and disulfides (-S-S-), which can be distinguished in intra- or intermolecular disulfide bonds with catalytic or structural properties based on their half-life [18, 19]. The term “allosteric disulfide” was introduced since a strict discrimination between these classic disulfides was not always possible [20]. It describes a structural disulfide bond, which is susceptible to reduction and therefore sensitive to alterations in redox states with an impact on protein conformation and function under oxidative stress. The molecular geometry directly affects the reactivity of a cysteinyl residue [21] and includes three parameters: bond length, bond angles between three atoms, and dihedral angles between three bonds, but it is insufficient for explaining or predicting a thiol switch [17]. The reactivity of a cysteinyl residue is highly dependent on the microenvironment generated by the neighboring residues [22] (proton acceptors or ionic interactions with positively charged residues) that are able to perturb the normally high pK_a (~8.5) of cysteine thiols up to 3.5 [23]. The deprotonated thiolate is the basis for an active site cysteine residue since the thiolate is able to start a nucleophilic attack at a hydrogen peroxide, converting the cysteinyl residue to a sulfenic acid, which is an important source of disulfides [17]. Additional features that enhance the reactivity may include the presence of acid-base catalysts [24] and specialized substrate docking sites [25]. Thiol modification can occur at active site cysteines [25, 26] or at non-active site but regulatory cysteines [27, 28]. Redox signaling mechanisms require a primary signaling molecule, sensor, transducer, effector, and termination reaction [29], which is well described in the Orp1/Yap1 couple from yeast. Orp1 acts as a sensor for H_2O_2 and becomes oxidized at its attacking cysteine. The originated sulfenic acid is reduced by Yap1, which results in disulfide formation inside Yap1. Oxidized Yap1 acts as a transducer of this oxidation signal and promotes the transcription of specific genes. Trx terminates this signal by reducing the disulfide bond in Yap1 [30].

1.3 Peroxiredoxins

Even when the specific catalytic rate constant of catalase or glutathione peroxidase is much higher than those of peroxiredoxins ($\sim 10^7\ M^{-1}\ sec^{-1}$), the high abundance of Prxs (1% or more of cellular proteins) is capable for their role as the dominant cellular peroxide-reducing enzymes [31]. Prxs (EC 1.11.1.15) are ubiquitous cysteine-dependent peroxidases and can regulate the intracellular messenger function of H_2O_2. They are able to reduce endogenous and exogenous H_2O_2, peroxynitrite ($ONOO^-$), and organic hydroperoxides (ROOH) [32], and their recycling depends on redoxins such as Trx or Grx. Prxs can be localized in the cytosol, mitochondrion, nucleus, and even in plastids. They can interact with and inhibit the function of certain oncoproteins [33, 34], can enhance the toxic effect of natural killer cells [35], maintain genome stability, promote longevity [36], and can be induced by proliferative stimuli [37], nitric oxide [38], and oxidative stress [39].
Peroxiredoxins are very sensitive to hyperoxidation, which leads to an inactivation and can be regulated by enzymes such as sulfiredoxin. This at the first glance disadvantage of Prxs was shown to be more likely an advantage. At low hydrogen peroxide concentrations, Prxs implement their peroxidase function but will be oxidized with time as well as their specific reductant. Moreover, redox-sensitive transcription factors such as Pap1 are oxidized due to the oxidized reductant, migrate to the nucleus, and can induce the adaptive response of transcription to persisting oxidative stress. At high H_2O_2 concentrations, Prx is rapidly hyperoxidized and will not act as a peroxidase. The reductant will not be oxidized since it is not able to deliver electrons to the hyperoxidized Prx, stays reduced as well as the transcription factor and therefore does not induce an adaptive response. Surprisingly, this leads to a higher survival rate [40] since the pool of reductant can mediate their repair activity to other proteins needed for cell survival in order to overcome a strong oxidative assault [41]. Furthermore, Prx's sensitivity to hyperoxidation was shown to be very individual by finding sensitive and robust Prx groups [42]. Prxs are also found in parasites that affect human health such as pathogenic protozoa, helminths, and parasitic fungi, which are major contributors to the global burden of disease [43], where Prxs are important for defense against endogenous and host-derived ROS and $ONOO^-$. Fundamental research into the parasites' biochemistry and biology is needed in order to find new candidate drugs for clinical testing and overcome this global impact of neglected tropical diseases.

1.3.1 Classification of peroxiredoxins

Peroxiredoxins are subdivided into six evolutionary clusters or subfamilies (Prx1, Prx5, Prx6, Tpx, PrxQ, and AhpE) [44]. Inside one subfamily group, the oligomerization states, interfaces, or the localization of the resolving cysteine (C_R) can vary [45]. Furthermore, Prxs can be divided mechanistically into three subfamilies. Since this work emphasizes mechanistic details, the classification of the Prx-families will be oriented on the mechanistic subdivision. Based on the number of active site cysteines involved in the catalytic cycle, Prxs can be distinguished into 1-Cys and 2-Cys peroxiredoxins. The 2-Cys Prxs can further be subdivided into typical and atypical 2-Cys Prxs. 1-Cys Prxs contain only the highly conserved peroxidatic cysteine (C_P) in the characteristically N-terminal region and no C_R. Oxidized 1-Cys Prxs can be reduced by small molecules such as GSH. 2-Cys Prxs contain, along with the C_P, the C-terminal C_R as well. Typical 2-Cys Prxs form a stable disulfide bond between the oxidized C_P and the C_R of another second subunit (intermolecular), and the atypical 2-Cys Prxs build a disulfide with the C_P in the same polypeptide chain (intramolecular) in the resolving step (Figure 1) [46].

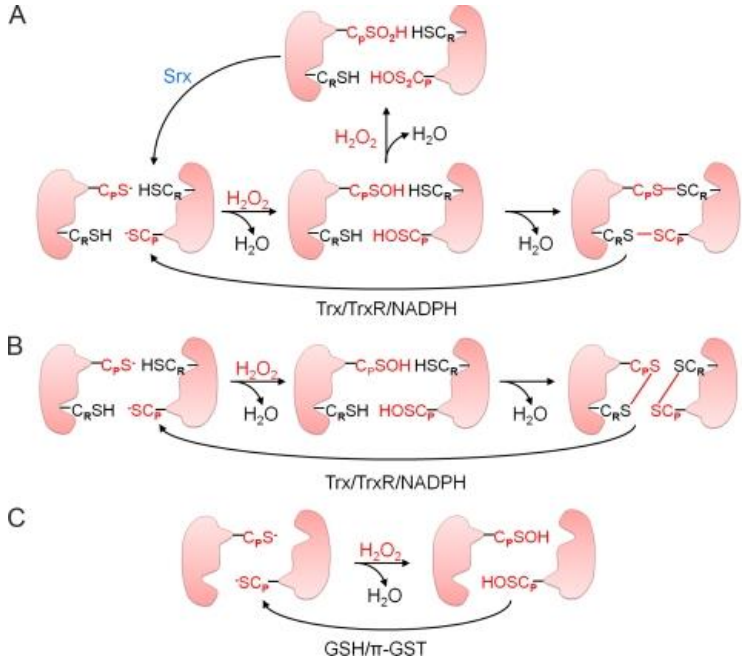

Figure 1: Reaction mechanism of peroxiredoxin enzymes. (A) typical 2-Cys Prx, (B) atypical 2-Cys Prx, and (C) 1-Cys Prx [47].

1.3.1.1 Structural features of peroxiredoxins

Although loop lengths and the conformation of the N-terminal and C-terminal extension of Prxs show variations across the subfamilies, they have a highly spatially conserved tertiary structure of the core. This core structure includes β-strands and α-helices organized as a central 5-stranded antiparallel β-sheet facing two additional β-strands and one α-helix on the one side and three α-helices on the other side [48] (Figure 2A). The peroxidatic cysteine is always located in the first turn of the α2-helix, where a local unfolding also takes place. When the Prx converts to the locally unfolding conformation, the helix will be unraveled at this point, and the C_P will be exposed in a loop segment. The geometry of the active sites of all fully folded Prxs is highly conserved and includes a Pro, a Thr, and an Arg [48] that are in contact with the C_P via van der Waals forces (Figure 2B).

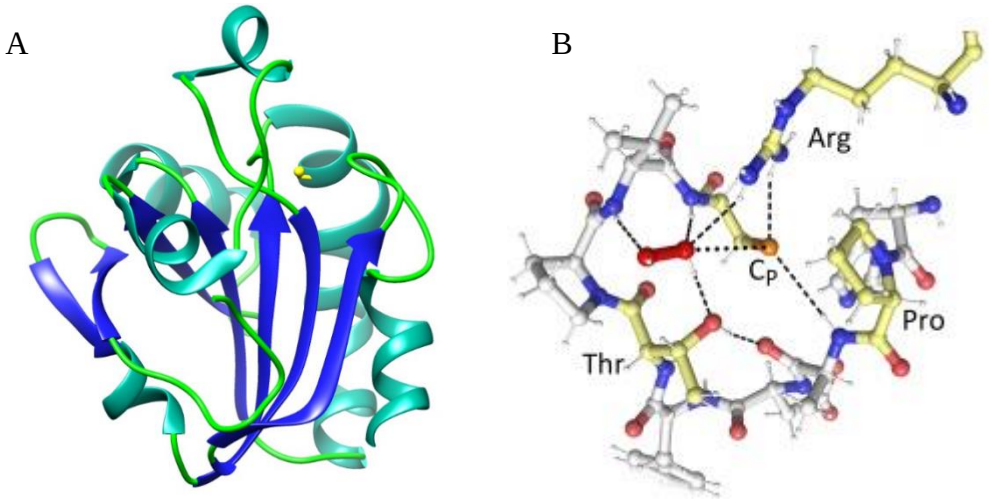

Figure 2: Characteristic structure of Prxs. (A) Stereoview of hPrx5 (PDB code 1HD2); the peroxidatic cysteine is represented in yellow. (B) The universally conserved active site of Prxs with its substrate H_2O_2. H-bonds are outlined as dashed lines. Figure 2B was modified according to [44].

Pro shields the C_P from water and plays a part in contributing to the position of the backbone amid the following Gly, which contributes to C_P activation. Arg also activates the C_P and influences the position and chemistry of the attacked peroxide oxygen, and Thr is seen as a proton shuttle between C_P and the peroxyl bond of the hydroperoxide. The peptide amid the C_P and the surrounding residues is also capable of influencing the position of the two resulting hydroxides [48]. When present, the resolving cysteine is located in the Trx-like fold and can occupy at least 5 different positions (on α2, α3, α5 helices) for intramolecular disulfides, and N-terminal (Nt) and C-terminal (Ct) types for intermolecular disulfides) [44].
In terms of oligomerization behavior, Prxs are reported to be dimers, octamers, decamers, and dodecamers, but rarely monomers [49]. All of these quaternary structures were formed by the association of two types of interfaces, the A-type and B-type (Figure 3). In A-type interface dimerization, the interaction of the core structure is supported in an end-to-end fashion, and B-type interface dimerization is defined as an antiparallel accretion of two monomers at their β-sheets in a head-to-tail manner. The C-terminal extension of some B-type Prx can stabilize these dimers (α_2), which can also interact to form toroidal complexes over the A-type dimer interface such as $(\alpha_2)_5$ decamers (and rare $(\alpha_2)_6$ dodecamers) [44]. Under some circumstances even larger complexes in a spherical aggregation or in an open-ended linear form can build up, often related to hyperoxidation and chaperone function [50, 51].

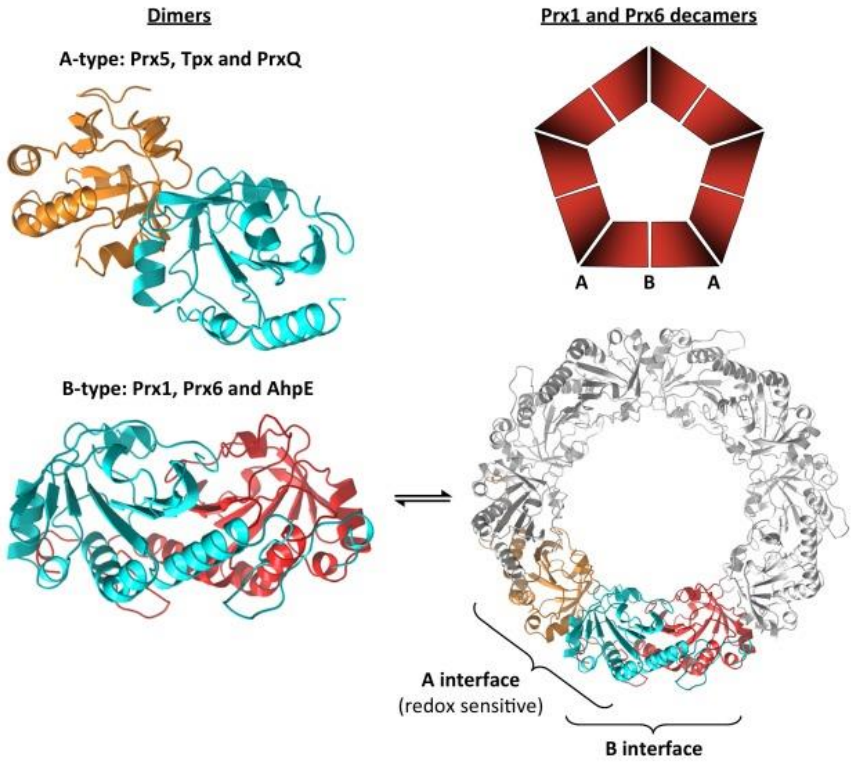

Figure 3: Quaternary structures of Prx [44].

It was shown that reduced Prxs occur in the decameric and oxidized Prxs in the dimeric state and that chaperone activity does not depend on this oligomerization. Hyperoxidation represents only one possibility to change the peroxidase function of Prxs to its chaperone function [52]. Other factors that can influence the structure of the enzyme are posttranslational modifications such as glutathionylation [53], phosphorylation [54], acetylation [55], and proteolysis [56].

1.3.2 Catalytic cycle of peroxiredoxins

The catalytic cycle begins with the thiolate (S^-) of the peroxidatic cysteine of reduced Prx. The Prx is now in the fully folded (FF) conformation and starts a nucleophilic attack at the peroxyl bond of the hydroperoxide substrate (ROOH), whereby the thiolate oxidizes to a sulfenic acid (SOH), and a hydroxide is released (peroxidation). Upon build-up of excess oxidative stress, this sulfenic acid can further oxidize to sulfinic acid (SO_2H) (overoxidation) or even to sulfonic acid (SO_3H). In many organisms the sulfinic acid can be reduced by enzymes such as the ATP-dependent sulfiredoxin (Srx) or sestrin proteins, which can reactivate the hyperoxidized (also called overoxidized) Prx (rescue). After the sulfenic acid is formed at the C_P, the Prx has to be recycled. For 1-Cys Prx, the thiol group involved comes from other proteins or small molecules (e.g. GSH), and in the 2-Cys Prxs, the resolving cysteine residue participates in this step both typically and atypically. The C_R forms a disulfide bond with the C_P, which is intermolecular in the typical 2-Cys Prxs and intramolecular in the atypical 2-Cys Prxs, and changes the Prx from the FF conformation to the locally unfolded (LU) conformation (resolution). The reduction of the disulfide is mediated by reductants such as Trx or Grx-like proteins, which contain an attacking cysteine and a resolving cysteine (CxxC-motif). First, the attacking thiol(ate) of the reductant forms a mixed disulfide with the Prx, which will be reduced by the resolving cysteine of the reductant in the second step. After this recycling step, the Prx is reduced and activated for another catalytic cycle [57] (recycling). The oxidized reductant has to be reduced by other enzymes (e.g. TrxR) in order to be available for another recycling step of the oxidized Prx (Figure 4).

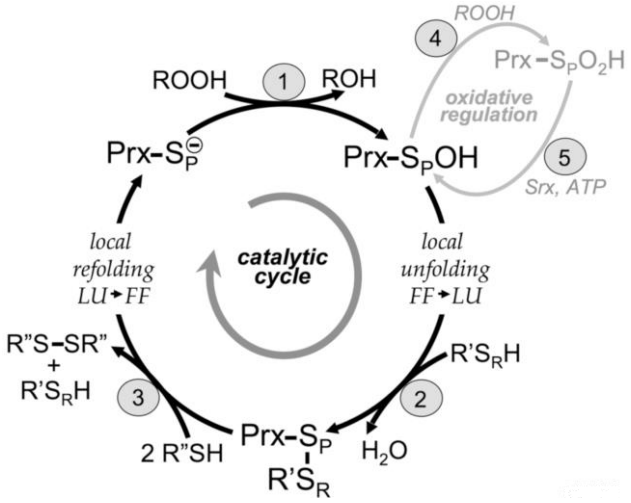

Figure 4: Catalytic cycle of peroxiredoxins. The catalytic steps of (1) peroxidation, (2) resolution, (3) recycling, (4) overoxidation, and (5) rescue are shown [47].

Peroxiredoxins can maintain intracellular H_2O_2 concentrations via their peroxidase activity. It was also shown that at persisting high levels of H_2O_2, the C_P can hyperoxidize, and no further reduction of H_2O_2 will take place, which could then affect other targets (floodgate hypothesis) [36, 42]. Signaling proteins (SP), which are regulated by oxidation, can be influenced directly by the Prx-controlled H_2O_2 concentration, but since the reactivity towards H_2O_2 is five to seven orders of magnitude lower than the reactivity of a Prx towards H_2O_2 and the abundance of SP is also lower, the SP cannot compete with a Prx for the peroxide. A second mechanism for oxidation signaling is transduction of the oxidation to an SP by oxidized Prx via the thiol-disulfide exchange mechanism, which facilitates the selective transfer of oxidation equivalents to downstream regulatory proteins [58]. Likewise, oxidized Trxs, which emerge from the

recycling step in the catalytic cycle, can transfer the oxidation signal to an SP [59, 60] (Figure 5).

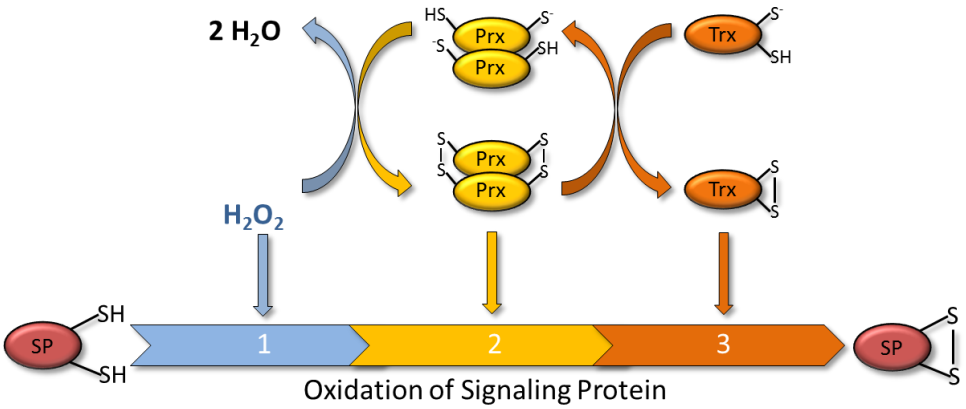

Figure 5: Mechanisms of H_2O_2 sensing. H_2O_2 reacts directly with an effector protein where peroxiredoxins can regulate the intracellular H_2O_2 concentration. Second, oxidized Prxs transduce the oxidation to a protein by forming a disulfide intermediate that is resolved by a C_R from the effector protein. Third, oxidized Prxs are reduced by thioredoxin (Trx), and the oxidized Trx transfers the oxidation to the target proteins**.** Modified according to Netto and Antunes [61].

1.4 Malaria and Plasmodium falciparum

3.4 billion people lived in areas with a high risk of infection with malaria parasites in 2013, which represents approximately half of the present world population. In 2015, this infectious disease affected up to 214 million people and caused about 438,000 cases of death [62]. The mosquito-borne infectious disease, also called marsh fever or tertian fever, received its name from the Medieval Italian words *mala aria*, which means 'bad air' based on the delusion that the malodorous air in the marshes was responsible for the transmission of malaria. However in 1880, the physician Alphonse Laveran was able to identify the true vector of this lethal disease [63]. Malaria is caused by the parasitic protozoan *Plasmodium*, an *Apicomplexa* that belongs to the taxonomic group of the *Alveolata*. The parasite is transmitted by the female *Anopheles* mosquito to mammals, reptiles, and birds. *Plasmodium vivax, P. ovale, P. malariae, P. knowlesi* and *P. falciparum* belong to the human pathogenic species, which cause various types of malaria (*malaria tertiana*, *malaria quartana*, and *malaria tropica*) with their respective spectrum of symptoms. All types of malaria cause symptoms such as fever, fatigue, vomiting, and headaches as well as hepatomegaly and splenomegaly. The most severe form of malaria, *malaria tropica*, can also cause chills, gastrointestinal afflictions, anemia, and icterus and is often lethal. Particularly in high risk areas of Central and South Africa *P. falciparum* is responsible for 75–100% of all malaria cases [64]. Therefore, *P. falciparum* belongs to the leading global causes of death caused by a single organism. The most vulnerable groups are children under five years as well as the elderly and pregnant women.

The typical fever attacks are caused by a rupture of erythrocytes at the end of each stage. *P. falciparum* infects every age of erythrocytes, leading to a parasitemia up to 50% (peak of superinfection). *P. falciparum* also induces the formation of the surface antigen *Pf*EMP1 (*P. falciparum* exterior membrane antigen) which acts as an adhesion protein and is cytoadherent. *Pf*EMP1 is therefore responsible for the adhesion of infected red blood cells to the endothelial wall, which as a consequence cannot be removed by the spleen, leading to a higher parasitemia. *Pf*EMP1 can likewise trigger the adhesion of parasitized erythrocytes among each other (rosette formation), which reduces the blood flow and leads to organ infarctions (brain, heart, lung, placenta, etc.) [65].

1.4.1 Life cycle of *P. falciparum*

The life cycle of *P. falciparum* is divided into a sexual phase, which is executed inside the *Anopheles* mosquito, and an asexual phase, which is executed in the intermediate host, the human body (Figure 6). Asexual multiplication is differentiated into two consecutive generation cycles, the exo-erythrocytic (hepatic) tissue schizogony and the erythrocytic schizogony. The cycle starts with the transmission of sporozoites through the bite of an infected fertilized female *Anopheles* mosquito, carrying the parasite in its salivary glands, to the human host. Once in the blood stream, the sporozoites will migrate rapidly to the liver and penetrate the hepatocytes, where the parasite will multiply asexually and develop into schizonts (liver stage) [66]. Mature schizonts rupture the hepatocyte and release merozoites into the blood stream, which enter the erythrocytes. Once in the erythrocytes, the intraerythrocytic cycle starts (blood stage), where the merozoites develop asexually to a ring form and later into trophozoites and mature schizonts, which rupture the erythrocyte and releases merozoites into the blood stream that are able to infect further erythrocytes. A small amount of merozoites differentiate into male and female gametocytes that can be ingested by another mosquito bite. Inside the mosquito (mosquito stage), gametocytes reach the midgut and develop into micro- and macrogametes. After fertilization these sexual forms fuse to form a diploid zygote, which develops into ookinetes and after transit of the midgut epithelial cell wall into mature oocysts. The midgut cells rupture and release sporozoites to invade the salivary gland and can be transmitted with the next mosquito bite.

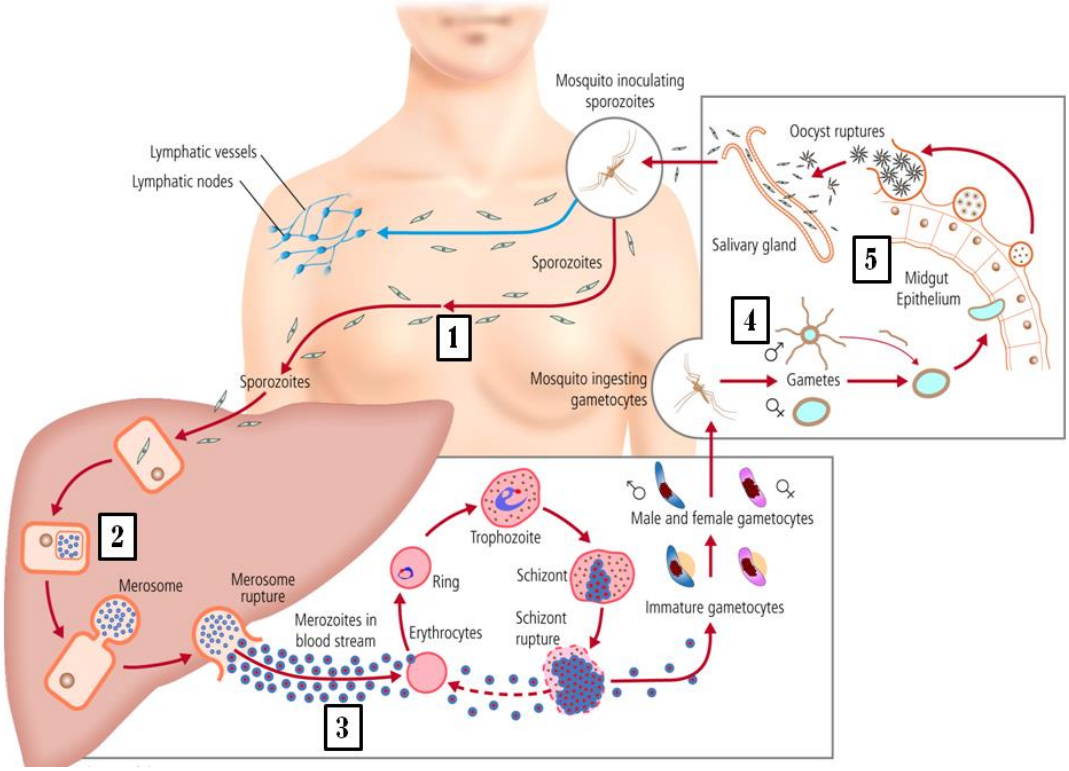

Figure 6: Life cycle of *P. falciparum* with different targets of malaria vaccines. Sporozoites targeted by pre-erythrocytic vaccines. (2) Liver stages of parasite targeted by pre-erythrocytic vaccines. (3) Asexual blood stages, mainly merozoites. (4) Parasite sexual stage in the mosquito midgut. (5) Midgut wall antigens (vector-stage vaccines, indirectly acting against the ookinete stage of the parasite) [66].

1.4.2 Maintenance of the intracellular redox balance in *P. falciparum*

During the life cycle of *P. falciparum*, the parasite is physiopathogenically exposed to high levels of oxidative stress. Large quantities of toxic redox-active byproducts are generated by its high metabolic rate and the degradation of host hemoglobin by the parasite [67]. Moreover, the production of ROS by the host immune system can further enhance overall oxidative stress in the parasite [68, 69]. Toxic free heme (ferri/ferroprotoporphyrin IX; FP) and ROS result from the degradation of hemoglobin in the food vacuole [70]. This FP can biocrystallize to hemozoin [71] and is therefore detoxified (Figure 7). When small amounts of FP escape this neutralization, it can cause damage to host and parasite proteins and membranes and can lyse the erythrocyte. To maintain redox equilibrium, *P. falciparum* relies on a well-equipped antioxidant mechanism composed of small molecules such as glutathione and antioxidant enzymes. These enzymes are glutathione and thioredoxin-dependent proteins [72, 73] as well as superoxide dismutase. The importance of these proteins is furthermore intensified since potent antioxidant enzymes such as catalase and glutathione peroxidase are not possessed by *P. falciparum* [74].

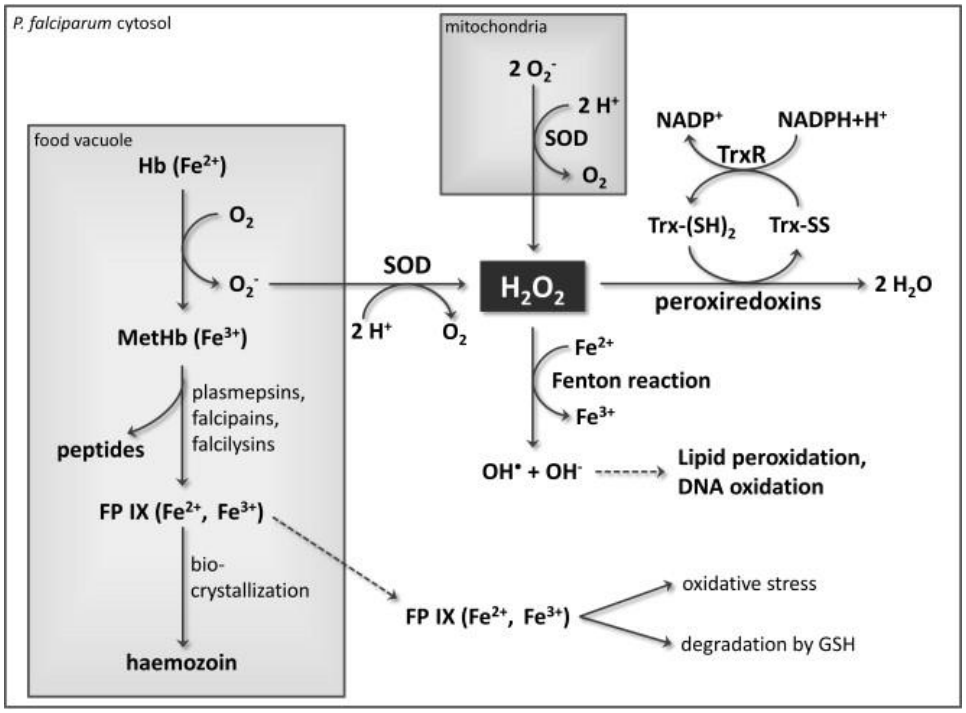

Figure 7: Redox metabolism in *P. falciparum* [75].

1.4.2.1 Thioredoxin system of *P. falciparum*

P. falciparum possesses two isoforms of thioredoxin reductases located in the cytosol and in the mitochondria [76] with similar kinetic properties [77]. *Pf*TrxR catalyzes the reduction of oxidized thioredoxin and can also transfer electrons to low molecular weight compounds [75]. In the catalytic cycle the TrxR transfers two electrons from NADPH to FAD and afterwards to the oxidized substrate (for more details see Chapter 1.5.1). *Pf*TrxR and human TrxR show high homology, although the C-terminal loop in the *Pf*TrxR contains a CxxxxC motif instead of a cysteine-selenocysteine motif [78]. Since the *Pf*TrxR is essential for the intraerythrocytic stages of the parasite, it is seen as a feasible drug target [79]. The physiological substrate of TrxR is thioredoxin. Trxs are a group of small proteins (~12 kDa) with redox-active properties

belonging to the Trx superfamily showing a characteristic Trx fold [80], which is composed of a central four-stranded β-sheet surrounded by α-helices [72, 81]. The three classic Trxs in *P. falciparum* (*Pf*Trx1-3) are located in the cytosol and mitochondria, and all of them perform their redox-regulating activity via a dithiol mechanism. The cytosolic *Pf*Trx1 plays the most important role in the parasite's redox-homeostasis. It can be reduced by *Pf*TrxR and is able to reduce many cellular targets such as Trx-dependent peroxiredoxins with its WCQAC motif (Figure 8). In this way, the attacking cysteine at the N-terminus starts a nucleophilic attack at the disulfide bridge of the oxidized target and forms a mixed disulfide with the substrate, which will be reduced by the resolving cysteine of the Trx at the C-terminus [22, 82]. *Pf*Trx1 also acts as a backup system for the glutathione system since it is able to reduce GSSG directly [83]. It is located in the cytosol and interacts with proteins in protein folding, transcription and translation, glycolysis, and signal transduction [84] and is also involved in protein *S*-glutathionylation [85]. Plasmoredoxin (Plrx), a Trx-superfamily member exclusively found in *Plasmodium*, is reduced by *Pf*Trx, *Pf*Grx, and GSH but is not essential for survival of the parasite. Physiological reducing partners are still unknown [86] although an interaction analysis could identify 21 potential interacting proteins [84].

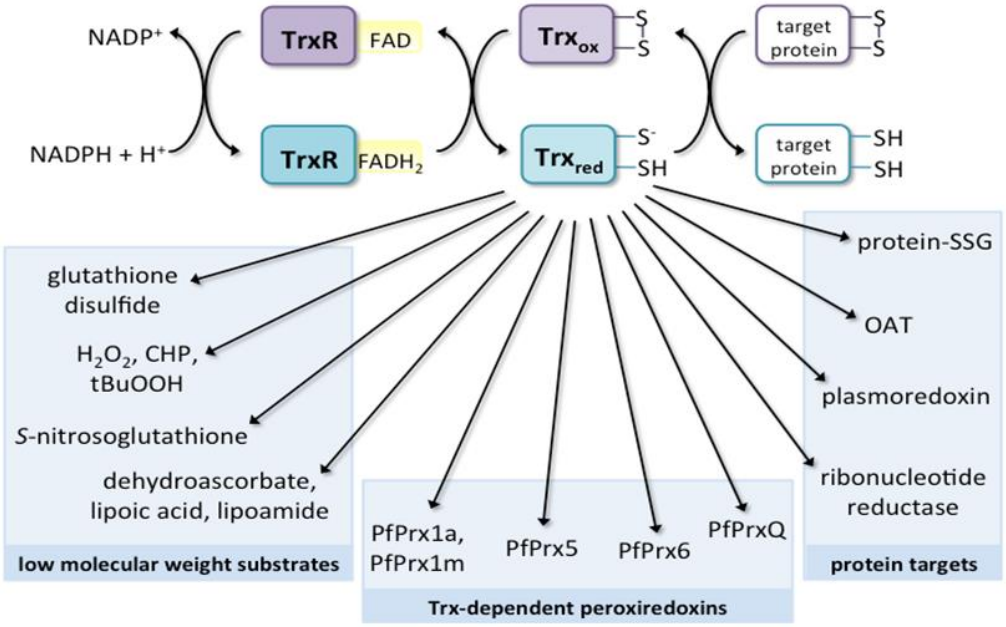

Figure 8: The thioredoxin system in *P. falciparum* [75].

1.4.2.2 Glutathione system of *P. falciparum*

The second central antioxidative system is the glutathione system, which consists of NADPH, glutathione (GSH), glutathione reductase (GR), and glutaredoxin (Grx). GSH reduces toxic peroxides, supports detoxification of xenobiotics, maintains the redox status of proteins by reducing oxidized cysteines, and participates in the regulation of the cell cycle and gene expression [87]. GSH is synthesized by γ-glutamyl-cysteine synthetase and glutathione synthetase and is essential for the development of *P. falciparum* in red blood cells. *P. falciparum* is not able to take up significant amounts of exogenous GSH, with the result that the intracellular GSH/GSSG ratio is closely regulated by its biosynthesis, the expression level of glutathione reductase, and GSSG efflux [88]. GR reduces the oxidized glutathione in an NADPH- and FAD-dependent reaction, which maintains the majority of the intracellular glutathione pool in a reduced state [75]. The intracellular GSH concentration (about 2 mM) is

higher than the concentration of NADPH (< 100 µM) and Trx (about 10 µM), and has to be kept in a reduced state since levels of GSSG over 100 µM are cytotoxic [73]. *Pf*GR and human GR are very similar but differ in their respective cavity of the dimer interface [89], and the enzyme is located in the cytosol and in the apicoplast [76]. Notably, a lack of GR from *P. berghei* is not lethal for the parasite [83, 90]. However, for *P. falciparum* this remains to be studied. Antimalarial compounds such as methylene blue are able to inhibit *Pf*GR as a redox-cycling substrate by turning the GR into a pro-oxidative enzyme [91] or by binding to specific sequence motifs [75]. Another member of the thioredoxin superfamily is glutaredoxin, which shows the common structural motif of the thioredoxin fold (four stranded β-sheets and three flanking α-helices) and a similar active site [92]. Grxs reduce disulfide bridges, can deglutathionylate proteins, and are reduced non-enzymatically by GSH instead of reduction by a specific reductase. In *P. falciparum* only one dithiol Grx has been described so far (*Pf*Grx), which contains the active site motif CPYC and is located in the cytosol. Three monothiol forms have also been found, which contain a CxxS motif and are named glutaredoxin-like proteins (Glp 1-3) [93].

1.4.3 Peroxiredoxins of *P. falciparum*

As described in Chapter 1.3.2.1, peroxiredoxins are thioredoxin-dependent enzymes and belong to the first line of defense against ROS and peroxinitrite [36]. *P. falciparum* possesses five peroxiredoxins, which are located in distinct cell compartments and have different substrate specifities (Figure 9). Additionally, *Plasmodium* is able to import the human Prx2 out of the host's erythrocytes and can accept *Pf*Trx1 as a substrate, which accounts for up to 50% of the total thioredoxin peroxidase activity in the parasite [94]. Peroxiredoxins are suggested to be key antioxidants that guarantee parasite survival under enhanced oxidative stress [95].

*Pf*Prx1a belongs to the typical 2-Cys Prx family with its peroxidatic cysteine at position C50 and its resolving cysteine at position C170; it is located in the cytosol. It is constitutively expressed during the complete life cycle [76] and reduces not only H_2O_2, with a catalytic efficiency of 6.7×10^6 M^{-1} sec^{-1} [96], but also $ONOO^-$, tBuOOH, and CHP by accepting *Pf*Trx and *Pf*Plrx as electron donors [97, 98]. It was shown that *Pf*Prx1a is very sensitive to heat stress [99]. A knockout in *P. berghei* showed no effect on its asexual proliferation but caused a defect in gametocyte development [100] and may be involved in development during multiplying stages such as sporozoites and exo-erythrocytic forms [101].

The mitochondrial *Pf*Prx1m is also a member of the typical 2-Cys Prx family, which detoxifies reactive oxygen species generated during the respiratory chain. It is Trx-dependent but cannot be reduced by GSH or dihydrolipoamide [102]. *Pf*Prx1m contains its peroxidatic cysteine at position C67 and its resolving cysteine at position C187 and could be crystallized by Boucher *et al.* (PDB 2C0D).

*Pf*Prx5, also called the plasmodial antioxidant protein *Pf*AOP, is located in the apicoplast and belongs to the 1-Cys Prx family, with the peroxidatic cysteine at position C117. It was shown to interact with tBuOOH, H_2O_2, GSH, and *Pf*Grx [77, 103] and was crystalized in a homodimeric state with a resolution of 1.8 Å (PDB 1XIY) [104]. *Pf*Prx5 contains a second cysteine at position 143, whose relevance has not yet been clarified. Since it has no effect on catalysis, subunit cooperativity, and enzyme activation, it is hypothesized that the enzyme might be involved in redox-dependent signal transduction, might lower the inactivation rate due to hyperoxidation, might be involved in the rescue reaction of the enzyme, or might act as a slow-acting resolving cysteine for (accidentally) formed disulfide bonds between *Pf*Prx5 and

other proteins. It can also be glutathionylated at Cys143, although it is buried in the crystal structure [103].

The cytosolic 1-Cys Prx family member is *Pf*Prx6 with a peroxidatic cysteine at C47. It shows peroxidase activity in a GSH-dependent [105] and a Trx-dependent [106] enzyme assay, can reduce H_2O_2 and tBuOOH, and also accepts Grx as an electron donor [77]. *Pf*Prx6 can be *S*-glutathionylated [85] and was suggested to bind to heme [107].

More recently, a fifth *Pf*Prx called *Pf*PrxQ was found in the parasitic nucleus. It prefers Grx over Trx and detoxifies H_2O_2 and CHP. *Pf*PrxQ is associated with chromatin in a genome-wide manner, suggesting an important role in protecting nuclear components or being involved in maintaining chromatin structure [108]. The nuclear enzyme contains, very similarly to linker histone H1, a C-terminal lysine-rich tail and is therefore speculated to potentially have the same property of a direct linker binding to the DNA [109].

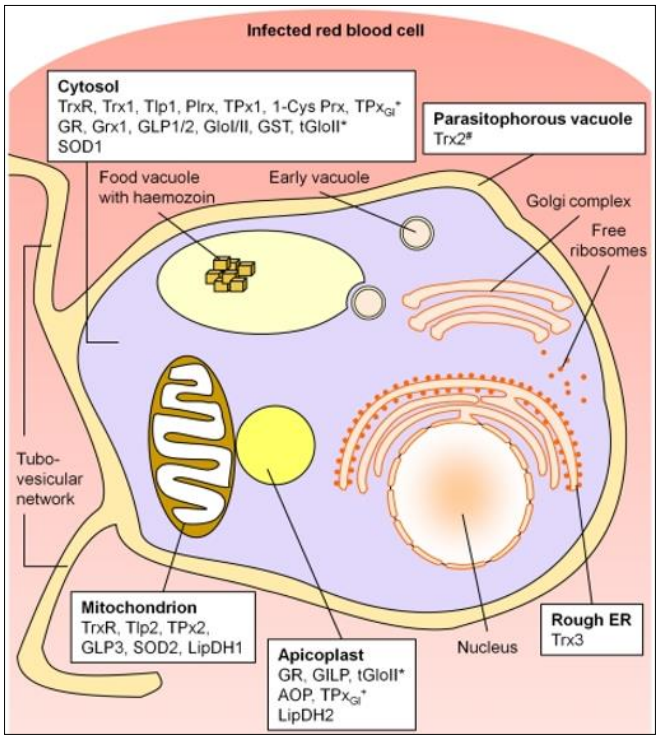

Figure 9: Compartmentation of the redox system in *P. falciparum* [110].

Prxs have been found in a great number of eukaryotic and prokaryotic human pathogens, and knock-out studies have proved that Prxs are essential for their survival and virulence, suggesting these proteins to be potential drug targets [111]. Conoidin A (2,3-bis(bromomethyl)-1,4-dioxide-quinoxaline; BBMQ) was reported to irreversibly inhibit the peroxidase activity of Prx in *Toxoplasma gondii* [112], which covalently binds to the C_P [113], and other quinolone derivatives are reported to reversibly inhibit Prx1a of *Leishmania major*, which binds in a cavity near the C_P [114]. The high conservation of Prx's active site structure, as well as the fact that most known inhibitors are electrophilic reagents with great affinity for thiols and by that are able to react in principle with all available Cys residues, are the most challenging obstacles in developing clinically useful drugs [113] for Prx inhibition.

1.5 Thioredoxin glutathione reductase

Until now, three kinds of thioredoxin reductases (TrxR1, TrxR2, and TGR) have been characterized. They are all members of the pyridine nucleotide disulfide oxidoreductase family [115] and are found in the cytosol and mitochondria, where TrxR1 and TrxR2 were shown to be essential for embryogenesis [116, 117]. The third form, thioredoxin glutathione reductase (TGR) (EC 1.8.1.B1), is mainly found in testes and shows high homology to the other two variants. TGR and TrxR1 generally co-occur in mammals, but could not be identified in all mammalian genomes, due perhaps to incomplete genome sequences and a lack of expressed sequence tags [118]. First described in *Mus musculus* [119], *Schistosoma mansoni* (*S. mansoni*) [120], and *Echinococcus granulosus* [121], TGR could be shown to be a linked combination of the TrxR and GR redox systems that contains TrxR, glutathione reductase (GR), and glutaredoxin activities and thereby represents an unusually wide range of substrate specificity.

TrxR and GR are completely replaced by TGR in *S. mansoni*, which contributes a significant amount of Grx activity present in the parasite. During an infection with *S. mansoni*, the parasite is exposed to high levels of oxidative stress initiated by the host's immune response, whereby the TGR plays a key role in the parasite's redox defense [122]. Due to the versatile functions of *Sm*TGR in the redox system, the enzyme could be an attractive drug target for future development of novel chemotherapeutic agents against schistosomiasis [120].

First discovered in formate dehydrogenese [123] and glycine reductase [124], it was shown that enzymes can contain selenium, which plays a key role in the enzymes' active site, especially from antioxidant enzymes. Selenocysteine (Sec) represents the major biological form of selenium and can act as an electron donor. Selenium and sulfur are nearly isosteric but exhibit significant, distinct chemical properties. The biggest advantage of Sec compared to a thiol is the much lower pK_a of Sec (5.2 vs. 8.0), depending on the neighboring residues, and is with that a more reactive nucleophile and is sometimes even called the 'superreactive cysteine'. It was also reported that Sec residues can adopt more varied conformations than Cys residues [125]. Sec is not coded directly in the genetic code as other amino acids because it is encoded by the UGA codon, which normally acts as the stop codon. Decoding the UGA codon in the mRNA and incorporating Sec requires a complex multi-component system and several reactions such as the synthesis of the selenium donor (monoselenophosphate), the conversion of seryl-tRNA^{Sec} to selenocysteyl-tRNA^{Sec}, and the formation of a cotranslational incorporation complex (SECIS element) [126]. Selenoproteins are involved in redox regulation of intracellular signaling, redox-homeostasis, and thyroid hormone metabolism and are closely linked to cancer and carcinogenesis [127]. In redox homeostasis the thioredoxin reductases are known to be one of the most important redox-regulating proteins and also belong to the group of proteins containing selenocysteine.

1.5.1 Thioredoxin reductase

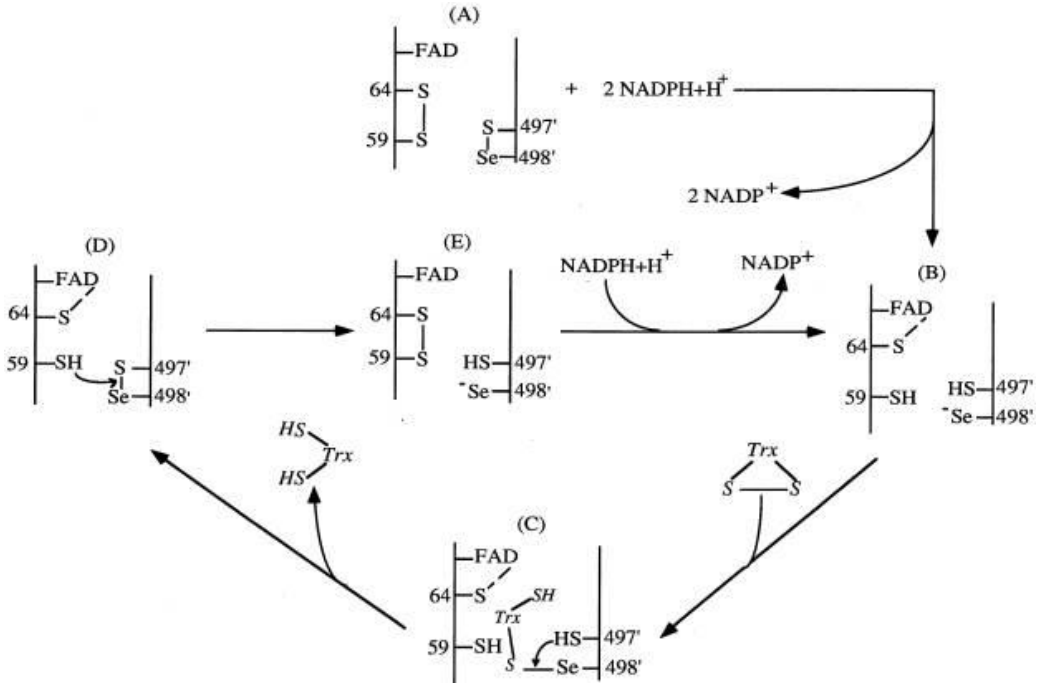

Figure 10: Postulated mechanism for Trx reduction by mammalian TrxR [128]. (For details see text below)

The human thioredoxin reductase (TrxR, EC 1.8.1.9) is an enzyme that contains Sec and acts as a homodimer. The hTrxR possesses two redox centers. The first is located at the N-terminus (Cys59 and Cys64) and is buried in the protein. The second is located at a flexible and highly accessible C-terminal arm of the other subunit (Cys497′ and Sec498′), which is used for electron transport to its substrates by using a guiding bar for stabilized, controlled transfer [129]. All mammalian TrxRs have a conserved -Gly-Cys-Sec-Gly motif at the C-terminal end and a subunit homologous to glutathione reductase even in the conserved active site. The catalytic cycle starts with an oxidized TrxR (E_{ox}), which is reduced by 2 molecules of NADPH to the fully reduced enzyme (EH_4) (Figure 10). Here, one NADPH reduces FAD (NADPH-FAD and $FADH^-$-$NADP^+$ charge transfer complexes as intermediates) to the transient $FADH^-$ in order to reduce the disulfide bond (thiolate-flavin charge transfer complex) within the sequence -Cys^{59}-Val-Asn-Val-Gly-Cys^{64}. The second NADPH reduces selenenylsulfide to the selenolate anion, which subsequently attacks the disulfide bond of the oxidized thioredoxin at position $Cys32^{hTrx}$ and creates a mixed selenenylsulfide between TrxR and Trx. The thiol then attacks the mixed selenenylsulfide at position 497' to reconstruct the selenenylsulfide between Cys497' and Sec498', thereby releasing the newly reduced Trx. The active site Cys of the first subunit will reduce the selenenylsulfide, leading to a disulfide bond at positions 59 and 64 that can be reduced by NADPH. In this manner, the active site dithiols are able to maintain the selenol in its reductive state [128]. The formation of the thiolate-flavin charge transfer complex can be determined by an increase of absorbance at 540 nm and a decrease at 463 nm. At 463 nm the absorbance decreases due to FAD reduction and increases due to flavin reoxidation, and at 540 nm the absorbance decreases due to a loss of the $FADH^-$-$NADP^+$ charge transfer complex and increases due to the formation of the thiolate-FAD charge transfer complex [130]. Due to this, hTrxR is reported to be able to reduce other substrates involved in DNA and selenium metabolism, antioxidant defense, and cell growth regulation [131, 132]. Furthermore, it is the most promising target in chemotherapy treatment based on induced redox stress [133-135].

1.5.2 Glutathione reductase

The glutathione reductase (GR; EC 1.8.1.7) is also a homodimer where each subunit contains an FAD binding site formed by a Rossmann-fold. It also contains an NADPH and a GSSG binding site formed by both subunits [136], which are linked by a cysteine disulfide bond [137-139]. GR plays a central role in glutathione metabolism by linking the cellular NAPDH pool with the thiol/disulfide pool [18]. The GR activity is composed of two distinct half reactions. The reductive half reaction is initiated by the reduction of the prosthetic group FAD by NADPH to the transient $FADH^-$, transporting electrons from NADPH to the isoalloxazine ring of FAD, which reduces the disulfide bond between the active site cysteines of the GR, forming the charge-transfer complex between the flavin and Cys63, which is located closer to the C-terminal end. Oxidized $NADP^+$ is released and replaced by a new reduced NADPH at the end of this first step. The oxidative half reaction starts by binding GSSG, where the more N-terminally located Cys58 of the GR attacks the Cys_I of GSSG to form a mixed disulfide and releases the GSH_{II} followed by a disulfide re-formation of the intramolecular cysteines of the GR that release GSH_I [140]. Some TGRs are reported to show the existence of a lag time before catalysis (hysteretic kinetic behavior) in the GR assay, but the underlying mechanism for this inhibition of initial velocity has not been clarified. The hypotheses range from *S*-glutathionylation at Cys88 for the enzyme's activation at high GSSG concentrations [141, 142] to substrate inhibition [143]. Gene knock-out strains of yeast GR are viable but more sensitive to oxidants and accumulate higher GSSG levels in the cytosol [144, 145].

1.5.3 Glutaredoxin

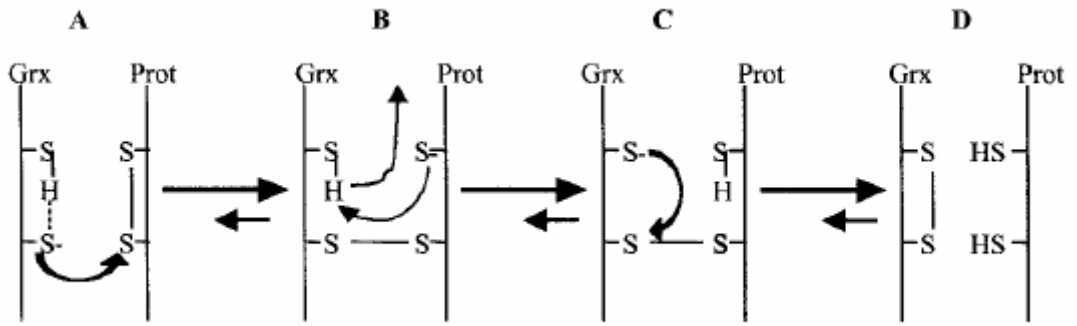

Figure 11: The glutaredoxin dithiol oxidoreductase mechanism. The reduced Grx starts a nucleophilic attack with its N-terminal cysteine at the disulfide bridge of an oxidized target protein. B) A mixed disulfide build up, and the C-terminal cysteine of Grx becomes deprotonated. C) The deprotonated C-terminal cysteine of Grx starts a nucleophilic attack at the mixed disulfide intermediate. D) The target protein is now fully reduced and the Grx is in its oxidized form [146].

Grxs are glutathione-dependent thiol/disulfide oxidoreductases that can catalyze thiol–disulfide exchange reactions. All Grx isoforms share an exposed active site cysteine residue at the N-terminus. Depending on the existence of a second more C-terminal cysteine, Grxs are distinguished into monothiol and dithiol Grxs. Additionally, some contain a third cysteine residue after the GG-motif at the N-terminus of helix α_4 [18] whose function has not yet been elucidated. Grxs are mostly monomers but have also been found as non-covalently linked [147-149] and covalently linked dimers [147] and were found to be able to bind Fe/S clusters with glutathione as a ligand, which can lead to the formation of dimers and tetramers [150-152]. In the glutaredoxin oxidoreductase mechanism, a dithiol reduction mechanism, the N-terminal cysteine of the CxxC motif of Grx starts a nucleophilic attack on one cysteine, which is part of

a disulfide bridge in the target protein, building a mixed disulfide between Grx and the target protein. In this step, the remaining C-terminal cysteine of Grx becomes deprotonated in order to start an attack on the N-terminal sulfur atom, which is involved in the mixed disulfide between Grx and the target protein, in order to generate a reduced target protein and oxidized Grx (Figure 11). In the monothiol mechanism, where Grx is able to reduce protein-SG mixed disulfides due to its higher affinity to GSH, Grx uses its N-terminal cysteine thiol to interact with the GSH moiety of the GSH mixed target protein. In doing so, Grx generates a covalent Grx-SG intermediate and releases the protein in its reduced form. A second GSH reduces the Grx-SG intermediate by generating GSSG (Figure 12) [146].

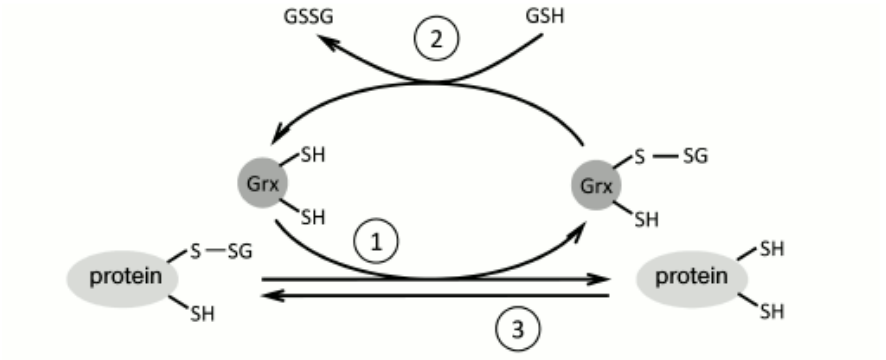

Figure 12: The monothiol mechanism of glutaredoxins. In step 1, the reduced Grx is able to transfer the GSH moiety from a glutathionylated protein to its N-terminal active site cysteine. Step 2 describes the dissociation of the glutathione moiety by a high level of free GSH by forming GSSG. The reduced glutathione-free protein is able to be glutathionylated again (step 3) [153].

1.5.4 Mammalian thioredoxin glutathione reductase

Sun and colleagues were the first to describe the existence of the human thioredoxin glutathione reductase (hTGR) in 1999 [154]. Although almost two decades have elapsed since this detection, further studies on mammalian TGR have mainly been conducted on mouse TGR [118, 154-159]. The TGR was shown to be a fusion of an N-terminal glutaredoxin domain with a thioredoxin reductase module, representing a combination of the most important redox-regulating systems inside the cell. Mammalian TGR is found in small amounts in the liver, kidney, brain, lung, heart, muscle, and prostate, as well as puberty-dependent in large amounts in post-pubertal testes [155]. In the proposed reaction mechanism from Sun *et al.* [118] the reducing equivalents are transferred from NADPH to FAD to the N-terminal active center and to the C-terminal selenenylsulfide active center of the second subunit and finally to the monothiol of the Grx domain of the first subunit (Figure 13). They also showed that all reactions catalyzed by TGR are selenocysteine dependent in order to achieve full efficiency and that a cysteine mutant can only partially compensate the lack of Sec. Furthermore, they were able to identify the Grx domain as responsible for the GR activity of the TGR.

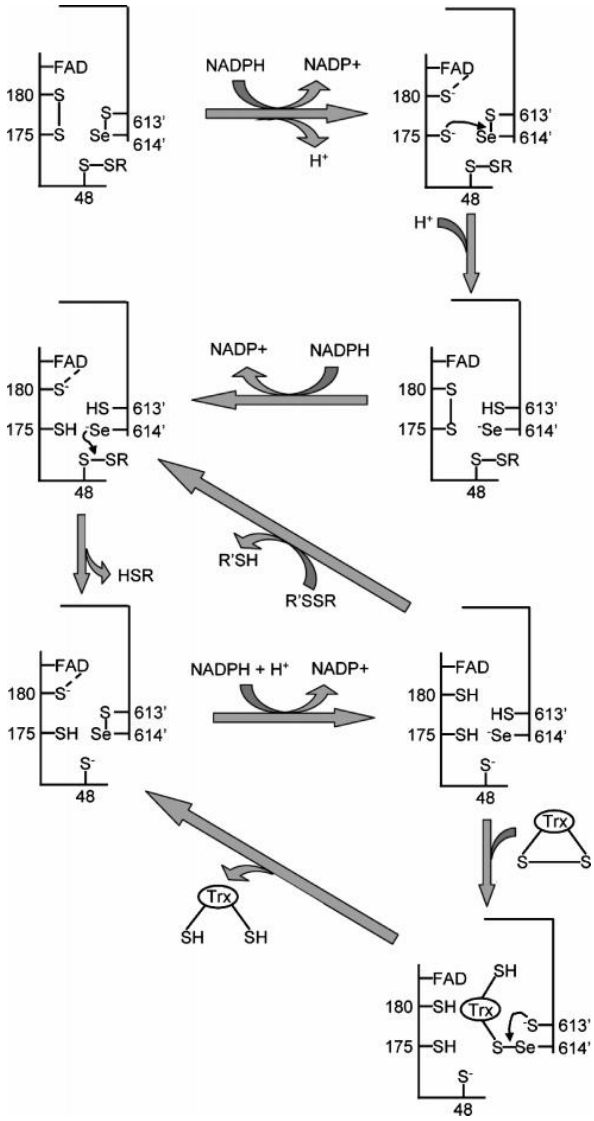

Figure 13: Proposed reaction mechanism for TGR [118].

The hTGR (UniProtKB – Q86VQ6) is a homodimer with a monomeric size of about 70 kDa and is encoded by the human *txnrd3* gene on the long arm of chromosome 3 (3q21.3). Along with an NADPH and FAD-binding domain, the sequence of hTGR also includes a dimer interface domain and a thiol/disulfide redox-active center. Due to the hTrxR domain, hTGR is an enzyme that contains selenocysteine. Here, Sec is placed as the penultimate amino acid at the C-terminal extension, encoded by a UGA codon that requires a SECIS element (cis-acting Sec insertion sequence) for proper recognition as an amino acid instead of a stop codon. Furthermore, hTGR contains an N-terminal GSH-binding motif, which is characteristic for the Grx domain. Moreover, in mammalian TGR this GSH-binding motif is a monothiol and contains only one active site Cys residue (CxxS), whereas the parasitic Grx domain contains a dithiol (CxxC). *Sm*TGR and hTGR show 48.7% sequence identity and 64.1% sequence similarity where the thiol/disulfide redox-active center and the thioredoxin active sites are conserved (Figure 14). Mammalian TGR targets include proteins that form structural components of the sperm, implying its role in the process of sperm maturation [155]. Moreover, its composition of redox-regulating systems might indicate an important role in testis-specific redox homeostasis and thereby a function in cancer prevention.

```
SmTGR       ADGTSQWLRKTVDSAAVILFSKTTCPYCKKVKDVLAEAKIKHATIELDQLSNGSAIQKCL    63
SjTGR       IDGTSQWLQRTIESAAVIVFSKTTCPFCKKLKDVLAEAKIKHATIELDQLSNGSVIQKAL    69
HsTGR       REELRRHLVGLIERSRVVIFSKSYCPHSTRVKELFSSLGVECNVLELDQVDDGARVQEVL    111
MmTGR       REELRRRLRDLIEGNRVMIFSKSYCPHSTRVKELFSSLGVVYNILELDQVDDGASVQEVL    120
             :   : *   ::   *::***: **...::*:::::.  :    :****:.:*: :*: *

SmTGR       GKEAAKYGAKTAVLDYVEPTPIGTTWGLGGTCVNVGCIPKKLMHQAGLLSHALEDAEHFG    182
SjTGR       GKEAAKYGAKIAVLDYVEPTPMGTTWGLGGTCVNVGCIPKKLMHQAGLLSHSLEDAQHFG    188
HsTGR       AKEAAILGKKVMVLDFVVPSPQGTSWGLGGTCVNVGCIPKKLMHQAALLGQALCDSRKFG    231
MmTGR       AKEAANLGKKVMVLDFVVPSPQGTTWGLGGTCVNVGCIPKKLMHQAALLGHALQDAKKYG    240
            .****  * *  ***:* *:* **:*********************.**.::* *:.::*

SmTGR       GPNAGEITQGYAVAIKMGATKADFDRTIGIHPTCSETFTTLHVTKKSGVSPIVSGCCG      598
SjTGR       GPNAGEITQGYAVAIKMGATKEDFDRTIGIHPTCSETFTTLHVTKRSGGSAAVTGC--      602
HsTGR       GPNAGEVTQGFAAAMKCGLTKQLLDDTIGIHPTCGEVFTTLEITKSSGLDITQKGCUG      643
MmTGR       GPNAGEITQGFAAAMKCGLTKQLLDDTIGIHPTCGEVFTTLEITKSSGLDITQKGCUG      652
            ******:***:*.*:* * **  :* ********.*.****.:** ** .   .**
```

Figure 14: Partial sequence comparison of TGR from different species. *Sm*TGR (UniProtKB – Q962Y6), *Sj*TGR (UniProtKB - B5THG7), hTGR (UniProtKB – Q86VQ6), *Mm*TGR (UniProtKB - Q99MD6). The glutaredoxin-active site is colored in green, the thiol-disulfide redox active center is colored in blue and the thioredoxin active site is colored in yellow. * identical residues, **:** very similar residues, **.** similar residues

To date there are no published data available that address overexpression conditions, purification, kinetics, reaction mechanism, or structure of the human homolog of TGR, which was part of this present dissertation.

1.6 Objectives of the study

As already mentioned, redox homeostasis is essential for every organism living in an aerobic environment. To counterbalance the toxic effect of excess ROS, organisms are equipped with several antioxidant systems. Prxs are known as the dominant cellular peroxide-reducing enzymes and can maintain intracellular H_2O_2 concentrations. Moreover, Prxs are able to transfer oxidation equivalents selectively to downstream proteins. In both cases, disulfide-dithiol exchange processes are involved. To gain further insights into the recycling step of oxidized plasmodial Prxs and the protein-protein interaction of *Pf*Prxs, the following major topics have been addresses within this thesis:

(i) Development of a surface plasmon resonance-based method for characterization of protein-protein interactions in *Plasmodium falciparum* peroxiredoxins and their redoxins in the recycling step of the catalytic cycle at molecular detail.

(ii) Identification of potential interaction partners of 2-Cys *Plasmodium falciparum* peroxiredoxins via a pull-down assay and mass spectrometry.

(iii) Determination of the catalytic cysteine pK_a of *Plasmodium falciparum* peroxiredoxins with the horseradish peroxidase competition assay and crystallization of the recently discovered nuclear *Pf*PrxQ.

Since enzymatic redox control represents an excellent field of study in the context of drug development in the fight against parasitic organisms, the redox control of their hosts should be under intensive investigation as well. The most important enzymes for redox homeostasis inside the human body are the thioredoxin reductase and glutathione reductase systems. Both proteins

are combined in a single multifunctional enzyme, the thioredoxin glutathione reductase, in many parasites, including *Schistosoma* and platyhelminths such as *Taenia* and *Echinococcus*, which demonstrates that TGR is the major enzyme addressed for drug development in the context of redox maintenance. Due to this, the human body also possesses this hybrid enzyme, although TrxR and GR are found as dominant isolated proteins as well. The detection of differences in structure and kinetic behavior between the host's and the pathogen's TGR are therefore highly relevant. To characterize human TGR the following objectives were contents of this thesis as well:

(iv) Heterologous overexpression, purification, and kinetic characterization of the human selenoprotein human thioredoxin glutathione reductase compared to with a Sec→Cys mutant and other selective mutants.

2 MATERIAL

2.1 Instruments

Instrument	Company
Autoclave	Webeco, Bad Schwartau
Autoclave VX-95	Systec, Wettenberg
Äkta FPLC system (Pump P-920, monitor UPC-900, injection valve INV-907, mixer M-925, Fraction collector Frac-900, column XK16/60, column material Superdex 200 prep grade)	GE Healthcare, Freiburg
Biacore T200	GE Healthcare, Munich
Centrifuge Megafuge 1.0 R	Heraus Instruments, Hanau
Centrifuge MiniSpin	Eppendorf, Hamburg
Centrifuge Sorvall RC5Plus (rotor SS-34 and SLA-3000)	Kendro Laboratory Products, Langenselbold
Centrifuge Sorvall RC 6+ (rotor SS-34 and F9S-4x1000y)	Thermo Scientific
Centrifuge 5415R	Eppendorf, Hamburg
Crystallization robot Honeybee 961	Digilab, Marlborough
Electrophoresis Chamber Mini-PROTEAN 3 cell	BioRad, Munich
Electrophoresis Chamber B1, B1A, B2	Owl Separation System Inc., Portsmouth, USA
Electrophoresis Power Supply-EPS 200	Pharmacia Biotec, Dübendorf Switzerland
GelDoc 2000	BioRad, Munich
Heating block neoBlock II	neoLab, Heidelberg
High-purity water system Astacus	MembraPure, Bodenheim
Hybridization oven OV 2	Biometra, Göttingen
Icemaker F80C	Icematic Deutschland, Meerbusch
Incubation shaker mytron	Thermo Scientific, Dreieich
Incubation shaker KS 500	Junke & Kunkel, IKA-Werke, Staufen
Incubation shaker SM25	Edmund Bühler GmbH, Tübingen
Magnetic stirrer CAT M15	MAGV Laborbedarf, Rabenau-Londorf
Magnetic stirrer color squid	IKA Werke, Staufen
Magnetic stirrer HI 300N	Hanna instruments, Kehl am Rhein
Magnetic stirrer RCTbasic	IKA Werke, Staufen

Multichannel pipette Discovery 1-10 µL	HTL Lab Solutions, Warschau
Multichannel pipette Discovery 20-200 µL	HTL Lab Solutions, Warschau
Multichannel pipette Transferpette 2-20 µL	Brand GmbH, Wertheim
OptimaTM TLX Ultracentrifuge	Beckmann, Munich
Peltier Cryobath System TPS 1500W	Thermo Scientific
PCR cycler Mastercycler	Eppendorf, Hamburg
PCR cycler Mastercycler gradient	Eppendorf, Hamburg
Peleus ball	Deutsch & Neumann, Berlin
pH meter model Φ 350 pH/Temp/mV Meter	Beckman, Krefeld
Pipette Eppendorf Research	Eppendorf, Hamburg
Pipette Gilson Pipetman P10, P20, P100, P200, P1000	Gilson, Middleton
Pipetting robot Lissy	Zinsser Analytic, Frankfurt
Precision scale ABT 120-5 DM	Kern & Sohn, Balingen
Precision scale AJ100	Mettler-Toledo, Giessen
Precision scale SBC 22	Scaltec Instruments, Göttingen
Scale 474-32	Kern & Sohn, Balingen
Scale Bosch PE626	Bosch & Sohn, Jungingen
Shaker Heidolph Unimax 2010	MAGV GmbH
Spectrophotometer BioPhotometer	Eppendorf, Hamburg
Spectrophotometer NanoDrop ND-1000	Thermo Scientific
Spectrophotometer U-2001	Hitachi, Schwäbisch Gmünd
Stereomicroscope M165 C	Leica Mikrosysteme, Wetzlar
Tecan infinite M 200 multiplate reader	Tecan, Männedorf, Switzerland
Ultracentrifuge, Optima TLX	Beckmann, Munich
Ultrasound device (GM 2070; UW 2070; SH 706; MS 73)	Bandelin Electronic, Berlin
Ultrasound water bath Sonorex RK100	Bandelin Electronic, Berlin
UV/VIS-Spectrophotometer Evolution 300	Thermo Scientific, Dreieich
Vortex mixer MS2 Minishaker	IKA Werke, Staufen
Western Blot Trans-Blot SD Semi-dry transfer cell	BioRad, Munich
X-Ray Cassette IEE 60406	Rego X-Ray GmbH, Augsburg

2.2 Chemicals

Chemical	Company
Acetate buffer (pH 5.5 - 4.0)	GE Healthcare, Munich
Acetic acid	Roth, Karlsruhe
Acrylamide/Bisacrylamide (Rotiphorese Gel 30 (37.5:1))	Roth, Karlsruhe
Agar-Agar	Roth, Karlsruhe
Agarose (peqGold Universal Agarose)	Roth, Karlsruhe
5-Amino-2,3,-dihydro-1,4,-phthalazinedione (Luminol)	Sigma, Steinheim
6-Aminohexanoic acid	Merck, Hohenbrunn
APS (Ammonium persulfate)	Roth, Karlsruhe
ATP (adenosine triphosphate)	Boehringer, Mannheim
Bradford reagent (BioRad Protein Assay)	BioRad, Munich
Bromphenol blue	Sigma, Steinheim
BSA (bovine serum albumin)	Roth, Karlsruhe
Calcium chloride	Roth, Karlsruhe
Carbenicillin	Roth, Karlsruhe
Coomassie Brilliant Blue R250	Sigma, Steinheim
Cumaric acid	Sigma, Steinheim
Cystatin	Sigma, Steinheim
L-Cystine	Sigma, Steinheim
DMSO (dimethyl sulfoxide)	Roth, Karlsruhe
DNase I	Roth, Karlsruhe
DTNB (5,5'-dithiobis-2-nitrobenzoic acid), Ellmans reagent	Roth, Karlsruhe
DTT (dithiotreitol)	Roth, Karlsruhe
Ethanol	Roth, Karlsruhe
Glycerol	Roth, Karlsruhe
GSH (glutathione)	Sigma, Steinheim
GSSG (glutathione disulfide)	Roche, Karlsruhe
HCl (fuming, 37 %)	Roth, Karlsruhe
HEPES (2-(4-(2-hydroxyethyl)-1-piperazine)-ethanesulfonic acid)	Roth, Karlsruhe
HRP (horseradish peroxidase)	Sigma, Steinheim

Hydrogen peroxide	Roth, Karlsruhe
Imidazole	Roth, Karlsruhe
IPTG (isopropyl-β-D-1-thiogalactopyranoside)	Roth, Karlsruhe
Kanamycin sulfate	Roth, Karlsruhe
Magnesium acetate, $Mg(CH_3COO)_2$	Sigma, Steinheim
MES (2-(N-morpholino)-ethanesulfonic acid)	Roth, Karlsruhe
Methanol	Roth, Karlsruhe
L-methionine	Merck, Darmstadt
Milk powder	Roth, Karlsruhe
MPD (2-methyl-2, 4-pentanediol)	Roth, Karlsruhe
NADPH (Nicotinamid adenine dinucleotide phosphate, reduced)	Biomol GmbH, Hamburg
Ni-NTA Agarose (nickel nitrilotriacetic acid)	Invitrogen, Karlsruhe
PEG (polyethylene glycol)	Sigma, Steinheim
Pepstatin A	Sigma, Steinheim
PMSF (phenylmethanesulfonylfluoride)	Roth, Karlsruhe
Polyethylene glycol (PEG) 200, 550, 600, 1000, 3350	Sigma, Steinheim
Ponceau S	Sigma, Steinheim
Potassium chloride, KCl	Roth, Karlsruhe
Potassium dihydrogenphosphate, KH_2PO4	Roth, Karlsruhe
Di-Potassium hydrogenphosphate, K_2HPO4	Roth, Karlsruhe
Potassium hydroxide, KOH	Roth, Karlsruhe
Select Agar	Invitrogen, Karlsruhe
Sodium acetate	Roth, Karlsruhe
Sodium chloride, NaCl	Roth, Karlsruhe
Sodium citrate	Sigma, Steinheim
SDS (Sodium dodecyl sulfate)	Sigma, Steinheim
Sodium hydroxide, NaOH	Roth, Karlsruhe
Sodium selenite	Honeywell, Seelze
Surfactant P20	GE Healthcare, Munich
Talon Metal Affinity Resin	Clontech, Takara Bio Europe SAS, Saint-Germain-en-Laye, France
TEMED (N, N, N', N'-tetramethylethylenediamine)	Sigma, Steinheim
TRIS (tris-(hydroxymethyl)-aminomethane)	Roth, Karlsruhe

Triton X-100	Sigma, Steinheim
Tryptone/Peptone	Roth, Karlsruhe
TWEEN 20 (polyethyleneglycol-sorbitan-monolaurate)	Sigma, Steinheim
Yeast extract	Oxoid LTD, Basingstdoke Hampshire

2.3 Consumables

Consumables	**Company**
CNBr-activated Sepharose 4B (Amersham)	GE Healthcare, Munich
Crystallization plate, 24 well, VDX plate	Hempton Research, Jena
Crystallization plate, 96 well, MRC 2 well	Jena Bioscience, Jena
Cuvettes, polystyrol	Sarstedt, Nümbrecht
Cuvettes, micro, UV	Brand GmbH, Wertheim
Halfmicro cuvettes 10x4x45 mm, polystyrol	Sarstedt, Nümbrecht
Falkon tube 15 mL, 50 mL	Greiner Bio-One, Frickenhausen
High performance chemiluminescence film Amersham hyperfilmTMECL	GE Healthcare, Freiburg
Glas capillaries 5 µL	Brand GmbH, Wertheim
Membrane filter ME 25, 0.45 µm	Whatman GmbH, Dassel
Micro pipettes	Brand, Wertheim
Microplate 96 well, PP, V-bottom, transparent	Greiner Bio-One, Frickenhausen
Microplate 96 well, PP, half area, flat bottom, clear	Greiner Bio-One, Frickenhausen
Microplate 96 well, PS, half area, black	Greiner Bio-One, Frickenhausen
Microplate 96 well, PS, half area, white	Greiner Bio-One, Frickenhausen
Microscope lens paper	Glaswarenfabrik Karl Hecht, Sondheim
Multiply PCR tube 0.2 mL	Sarstedt, Nümbrecht
Nitrocellulose blotting membrane, 0.45 µm	GE Healthcare, Freiburg
Parafilm ’M’ laboratory film	Pechiney Plastic Packaging, Menasha USA
Pasteur pipette 150 mm	Hirschmann Laborgeräte, Eberstadt
Petri dish, 15 cm Ø	Sarstedt, Nümbrecht
Pipette tips and tubes, disposable	Eppendorf, Hamburg
Pipette tips Omnitip FastRack 10 µL, 200 µL	Ulplast, Warschau
Plastic Vials	GE Healthcare, Munich

Protein ladder unstained protein MW marker	Fermentas, St. Leon-Rot
Protein ladder 6xHis	Qiagen, Hilden
PVDF membrane	Roth, Karlsruhe
Rubber Caps	GE Healthcare, Munich
Series S Sensor Chip CM5	GE Healthcare, Munich
Silicone oil 550	Merck, Darmstadt
Sterile filters 0.2 µm FP030	Schleicher & Schüll, Kassel
Syringe 1 mL Plastipak	Becton Dickson, Madrid
Syringe 10 mL	B. Braun, Melsungen
24 Bottom Wells 1.7x1.6 cm MP	Biochemicals Inc., U.S.A
Vivaspin 20, 3,000 MWCO, 10,000 MWCO and 30,000 MWCO	Sartorius Stedim Biotech, Göttingen
X-ray film Processore, Optimax	Protec, Oberstenfeld
Zeba^{TM} Desalt Spin Columns	Thermo Scientific, Rockford, USA

2.4 Kits

Kit	**Company**
Biacore ^{TM} Maintenance Kit Type 2	GE Healthcare, Munich
Bradford Assay Kit	Bio-Rad, Munich
QIAprep Spin Miniprep Kit	Qiagen, Hilden
QIAquick PCR Purification Kit	Qiagen, Hilden
Pierce Silver Staining Kit	Thermo Scientific, Rockford, USA

2.5 Enzymes

2.5.1 Restriction enzymes

Enzyme	**Company**	**Restriction site**
DpnI	Thermo Scientific	5´...GA^{-CH3}^TC...3´
EcoRI	Thermo Scientific	5´...G^AATTC...3´

2.5.2 Enzymes for molecular biology

Enzyme	Company
Pfu DNA Polymerase	Promega, Mannheim
RedTaq® Polymerase	Sigma, Steinheim
T4 Ligase	Fermentas, St. Leon-Rot

2.5.3 Recombinant enzymes

Enzyme	
*Pf*Prx1a	*Pf*Prx1m
*Pf*Prx1a^{C50S}	*Pf*Prx1m^{C67S}
*Pf*Prx1a^{C170S}	*Pf*Prx1m^{C187S}
*Pf*Prx1a^{C74A}	*Pf*Prx1m$^{C67S/C187S}$
*Pf*Prx1a$^{C50S/C170S}$	*Pf*Prx6
*Pf*Prx1a$^{C50S/C74A/C170S}$	*Pf*Prx6^{C47S}
*Pf*Prx1a$^{C50S/C74A}$	hTGR
*Pf*Prx1a$^{C74A/C170S}$	hTGR^{U642C}
*Pf*Prx5	hTGR$^{1-150}$
*Pf*Prx5^{C117S}	hTGR$^{151-643}$
*Pf*Prx5^{C143S}	hTGR^{H78A}
*Pf*Prx5$^{C117S/C143S}$	hTGR^{C133S}
Truncated *Pf*PrxQ$^{1-164}$	hTGR^{D134A}
Truncated *Pf*PrxQ$^{1-164/C56S}$	hTGR$^{C133S/D134A}$
Truncated *Pf*PrxQ$^{1-164/C103S}$	hGR
Truncated *Pf*PrxQ$^{1-164/C56S/C103S}$	hTrxR^{U498S}

2.6 Antibodies

Antibody	Company
Mouse anti-His-tag IgG	Jackson Immuno Research, West Grove
Rabbit anti-mouse IgG HRP	Dianova, Hamburg
Mouse anti-glutathione IgG	Virogen, Watertown
Rabbit anti-*Pf*Trx1 IgG	Bioscience, Heidelberg
Rabbit anti-*Pf*Prx1a IgG	Bioscience, Heidelberg
Goat anti-rabbit IgG HRP	Dianova, Hamburg

2.7 *E. coli* cells

Strain	Genotype
XL-1 blue	F'::Tn10 proA^{+}B^{+} lacI^{q} Δ(lacZ)M15/recA1 endA1 gyrA96 (Nal^{R}) thi hdgR17 (rK^{-} mK^{+}) glnV44 relA1 lac
BL21 (DE3)	*E. coli* B F^{-} dcm *omp* T *hsd*S(r$_{B}^{-}$ m$_{B}^{-}$) gal λ(DE3)
Single Step (KRX) Competent Cells	[F', traD36, Δ*omp*P, proA^{+}B^{+}, lacI^{q}, Δ(lacZ)M15] Δ*omp*T, endA1, recA1, gyrA96(Nal(r)), thi^{-}1, *hsd*R17 (r(k)$^{-}$, m(k)$^{+}$), e14^{-} (McrA^{-}), relA1, supE44, Δ(lac- proAB), Δ(rhaBAD)::T7 RNA polymerase
M15	nalS, StrS, rifS, KmR, lac^{-}, ara^{-}, gal^{-}, mtl^{-}, F^{-}, recA^{+}, uvr^{+}

2.8 Cloning and expression vectors

Vector	Properties
pET28a^{+}	Kanamycin resistance, T7 promotor, His$_{6}$-tag coding sequence, T7 tag coding sequence, lac I coding sequence, T7 terminator
pQE30	Carbenicillin resistance, T5 promotor, His-tag coding sequence, lac operator
pSelABC	Chloramphenicol resistance, *selAB*, *selC* coding sequence (kindly provided by E. Arnér, Karolinska Institute, Stockholm)

2.9 Solutions and buffers

2.9.1 Buffer for Ni-NTA-affinity chromatography

Buffer	Composition
Elution buffer *Pf*Prx1a	50 mM Na_2HPO_4, 300 mM NaCl, pH 8.0
	20, 75, 200 and 500 mM imidazole
	0.5 mM DTT
Elution buffer *Pf*Prx1m	50 mM Na_2HPO_4, 300 mM NaCl, pH 8.0
	20, 50, 100, 200 and 500 mM imidazole
Elution buffer *Pf*Prx5	50 mM Na_2HPO_4, 300 mM NaCl, pH 8.0
	30, 100 and 500 mM imidazole
Elution buffer *Pf*Prx6	50 mM Tris, 300 mM NaCl, pH 8.0
	with 30, 50, 100 ad 500 mM imidazole
	0.5 mM DTT
Elution buffer *Pf*PrxQ$^{1\text{-}164}$	50 mM Na_2HPO_4, 300 mM NaCl, pH 8.0
	10, 30, 50 and 200 mM imidazole

Elution buffer hTGR	50 mM Na_2HPO_4, 300 mM NaCl, pH 7.2
	20, 30, 200 and 500 mM imidazole
Elution roGFP2-Orp	50 mM Na_2HPO_4, 300 mM NaCl, pH 8.0
	10, 50, 200 and 500 mM imidazole
Ultrasonication (US) buffer	50 mM Na_2HPO_4, 300 mM NaCl, pH 8.0

2.9.2 Buffers for electrophoresis

Buffer	**Composition**
Stacking gel buffer	0.5 M Tris, pH 6.8
Separating gel buffer	1.5 M Tris, pH 8.8
SDS chamber buffer	192 mM glycine, 25 mM Tris-HCl, pH 8.3
	0.1% (w/v) SDS
SDS sample buffer 1x	62.5 mM Tris-HCl pH 6.8, 25% glycerin
	20 mL 10% (w/v) SDS
	2 mL 0.5% (w/v) bromophenol blue, 50 mM DTT, 40.5 mL H_2O
	storage at room temperature
	before usage 5% (v/v) 2-ME were added
SDS sample buffer 4x	3 mL stacking gel buffer, 300 mg DTT
	400 mg SDS, 2 mL glycerin
	tip of a spatula bromophenol blue
Coomassie staining solution	160 mg Coomassie Brilliant Blue R 250 ad 1 L ddH_2O, 2 h stirring, add 3 mL concentrated HCl

2.9.3 Buffers for semi-dry Western blot

Buffer	**Composition**
Anode buffer I	300 mM Tris
Anode buffer II	25 mM Tris
Cathode buffer	40 mM 6-Aminohexanoic acid
TBS	10 mM Tris
	55 mM NaCl, pH 7.4
TBST	10 mM Tris
	55 mM NaCl
	0.05% (v/v) TWEEN 20, pH 7.4

Ponceau S staining	1% (w/v) ponceau S
	5% (v/v) acetic acid
Ponceau S destaining	1% (v/v) acetic acid
Luminol	1.25 mM luminol
	0.0093% (v/v) H_2O_2
	0.1 M Tris-HCl, pH 8.6
ECL-reagent	1 mL luminol, 10 µL cumaric acid

2.9.4 Gels for electrophoresis

Gel	**Composition**
15 % separating gel (4 gels)	3.6 mL ddH_2O
	3.75 mL separating gel buffer
	7.5 mL acrylamide/bisacrylamid (30% (v/v))
	0.15 mL SDS (10% (w/v))
	75 µL APS (10% (w/v))
	7.5 µL TEMED
12 % separating gel (4 gels)	5.1 mL ddH_2O
	3.75 mL separating gel buffer
	6 mL acrylamide/bisacrylamid (30% (v/v))
	0.15 mL SDS (10% (w/v))
	75 µL APS (10% (w/v))
	7.5 µL TEMED
4 % stacking gel (4 gels)	3.05 mL ddH_2O
	1.25 mL stacking gel buffer
	0.65 mL acrylamide/bisacrylamid (30% (v/v))
	0.05 mL SDS (10% (w/v))
	25 µL APS (10% (w/v))
	5 µL TEMED

2.9.5 Assay buffers and solutions

Assay solution	**Composition**
DTNB Assay	
Assay buffer	47.4 mM KH_2PO_4, 52.6 mM K_2HPO_4, pH 7.4

NADPH	4 mM in assay buffer
DTNB	100 mM in DMSO
Thioredoxin Reductase Assay	
Assay buffer	47.4 mM KH_2PO_4, 52.6 mM K_2HPO_4, pH 7.4
NADPH	4 mM in in assay buffer
$hTrx^{C72S}$	1.57 mM in assay buffer
Glutathione Reductase Assay	
Assay buffer	20.5 mM KH_2PO_4, 26.5 mM K_2HPO_4, 1 mM EDTA, 200 mM KCl, pH 6.9
NADPH	4 mM in assay buffer
GSSG	100 mM in assay buffer
HEDS/Grx Activity Assay	
Assay buffer	100 mM Tris, 1 mM EDTA, pH 8.0
NADPH	4 mM in assay buffer
GSH	100 mM in assay buffer
HEDS	7.5 mM in assay buffer
HRP Competition Assay	
10 x BPCD	100 mM Na_2HPO_4, 100 mM $C_6H_5Na_3O_7$, 100 mM BH_3O_3, 1 mM EDTA, 1 M NaCl
	Dilute to 2x BPCD and adjust to pH 2.5-10
HRP	5 mM in US buffer
DTT	1 M in US buffer
H_2O_2	45 µM in US buffer
Pull-down Assay	
Suspension buffer	1 mM HCl
Lysis, wash and elution buffer	100 mM Tris, 500 mM NaCl, pH 8.0
	For elution ad 10 mM DTT, freshly
Coupling buffer	100 mM $NaHCO_3$, 500 mM NaCl, 0.5 mM DTT, pH 8.3
Blocking buffer	100 mM Tris-HCl, 0.5 mM DTT, pH 8.0

pH shift buffer I	100 mM $C_2H_3NaO_2$, 500 mM NaCl, 0.5 mM DTT, pH 4.0
pH shift buffer II	100 mM Tris-HCl, 500 mM NaCl, 0.5 mM DTT, pH 8.0 DTT was freshly added prior to each experiment
Interaction Analysis (SPR)	
HBS-EP$^+$ buffer (10x)	0.1 M Hepes, 1.5 M NaCl, 30 mM EDTA, 0.5% Surfactant P20 (v/v), pH 8.0

2.9.6 Stock solutions

Stock solution	**Composition**
APS	10% (w/v) in ddH_2O, storage at -20 °C
Carbenicillin	50 mg/mL in 50% (v/v) EtOH, storage at -20 °C
Chloramphenicol	35 mg/mL, 100% EtOH, storage at -20 °C
Cystatin	40 µM in US buffer, storage at -20 °C
DTT	200 mM in ddH_2O, storage at -20 °C
HRP (Horseradish peroxidase)	5 mM in PO_4-buffer
IPTG	1 M in ddH_2O, sterile filtration 0.2 µm, storage at -20 °C
Kanamycin	25 mg/mL in ddH_2O, sterile filtration 0.2 µm, storage at -20 °C
Pepstatin	0.3 mg/mL in US buffer, storage at -20 °C
Ponceau S	2% ponceau S (v/v), 3% TCA (v/v)
PMSF	100 mM in DMSO, storage at 23 °C
Sodium selenite	50 mM in ddH_2O

2.10 Media for bacterial culture

After preparing, the medium suspension will be autoclaved for 30 min at 120 °C and stored at 4 °C. Adding the respective antibiotic took place directly before inoculation.

Medium	**Composition**
Lysogeny broth (LB)	10 g/L tryptone, 5 g/L yeast extract, 10 g/L NaCl
Terrific broth (TB)	12 g/L tryptone, 24 g/L yeast extract, 9.4 g/L KH_2PO_4, 2.2 g/L K_2HPO_4, 4 mL/L glycerin, pH 7.0
2xYT (Yeast Extract Tryptone)	5 g/L NaCl, 16 g/L tryptone, 10 g/L yeast extract
modified LB (Bar-Noy)	12 g/L tryptone, 24 g/L yeast extract, 5 g/L NaCl, 5 g/L K_2HPO_4, 0.142 g/L Na_2SO_4, 40 mL/L glycerol

2.11 Protein crystallization screens

Crystallization screens	**Source**
$(NH_4)_2SO_4$	Becker lab
JBScreen Classic HTS I	Jena Bioscience, Jena
JBScreen Classic HTS II	Jena Bioscience, Jena
JCSG Core Suite I	Qiagen, Hilden
JCSG Core Suite II	Qiagen, Hilden
JCSG Core Suite III	Qiagen, Hilden
JCSG Core Suite IV	Qiagen, Hilden
MPD	Becker lab
PEG part I	Becker lab
PEG part II	Becker lab
Isopropanol Screen	Becker lab

2.12 Oligonucleotides

Primers for cloning	**Sequence (5'-3')**
OhTGRN	GCGGATCCCTGGAGCGGTCGCCGCCGCAGT
OhTGR-GrxN	GCGGATCCGAAGATTTGGCATATGATTATGATCTC

Primers for generating the SECIS-element (in lower case, with stop codon in italics and the Sec codon boxed)	
OhTGRselR1	gcagacctgcaaccgatgg*CTA*GCCTCAGCAGCCTTTCTGAGTGATG
OhTGRselR2	CGAAGCTTctagctagcgattggtgcagacctgcaaccgatgg*CTA*GCC
Primers for site-directed mutagenesis	
OhTGR^{C133S}s	AAGTGCATGTAGGTGGATCTGACCAAACTTTCCAGGCA
OhTGR^{C133S}as	TGCCTGGAAAGTTTGGTCAGATCCACCTACATGCACTT
OhTGR^{D134A}s	GCATGTAGGTGGATGTGCCCAAACTTTCCAGGCA
OhTGR^{D134A}as	TGCCTGGAAAGTTTGGGCACATCCACCTACATGC
OhTGR^{H78A}s	CAAGAGCTACTGTCCCGCTAGTACTCGGGTGAAA
OhTGR^{H78A}as	TTTCACCCGAGTACTAGCGGGACAGTAGCTCTTG
OhTGR^{C133SD134A}s	AAGTGCATGTAGGTGGATCTGCCCAAACTTTCCAGGCA
OhTGR^{C133SD134A}as	TGCCTGGAAAGTTTGGGCAGATCCACCTACATGCACTT
*Pf*Prx1a^{C50S}s	TTTTACGTTTGTATCTCCATCTGAAATC
*Pf*Prx1a^{C50S}as	GATTTCAGATGGAGATACAAACGTAAAA
*Pf*Prx1a^{C170S}s	AACATGGAGATGTTTCCCCAGCAAAC
*Pf*Prx1a^{C170S}as	GTTTGCTGGGGAAACATCTCCATGTT
*Pf*Prx1m^{C67S}s	CTATACCTTTGTCTCTCCAACCGAAAT
*Pf*Prx1m^{C67S}as	ATTTCGGTTGGAGAGACAAAGGTATAG
*Pf*Prx1m^{C187S}s	TCTGGTGAAGTTTCTCCGATCAATTG
*Pf*Prx1m^{C187S}as	CAATTGATCGGAGAAACTTCACCAGA
*Pf*Prx5^{C117S}s	ATTTACGCCTACTTCCAGTACAAAAATG
*Pf*Prx5^{C117S}as	CATTTTTGTACTGGAAGTAGGCGTAAAT
*Pf*Prx5^{C143S}s	GATGACATTTATTCTATTACTAATAATG
*Pf*Prx5^{C143S}as	CTACTGTAAATAAGATAATGTTATTAC
*Pf*Prx6^{C47S}s	ATTTTACTCCCGTTTCTACCACTGAAC
*Pf*Prx6^{C47S}as	GTTCAGTGGTAGAAACGGGAGTAAAAT
Truncated *Pf*PrxQ$^{1\text{-}164/C56S}$s	CAAACACTCCTGGTTCCACAAAACAAG
Truncated *Pf*PrxQ$^{1\text{-}164/C56S}$as	CTTGTTTTGTGGAACCAGGAGTGTTTG
Truncated *Pf*PrxQ$^{1\text{-}164/C103S}$s	GTATGAATTGCTGTCTGATGTTGATAAG
Truncated *Pf*PrxQ$^{1\text{-}164/C103S}$as	CTTATCAACATCAGACAGCAATTCATAC

3 METHODS

3.1 Molecular biological methods

3.1.1 Plasmid preparation

To purify plasmid DNA from *E. coli* cells the QIAprep Spin Miniprep Kit (Qiagen, Promega) was used following the manufacturer's protocol. In brief, the pellet of 1-3 mL overnight culture containing the favored plasmid was lysed, neutralized, and centrifuged. The plasmid DNA comprising supernatant was than purified over a silica membrane column.

3.1.2 Determination of DNA concentration

DNA concentration was determined spectrophotometrically at 260 nm in UV cuvettes using a biospectrophotometer (Eppendorf) (1 OD_{260nm} unit = 50 µg/mL). The degree of purity was delineated by the ratio of absorbance at 260 nm to 280 nm (for DNA a ratio of ~ 1.8 is generally accepted as "pure") calculated by the following formula:

$$\text{DNA purity } (A_{260}/A_{280}) = A_{260}\text{ reading} \div A_{280}\text{ reading}$$

3.1.3 Site-directed mutagenesis for *Pf*Prxs

Selected cysteines of the *Pf*Prxs were mutated with site-directed mutagenesis via PCR. Respective *Pf*Prxs, each in pQE30, were used as gene templates, and oligonucleotide primers containing the respective mutated codons (Chapter 2.12) were used to insert the mutation using Pfu polymerase.

Reaction mix	
Template DNA	0.5 µL (~100 ng/µL)
Forward primer (100 pmol/µL)	1 µL
Reverse primer (100 pmol/µL)	1 µL
dNTP mix	1 µL (10 mM)
10x Pfu buffer	5 µL
Pfu polymerase (3 U/µL)	1 µL
DMSO	2.5 µL
Sterile H_2O	38 µL
PCR program	
Denaturation	90 sec 94 °C
Cycles	24
Denaturation	30 sec 94 °C
Annealing	60 sec 58 °C
Elongation	14 min 68 °C
Final elongation	13 min 68 °C

The PCR reaction products were purified with the QIAquick® PCR purification kit following the manufacturer's protocols. In a second step, a DpnI-digestion of the template was performed

for 1 h at 37°C (for details please see below), and purified again. In doing so, the methylated template could be eliminated.

Component	
Nuclease-free water	16 µL
10x Buffer Tango	2 µL
DNA (0.5-1 µg/µL)	1 µL
DpnI	1 µL

Mutated samples were sequenced at an in-house sequencing facility [160]. By reference to the chromatograms and with the help of the program FinchTV, the constructed mutations could be controlled.

3.1.4 Site-directed mutagenesis for hTGR

The coding sequence for hTGR (UniProtKB Q86VQ6) was amplified via PCR by using human cDNA (lung tissue, AG Becker) as a template. By changing the TGA-Sec-codon to a TGC-Cys-codon within the reverse primer, Sec was mutated to Cys. The product - 1929 bp - was cloned into the expression vector pET28a using BamHI and HindIII and verified by sequencing in an in-house sequencing facility. This N-terminally His-tagged gene was used for overexpression of $hTGR^{U642C}$ in *E. coli*.

To obtain wild type hTGR, Cys642 of the $hTGR^{U642C}$ construct was back-mutated to a Sec and the SECIS element of *E. coli* formate dehydrogenase was introduced into the sequence downstream of the stop codon via PCR by using primer elongation [161]. For this, a first PCR was conducted by using OhTGRN (or OhTGR-GrxN for the 'TrxR-part', $hTGR^{151-643}$) and OhTGRselR1 as primers. The resulting PCR product was then used as template for a second PCR with the primers OhTGRN (or OhTGR-GrxN for the 'TrxR-part', $hTGR^{151-643}$) and OhTGRselR2. The PCR products were also cloned into the expression vector pET28a using BamHI and HindIII.

To obtain the N-terminal part of hTGR representing the glutaredoxin domain, $hTGR^{1-150}$, was ordered as a synthetic gene (Eurofins MWG, Ebersberg) with codons optimized for expression in *E. coli*. By using this strategy, it was possible to overcome problems with the very high GC content in the N-terminal part of the gene. $hTGR^{1-150}$ was then cloned into the expression vector pET28a by using BamHI and HindIII.

3.1.5 Molecular cloning

To clone the desired genes into expression vectors, the vector DNA and the DNA to be cloned were digested using restriction endonucleases (Chapter 2.5.1) creating compatible ends at their cleavage sites following the manufacturer's protocols. Recombinant DNA was formed after linking the cleaved vector with the cleaved foreign DNA via ligation with the T4-DNA ligase following the manufacturer's protocols.

3.2 Microbiological methods

3.2.1 Transformation

Transformation is the process of incorporating plasmids into competent *E. coli* cells. In our approach, the method of heat shock-induced DNA uptake was utilized [162].

Cells and plasmids were thawed on ice, and approximately 100 ng of plasmid was added to 125 µL of $CaCl_2$ treated competent *E. coli* cells and incubated for 30 min on ice. During incubation, the plasmids bound to the *E. coli* cell membrane. A heat shock for 90 sec at 42 °C stressed the bacterial cells so that they took up the plasmids. Cells were allowed to rest for 1 min on ice and were incubated with 300 mL of LB medium at 37 °C for 1 h while shaking. 200 µL of cell suspension was plated out onto agar plates containing the respective antibiotics, incubated for 16 h at 37 °C, and stored at 4 °C.

3.2.2 Heterologous overexpression in *E. coli*

For heterologous overexpression of the respective gene, 3 mL of medium containing the respective antibiotic was inoculated with one colony or 3 - 5 µL glycerol stock of transformed *E. coli* at 37 °C for eight hours in a shaking incubator. This first preculture was transferred to 50 mL of rich medium containing antibiotics and was incubated over-night at 37 °C while shaking. The next day, 25 – 35 mL of the second preculture was added to 1 L of preheated rich medium with the required antibiotics up to an optical density of about 0.1 at 600 nm (OD_{600}). *E. coli* was grown to an OD_{600} of 0.6 or 2.0, depending on the optimal expression conditions of the respective gene, at 37 °C, followed by an expression induction with isopropyl-β-D-1-thiogalactopyranoside (IPTG). IPTG is an artificial inductor of the *lac* operon. IPTG binds to the *lac* repressor and by that deallocates the repressor from the *lac* operator, which enables the transcription of the recombinant genes. The induced culture was incubated for 2.5, 4, or 24 h at 37 °C or room temperature (25 °C) according to the protocol while constantly shaking.

3.2.2.1 Heterologous overexpression of *Pf*Prxs in *E. coli*

_Pf_Prx1a

*Pf*Prx1a, *Pf*Prx1a^{C50S}, *Pf*Prx1a^{C170S}, *Pf*Prx1a^{C74S}, *Pf*Prx1a$^{C50S/C170S}$, and *Pf*Prx1a$^{C50S/C74A/C170S}$ were heterologously overexpressed in competent *E. coli* M15 cells using pQE30 as a vector with an N-terminal His_6-tag. Cells were grown in LB medium containing 50 µg/mL kanamycin and 100 µg/mL carbenicillin at 37 °C (while shaking) up to an OD_{600} of 0.6. Gene expression was induced with 1 mM IPTG for 4 h at 37 °C.

_Pf_Prx1m

*Pf*Prx1m, *Pf*Prx1m^{C67S}, *Pf*Prx1m^{C187S}, and *Pf*Prx1m$^{C67S/C187S}$ were heterologously overexpressed in competent *E. coli* M15 cells using pQE30 as a vector with an N-terminal His_6-tag. Cells were multiplied in TB medium containing 50 µg/mL kanamycin and 100 µg/mL carbenicillin at 37 °C (while shaking) up to an OD_{600} of 0.6. Gene expression was induced by 0.5 mM IPTG for 24 h at RT.

_Pf_Prx5

*Pf*Prx5, *Pf*Prx5^{C117S}, *Pf*Prx5^{C143S}, and *Pf*Prx5$^{C117S/C143C}$ were heterologously overexpressed in competent *E. coli* M15 cells using pQE30 as vector with an N-terminal His_6-tag. Cells were

grown in LB medium containing 50 µg/mL kanamycin and 100 µg/mL carbenicillin at 37 °C (while shaking) up to an OD_{600} of 0.6. Gene expression was induced by 1 mM IPTG for 4 h at 37 °C.

***Pf*Prx6**

*Pf*Prx6 and *Pf*Prx6^{C47S} were heterologously overexpressed in competent *E. coli* BL21 cells using pET28a$^+$ as a vector with an N-terminal His_6-tag. Cells were grown in LB medium containing 50 µg/mL kanamycin at 37 °C (while shaking) up to an OD_{600} of 0.6. Gene expression was induced by 1 mM IPTG for 4 h at 37 °C.

***Pf*PrxQ$^{1\text{-}164}$**

Truncated constructs of *Pf*PrxQ$^{1\text{-}164}$, *Pf*PrxQ$^{1\text{-}164/C56S}$, *Pf*PrxQ$^{1\text{-}164/C103S}$, and *Pf*PrxQ$^{1\text{-}164/C56S/C103S}$ were heterologously overexpressed in competent *E. coli* M15 cells using pQE30 as a vector with an N-terminal His_6-tag. Cells were grown in LB medium containing 50 µg/mL kanamycin and 100 µg/mL carbenicillin at 37 °C (while shaking) up to an OD_{600} of 0.6. Gene expression was induced by 1 mM IPTG for 2.5 h at 37 °C.

3.2.2.2 Heterologous overexpression of hTGR and mutants in *E. coli*

Recombinant hTGR and hTGR$^{151\text{-}643}$, hTGR^{H78A}, hTGR^{C133S}, hTGR^{D134A}, and hTGR$^{C133S/D134A}$ all in pET28a$^+$ (N-terminal His_6-tag) were cotransformed with pSU SelABC into *E. coli* BL21 (DE3) cells. Cells were grown in lysogeny broth (LB) medium, according to Bar-Noy with slight modifications. The medium contained 0.142 g Na_2SO_4 per liter of medium supplemented with kanamycin (50 µg/mL) and chloramphenicol (17.5 µg/mL), 0.1 g cystine and 0.37 g methionine at 37 °C. After reaching an OD_{600} of 2.0, the temperature was shifted to 21 °C for 1 h. Expression was induced with 0.4 mM isopropyl-D-thiogalactopyranoside (IPTG), 5 µM sodium selenite, as well as riboflavin, nicotinic acid, and pyridoxine (20 mg/L each) for 24 h [163].

E. coli BL21 (DE3) cells were transformed with pET28a$^+$ coding for hTGR^{U642C}. Expression of the cysteine mutant was performed in LB medium in accordance with Bar-Noy and contained kanamycin (50 µg/mL), 0.1 g cystine, and 0.37 g methionine at 37 °C to an OD_{600} of 2.0. Induction was initialized by 0.4 mM IPTG, riboflavin, nicotinic acid, and pyridoxine (all 20 mg/L) and was conducted for 24 h.

hTGR$^{1\text{-}150}$ was heterologously overexpressed in competent *E. coli* BL21 cells using pET28a$^+$ as a vector. Cells were grown in LB medium that contained 50 µg/mL kanamycin at 37 °C while shaking up to an OD_{600} of 0.6. Gene expression was induced by 1 mM IPTG for 24 h at RT.

3.2.3 Cell harvest

Cells were harvested via centrifugation in an SLA rotor at 8,000 rpm and 4 °C for 15 min, and cell pellets were resuspended in the respective buffer containing protease inhibitors (100 µM PMSF, 150 nM pepstatin, and 40 nM cystatin) and stored at -20 °C.

3.3 Protein biochemical methods

3.3.1 Cell disruption

For cell disruption, the suspension was thawed, and 16 mg of lysozyme and an aliquot of DNase I were added to one liter of *E. coli* culture pellets. The lysis was done on ice on a magnetic stirrer. While stirring, the lysozyme, out of egg albumen, cleaved the β-1.4-glycosidic bond between *N*-acetylmuramic acid and *N*-acetyl-D-glucosamine residues in the sugar chains of the peptidoglycan scaffold from the bacteria cell wall. DNase I is an endonuclease that cleaves phosphodiester bonds in the bacterial DNA. Chemical lysis of the cell suspension was followed by mechanical lysis with an ultrasonic treatment. Here the lysate was further cleaved via ultrasonication for 3 x 30 sec at 70% of maximum power. Subsequently, the suspension was centrifuged for 30 min at 4 °C and 18,000 rpm in an SS34 rotor to extract the proteins in the supernatant. This supernatant should contain the overexpressed protein next to the cytosolic proteins of *E. coli.*

3.3.2 Purification with Ni-NTA affinity chromatography

The purification of cell lysate took place under native conditions via immobilized metal ion affinity chromatography (IMAC) [164] using a nickel-nitrilotriacetic acid (Ni-NTA) resin. In this technique, the histidine rich side chain of proteins reversibly binds to the immobilized metal ion (nickel), which is bound to a Sepharose agarose. The crude extract of the *E. coli* culture was applied to the resin material, which had previously been equilibrated with buffer, and was run through the matrix with a speed of one drop per six sec. In doing so, the hexahistidyl-tag (His_6-tag), which was attached to the recombinant protein, bound reversibly to the column. Afterwards the loaded resin was washed with buffer to remove unspecifically bond proteins. After washing, the remaining bound proteins were eluted with an increasing gradient of imidazole. Imidazole holds a very similar structure to histidine and is capable of replacing and liberating the bonded histidine-containing proteins. At low concentrations of imidazole, proteins with an unspecific or weak bonding were replaced. The fractions of eluates were collected in Eppendorf cups and stored at 4 °C.

3.3.2.1 Purification of *Pf*Prxs

The His_6-tagged proteins were purified via affinity chromatography using different column materials, additives, and buffers (Table 1).

Table 1: General purification procedure for different Prxs.

Protein	***Lysis***	***Column material***	***Volume of column material for 1 L cell culture***	***Additive***	***Buffer***
*Pf*Prx1a	45 min	Ni-NTA	1 mL	0.5 mM DTT	US buffer
*Pf*Prx1m	30 min	Ni-NTA	1 mL	-	US buffer
*Pf*Prx5	30 min	Ni-NTA	3 mL	-	US buffer

*Pf*Prx6	30 min	Ni-NTA	4 mL	0.5 mM DTT	Tris buffer
*Pf*PrxQ$^{1-164}$	30 min	Talon	4 mL	-	US buffer

The respective proteins were eluted using an imidazole gradient (please see Chapter 2.9.1). Eluted samples were checked for purity using a sodium dodecyl sulfate polyacrylamide gel electrophoresis (SDS-PAGE). Protein samples with high purity were pooled using vivaspins 20 with a molecular weight cut-off (MWCO) of 10,000 Da and stored on ice or at -20 °C in 20% glycerol depending on the intended use.

3.3.2.2 Purification of hTGR

For hTGR, hTGR^{U642C}, and hTGR$^{151-643}$, the supernatant was brought to 20 mM imidazole, and all proteins were purified utilizing a nickel affinity column. Purified recombinant protein was eluted in 200 and 500 mM imidazole. Eluted samples were checked for purity using an SDS-PAGE. Protein samples with high purity were pooled using vivaspins 20 with a MWCO of 30,000 Da and stored on ice.

3.3.3 SDS polyacrylamide gel electrophoresis

The purified protein was separated by its molecular weight in an electric field via sodium dodecyl sulfate polyacrylamide gel electrophoresis (SDS-PAGE) according to Laemmli [165]. SDS denatures and covers the given charge of the protein, resulting in an overall negatively charged protein. This charge is proportional to the molecular mass of the protein. The negatively charged proteins are then able to migrate through an electric field towards the anode fractionated by their size. To denature the protein and break present disulfide bonds, SDS buffer containing 50 mM DTT was added to the protein samples and heated for 5 min at 95 °C. The covered proteins were loaded on an SDS gel and were able to migrate through the gel at a constant voltage of 200 V. Subsequently, gels were washed with ddH_2O for 2 x 10 min after short boiling (40 sec) in a microwave. Staining was conducted with Coomassie Brilliant Blue G-250 for 15 min after short boiling, followed by washing with ddH_2O for 2 x 10 min.

3.3.4 Size exclusion chromatography

An additional purification step of all proteins that are the subject matter of this thesis was not necessary since the given purity after the respective affinity chromatography was very high (>95%). Size exclusion chromatography (via fast protein liquid chromatography, FPLC) was used to determine the molecular mass of oligomeric forms of the recombinant protein under different conditions. Native gel filtration was conducted using a HiLoad^{TM}16/60 Superdex^{TM} 200 prep grade column connected to an ÄKTA/Unicorn FPLC system (GE Healthcare). A final volume of 0.8 mL of purified and concentrated recombinant protein was loaded onto the gel filtration column (previously equilibrated with 1.5 column volumes of the respective buffer of interest). Proteins were eluted at a flow rate of 1 mL/min with an eluate fraction size of 2 mL and a column pressure limit of 0.3 MPa and were detected spectrophotometrically at 280 nm. With this technique, proteins are separated according to their molecular mass, with smaller molecules migrating more slowly than larger molecules. The respective molecular mass of the

eluted proteins was determined by comparison with protein standards of low and high molecular mass (GE healthcare).

3.3.5 Determination of protein concentration

Protein concentration was determined via the Bradford assay [166], using BSA for the standard curve, and by measuring the absorption of protein solutions (in 6 M guanidine hydrochloride, 20 mM potassium phosphate, pH 6.5) at 280 nm taking into account their specific extinction coefficients (see Chapter 3.4) with the following formula:

$$[\text{Protein}] \text{ in mM} = \frac{A_{280}}{\varepsilon \left(\text{cm}^{-1}\text{mM}^{-1}\right) * \text{d (cm)}}$$

ε = molar extinction coefficient at λ of 280 nm
d = distance moved by the light in a cuvette (= 1 cm)

3.3.6 Western blot

Semi-dry western blot analysis was used for protein identification [167] for His_6-tagged proteins or *S*-glutathionylated proteins. After protein separation via SDS-PAGE, the proteins were electrophoretically transferred to a polyvinylidene difluoride (PVDF) membrane. For this, the stacking gel was removed from the SDS gel and soaked in cathode buffer together with five filter papers. Two filter papers and the preactivated PVDF membrane (with 100% methanol) were soaked in anode buffer II, and three filter papers were soaked in anode buffer I. After 15 min of equilibration in the respective buffers, the blot sandwich was built up air bubble-free into the transfer cassette. Starting from the anode, three filter papers from the anode buffer I were followed by two filter papers from the anode buffer II, the PVDF membrane, the SDS gel, and finally five filter papers from the cathode buffer. The separated proteins from the SDS gel were blotted onto the PVDF membrane at 13 V for 30 min.

Upon completion of the transfer, the PVDF membrane was rocked in Ponceau S for 30 sec and was washed with 1% acetic acid to visualize transferred proteins (blot control). After washing the membrane with TBST for five minutes, the free surface of the blot was blocked with 5% non-fat milk in TBST for 1 h at room temperature or overnight at 4 °C. The PVDF membrane was then washed 3 times with TBST for 5 min and incubated with the first antibody for 1 h at room temperature. After incubation, the membrane was washed again 3 times with TBST followed by an incubation with the secondary antibody for 1 h at room temperature. Afterwards, the membrane was washed 3 times with TBST followed by chemiluminescent detection. For this, the membrane was incubated with the enhanced chemiluminescence (ECL)-reagent for 1 min at room temperature. During incubation the horseradish peroxidase (HRP)-tagged secondary antibody oxidized the ECL reagent containing luminol, whose oxidized form releases a chemiluminescence, which was detected with an X-ray film.

3.3.6.1 Western blot analysis for hTGR

Samples were loaded onto an SDS-PAGE gel and the separated proteins were transferred to a PVDF membrane. The membrane was blocked overnight with 5% dry milk in Tris-buffered saline (TBS, 10 mM Tris, 0.9% NaCl, pH 7.4) containing 0.05% Tween 20 (TBST). After washing the membrane with TBST the primary antibody (mouse anti-his-tag IgG) (1:1,000 in

3% BSA) was added and incubated for 1 h at RT. The membrane was washed again with TBST, followed by an incubation with the secondary antibody (rabbit anti-mouse IgG HRP) (1:20,000 in 5% milk) for 1 h and subsequent development with the ECL system containing luminol, whose oxidized form release a chemiluminescence which was detected by an X-ray film.

3.3.7 Protein-protein interaction analysis

3.3.7.1 Pull-down assay

To identify interacting partners that are addressed for H_2O_2 signal transduction and reduction with plasmodial peroxiredoxins *in vitro*, a pull-down assay where covalent disulfide-bonded reaction intermediates can be visualized was developed. For this purpose, the respective protein was immobilized on CNBr-activated Sepharose 4B beads via amine coupling and then was incubated with parasite lysate from *Plasmodium falciparum* 3D7 containing all soluble proteins and putative interaction partners (Figure 15). All experiments were conducted in triplicate. The eluted samples containing the interacting partners were visualized via silver staining after gel electrophoresis and analyzed via mass spectrometry by Claire Delahunty, Ph.D. (The Scripps Research Institute, laboratory of Professor John R. Yates III, Ph.D., La Jolla, California).

CNBr-activated Sepharose 4B beads are supplied lyophilized in the presence of additives, which had to be washed away with a low pH buffer (pH 3) before protein coupling. Additionally, the low pH preserves the activity of the reactive CNBr groups (cyanate esters). These reactive groups are able to react with primary amines to couple proteins onto the agarose matrix, building isourea derivatives immobilized at the Sepharose beads. Saturated groups were not blocked with buffer containing the small primary amine Tris. To remove ligands that were bound ionically to the immobilized protein, the matrix was washed with low and high pH buffers containing 500 mM NaCl.

Ligand coupling

5.7 mg of lyophilized CNBr-activated Sepharose 4B beads were suspended in 20 µL of 1 mM HCl. The swollen material was washed for 10 min with 800 µL 1 mM HCl followed by centrifugation for 90 sec at 13,400 rpm in a MiniSpin centrifuge. The supernatant was discarded, and the beads were washed again for 5 min with 400 µL of 1 mM HCl. After centrifugation for 90 sec at 13,400 rpm, the supernatant was discarded again. For ligand coupling, the respective protein was dialyzed 3 times for 30 min in coupling buffer (see Chapter 2.9.5). 2 mg of reduced protein in coupling buffer were blended with washed beads and slightly swiveled for 1 h at 4 °C using a hybridization oven (OV 2, Biometra). The mixture was centrifuged again for 90 sec at 13,400 rpm, and the supernatant was discarded. The excess of ligand, which had not been bound to the Sepharose beads, was washed away by 3 cycles of inverting the material with 200 µL of coupling buffer and 90 sec of centrifugation at 13,400 rpm. Unsaturated groups were blocked with 200 µL of blocking buffer (see Chapter 2.9.5) for 2 h, at RT. After blocking, the medium was washed with 3 cycles of 200 µL of pH shift buffer I, alternating with 200 µL of pH shift buffer II (see Chapter 2.9.5). After each step of the pH seesaw, centrifugation for 90 sec at 13,400 rpm and discarding of the supernatant followed. To keep the decameric state of the recombinant peroxiredoxins, all immobilization steps were performed in the presence of 0.5 mM DTT.

Parasite lysate preparation

For parasite lysate preparation, a pellet from eight large culturing plates (45 mL) of *P. falciparum* 3D7 with 5% hematocrit, and 7% parasitemia was blended with 1.5 mL wash buffer

in an Eppendorf cup, which was additionally sealed with Parafilm. Parasite pellets were generated according to Chapter 3.5. The cup was frozen in liquid nitrogen for 2 min and thawed in lukewarm water until the suspension was liquid again. The freeze and thaw cycle was repeated 4 times in order to lyse the parasite cells. Subsequently, the medium was transferred into centrifuge tubes and centrifuged at 50,000 rpm for 30 min at 4 °C in an ultracentrifuge (Beckmann). The protein concentration of the resulting parasite lysate was determined with the Bradford assay at 595 nm.

Pull-down assay

Approximately 6 mg of parasite lysate proteins were incubated with the loaded beads at RT for 2 h while slightly swiveling. The beads were washed again with 200 µL of wash buffer in order to remove unbound parasite proteins. This washing step was repeated as long as no protein could be observed in the supernatant by determining the protein concentration at 280 nm in a UV cuvette using a biophotometer (Eppendorf). For elution of covalently bound parasite proteins, beads were incubated with 70 µL of wash buffer containing 10 mM of DTT for 30 min at RT while occasionally inverting the mixture. After incubation, the cup was centrifuged again, and the supernatant was stored at -20 °C until used for MS analysis.

Visualization

To visualize the outcome of the pull-down assay, an SDS-PAGE was conducted with aliquots of parasite lysate, different washing steps, and the eluate. 1 µL of parasite lysate was mixed with 15 µL of 1 x sample buffer, 5 µL of the first washing step was mixed with 15 µL of 1 x sample buffer, 15 µL of an intermediate and 15 µL of the last washing step were mixed with 4 x sample buffer, and 15 µL of the eluate was mixed with 4 x sample buffer. The SDS-PAGE was accomplished as described in chapter 3.3.3. Since the concentration of the proteins in the eluate fraction was very low according to expectations, silver staining was used. The staining was carried out following the manufacturer's protocol (Pierce Silver Stain Kit, Thermo Scientific).

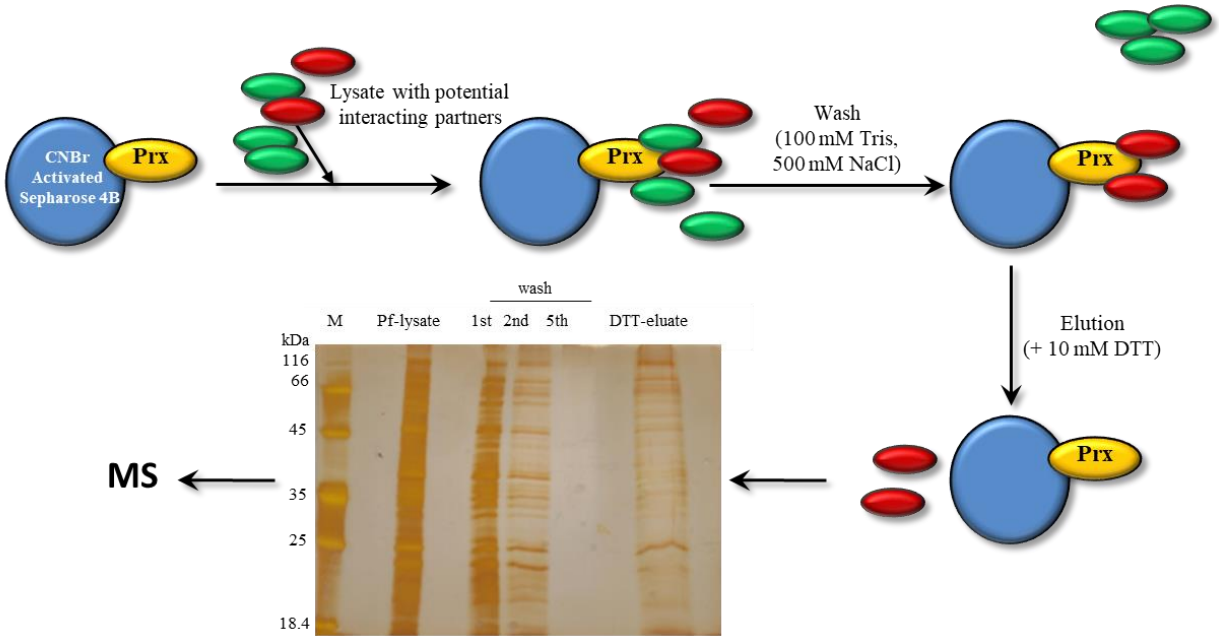

Figure 15: Scheme of pull-down assay implementation.

Sample preparation for mass spectrometry analysis

For MS analysis, the eluates were sent in a dry ice parcel to The Scripps Research Institute, La Jolla, California. Samples were then mixed with 60 µL of 200 mM Tris and 57 mg of solid urea. 30 µL of Ni-NTA agarose, which had been washed and equilibrated in 100 mM Tris, pH 8.5, was added to each sample to remove the recombinant His-tagged *Pf*Prxs. The slurry was shaken at RT for 1 hour. Samples were centrifuged at top speed for 30 minutes, and the supernatant was transferred to a new microcentrifuge tube. Supernatants were spun again for 20 minutes, and supernatants were removed and moved to a new tube. Samples were reduced with 6 µL 100 mM TCEP and alkylated with 6 µL of 250 mM IAA. 1 µg of Endo-LysC was added, and the reaction was allowed to proceed for 4 hours at 37 °C. Samples were diluted with 360 µL 100 mM Tris pH 8.5, and 2 µg of trypsin was added. Samples were shaken at 37 °C for 18 hours, quenched with 25 µL of formic acid and spun for 20 minutes.

Mass spectrometry analysis

After transfer to another tube, the supernatant was filtered through a 100 µm capillary column with a frit. Filtered supernatants were pressure loaded onto a fused silica microcapillary column containing 2.5 cm of Partisphere strong cation exchanger (Whatman) followed by 2.5 cm of 10 cm Aqua C18 (Phenomenex) packed into a 250 µm inside diameter (i.d.) capillary (Polymicro Technologies) with a 1 cm frit. The column was washed for 60 min with buffer A. After washing, a 100 µm i.d. capillary with a 5 µm pulled tip packed with 15 cm of 3 µm Aqua C18 material (Phenomenex) was attached via a union, and the entire split column was placed in line with an Agilent 1100 quaternary high performance liquid chromatography (HPLC) and analyzed using a nine-step separation. The buffer solutions used for separation were 5% acetonitrile / 0.1% formic acid (Buffer A), 80% acetonitrile / 0.1% formic acid (Buffer B), and 500 mM ammonium acetate / 5% acetonitrile / 0.1% formic acid (Buffer C). Step 1 consisted of a 90 min gradient from 0% to 100% buffer B. Steps 2–9 had the following profile: 10 min of X% buffer C, a 15 min gradient from 0% to 5% buffer B, and a 95 min gradient from 15% to 100% buffer B. The 10 min buffer C percentages (X) were 10%, 20%, 30%, 40%, 50%, 60%, 70%, and 100%, respectively, for the nine-step analysis. As peptides eluted from the microcapillary column, they were electrosprayed directly into an Orbitrap Velos mass spectrometer (ThermoFisher) with the application of a distal 2.4 kV spray voltage. A cycle of one full-scan mass spectrum (400–1,800 m/z) followed by 15 data-dependent tandem mass spectrometry spectra at a 35% normalized collision energy was repeated continuously throughout each step of the multidimensional separation. The application of mass spectrometer scan functions and HPLC solvent gradients was controlled via the XCalibur data system.

Mass spectrometry data analysis

Tandem mass spectra were analyzed with Integrated Proteomics Pipeline-IP2 (Integrated Proteomics Applications, Inc., San Diego, CA. http://www.integratedproteomics.com) using ProLuCID [168] and DTASelect2.0 [169, 170]. Spectrum raw files were extracted into MS1 and MS2 files using RawExtract 1.9.9 (http://fields.scripps.edu/downloads.php) [171], and tandem mass spectra were searched against the PlasmoDB database (release date 03/30/15). To accurately estimate peptide probabilities and false discovery rates, a decoy database containing the reversed sequences of all proteins appended to the target database [172] was used. Tandem mass spectra were matched to sequences using the ProLuCID algorithm with 50 ppm peptide mass tolerance [173] where at least 2 peptides per protein had to pass the filtering process with a minimum peptide length of 6 aa. The search space included all peptide candidates without restriction to tryptic cleavage that fell into the mass tolerance window. Modifications of +57.02146 on C owing to IAA treatment as part of the sample preparation were considered to

be a potential modification. The validity of peptide/spectrum matches was assessed according to Wang *et al.* (2015) [173] with a protein confidence of 97% as the minimum threshold and a peptide delta mass limitation of 15 ppm maximum, resulting in a peptide false discovery rate below 1.5%.

3.3.7.2 Surface plasmon resonance spectroscopy

When light is reflected off a thin metal film (e.g. gold or silver) at a defined angle, surface plasmon resonance occurs [174]. Incident light is not only reflected at a metal film, a fraction of light energy stimulates the resonant oscillation of electrons (plasmon), enhancing the evanescent field amplitude at the conducting material and leading to an electromagnetic surface wave (surface plasmon polariton, SPP), which propagates along a metal-dielectric interface (Figure 16) [175]. The SPPs are located at the boundary of the metal film and the external medium, with the result that these waves are very sensitive to alterations in this environment. SPPs reduce the reflected light intensity and therefore the refractive index at the backside of the metal film, which is determined with a two-dimensional detector array monitored as a characteristic drop in the reflected light intensity [176]. A change at the boundary can be induced by binding molecules to the conducting surface, resulting in a change of the local refractive index and leading to a detectable change in the surface plasmon resonance (SPR) angle.

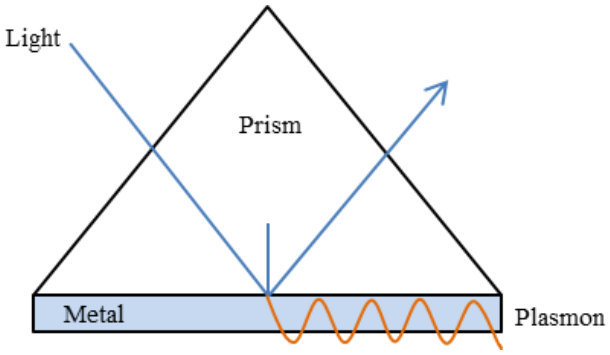

Figure 16: Simplified depiction of surface plasmon polariton formation (Kretschmann configuration).

A surface plasmon resonance (SPR) biosensor (BiacoreT200) is able to detect those angle shifts in reflected light, depending on the mass of molecules binding to the surface layer. For interaction analysis, biomolecules are bound to the gold-covered surface (ligand) and can be challenged with other biomolecules free in solution (analyte) via a microfluidic system (flow channel; FC). If binding occurs, a local increase in the refractive index is produced, inducing an SPR angle shift [177]. The change in the refractive index can be monitored in real time as a plot of resonance signal versus time measured in resonance units (RU), which correlates with a mass increase (Figure 17) [178], where the angle shift of 0.0001° is defined as 1 response unit and equals 1 pg/mm^2. This response is directly proportional to the concentration of biomolecules attaching to the surface.

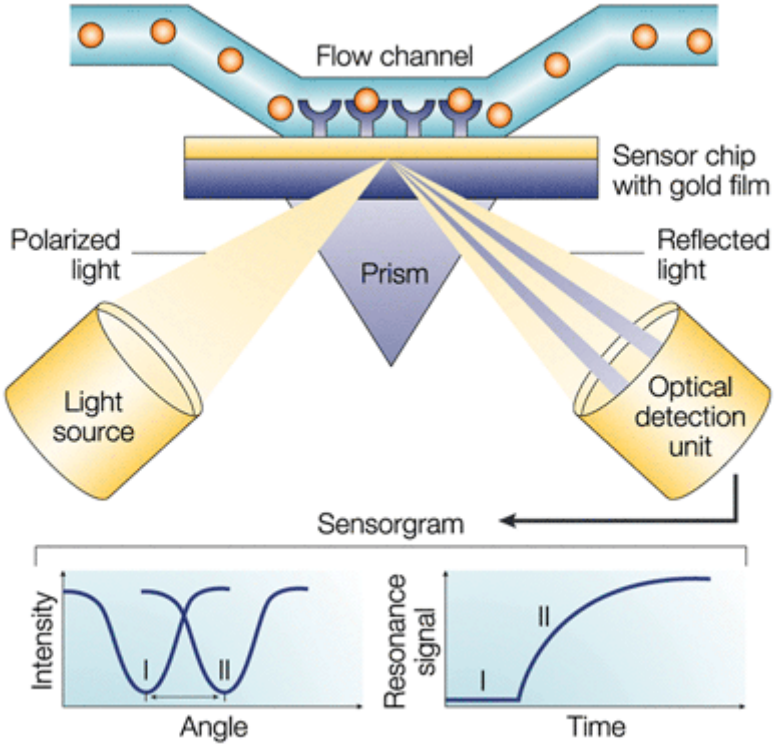

Figure 17: General setup for an SPR biosensor Molecules in solution can bind to the surface-immobilized ligands. This binding can alter the refractive light index near the surface, which can be monitored in real time [178].

For protein-protein interaction (PPI) analysis, proteins can be attached via many different approaches onto the gold surface. For the experiments performed during this thesis, a covalent immobilization via amine coupling was chosen, where the proteins were bound through a covalent chemical link, most likely at the amine group of a lysine. Commercially available sensor chips (Series S Sensor Chip CM5, GE Healthcare) are covered with a carboxymethylated dextran matrix, which provides a hydrophilic interaction environment and relatively high freedom of mobility of the biomolecules attached to the surface due to the unbranched polymer chains of the matrix. They also provide the chemical basis for the covalent attachment of the respective proteins.

As a first step of immobilization, the carboxyl groups have to be activated by 1-ethyl-3-(3-dimethylaminopropyl)-carbodiimide (EDC) and N-hydroxysuccinimide (NHS). EDC activates the carboxyl group by forming reactive O-acylisourea, which is relatively unstable and has to be stabilized with NHS, building the NHS ester intermediate, which has a longer half-life (Figure 18).

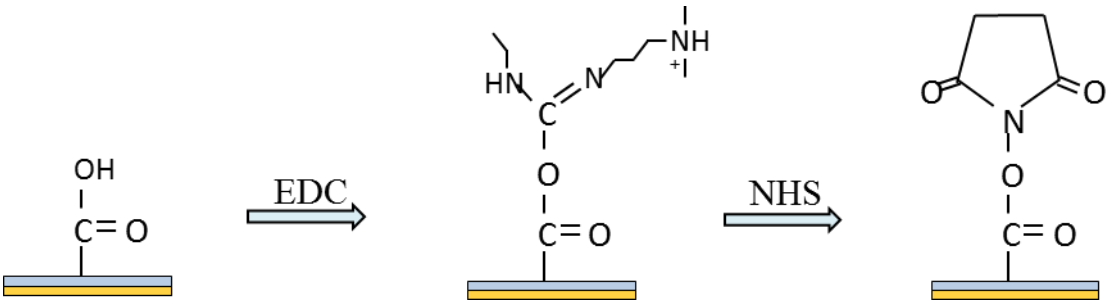

Figure 18: Activation of carboxymethyl dextran.

The reactive succinimide ester reacts spontaneously with primary amines of the ligand, which is passed over the surface to link the protein covalently to the dextran matrix. In this step, 50% of the COO^- will be activated to retain the negative charge of the surface. To enable a pre-concentration of the ligand on the dextran matrix, electrostatic attraction is used. The carboxymethylated dextran surface is negatively charged at pH values above 3.5. To generate positively charged ligands, a pH scouting for the ligand is generally used prior to immobilization to ascertain an optimal pH that should lie between the isoelectric point of the ligand and the pK_a of the surface (Table 2).

Table 2: Peroxiredoxins and the respective pH used for immobilization.

Ligand	*pH for immobilization*	*pI*
*Pf*Prx1a	5.5	6.65
*Pf*Prx1a^{C50S}, *Pf*Prx1a$^{C50S/C170S}$, *Pf*Prx1a^{C74A}	4.5	6.65
*Pf*Prx1m	5.0	8.81
*Pf*Prx1m^{C67S}, *Pf*Prx1m$^{C67S/C187S}$	4.5	8.81
*Pf*Prx1m^{C187S}	4.0	8.81
*Pf*Prx5, *Pf*Prx5^{C117S}	5.0	7.64
*Pf*Prx5^{C143S}	4.0	7.64
*Pf*Prx6, *Pf*Prx6^{C47S}	4.5	6.31
*Pf*Prx$^{1-164}$Q, *Pf*PrxQ$^{1-164/C56S}$, *Pf*PrxQ$^{1-164/C103S}$	4.0	4.96
*Pf*PrxQ$^{1-164/C56S/C103S}$	4.5	4.96

A 1:1 (v/v) mixture of 400 mM EDC and 100 mM NHS was injected for 7 min at 10 µL/min for surface activation. Freshly purified ligand was diluted to a final concentration of 50 µg/mL in 10 mM sodium acetate buffer with the respective pH, and was injected at 10 µL/min for 7 min. To deactivate remaining reactive groups 1 M ethanolaminehydrochloride pH 8.5 was injected for 7 min at 10 µL/min, at 25 °C.

Analytes used for PPI detection were already constructed prior to this thesis, namely *Pf*Trx wild type [83], *Pf*Trx^{C30S} (*Pf*Trx^{SCC}), *Pf*Trx^{C33S} (*Pf*Trx^{CSC}), *Pf*Trx^{C43S} (*Pf*Trx^{CCS}), *Pf*Trx$^{C30S/C33S}$ (*Pf*Trx^{SSC}), *Pf*Trx$^{C33S/C43S}$ (*Pf*Trx^{CSS}), *Pf*Trx$^{C30S/C43S}$ (*Pf*Trx^{SCS}), *Pf*Trx$^{C30S/C33S/C43S}$ (*Pf*Trx^{SSS}) [84], *Pf*Grx wild type [93], *Pf*Grx^{C29S} (*Pf*Grx^{SCC}), *Pf*Grx^{C32S} (*Pf*Grx^{CSC}), *Pf*Grx^{C88S} (*Pf*Grx^{CCS}), *Pf*Grx$^{C29S/C32S}$ (*Pf*Grx^{SSC}), *Pf*Grx$^{C32S/C88S}$ (*Pf*Grx^{CSS}), *Pf*Grx$^{C29S/C88S}$ (*Pf*Grx^{SCS}), and *Pf*Grx$^{C29S/C32S/C88S}$ (*Pf*Grx^{SSS}) [84].

The approach for identifying regioselectivity between redoxins and *Pf* peroxiredoxins were established within this study. Therefore, the protocol for this application is implemented in the results part of this thesis.

3.3.7.3 Electrophoretic mobility shift assay

To evaluate covalent protein-protein bindings of *Pf*Prx1a and *Pf*Trx, an electrophoretic mobility shift assay (band shift assay) was conducted. To achieve this, recombinant *Pf*Prx1a wild type, *Pf*Prx1a$^{C50S/C74A}$, *Pf*Prx1a^{C170S}, and *Pf*Trx^{CSC} were reduced with 0.5 mM TCEP for 30 min and desalted using Zeba^{TM} Spin desalting columns. Afterwards, *Pf*Prx1a was oxidized with 0.5 mM DTNB for 5 min and desalted again. Reduced *Pf*Trx^{CSC} and oxidized *Pf*Prx1a were incubated for 1 h at RT. Protein binding was visualized with SDS electrophoresis under reducing and non-reducing conditions. Moreover, antibodies detecting *Pf*Prx1a, *Pf*Trx, and His_6-tags were used in western blot analyses to identify the respective protein bands. His-tagged (*Pf*Prx1a and *Pf*Trx) proteins were identified using mouse anti-His-tag IgG (1:1,000 in 3% BSA) as primary antibodies and rabbit anti-mouse IgG HRP (1:20,000 in 5% milk) as secondary antibodies on a PVDF membrane. For exclusive immunoblotting of *Pf*Prx1a, rabbit anti-*Pf*Prx1a IgG (1:2,000 in 5% milk) was used as a primary antibody and goat anti-rabbit IgG HRP (1:20,000 in 5% milk) as a secondary antibody on a nitrocellulose membrane. For detection of *Pf*Trx, rabbit anti-*Pf*Trx IgG (1:20,000 in 5% milk) was used as a primary antibody and goat anti-rabbit IgG HRP (1:20,000 in 5% milk) as a secondary antibody on a nitrocellulose membrane.

3.3.7.4 Microscale thermophoresis

Within a temperature gradient, particles are able to enforce a direct motion, called thermophoresis, thermal diffusion, or the Soret effect [179]. This phenomenon can be used to monitor direct movements of fluorescent molecules through a microscopic temperature gradient (MicroScale Thermophoresis, MST) and is employed to analyze binding events [180]. A movement in aqueous solutions is typically directed from regions of elevated temperature and will be monitored inside a small capillary (50 × 50 µm cross section). An infrared laser (emission wavelength: 1480 nm) locally applies the temperature gradient, where the concentration of molecules is observed with a fluorescent tag on the respective molecule [181]. The differences in thermophoresis of a protein and a protein-ligand complex due to binding-induced changes in size, charge, and solvation energy, can be used to quantify the dissociation constant (K_d) in titration experiments [182] (Figure 19).

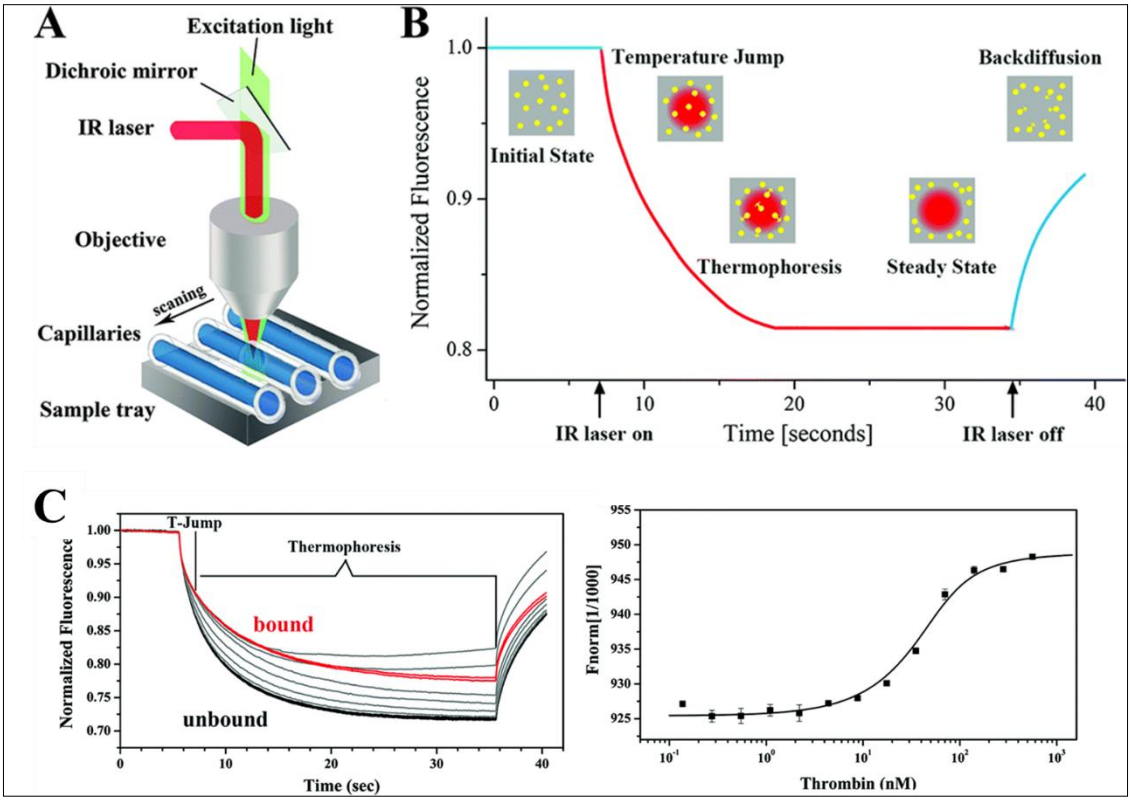

Figure 19: MST setup and thermophoresis assay. (A) Schematic representation of the MST optical system, (B) a typical thermophoretic curve. In the initial state the fluorescently labeled sample is homogenously distributed in the capillary. When the laser creates a temperature gradient, the labeled sample migrates out of the laser focal point observed in a fluorescence drop as it is sensitive to temperature. As soon as the laser is turned off, the fluorescence dye diffuses back. (C) MST time traces of titrations of an analyte against a ligand (left) and the temperature-jump signals fitted for calculating the dissociation constant of the ligand (here thrombin). Modified according to Liu *et al*. [183].

For interaction analysis of selected protein pairs (Trx and Prx), the thioredoxin mutants were chosen to be fluorescently labeled with the Monolith NT™ Protein Labeling Kit RED-NHS, following the manufacturer's protocol [179]. For this, Trx was diluted to 20 µM in 190 µl US buffer. 10 µL of red dye NT-647 (solved in DMSO) was added and incubated for 1 h at RT in the dark. Labeled Trxs were centrifuged and desalted using a gravity flow column B (NanoTemper Technologies), followed by reduction with TCEP (ad 0.5 mM) for 15 min, and then they were desalted again. Reduced Prxs were desalted using P-6 gel (equilibrated in US buffer) and were oxidized with DTNB and desalted. A dilution series (1:1 (v/v)) was prepared for the unlabeled Prx starting with a concentration of 66 µM down to 1 nM. 200 nM labeled Trx was then added to every titration step. The assay mixture was then filled into 5 µl capillaries via adhesion. The motion behavior of the labeled Trx in dependency of the Prx concentration in the MST was measured with the Monolith NT.115 (Blue/Red) from NanoTemper Technologies at Philipps University, Marburg. Data were assessed using Origin8 (OriginLab). The interaction profiles of *Pf*Prx1a wild type with *Pf*Trx^{CSC} and *Pf*Trx^{SSS} were chosen as representative interaction models.

3.3.7.5 Isothermal titration calorimetry

Biochemical reactions are accompanied by a release or uptake of heat due to physical and chemical processes that can be measured via isothermal titration calorimetry (ITC) [184]. In this way, the heat-sensing device in the microcalorimeter can measure the differences in heat between a reference cell (water) and an analytical cell (sample). When binding occurs, which will lead to a temperature change, the calorimeter compensates the temperature difference between the cells. The amount of energy needed for compensation reveals the read out data (Figure 20). The detected heat transfer (isotherm) is used in order to determine binding constants (K_D), reaction stoichiometry (n), enthalpy (ΔH), and entropy (ΔS). In the experiment, one sample is titrated into a second sample until no further heat changes (in µcal or µJ) are detected due to saturation of the second reactant. The resulting raw data is converted to a binding isotherm that can be fitted to a binding model.

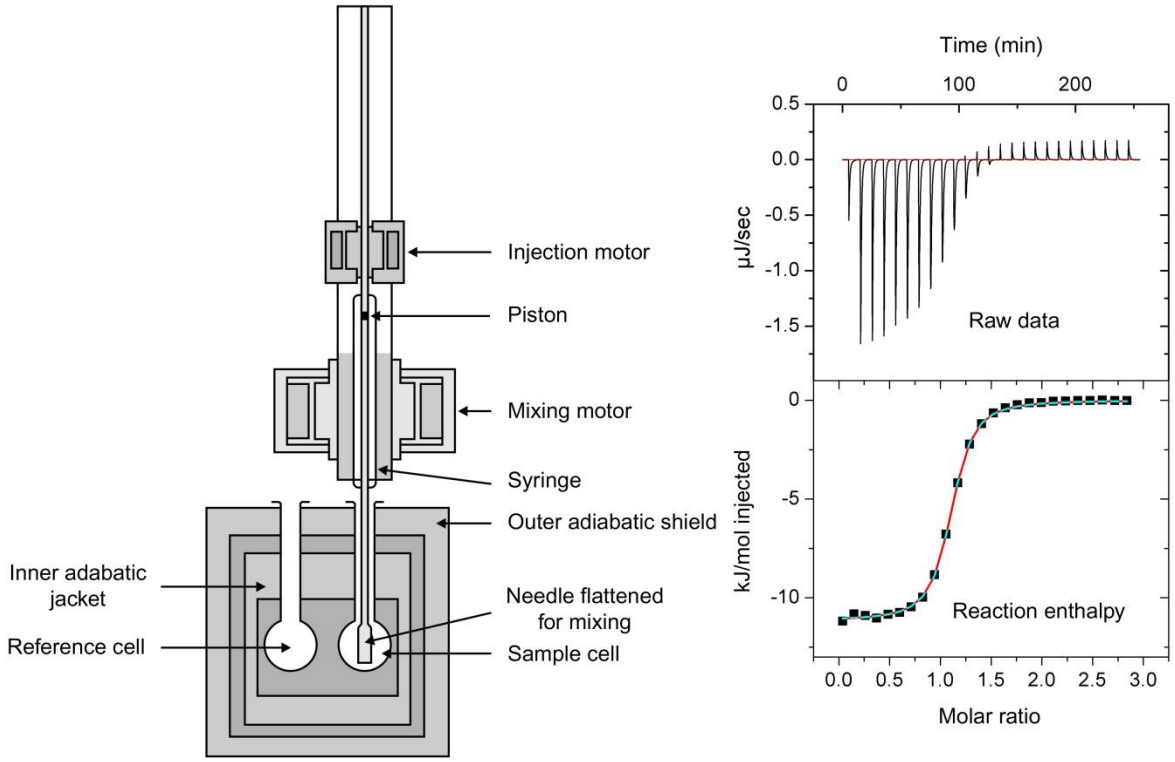

Figure 20: Schematic representation of the isothermal titration calorimeter. ITC (left) and a characteristic titration experiment (isotherms) (upper right) with its evaluation (lower right) [185].

For sample preparation, samples were reduced with 1 mM TCEP for 30 min or oxidized with 0.5 mM DTNB and desalted using desalting columns. These proteins were used for association experiments. In a second approach, the oxidized Prx and the reduced Trx were desalted and incubated for 1 h and applied as a protein-ligand-couple as injectant for dissociation experiments. Samples were degassed for 5 min (MicroVal, MicroCal) at 20 °C in a 5 mL vial. The syringe was filled with 300 µL of injectant and the analytical cell with 1.4 mL of buffer/protein solution. Titration experiments were performed automatically at 25 °C for a maximum of 30 injections of 10 µL (100 µM of Trx or 30 µM Prx-Trx) of injectant with an initial delay of 60 sec and a 120 sec lag between each injection into the analytical cell (10 µM of Prx or 0.5 mM TCEP). Stirring speed was adjusted to 286 rotations/min, and the reference power was set to 10 µcal/sec. Data were evaluated using Origin7. Control titrations of protein into buffer and buffer into buffer were performed and subtracted from the resulting isotherms.

The isotherms of *Pf*Trx^{CSC} with *Pf*Prx1a wild type as well as *Pf*Trx^{SSS} with *Pf*Prx1a wild type were chosen as representative interaction models of a covalent and non-covalent interaction, respectively.

3.3.8 Absorption titration spectrum

To verify the successful incorporation of FAD into hTGR and the presence of a charge transfer complex, an NADPH titration was performed. 20 µM of enzyme in 300 µL of US buffer pH 7.2 was titrated with 4, 12, and 20 µM NADPH, followed by a single dose of 50 µM hTrx in UV cuvettes at 25 °C. For every titration step, a spectrum from 200–800 nm was recorded with the UV/VIS spectrophotometer Evolution 300 (Thermo Scientific). Spectra were plotted and smoothed with SigmaPlot 8.0.

3.3.9 Measurement of the catalytic cysteine pK_a

To determine the pK_a of the catalytic cysteine for the plasmodial peroxiredoxins, a HRP competition assay was conducted [186, 187]. With this, the second-order rate constant for the active site Cys was obtained at different pH values varying from 5 to 10.

The competition assay was used to monitor the enzyme's ability to compete with HRP. HRP reacts with hydrogen peroxide to form the so-called compound I with a second order rate constant of $1.78 \times 10^7\ M^{-1}\ sec^{-1}$ over a wide pH range [188], and the formation of this compound I can be measured spectroscopically at 403 nm. When reduced Prx (Prx-S_P^-) is also involved in this reaction, it too will react with H_2O_2 to form sulfenic acid (Prx-S_POH) so that less peroxide is available to oxidize HRP, with the result that compound I formation will decrease (Figure 21).

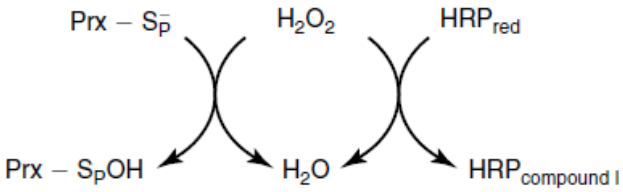

Figure 21: Basic principle of Prx activity determination by the HRP competition assay [187].

With this assay, Prx activity can be detected as a function of the decreased formation of compound I as the Prx competes with HRP for the available peroxide. Since formation of compound I will decrease as Prx concentration increases, the relative amount of H_2O_2 reacting with HRP and Prx can be used to calculate the second order rate constant for each implemented Prx concentration (k_{Prx}). These values are plotted against Prx concentration and fitted via linear regression. This competition assay was conducted in a wide range of different pH values. The slopes of each linear regression out of the different pH milieus (Figure 22) can be plotted against the pH values and will give pH dependency and by association the pK_a of the respective catalytic cysteine inside the Prx [187].

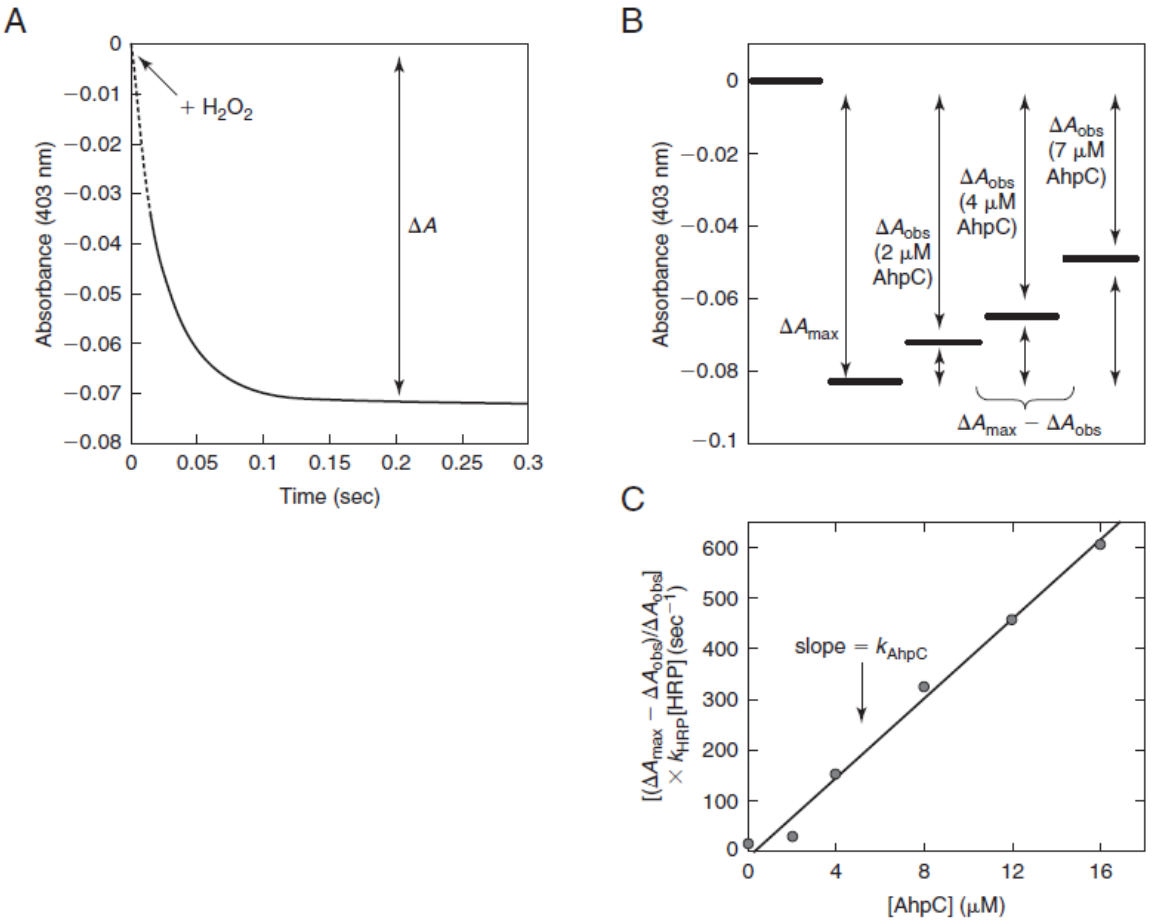

Figure 22: Determination of k_{Prx} with the HRP competition assay. At 403 nm, HRP absorbance decreases via compound I formation due to oxidation of HRP with H_2O_2. (B) When [Prx] increases, the amount of compound I formation decreases since Prx is competing with HRP for the available H_2O_2. The apparent second order rate constant of each [Prx] can be calculated $[(\Delta A_{max}\text{-}\Delta A_{obs})/\Delta A_{obs}] \times k\text{HRP}_{[HRP]}$. (C) $k_{[Prx]}$ values are plotted against [Prx] and fitted via linear regression. The slope of the linear regression provides the k_{Prx} for H_2O_2 at a defined pH. k_{Prx} values across a range of different pH values are plotted against pH in order to determine the pK_a of the catalytic cysteine of the respective Prx [187].

Prxs, stored at -20 °C with 10 mM DTT and 20% glycerol, were used for the HRP competition assay. Prxs were reduced again with 10 mM DTT for 30 min prior to every experiment and were desalted over desalting columns (Zeba spin). Before the reaction was induced, a 52 µM H_2O_2 stock was freshly prepared in US buffer, and the HRP concentration was determined. Assay mixtures containing 15 µM HRP and reduced Prx (0, 10, 15, 20, 30, and 40 µM) in US buffer were prepared (mix 1), and 2x BPCD buffers were adjusted to pH 2.5-10 (mix 2). 75 µL of mix 1 and 75 µL of mix 2 were transferred 1:1 (v/v) into a transparent 96-well plate (half area from Greiner Bio-One) with a multichannel pipette and were pipetted up and down very carefully to avoid air bubbles. Absorbance at 403 nm was measured with a multiplate reader at 25 °C (Tecan infinite M 200). Directly after adding 10 µL of the H_2O_2 stock and carefully mixing the assay solution, absorbance at 403 nm was measured again since the formation of compound I is stable for only 90 sec. Measurements were performed for at least three independent samples with four replicates each. To determine ΔA_{obs}, absorbance after adding H_2O_2 was subtracted from the average change in absorbance during the absence of Prx (ΔA_{max}). The respective k_{Prx} values were calculated for each well using a second order rate constant of 1.78 x 10^7 M^{-1} sec^{-1} for the reaction of HRP with 7.5 µM H_2O_2 [188]. Every k_{Prx} value was plotted against the peroxiredoxin concentration and was fitted to linear regression using Excel. The corresponding slope of this line gives the second order rate constant of the respective Prx

reacting with hydrogen peroxide. To determine the pK_a of the catalytic cysteines (C_P), k_{Prx} values obtained at different pH values were plotted against pH and were used to calculate the pK_a with GraphPad Prism5 via sigmoidal fitting and the three-parameter logistic equation.

3.4 Determination of kinetic parameters

Enzyme activities were all measured at 25 °C using either a HITACHI U-2001 spectrophotometer (total assay volume 500 µL) or an Evolution 300 UV/VIS spectrophotometer (Thermo Scientific) (total assay volume 600 µL), and the extinction coefficients of NADPH (6.22 mM^{-1} cm^{-1}) and TNB^- (13.6 mM^{-1} cm^{-1} (×2)) were used for calculations. To determine K_M and V_{max} values, the final concentrations of the respective substrates were varied at standard assay concentrations of the second substrate (see assay descriptions below), and kinetic values were calculated via nonlinear regression of the Michaelis-Menten equation; k_{cat} values were calculated on the basis of the V_{max} values; specific activities were determined at standard assay conditions. The reaction velocity was plotted against the substrate concentration using GraphPad Prism5. All measurements were carried out in at least three independent experimental series.

$$\text{Specific activity [µmol * min}^{-1}\text{ * mg}^{-1}\text{]} = \left(\frac{\mu mol}{min * mL}\right) * \left(\frac{mL}{mg}\right)$$

$$k_{cat}\text{ [molecules * min}^{-1}\text{]} = \left(\frac{\mu mol}{min * mL}\right) * \left(\frac{mL}{\mu mol}\right)$$

For calculations of stock solution concentrations and kinetic parameters, the specific extinction coefficients of the respective proteins (calculated by the ProtCalc online tool of JustBio, www.justbio.com) and substrates were used.

ε_{280} (*Pf*Prx1a)	= 21.7 $mM^{-1} * cm^{-1}$	ε_{280} ($hTGR^{1-150}$)	= 2.71 $mM^{-1} * cm^{-1}$
ε_{280} (*Pf*Prx1m)	= 21.8 $mM^{-1} * cm^{-1}$	ε_{280} ($hTGR^{151-643}$)	= 62.04 $mM^{-1} * cm^{-1}$
ε_{280} (*Pf*Prx5)	= 20.4 $mM^{-1} * cm^{-1}$	ε_{340} (NADPH)	= 6.22 $mM^{-1} * cm^{-1}$
ε_{280} (*Pf*Prx6)	= 30.9 $mM^{-1} * cm^{-1}$	ε_{412} (TNB^-)	= 13.60 $mM^{-1} * cm^{-1}$
ε_{280} (*Pf*PrxQ)	= 13.5 $mM^{-1} * cm^{-1}$		
ε_{280} (hTGR)	= 64.8 $mM^{-1} * cm^{-1}$		

3.4.1 Thioredoxin reductase activity assays

The enzyme's ability to reduce thioredoxin was determined using a thioredoxin reductase (TrxR) assay. The decrease in absorption at 340 nm was detected since the reduction of oxidized hTrx converts the co-substrate NADPH to $NADP^+$, which leads to a shift in absorption at 340 nm [189]. To determine thioredoxin-reducing activity, hTGR (and variants) were added to an assay mixture consisting of 100 mM potassium phosphate, 2 mM EDTA, pH 7.4, and 100 µM NADPH. After monitoring the baseline, the reaction was started by adding human Trx^{C72S} (20 µM final concentration), and the initial ΔA/min was monitored at 340 nm.

The capability to reduce the artificial substrate 5,5'-dithiobis-(2-nitrobenzoic acid) (DTNB, Ellman's reagent) was detected with a DTNB assay. DTNB is reduced to the yellow colored 2-nitro-5-thiobenzoate (TNB^-) stoichiometrically by thiols, leading to an increase in absorbance at 412 nm [190]. The standard 2-nitro-5-thiobenzoate (DTNB) reduction assay contained 100

mM potassium phosphate, 2 mM EDTA, pH 7.4, 100 µM NADPH, and 3 mM DTNB (dissolved in DMSO). After monitoring the baseline, the reaction was initiated by adding the enzyme. The reaction was followed by measuring the initial change in absorbance at 412 nm.

3.4.2 Grx activity assay

The HEDS reduction assay was used to determine the enzyme's ability to deglutathionylate a substrate via a monothiol mechanism. In this coupled assay, GSH and the disulfide substrate bis(2-hydroxyethyl)disulfide (HEDS) react non-enzymatically with each other to form the mixed disulfide GSSEtOH, which is the actual substrate for the Grx domain. The active site cysteine in its thiolate form attacks GSSEtOH in the oxidative half reaction and becomes glutathionylated. A second GSH molecule subsequently regenerates the enzyme during the reductive half reaction, releasing GSSG [191-193]. The GSSG that originates is then reduced by hGR in the presence of NADPH, leading to a decrease in absorption at 340 nm due to NADPH consumption. The assay mixture contained 100 mM Tris, 1 mM EDTA, pH 8.0, 100 µM NADPH, 0.25 U/ml of human GR, 1 mM reduced glutathione (GSH) and 750 µM HEDS. The reaction was initiated by adding hTGR. A decrease in NADPH absorbance was monitored at 340 nm for 1 min. The initial reaction of all assay components, excluding the hTGR, generates a background reaction that depends on the HEDS concentration and was subtracted from the respective absorbance changes.

3.4.3 Glutathione reductase activity assay

To evaluate GR activity of hTGR a glutathione reductase (GR) assay was conducted. An enzyme with GR activity is able to reduce GSSG in the presence of NADPH. The decrease in absorbance at 340 nm was detected for 1 min after adding GSSG. To detect GR activity [194], hTGR was added to an assay mixture comprising 20.5 mM KH_2PO_4, 26.5 mM K_2HPO_4, 1 mM EDTA, 200 mM potassium chloride, pH 6.9, and 100 µM NADPH. After monitoring the baseline, the reaction was started by adding 0.2 mM GSSG, and the initial decrease in absorbance at 340 nm due to NADPH consumption was monitored. Recombinant hGR served as a positive control.

3.4.4 Hysteretic effect

The time-based dependency of the enzymatic reaction on present and past inputs (hysteresis) was detected with the GR assay as described above. For this, the assay was conducted in the presence of varying GSSG concentrations in order to detect its influence on the initial velocity of the enzyme's reaction. 0.45 µM hTGR was incubated with 0.1 – 4 mM GSSG and 100 µM NADPH. The following decrease in absorbance at 340 nm was recorded for 6.5 h.

3.4.5 Protein-*S*-glutathionylation

For glutathionylation studies, hTGR wt was reduced with 5 mM DTT for 30 min at 4 °C and desalted using Zeba™ Spin Desalting Columns. The reduced enzyme was incubated with 5 mM GSSG for 5 min at 37 °C and loaded onto a 12% SDS gel for western blot analysis. For immunoblotting, the first antibody (mouse anti-glutathione antibody) was diluted 1:500, and the secondary antibody (rabbit anti-mouse IgG HRP) was diluted 1:5,000 in 5% milk powder.

For mass spectrometry analysis, proteins were loaded onto a 12% polyacrylamide gel followed by SDS-PAGE. Protein containing gel pieces of interest were excised, digested with trypsin and analyzed by matrix-assisted laser desorption ionization time-of-flight (MALDI-TOF) mass spectrometry (Ultraflex I, Bruker Daltonics, Bremen) (by Protein Analytics, Prof. Lochnit, Giessen).

3.5 *P. falciparum* cell culture methods

The chloroquine-sensitive strain 3D7 was maintained in cell culture according to Trager and Jensen with modifications [195]. In brief, parasites were grown in red blood cells (A^+) at 5% hematocrit with a parasitemia not higher than 8% to avoid cell death at steady 37 °C, purged with a gas mixture containing 3% O_2, 3% CO_2, and 94% N_2. Parasite growth was monitored via Giemsa staining. To ensure synchronous parasites, sorbitol synchronization was performed according to Lambros and Vanderberg [196]. Once parasites became trophozoites, saponin lysis was conducted to remove red blood cells and obtain the parasite pellet [197]. The pellets were stored at - 80 °C until use.

3.6 Protein crystallization

Atomic resolution structures of proteins provide a deep and unique understanding of protein function and help unravel the inner workings of the living cell [198]. To obtain the three-dimensional structure, proteins must be purified to homogeneity, which is a key factor in obtaining crystals that diffract to high resolution [199]. For crystallization, the protein has to be brought to supersaturation and should therefore be concentrated as highly as possible without causing aggregation or precipitation of the macromolecule. Precipitating agents (e.g. salt, organic solvents, or polyethylene glycols (PEG)) can promote the nucleation of protein crystals in the solution [198]. The salt concentration in the sample has to be kept as low as possible because salt itself tends to crystallize at a high concentration, and a higher salt concentration is inversely connected to a decrease in protein solubility. Organic solvents decrease the water content of the solution and the dielectric constant of the medium, and PEG, as a polymer, uses its volume exclusion property to lower the solubility of the solution [200]. Vapor diffusion and batch crystallization are the main techniques for obtaining protein crystals, and the former was used in the present thesis. For vapor diffusion, an unsaturated precipitant-containing protein solution is sealed in a chamber with pure precipitant. Vapor equilibration of the drop and reservoir induces dehydration of the drop to reach a supersaturation level where nucleation and crystal growth can occur and can be carried out with the hanging drop or sitting drop method. For initial screening of appropriate crystallization conditions, different screens were performed in microplates using the sitting drop method. With the HoneyBee 961 crystallization robot, commercially available and self-arranged crystallization screens (see Chapter 2.11) were set up using 200 nL of protein-precipitant mixture, which enables a simultaneous test of 96 different conditions in one plate. For crystallization setup, an initial protein concentration of 17 mg/mL (*Pf*PrxQ$^{1\text{-}164}$) was used. Once a promising condition was found, further crystallization trials were performed with the hanging drop method. For this, 2 µL of protein solution and 2 µL of precipitant were mixed on a cover slip and were applied upside down onto a well filled with precipitant (800 µL), sealed with silicon oil to avoid dehydration and enable vapor diffusion. Visual controls and protocols of the protein drops were regularly performed with a stereomicroscope (Leica). Protein crystals of appropriate quality were brought to an X-ray source at the Max Plank Institute for Medical Research, Heidelberg.

4 RESULTS

4.1 The interactome of *Plasmodium falciparum* 2-Cys peroxiredoxins

To study the interactome of *Plasmodium falciparum* 2-Cys Prxs (Chapter 4.1) and to further investigate the recycling step of Prxs via its redoxins (Chapter 4.2), multiple active site Cys mutants of Prxs were constructed and new overexpression and purification protocols were established, which are described in the following. Due to this, the pK_a of different *Pf*Prxs could be determined using the HRP competition assay and the truncated *Pf*PrxQ$^{1\text{-}164}$ could be crystallized, which shall be described at the end of Chapter 4.2.

4.1.1 Site-directed mutagenesis of *Pf*Prxs

For the investigation of redox-regulated cysteines in the *Pf*Prxs the respective peroxidatic and resolving cysteines were mutated, in most cases, to serine, which is the closest replacement to cysteine in terms of size. A cysteine to alanine substitution was used, in one case, to maintain the hydrophobicity at the buried C74 in *Pf*Prx1a. Within this thesis, mutants of *Pf*Prx1a (*Pf*Prx1a^{C50S}, *Pf*Prx1a^{C170S}, *Pf*Prx1a$^{C50S/C74A}$, *Pf*Prx1a$^{C74A/C170S}$, *Pf*Prx1a$^{C50S/C170S}$, *Pf*Prx1a$^{C50S/C74A/C170S}$), *Pf*Prx1m (*Pf*Prx1m^{C67S}, *Pf*Prx1m^{C187S}, *Pf*Prx1m$^{C67S/C187S}$), *Pf*Prx5 (*Pf*Prx5^{C117S}, *Pf*Prx5^{C143S}), *Pf*Prx6 (*Pf*Prx6^{C47S}), and mutants of the truncated form of *Pf*PrxQ$^{1\text{-}164}$ (*Pf*PrxQ$^{1\text{-}164/C56S}$, *Pf*PrxQ$^{1\text{-}164/C103S}$, *Pf*PrxQ$^{1\text{-}164/C56S/C103S}$) were constructed with site-directed mutagenesis.

4.1.2 Heterologous overexpression and purification of *Pf*Prxs and mutants

The heterologous overexpression and purification of *Pf*Prx mutants (*Pf*Prx1a^{C50S}, *Pf*Prx1a^{C170S}, *Pf*Prx1a$^{C50S/C170S}$, *Pf*Prx1m^{C67S}, *Pf*Prx1m^{C187S}, *Pf*Prx1m$^{C67S/C187S}$, *Pf*Prx5^{C117S}, *Pf*Prx5^{C143S}, *Pf*Prx6^{C47S}, *Pf*PrxQ$^{1\text{-}164/C56S}$, *Pf*PrxQ$^{1\text{-}164/C103S}$, *Pf*PrxQ$^{1\text{-}164/C56S/C103S}$) was performed using the same protocol as for the wild type *Pf*Prxs. Within this thesis, overexpression and purification conditions of the truncated form of *Pf*PrxQ^{164} were optimized to obtain about 150 mg purified protein out of 1 L *E. coli* culture. Figure 23 represents respective purification results via Ni-NTA affinity chromatography for all five *Pf*Prxs. The purification of *Pf*Prx1a and *Pf*Prx5 required the presence of a reducing agent during all involved steps, which was realized by the addition of 0.5 mM TCEP to prevent hyperoxidation. For all further experiments, only fractions with the highest purity were pooled. After elution, the purified proteins were stored at either 4 °C or with 10 mM DTT and 20% glycerol at -20 °C.

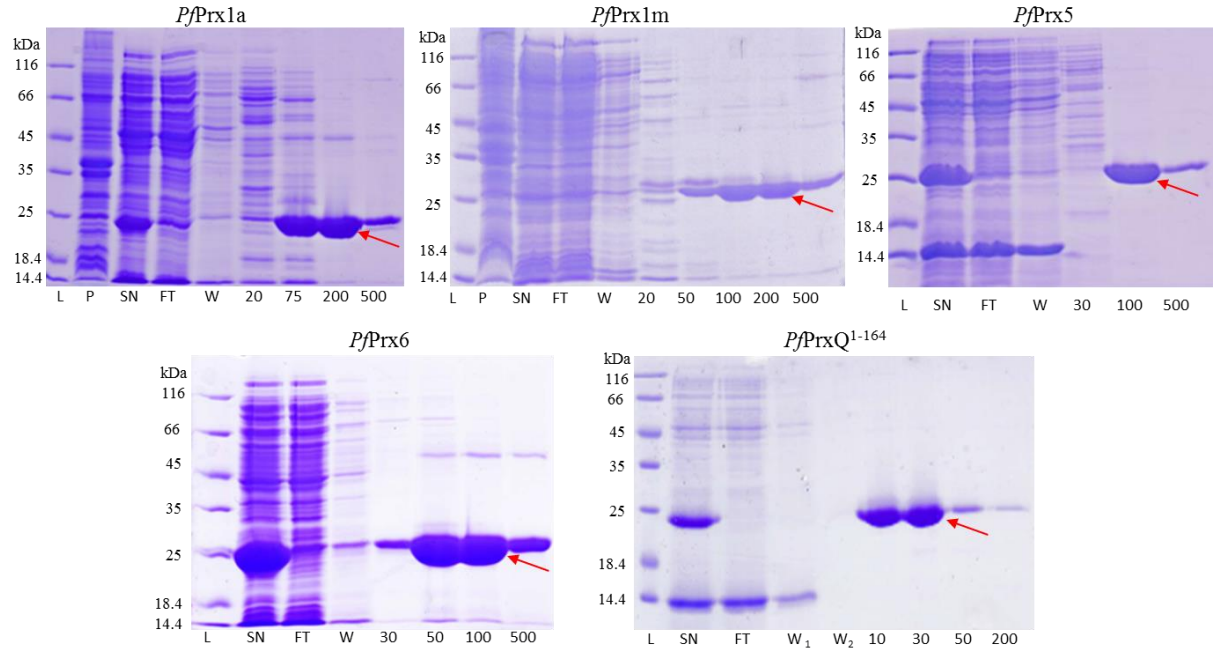

Figure 23: Purification of *Pf*Prxs via Ni-NTA affinity chromatography. *Pf*Prx1a, *Pf*Prx1m, *Pf*Prx5, and *Pf*Prx6 were purified using Ni-NTA affinity resin, and *Pf*PrxQ$^{1-164}$ was purified using talon affinity resin. L: protein ladder, P: pellet, SN: supernatant, FT: flow through, W: wash. Numbers indicate the concentration of imidazole for protein elution. Red arrows indicate the respective protein.

To study the oligomerization behavior of *Pf*PrxQ$^{1-164}$ size-exclusion chromatography using a HiLoad^{TM}16/60 Superdex^{TM} 200 prep grade column was also performed in the master's thesis of Kathrin Pauli in parallel to this thesis [201]. For this, the protein was analyzed in its reduced and oxidized form by adding 5 mM of DTT or 10 mM of H_2O_2, respectively (Figure 24).

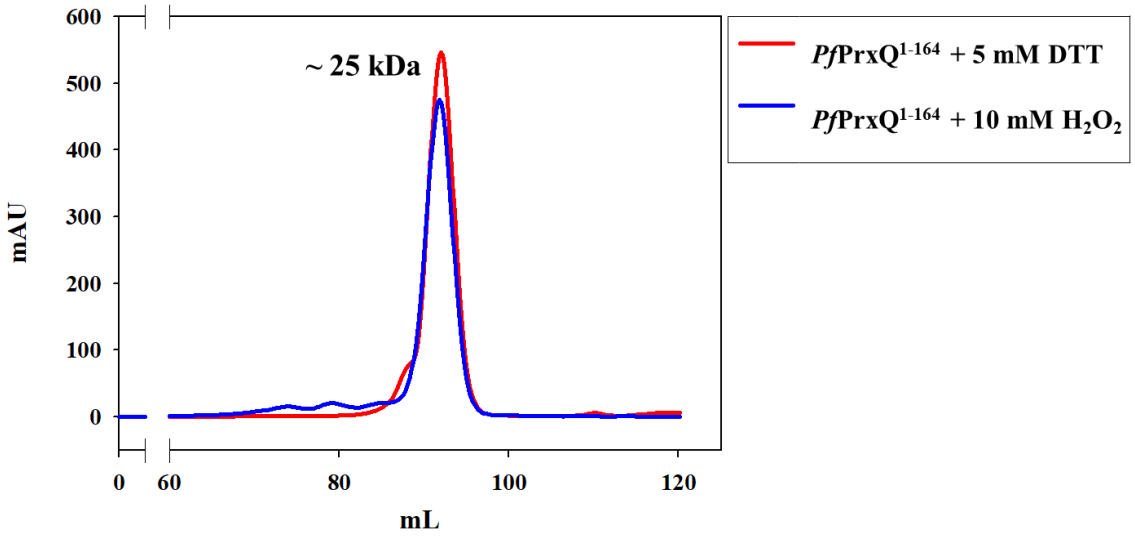

Figure 24: Size-exclusion chromatogram of *Pf*PrxQ$^{1-164}$ under reducing and oxidizing conditions.

The resulting chromatogram demonstrated *Pf*PrxQ$^{1-164}$ (monomeric size = 19.7 kDa) as a monomeric Prx independently from its redox state.

4.1.3 Pull-down assay with 2-Cys *Pf*Prxs

In the used pull-down procedure, where immobilized *Pf*Prxs are able to capture interacting proteins via a dithiol-disulfide mechanism, *Pf*Prx1a and *Pf*Prx1m are confronted with 500 mM NaCl containing buffers. To confirm a constant oligomerization state of the respective Prxs, under the used salt concentration, size exclusion chromatography of the applied Prxs was conducted. The elution profile of both proteins could demonstrate uniform oligomerization in the different buffers. All peaks in the elution profiles correspond to the respective decameric Prx (Figure 25).

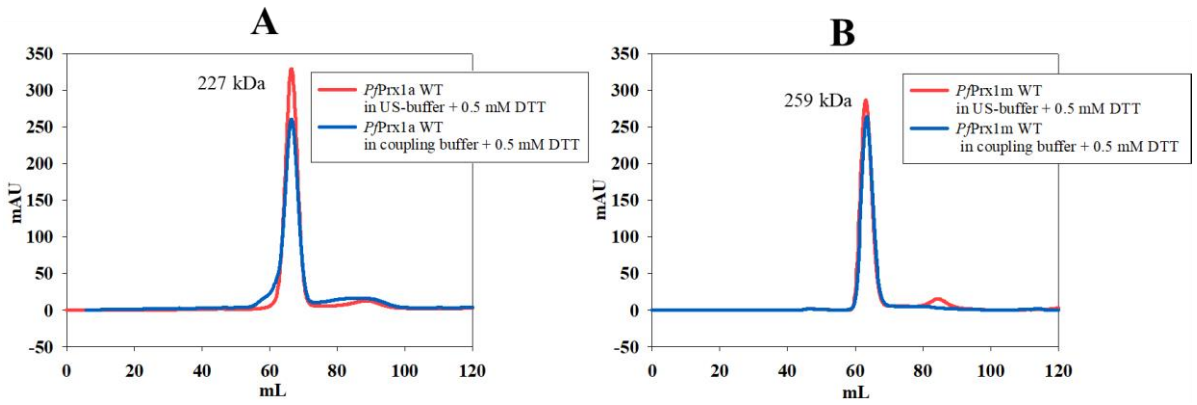

Figure 25: Size-exclusion chromatography profile of *Pf*Prx1a wt and *Pf*Prx1m wt. A) In red: reduced *Pf*Prx1a wt elution profile in US buffer, in blue: reduced *Pf*Prx1a wt elution profile in coupling buffer. B) In red: reduced *Pf*Prx1m wt elution profile in US buffer, in blue: *Pf*Prx1m elution profile in coupling buffer.

For pull-down experiments, the 2-Cys peroxiredoxins (*Pf*Prx1a and *Pf*Prx1m), their resolving cysteine mutants (*Pf*Prx1a^{C170S} and *Pf*Prx1m^{C187S}), and their peroxidatic cysteine mutants (*Pf*Prx1a^{C50S} and *Pf*Prx1m^{C67S}) were used. Additionally, 2-Cys *Pf*Prxs lacking their peroxidatic and resolving cysteines were used as bait for mixed disulfides with parasitic proteins (*Pf*Prx1a$^{C50S/C170S}$ and *Pf*Prx1m$^{C67S/C187S}$) (Figure 26).

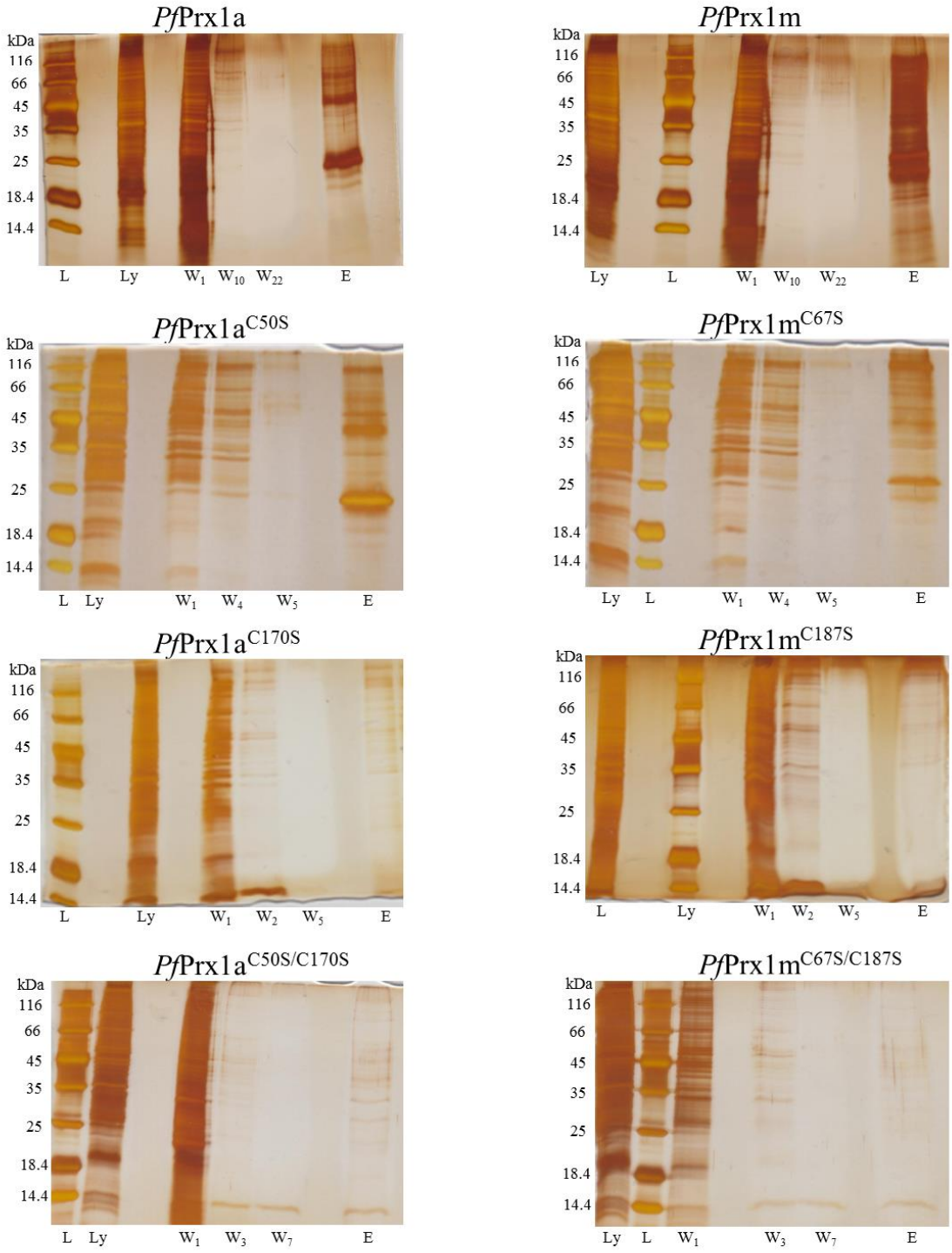

Figure 26: Elution profile of 2-Cys *Pf*Prxs during pull-down assays. Representative elution profiles of the pull-down experiment on an SDS page, dyed with silver staining after gel electrophoresis. L: protein ladder, Ly: parasite lysate, W: number of washing step, E: eluate with 10 mM DTT.

Proteins in the elution fractions were identified via mass spectrometry. To account for unspecific protein binding of parasite lysate to the CNBr-activated Sepharose 4B beads, the immobilization of bait proteins to the beads were mimicked with water during the pull-down procedure, which was also conducted in triplicates. Parasitic proteins captured with empty beads were subtracted from all ensuing results.

Tables 3 and 4 provide an overview of proteins exclusively captured with the wild type enzyme, a peroxidatic or resolving cysteine mutant of *Pf*Prx1a and *Pf*Prx1m, and their double active site mutants. For *Pf*Prx1a, captured potentially interacting proteins are involved in carbohydrate metabolism, transcription and translation, protein degradation, and signaling. Interacting proteins for *Pf*Prx1m are involved in energy and lipid metabolism, and anti-oxidative stress response.

Table 3: Interaction partners of *Pf*Prx1a. Proteins located in the cytosol and exclusively captured by *Pf*Prx1a wild type, *Pf*Prx1a^{C50S}, *Pf*Prx1a^{C170S}, or *Pf*Prx1a$^{C50S/C170S}$. Listed proteins occurred in at least two independent experiments.

Protein name	**Accession number**	**Protein MW (Da)**	**pI**	**Sequence coverage (%)**		
***Pf*Prx1a wild type**				**1**	**2**	**3**
Serine repeat antigen 5 (SERA5)	PF3D7_0207600	111,768	5.4	7.6 %	10.9 %	6.2 %
Heat shock protein 40, putative	PF3D7_0213100	37,356	8.8	5.8 %	9.8 %	12.2 %
40S ribosomal protein S23, putative	PF3D7_0306900	16,130	10.8	8.3 %	0	8.3 %
40S ribosomal protein S15A, putative	PF3D7_0316800	14,874	10.0	30.0 %	30.8%	6.2 %
Proteasome regulatory protein, putative	PF3D7_0317800	26,466	6.9	0	9.8 %	4.9 %
40S ribosomal protein S3A, putative	PF3D7_0322900	30,047	9.8	6.9 %	21.8 %	9.9 %
Small GTP-binding protein sar1 (SAR1)	PF3D7_0416800	22,020	7.3	24.0 %	22.9 %	24.0 %
Eukaryotic initiation factor, putative	PF3D7_0422700	44,800	7.6	7.4 %	3.8 %	0
Translation initiation factor IF-2, putative	PF3D7_0607000	112,358	8.0	2.4 %	1.9 %	0
Nascent polypeptide associated complex alpha chain, putative	PF3D7_0621800	20,623	4.9	20.1 %	23.9 %	0
Ubiquitin carboxyl-terminal hydrolase, putative	PF3D7_0726500	373,171	7.9	0.3 %	0.3 %	0.6 %
Karyopherin alpha (KARalpha)	PF3D7_0812400	61,159	5.3	8.3 %	4.0 %	0
Eukaryotic translation initiation factor 3 subunit 5, putative	PF3D7_0918300	36,820	6.7	6.6 %	6.6 %	0
26S protease regulatory subunit 4, putative (RPT2)	PF3D7_1008400	49,839	7.5	10.9 %	0	2.0 %
S-adenosylmethionine decarboxylase/ornithine decarboxylase	PF3D7_1033100	168,169	6.4	3.2 %	0	1.5 %
Phosphoglycerate mutase, putative (PGM1)	PF3D7_1120100	28,770	8.3	13.2 %	14.0 %	8.4 %
40S ribosomal protein S18, putative	PF3D7_1126200	17,891	10.5	0	13.5 %	16.7 %
Casein kinase 1 (CK1)	PF3D7_1136500.1	37,631	9.3	23.8 %	16.4 %	0
Casein kinase 1 (CK1)	PF3D7_1136500.2	37,789	9.2	23.8 %	16.4 %	0
Protein phosphatase 2C (PP2C)	PF3D7_1138500	105,404	4.5	0	2.6 %	2.6 %
60S ribosomal protein L35ae, putative	PF3D7_1142600	16,265	10.5	8.6 %	0	15.0 %
40S ribosomal protein S21 (RPS21)	PF3D7_1144000	9,145	8.5	0	13.4 %	11.0 %
Eukaryotic translation initiation factor 3 subunit 8, putative	PF3D7_1206200	116,014	5.4	5.0 %	4.3 %	2.2 %
Eukaryotic translation initiation factor 3 subunit 10, putative	PF3D7_1212700	166,061	6.8	5.9 %	3.0 %	0
Endoplasmin, putative (GRP94)	PF3D7_1222300	95,018	5.4	10.2 %	9.6 %	4.6 %
Ras-related protein Rab-2 (RAB2)	PF3D7_1231100	24,424	6.8	11.3 %	6.1 %	0

Acyl-CoA synthetase (ACS11)	PF3D7_1238800	92,092	8.7	2.8 %	0	1.3 %
26S protease regulatory subunit 8, putative (RPT6)	PF3D7_1248900	49,545	7.0	5.1 %	0	2.5 %
26S protease regulatory subunit 10B, putative (RPT4)	PF3D7_1306400	44,677	8.9	0	3.1 %	9.9 %
Carbamoyl phosphate synthetase (cpsSII)	PF3D7_1308200	273,437	6.6	0.9 %	0	0.6 %
26S protease regulatory subunit 7, putative (RPT1)	PF3D7_1311500	46,835	6.7	9.8 %	0	5.0 %
Glutamine-tRNA ligase, putative	PF3D7_1331700	108,532	8.2	2.4 %	2.4 %	1.0 %
Lysine-tRNA ligase (KRS1)	PF3D7_1350100	67,591	7.4	9.4 %	3.1 %	0
60S ribosomal protein L17, putative	PF3D7_1351400	23,415	10.9	0	3.9 %	7.9 %
26S proteasome regulatory subunit RPN11, putative (RPN11)	PF3D7_1368100	35,212	6.7	4.2 %	0	7.1 %
Eukaryotic translation initiation factor 2 gamma subunit, putative	PF3D7_1410600	51,245	8.0	9.5 %	4.9 %	2.4 %
60S ribosomal protein L14, putative	PF3D7_1431700	19,297	10.2	7.9 %	13.9 %	4.2 %
***Pf*Prx1a^{C50S}**				**1**	**2**	**3**
Protein transport protein SEC31 (SEC31)	PF3D7_0214100	166,708	6.9	3.1 %	0	4.2 %
RING zinc finger protein, putative	PF3D7_0215100	34,401	7.0	16.8 %	0	16.8 %
Exportin-1, putative	PF3D7_0302900	147,938	6.0	2.6 %	0	3.4 %
RNA pseudouridylate synthase, putative	PF3D7_0511500	1187,631	7.5	0.3 %	0	0.3 %
Eukaryotic translation initiation factor 3 37.28 kDa subunit,	PF3D7_0716800	37,284	6.9	5.5 %	0	15.0 %
Serine--tRNA ligase, putative	PF3D7_0717700	62,454	7.0	2.8%	0	5.8 %
60S ribosomal protein L11a, putative	PF3D7_0719600	20,228	10.1	8.7 %	0	17.3 %
40S ribosomal protein S10, putative	PF3D7_0719700	16,478	9.7	10.9 %	0	34.3 %
Proteasome subunit alpha type-5, putative	PF3D7_0727400	28,388	5.1	20.7 %	0	27.7 %
26S proteasome regulatory subunit RPN10, putative (RPN10)	PF3D7_0807800	55,067	4.8	3.1 %	0	11.0 %
60S ribosomal protein L22, putative	PF3D7_0821700	16,382	10.2	10.1 %	0	16.5 %
Ubiquitin domain-containing protein DSK2, putative	PF3D7_1113400	42,706	4.7	9.3 %	0	9.3 %
Peptidyl-prolyl cis-trans isomerase (CYP19B)	PF3D7_1115600	21,731	7.6	13.3 %	0	25.6 %
Pyridoxine biosynthesis protein PDX2 (PDX2)	PF3D7_1116200.1	24,563	6.9	22.4 %	0	5.5 %
Box C/D snoRNP rRNA 2'-O-methylation factor, putative	PF3D7_1118500	69,390	5.9	5.4 %	0	18.7 %
Protein transport protein SEC13 (SEC13)	PF3D7_1230700	90,749	6.6	7.3 %	0	5.2 %
U4/U6.U5 tri-snRNP-associated protein 2, putative	PF3D7_1317000	74,636	7.9	6.1 %	0	15.6 %
Proteasome subunit alpha type-4, putative	PF3D7_1353800	27,948	6.1	22.8 %	0	26.4 %

Alanine-tRNA ligase (AlaRS)	PF3D7_1367700	165,135	8.9	1.6 %	0	1.0 %
Glycine-tRNA ligase (GlyRS)	PF3D7_1420400	104,306	7.9	3.7 %	0	12.5 %
Histidine-tRNA ligase, putative	PF3D7_1445100	133,668	7.7	1.6 %	0	2.5 %
***Pf*Prx1a^{C170S}**				**1**	**2**	**3**
Deoxyribose-phosphate aldolase, putative	PF3D7_1021600	28,980	7.2	0	4.2 %	4.2 %
60S ribosomal protein L23, putative	PF3D7_1331800	14,993	9.9	21.6 %	7.2 %	0
***Pf*Prx1a$^{C50S/C170S}$**				**1**	**2**	**3**
Elongation factor 1-beta (EF-1beta)	PF3D7_0913200	32,027	5.1	0	8.3 %	8.3 %
***Pf*Prx1a wild type, *Pf*Prx1a^{C50S}**				**1**	**2**	**3**
60S ribosomal protein P0 (PfP0)	PF3D7_1130200	34,967	6.7	0	9.2 %	6.0 %
Elongation factor 1-gamma, putative	PF3D7_1338300	47,777	7.4	4.6 %	0	20.9 %
60S ribosomal protein L6-2, putative	PF3D7_1338200	25,532	10.1	17.2 %	0	25.8 %
60S acidic ribosomal protein P2 (PfP2)	PF3D7_0309600	11,948	4.5	33.0 %	43.8 %	21.4 %
40S ribosomal protein S4, putative	PF3D7_1105400	29,772	10.1	22.6 %	27.2 %	8.0 %
Dolichyl-phosphate-mannose protein mannosyltransferase,	PF3D7_1010700	25,678	7.0	28.7 %	0	59.2 %
Purine nucleoside phosphorylase (PNP)	PF3D7_0513300	26,858	6.5	18.0 %	0	27.8 %
60S acidic ribosomal protein P1, putative (RPP1)	PF3D7_1103100	13,014	4.6	39.8 %	0	48.3 %
Translation initiation factor 4E (eIF4E)	PF3D7_0315100	26,948	8.3	15.0 %	0	29.1 %
26S proteasome AAA-ATPase subunit RPT3, putative	PF3D7_0413600	44,666	7.5	9.4 %	0	12.2 %
Hypoxanthine-guanine phosphoribosyltransferase (HGPRT)	PF3D7_1012400	26,362	7.7	19.0 %	0	48.9 %
Heat shock protein 70 (HSP70-3)	PF3D7_1134000	73,298	6.9	9.2 %	0	33.8 %
Heat shock protein 70 (HSP70-2)	PF3D7_0917900	72,388	5.3	29.1 %	14.3 %	15.5 %
Protein disulfide isomerase (PDI-11)	PF3D7_1134100	49,195	8.9	12.5 %	0	24.1 %
Phosphoribosylpyrophosphate synthetase	PF3D7_1325100	49,383	9.3	10.3 %	0	18.5 %
Enolase (ENO)	PF3D7_1015900	48,678	6.6	26.5 %	0	38.3 %
Fructose-bisphosphate aldolase (FBPA)	PF3D7_1444800	40,105	8.1	11.7 %	0	35.5 %
Erythrocyte membrane-associated antigen	PF3D7_0703500	264,915	8.6	1.4 %	0	4.2 %
Suppressor of kinetochore protein 1, putative (SKP1)	PF3D7_1367000	18,786	4.5	17.9 %	0	8.0 %

Phosphoethanolamine N-methyltransferase (PMT)	PF3D7_1343000	31,043	5.6	13.2 %	0	57.9 %
Ubiquitin carboxyl-terminal hydrolase 2, putative	PF3D7_0516700	156,332	6.8	4.6 %	0	10.2 %
Dihydropteroate synthetase (DHPS)	PF3D7_0810800	83,374	7.1	2.7 %	0	5.9 %
L-lactate dehydrogenase (LDH)	PF3D7_1324900	34,108	7.5	31.0 %	0	39.2 %
Asparagine--tRNA ligase (AsnRS)	PF3D7_0211800	70,498	6.7	15.2 %	0	25.4 %
1-cys peroxiredoxin (1-CysPxn)	PF3D7_0802200	25,164	6.8	30.5 %	0	36.8 %
Fibrillarin, putative (NOP1)	PF3D7_1407100	34,129	10.0	6.3 %	0	14.5 %
40S ribosomal protein S5	PF3D7_1447000	29,958	10.0	11.8 %	0	29.4 %
S-adenosyl-L-homocysteine hydrolase (SAHH)	PF3D7_0520900	53,839	5.9	20.9 %	0	21.7 %
Adenylate kinase (AK1)	PF3D7_1008900	27,611	8.9	5.8 %	19.0 %	18.6 %
60S ribosomal protein L3 (RPL3)	PF3D7_1027800	44,221	10.2	0	13.0 %	5.4 %
Casein kinase 2, alpha subunit (CK2alpha)	PF3D7_1108400	39,890	8.8	10.7 %	11.3 %	0
Phosphoglycerate kinase (PGK)	PF3D7_0922500	45,427	7.8	23.1 %	4.3 %	11.8 %
40S ribosomal protein S3	PF3D7_1465900	24,668	10.2	7.7 %	0	18.6 %
***Pf*Prx1a wild type, *Pf*Prx1a^{C170S}**				**1**	**2**	**3**
40S ribosomal protein S7, putative	PF3D7_1302800	22,481	9.8	14.9 %	4.6 %	0
Inosine-5'-monophosphate dehydrogenase	PF3D7_0920800	56,150	7.9	13.3 %	13.1 %	8.8 %
60S ribosomal protein L5, putative	PF3D7_1424100	33,998	9.8	7.1 %	7.1 %	6.1 %

Table 4: Interaction partners of *Pf*Prx1m. Proteins located in the mitochondrion and exclusively captured by *Pf*Prx1m wild type, *Pf*Prx1m^{C176S}, or *Pf*Prx1m^{C187S}. Listed proteins occurred in at least two independent experiments.

Protein name	**Accession number**	**Protein MW (Da)**	**pI**	**Sequence coverage (%)**		
***Pf*Prx1m wild type**				**1**	**2**	**3**
Diacylglycerol kinase, putative	PF3D7_1471400	57,643	8.8	11.4 %	2.8 %	0
***Pf*Prx1m^{C67S}**				**1**	**2**	**3**
GrpE protein homolog, mitochondrial, putative (MGE1)	PF3D7_1124700	35,043	8.9	33.9 %	0	13.6 %
Sortilin, putative	PF3D7_1451800	102,270	6.7	8.4 %	0	3.1 %
***Pf*Prx1m^{C187S}**				**1**	**2**	**3**
Ferrodoxin reductase-like protein	PF3D7_0720400	72,722	8.7	3.9 %	3.9 %	0
Superoxide dismutase [Fe] (FeSOD)	PF3D7_0814900	22,734	6.8	7.1 %	7.1 %	0
ATP synthase subunit beta, mitochondrial	PF3D7_1235700	58,394	6.4	2.1 %	9.0 %	0
Glutathione *S*-transferase (GST)	PF3D7_1419300	24,789	6.4	11.8 %	21.8 %	0
Glutathione reductase (GR)	PF3D7_1419800.1	56,492	7.9	5.4 %	3.0 %	0
Mitochondrial acidic protein MAM33, putative	PF3D7_1434800	28,872	5.0	15.9 %	15.9 %	0
***Pf*Prx1m wild type, *Pf*Prx1m^{C187S}**				**1**	**2**	**3**
Acyl-CoA synthetase (ACS10)	PF3D7_0525100	76,852	8.2	24.8 %	0	7.0 %

4.1.4 Measurement of the catalytic cysteine pK_a of *Pf*Prxs

For pK_a measurements of the catalytic cysteine residues, the enzyme's ability to reduce H_2O_2, and thus to compete with HRP for the available substrate, was detected for *Pf*Prx1a, *Pf*Prx5, and *Pf*PrxQ$^{1\text{-}164}$ at different Prx concentrations and varying pH values. The slopes of every linearized activity curve at different pH values were plotted against the respective pH values [187], where the highest corresponding activity was set to 100% to compensate for pipetting mistakes or slightly varying H_2O_2 or HRP concentrations. Figure 27 shows sigmoidal fits of the pH dependency of Prx activity and the corresponding pK_a value. The second order rate constants for hydrogen peroxide of *Pf*Prx1a (1.6×10^8 M^{-1} sec^{-1}), *Pf*Prx5 (2.8×10^8 M^{-1} sec^{-1}), and *Pf*PrxQ$^{1\text{-}164}$ (2.2×10^7 M^{-1} sec^{-1}) were determined with the same competition assay at a constant pH value of 7.4.

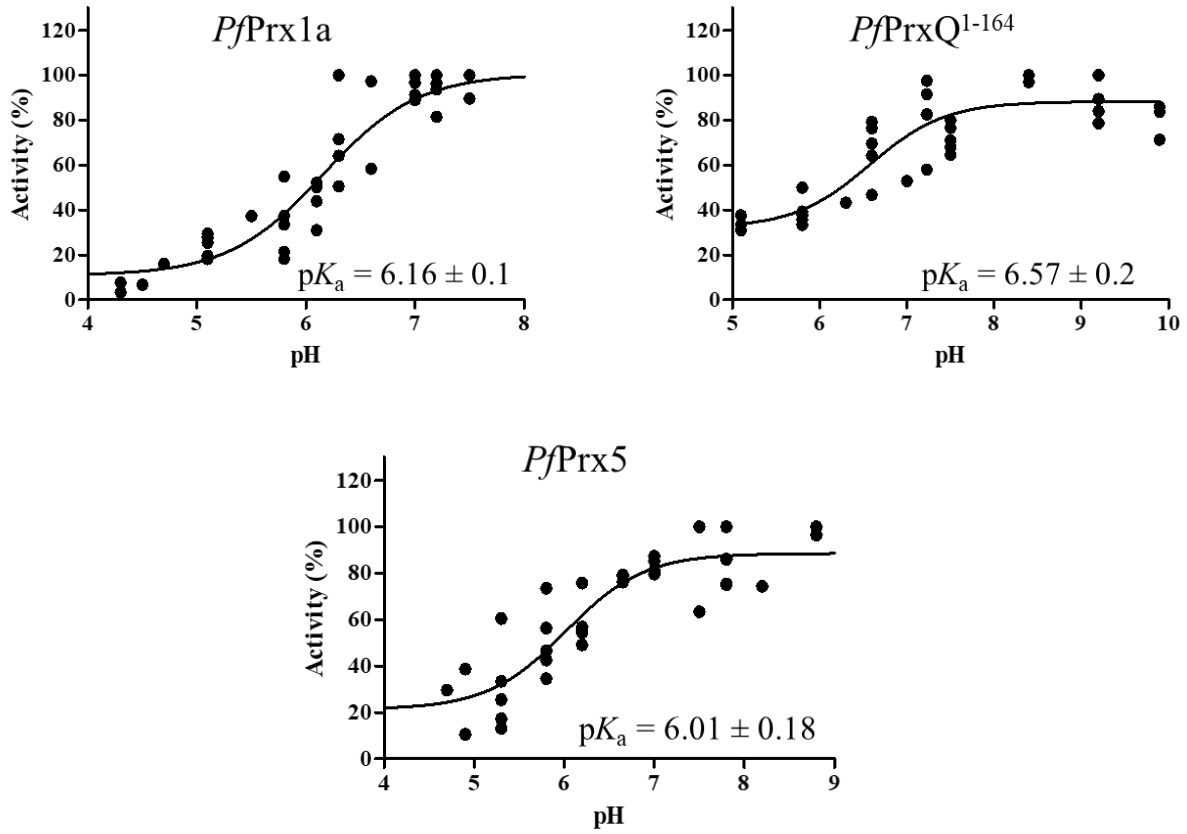

Figure 27: pH-dependent activity curves of *Pf*Prx1a, *Pf*PrxQ$^{1\text{-}164}$, and *Pf*Prx5. pK_a values are mean values ± SE. Measurements were performed in five independent experiments carried out in quadruplicate.

The pK_a determination for *Pf*Prx1m and *Pf*Prx6 were not possible, probably due to hyperoxidation of the enzymes, and delivered no reproducible data. The pK_a for *Pf*Prx5 had been determined prior to this thesis by Dr. Esther Jortzik.

4.1.5 Crystallization of the truncated *Pf*PrxQ$^{1\text{-}164}$

Protein needles of the truncated *Pf*PrxQ$^{1\text{-}164}$ were obtained within three days at RT using the initial Core Suite IV screen (Jena Bioscience). Based on these initial conditions, protein, glycerol, and PEG concentrations, as well as pH values and buffer systems were varied. This led to small protein crystals at pH values of 7.0 and 7.4 (Figure 28 A). Finally, the addition of

2 mM TCEP and 2 mM magnesium acetate to the protein solution and a higher protein concentration (45 mg/mL) provided large protein crystals at 4 °C within one week (Figure 30 B and C).

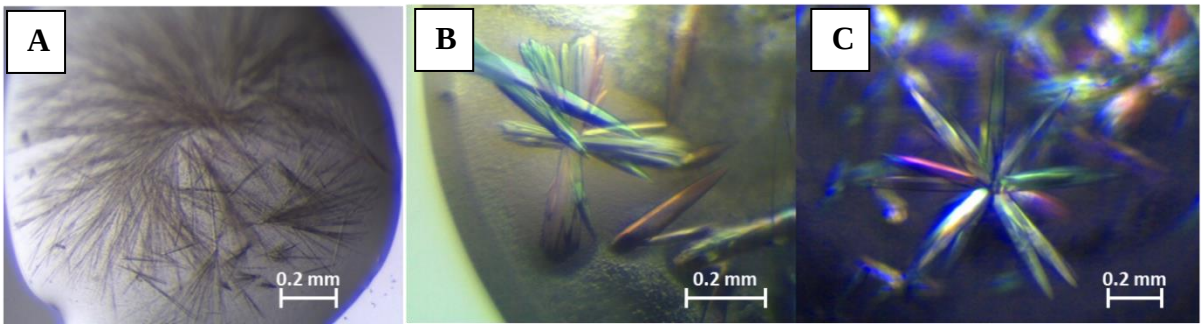

Figure 28: Protein crystals of *Pf*PrxQ$^{1-164}$. A) Protein needles obtained in the initial Core IV Screen (sitting drop): 0.1 M MES, pH 6.0, 30% PEG 600, 5% PEG 1000, 10% glycerol, [*Pf*PrxQ$^{1-164}$]: 17 mg/mL in 50 mM TrisHCl, pH 7.4. B) and C) hanging drop crystals after refinement: 0.1 M MES, pH 7.0, 30% PEG 600, 5% PEG 1000, 10% glycerol. [*Pf*PrxQ$^{1-164}$]: 45 mg/mL in 50 mM TrisHCl, pH 7.4, 2 mM TCEP, 2 mM $Mg(CH_3COO)_2$.

Protein crystals were obtained from truncated *Pf*PrxQ$^{1-164}$ and the truncated mutant *Pf*PrxQ$^{1-164/C103S}$. Single isomorphous replacement with mercury soaking was performed with crystals of truncated *Pf*PrxQ$^{1-164}$ for phasing purposes. Diffraction data of all three crystals were collected at the X10SA beam line of the Swiss Light Source at the Paul Scherrer Institute, Villigen, Switzerland, with a resolution up to 2.5 Å. Dr. Karin Fritz-Wolf assessed the measured data at the Max Plank Institute for Medical Research, Heidelberg. Diffraction patterns were processed with the XDS program package [202] to identify the position and intensity of reflections. The analyzed data showed a systematic obliteration of specific reflections, indicating a space group with a screw axis. However, space groups could not be exactly determined even when all crystals had similar unit cells. The program Xtriage (http://phenix-online.org/documentation/reference/xtriage.html) assumed a possible twinning in crystal symmetry based on the integrated sanity checks of the program. Since the data obtained was of poor quality and the underlying homology model (truncated cysteine mutant of yeast nuclear thiol peroxidase; PDB code: 2a4v) showed only 36% sequence similarity, molecular replacement was inapplicable.

4.2 Protein-protein interaction analysis of *Pf*Prxs and their redoxins

Surface plasmon resonance spectroscopy

A protocol for identifying interacting active site cysteines from peroxiredoxins and their reducing redoxins was developed within this thesis. Prxs, which were immobilized on a CM5 chip by amine coupling, were first oxidized with 500 µM DTNB (solved in running buffer) for 30 sec at 10 µL/min, called conditioning cycle, followed by 5 µM of the respective reduced redoxin for 60 sec at 10 µL/min. The dissociation time was set to 700 sec at a flow rate of 10 µL/min of running buffer. To resolve covalently bound proteins, 500 µM TCEP was injected for 30 sec at 10 µL/min in running buffer. As internal controls, the analytes, in our case the redoxins, were injected as duplicates, and a sample containing no protein was injected in between these replicates as a technical control. All analytes flowed over the active surface and over a reference surface where no protein was immobilized in order to account for unspecific binding events on the carboxymethylated dextran surface.

The prior reduction of the redoxins was performed by 1 mM TCEP for 15 min. The proteins were desalted using desalting columns (Zeba spin) via centrifugation at 2,200 rpm for 2 min following the manufacturer's protocol. Figures 29 shows representative sensograms for the interaction of *Pf*Prx and *Pf*Trx.

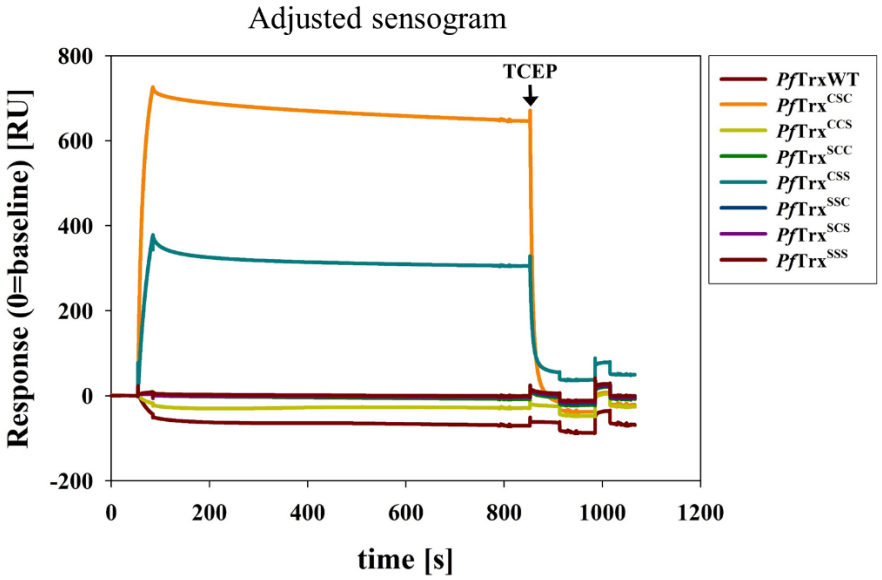

Figure 29: Interaction profile of *Pf*Prx1a^{C50S} with *Pf*Trx wild type and its Cys mutants. Ligand oxidation was achieved with 0.5 mM DTNB prior to every cycle. Reduced analytes were injected for 30 sec, followed by a 700 sec phase of dissociation with running buffer. After the dissociation phase, 0.5 mM TCEP was injected for 30 sec into the flow cell (black arrow) followed by 60 sec of running buffer injection and a conditioning cycle with 0.5 mM DTNB to oxidize the ligand for the next cycle.

In the corresponding sensogram, an interaction between the peroxiredoxin and the redoxin was observed as an increase in response units during the association phase. A decrease in RU displayed the dissociation of the redoxin. When this interaction event was mediated by a disulfide bridge, the RU stayed constant, representing a plateau in RU over time. The covalently bound redoxins were then resolved with the reducing agent TCEP at the end of the dissociation phase, resulting in an instant, steep decrease of RU within the plot. A covalent binding event was concluded every time a significant, steep drop of RU was observed directly after TCEP injection. To compare binding events between different Cys mutants of redoxins and Prxs the same amount of redoxins was used in the experiments (5 µM). With the used concentration of redoxins (and its mutants) some interactions resulted in very distinct sensograms (cylindrical) and others showed no interaction at all. Since only one concentration of analyte was used, it is not possible to calculate an association and a dissociation rate constant (describes kinetics), or the affinity constant (strength of interaction) via the described approach.

Covalent binding events were monitored between *Pf*Prx1a and *Pf*Trx^{CSC} as well as between *Pf*Prx1a and *Pf*Trx^{CSS}. The same result was found for the peroxidatic Cys mutant *Pf*Prx1a^{C50S}. The resolving Cys mutant *Pf*Prx1a^{C170S} and the mutant lacking both active site cysteines showed covalent binding with *Pf*Trx^{CSC} as well. Since in *Pf*Prx1a a third cysteine (Cys74) is located among the active site cysteines, an additional C74A mutant was used, which had already been constructed in the Becker lab for prior experiments. The Cys mutants containing a C74A mutation (*Pf*Prx1a$^{C50S/C74A}$, *Pf*Prx1a$^{C74A/C170S}$, *Pf*Prx1a$^{C50S/C74A/C170S}$) showed no covalent binding events except for the *Pf*Prx1a$^{C74A/C170S}$ and *Pf*Prx1a^{C74A} mutants. No covalent interaction of Grx with *Pf*Prx1a and all their mutants was found in the conducted experiments (Table 5).

Table 5: Interaction of *Pf*Prx1a with *Pf*Trx and *Pf*Grx. The x indicates a confirmed event.

	***Pf*Prx1a**		***Pf*Prx1a^{C50S}**		***Pf*Prx1a^{C170S}**		***Pf*Prx1a$^{C50S/C170S}$**	
	covalent binding	interaction	covalent binding	interaction	covalent binding	interaction	covalent binding	interaction
*Pf*Trx						**x**		**x**
*Pf*Trx^{CSC}	**x**		**x**		**x**		**x**	
*Pf*Trx^{CCS}						**x**		**x**
*Pf*Trx^{SCC}								
*Pf*Trx^{CSS}	**x**		**x**			**x**		**x**
*Pf*Trx^{SSC}								**x**
*Pf*Trx^{SCS}								
*Pf*Trx^{SSS}		**x**		**x**		**x**		**x**
*Pf*Grx		**x**		**x**				**x**
*Pf*Grx^{CSC}		**x**		**x**				**x**
*Pf*Grx^{CCS}		**x**		**x**				**x**
*Pf*Grx^{SCC}		**x**		**x**				**x**
*Pf*Grx^{CSS}		**x**		**x**				**x**
*Pf*Grx^{SSC}		**x**		**x**				**x**
*Pf*Grx^{SCS}		**x**		**x**				**x**
*Pf*Grx^{SSS}		**x**		**x**				**x**
	***Pf*Prx1a^{C74A}**		***Pf*Prx1a$^{C50S/C74A}$**		***Pf*Prx1a$^{C74A/C170S}$**		***Pf*Prx1a$^{C50S/C74A/C170S}$**	
	covalent binding	interaction	covalent binding	interaction	covalent binding	interaction	covalent binding	interaction
*Pf*Trx								
*Pf*Trx^{CSC}	**x**				**x**			
*Pf*Trx^{CCS}								
*Pf*Trx^{SCC}								
*Pf*Trx^{CSS}	**x**					**x**		
*Pf*Trx^{SSC}								
*Pf*Trx^{SCS}								
*Pf*Trx^{SSS}								
*Pf*Grx		**x**				**x**		
*Pf*Grx^{CSC}		**x**				**x**		
*Pf*Grx^{CCS}		**x**				**x**		
*Pf*Grx^{SCC}	**x**							
*Pf*Grx^{CSS}		**x**				**x**		
*Pf*Grx^{SSC}		**x**				**x**		
*Pf*Grx^{SCS}		**x**				**x**		
*Pf*Grx^{SSS}		**x**				**x**		

Concerning the interaction of *Pf*Prx1m with *Pf* redoxins, a covalent binding event was monitored for the interaction of *Pf*Prx1m with *Pf*Trx^{CSC}, and for the interaction of the peroxidatic cysteine mutant (*Pf*Prx1m^{C67S}) with *Pf*Trx^{CSC} and *Pf*Trx^{CSS} (Table 6). Our results indicate that the resolving cysteine mutant (*Pf*Prx1m^{C187S}) and the double active site mutant *Pf*Prx1m$^{C67S/C187S}$ were not covalently bound by thioredoxin or glutaredoxin and their respective active site cysteine mutants.

Table 6: Interaction of *Pf*Prx1m with *Pf*Trx and *Pf*Grx. The x indicates a confirmed event.

	***Pf*Prx1m**		***Pf*Prx1m^{C67S}**		***Pf*Prx1m^{C187S}**		***Pf*Prx1m$^{C67S/C187S}$**	
	covalent binding	interaction	covalent binding	interaction	covalent binding	interaction	covalent binding	interaction
*Pf*Trx		x						
*Pf*Trx^{CSC}	x		x			x		x
*Pf*Trx^{CCS}						x		
*Pf*Trx^{SCC}		x						
*Pf*Trx^{CSS}		x	x			x		x
*Pf*Trx^{SSC}		x						
*Pf*Trx^{SCS}		x						
*Pf*Trx^{SSS}						x		x
*Pf*Grx		x		x		x		x
*Pf*Grx^{CSC}		x		x		x		x
*Pf*Grx^{CCS}		x		x		x		x
*Pf*Grx^{SCC}		x						
*Pf*Grx^{CSS}		x		x				x
*Pf*Grx^{SSC}		x		x				x
*Pf*Grx^{SCS}		x		x				x
*Pf*Grx^{SSS}		x		x				x

A covalent binding was observed during the interaction of the peroxidatic Cys mutant of *Pf*Prx5 (*Pf*Prx5^{C117S}) with *Pf*Trx^{CSC}, however no covalent interaction between wild type *Pf*Prx5 and *Pf*Trx^{CSC} could be detected. *Pf*Prx5 wild type was generally prone to rapid hyperoxidation, known from prior experiments. To detect whether the second more N-terminal located cysteine (Cys143), which is not known to be part of the active site, is able to be bound by Trx, *Pf*Prx5^{C143S} was immobilized as a ligand, oxidized with DTNB, and confronted with *Pf*Trx and *Pf*Grx, and its cysteine mutants. Out of the arising sensograms it could be observed that *Pf*Trx^{CSC} was bound covalently to *Pf*Prx5^{C143S}. Additionally, non-covalent interactions between *Pf*Grx and its mutants with *Pf*Prx5^{C143S} were markedly decreased (Table 7).

Table 7: Interaction of *Pf*Prx5 with *Pf*Trx and *Pf*Grx. The x indicates a confirmed event.

	***Pf*Prx5**		***Pf*Prx5^{C117S}**		***Pf*Prx5^{C143S}**	
	covalent binding	interaction	covalent binding	interaction	covalent binding	interaction
*Pf*Trx		x				
*Pf*Trx^{CSC}		x	x		x	
*Pf*Trx^{CCS}		x		x		x
*Pf*Trx^{SCC}		x				x
*Pf*Trx^{CSS}						x
*Pf*Trx^{SSC}		x				x
*Pf*Trx^{SCS}		x				x
*Pf*Trx^{SSS}				x		x
*Pf*Grx		x		x		
*Pf*Grx^{CSC}		x		x		x
*Pf*Grx^{CCS}		x		x		

*Pf*Grx^{SCC}		x		x		
*Pf*Grx^{CSS}		x		x		
*Pf*Grx^{SSC}		x		x		
*Pf*Grx^{SCS}		x		x		
*Pf*Grx^{SSS}		x		x		

*Pf*Prx6 wild type and its peroxidatic Cys mutant *Pf*Prx6^{C47S} showed both covalent interaction events with the resolving Cys mutant of *Pf*Trx (*Pf*Trx^{CSC}). Non-covalent interaction between *Pf*Prx6 wild type and the redoxins *Pf*Trx and its mutants (excluding *Pf*Trx^{SSS}), and *Pf*Grx and its mutants could be observed (Table 8).

Table 8: Interaction of *Pf*Prx6 with *Pf*Trx and *Pf*Grx. The x indicates a confirmed event.

	***Pf*Prx6**		***Pf*Prx6^{C47S}**	
	covalent binding	interaction	covalent binding	interaction
*Pf*Trx		x		
*Pf*Trx^{CSC}	x		x	
*Pf*Trx^{CCS}		x		
*Pf*Trx^{SCC}		x		
*Pf*Trx^{CSS}		x		
*Pf*Trx^{SSC}		x		
*Pf*Trx^{SCS}		x		
*Pf*Trx^{SSS}				
*Pf*Grx		x		
*Pf*Grx^{CSC}		x		
*Pf*Grx^{CCS}		x		
*Pf*Grx^{SCC}		x		
*Pf*Grx^{CSS}		x		
*Pf*Grx^{SSC}		x		
*Pf*Grx^{SCS}		x		
*Pf*Grx^{SSS}		x		

*Pf*PrxQ$^{1\text{-}164}$ and the resolving Cys mutant *Pf*PrxQ$^{1\text{-}164/C103S}$ were both able to covalently interact with *Pf*Trx^{CSC}, whereas *Pf*PrxQ$^{1\text{-}164/C103S}$ was also able to build a covalent bond with *Pf*Trx^{CSS}. However, for the interaction of the peroxidatic Cys mutant of *Pf*PrxQ$^{1\text{-}164}$ (*Pf*PrxQ$^{1\text{-}164/C156S}$) with *Pf*Trx^{CSC} a covalent binding was not observed. All other combinations of Cys mutations in *Pf*Trx, as well as its wild type, showed non-covalent interactions or any observed interactions with *Pf*PrxQ$^{1\text{-}164}$ wild type or its Cys mutants. *Pf*Grx and all of its active site mutants showed interactions with all variants of active site mutations and the wild type of *Pf*PrxQ$^{1\text{-}164}$ (Table 9).

Table 9: Interaction of *Pf*PrxQ$^{1-164}$ with *Pf*Trx and *Pf*Grx. The x indicates a confirmed event.

	***Pf*PrxQ$^{1-164}$**		***Pf*PrxQ$^{1-164/C56S}$**		***Pf*PrxQ$^{1-164/C103S}$**		***Pf*PrxQ$^{1-164/C56S/C103S}$**	
	covalent binding	interaction	covalent binding	interaction	covalent binding	interaction	covalent binding	interaction
*Pf*Trx				x				
*Pf*Trx^{CSC}	x			x	x			x
*Pf*Trx^{CCS}		x		x		x		x
*Pf*Trx^{SCC}								
*Pf*Trx^{CSS}		x		x	x			
*Pf*Trx^{SSC}		x		x		x		x
*Pf*Trx^{SCS}						x		
*Pf*Trx^{SSS}		x		x		x		x
*Pf*Grx		x		x		x		x
*Pf*Grx^{CSC}		x		x		x		x
*Pf*Grx^{CCS}		x		x		x		x
*Pf*Grx^{SCC}		x		x		x		x
*Pf*Grx^{CSS}		x		x		x		x
*Pf*Grx^{SSC}		x		x		x		x
*Pf*Grx^{SCS}		x		x		x		x
*Pf*Grx^{SSS}		x		x		x		x

To confirm the observed results of the SPR based approach and to compare different methods of PPI-detection, electrophoretic mobility shift assays, microscale thermophoresis, and isothermal titration calorimetry were performed with *Pf*Prx1a and *Pf*Trx Cys mutants.

Electrophoretic mobility shift assay

As shown in Figure 30, *Pf*Trx^{CSC} is able to covalently bind *Pf*Prx1a wt under non-reducing conditions. Under reducing conditions and sample boiling, *Pf*Prx1a wt occurs mainly as a monomer at 23 kDa (lanes 1) and under non-reducing conditions as monomer and dimer at 23 kDa and 46 kDa, respectively (lanes 4). In the Coomassie-stained gel (A) as well as in the anti-*Pf*Trx Western blot (D; lane 2, 5 and 6), a second band of *Pf*Trx^{CSC} appears at ~25 kDa and it is therefore suggested to be a Trx dimer. A band shift due to covalent binding of both proteins to each other can be demonstrated in lanes 6 (non-reducing conditions without sample boiling) in contrast to lanes 3 (reducing conditions). All three Western blots (anti-His, anti-*Pf*Prx1a, and anti-*Pf*Trx) as well as the Coomassie-stained gel indicate a binding of both the *Pf*Prx1a monomer and dimer with *Pf*Trx^{CSC}.

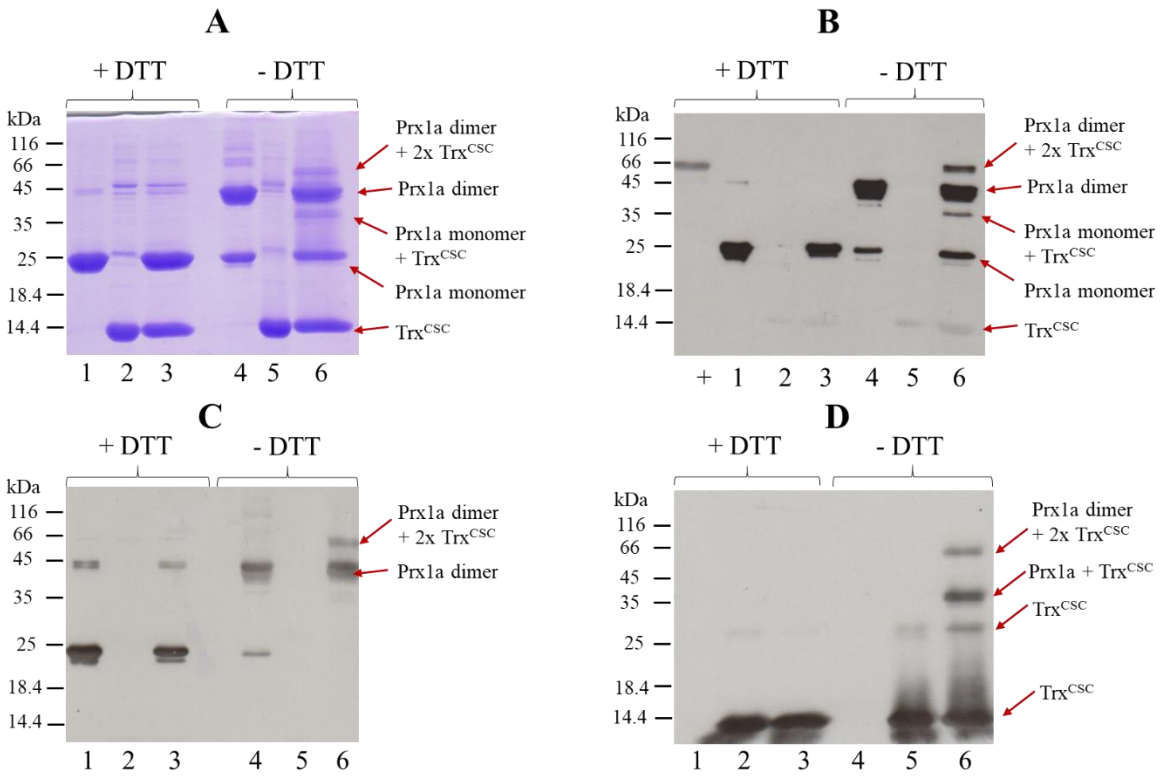

Figure 30: Western blot confirmation of covalent binding in *Pf*Prx1a and *Pf*Trx1. A) Coomassie staining, B) anti-His-tag Western blot containing a His-tagged *Pf*GR (57.2 kDa) as His-positive control marked with +, C) anti-*Pf*Prx1a Western blot, D) anti-*Pf*Trx1 Western blot 1: reduced *Pf*Prx1a wt, 2: reduced *Pf*Trx1, 3: reduced coupled *Pf*Prx1a wt + *Pf*Trx1, 4: oxidized *Pf*Prx1a wt, 5: reduced *Pf*Trx1, 6: coupled *Pf*Prx1a wt + *Pf*Trx1 without DTT. Arrows are indicating the respective protein, oligomerization or coupling.

Furthermore, a regioselectivity of *Pf*Trx towards the respective active site cysteines of *Pf*Prx1a was confirmed via electrophoretic mobility shift assays and add-on Western blot analyses (Figure 33). The protein immunoblots revealed a binding of *Pf*Trx^{CSC} to the C_P of *Pf*Prx1a as shown with the SPR-based approach. A binding of *Pf*Trx^{CSC} to the C_R of *Pf*Prx1a was not detected, which corresponds to the SPR data as well. When incubated with *Pf*Prx1a wt, *Pf*Trx^{CSC} was able to build stable complexes (under non-reducing conditions) with the Prx monomer (~35 kDa) and dimer (~70 kDa), following a 1:1 stoichiometry, which was confirmed with anti-*Pf*Prx1a and anti-*Pf*Trx Western blots (see Figure 31). *Pf*Trx^{CSC} was also able to bind covalently to *Pf*Prx1a^{C170S}, confirming the C_P as a target for *Pf*Trx^{CSC}. In Figure 32 a double band was observed for the *Pf*Prx1a^{C170S} monomer in the anti-His and in the anti-*Pf*Prx1a WB. Here, *Pf*Trx^{CSC} is able to bind both the full-length Prx monomer mutant and the fragmented monomeric Prx1a mutant, visible in the anti-*Pf*Prx1a and anti-*Pf*Trx WB. As shown in the immunoblots, *Pf*Trx^{CSC} was not able to bind the C_P mutants of *Pf*Prx1a (*Pf*Prx1a$^{C50S/C74A}$) demonstrated in all three WBs. Due to this, it should be noted that the applied antibodies recognizing *Pf*Prx1a and *Pf*Trx cross react slightly with both proteins. A distinct discrimination of identified proteins is however possible by comparing lanes 4 and 5 to lane 6. A covalent complex binding of both proteins (mobility shift) must cause every positive signal not visible in lanes 4 and 5 but occurring in lane 6.

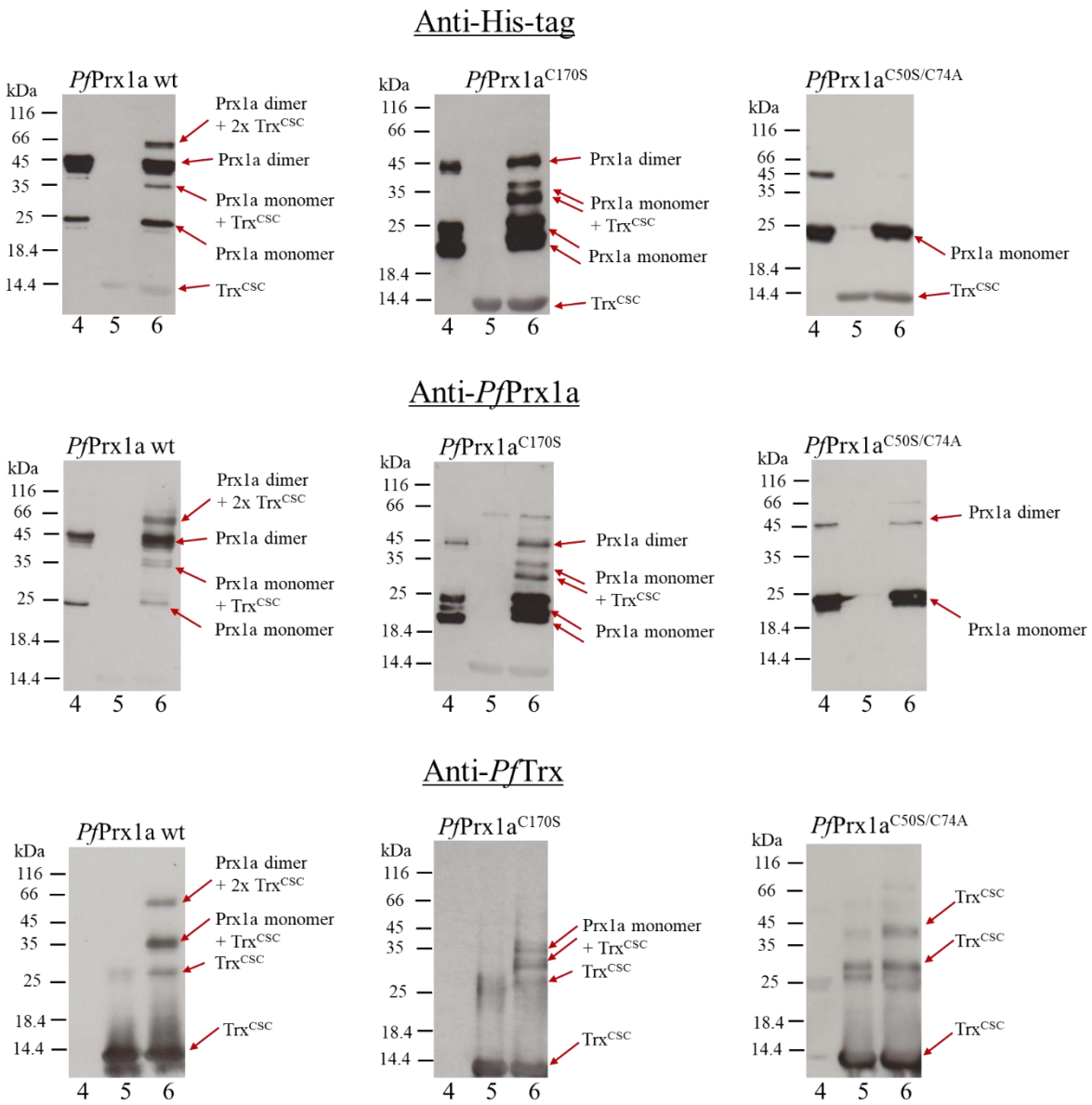

Figure 31: Western blot confirmation of cysteine-dependent regioselectivity of *Pf*Prx1a interacting with *Pf*Trx1. A juxtaposition of the anti-His, anti-*Pf*Prx1a, and anti-*Pf*Trx Western blots of *Pf*Prx1a wt, *Pf*Prx1aC170S, *Pf*Prx1a$^{C150S/C74A}$ and *Pf*Trx^{CSC} is represented. 4: oxidized *Pf*Prx1a wt, 5: reduced *Pf*Trx1, 6: coupled *Pf*Prx1a wt + *Pf*Trx1 without DTT. Arrows indicate the respective protein, oligomerization, or coupling.

Microscale thermophoresis

For protein interaction analyses via MST, two representative protein pairs were selected that showed different interaction behavior based on the SPR spectroscopy experiments performed. The interaction of *Pf*Prx1a wt and *Pf*Trx^{CSC} was chosen to represent a covalent binding and the interaction of *Pf*Prx1a wt and *Pf*Trx^{SSS} served as example for a non-covalent interaction event. All assays were performed in triplicate.

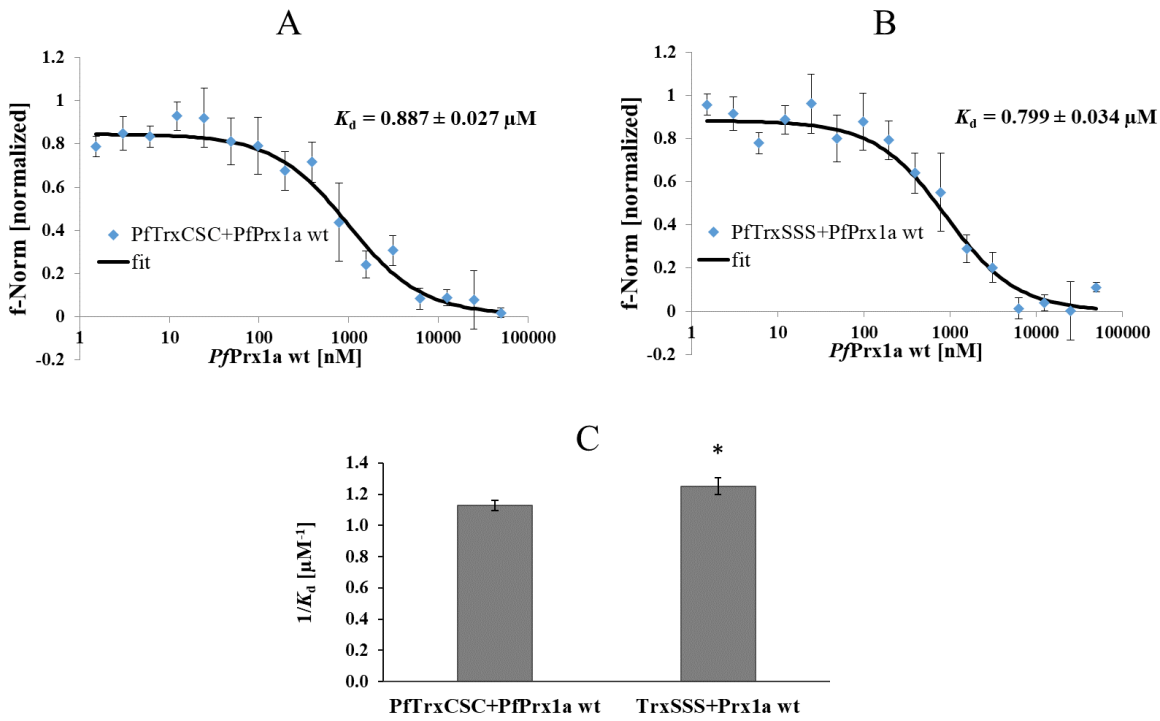

Figure 32: Quantitative determination of the interactions between *Pf*Prx1a and *Pf*Trx Cys mutants. A) Interaction analysis of *Pf*Prx1a wt and *Pf*Trx^{CSC}. B) Interaction analysis of *Pf*Prx1a wt and *Pf*Trx^{SSS}. C) Association constant (1/K_d) of the interaction between *Pf*Prx1a wt and *Pf*Trx^{CSC} or *Pf*Trx^{SSS}, respectively. A student's unpaired *t*-test with a 95% confidence level was performed in order to compare means. *p<0.05, **p<0.01, ***p<0.001

MST analysis showed a dissociation constant (K_d) of 0.887 ± 0.027 µM and an association constant (K_a) of 1.127 ± 0.034 µM^{-1} for the interaction of *Pf*Prx1a wt and *Pf*Trx^{CSC} and a K_d of 0.799 ± 0.034 µM and a K_a of 1.252 ± 0.053 µM^{-1} for the interaction of *Pf*Prx1a wt and *Pf*Trx^{SSS} (Figure 32). An interaction of the respective proteins was thereby proven. Both interactions showed a significant difference in K_d and K_a to each other, with a p-value of 0.025. Since both dose-response curves had similar shapes, a discrimination between covalent and non-covalent binding was not possible, and a covalent binding could not be concluded based on these data.

Isothermal titration calorimetry

In traditional association experiments with ITC, a titrant is titrated to a second molecule. The arising and fitted reaction enthalpy is thereby illustrated as a declining or ascending sigmoidal curve out of the emerging isotherms (rate of heat release) (see Fig. 20 in Material & Methods). In such experiments, initially titrated molecules are less abundant in the analytical cell and are bound immediately by the more abundant molecules already present in the cell. By injecting more titrant over time, the first molecules begin to saturate the second interaction partner, resulting in a sigmoidally shaped curve. Unfortunately, a test series of association experiments provided no reproducible data, and the assay set-up was shifted to dissociation experiments.

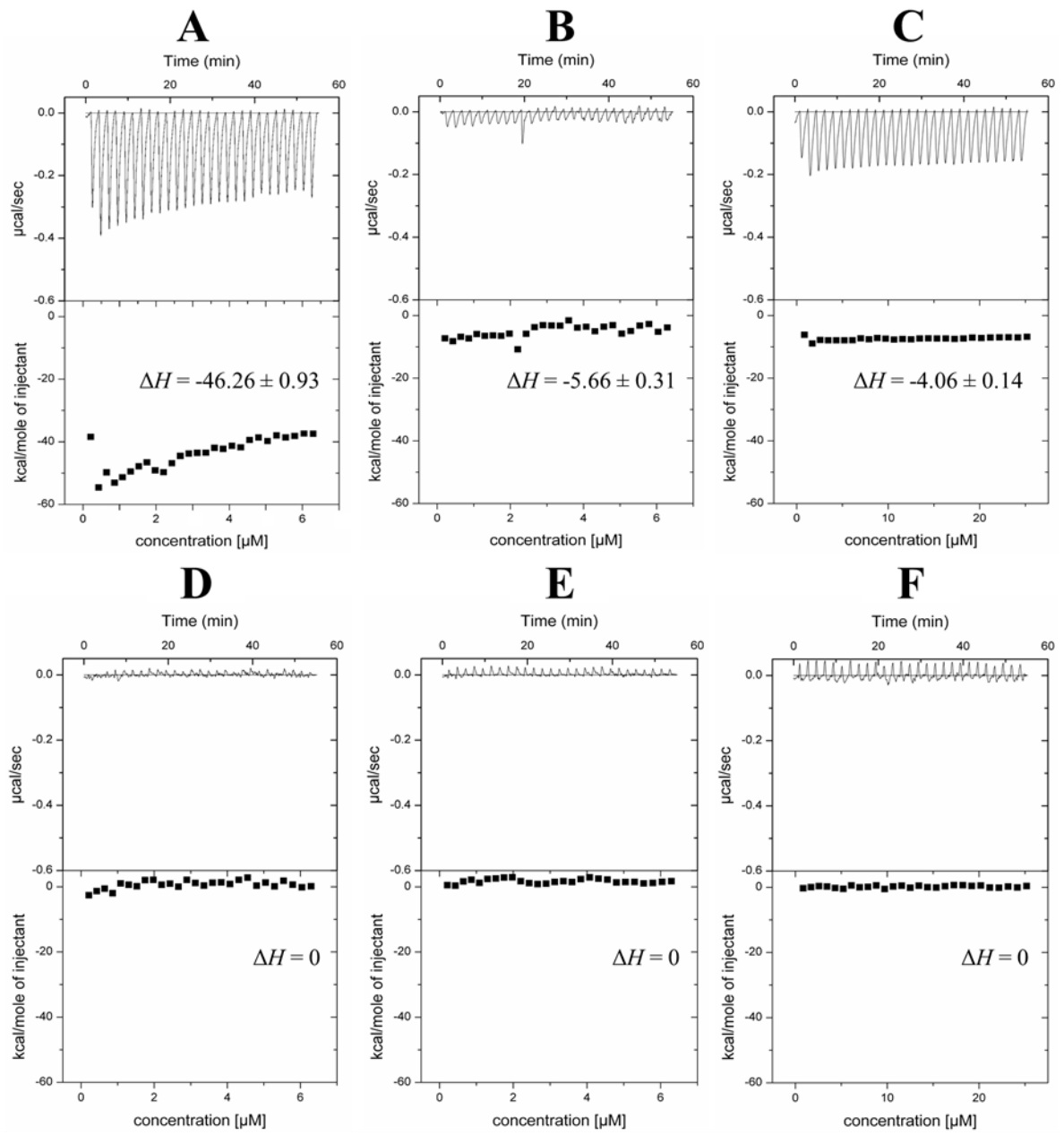

Figure 33: Dissociative calorimetric titration of *Pf*Prx1a wt coupled with *Pf*Trx^{CSC} and *Pf*Trx^{SSS}. In A) oxidized *Pf*Prx1a wt incubated with reduced *Pf*Trx^{CSC} and then titrated in US buffer containing 1 mM TCEP (n=3) and in B) oxidized *Pf*Prx1a wt incubated with reduced *Pf*Trx^{SSS} and then titrated in US buffer containing 1 mM TCEP (n=4) are shown. Controls are composed out of C) oxidized *Pf*Prx1a wt titrated in US buffer containing 1 mM TCEP (n=4), D) oxidized *Pf*Prx1a wt incubated with reduced *Pf*Trx^{CSC} and then titrated in US buffer (n=2), E) oxidized *Pf*Prx1a wt incubated with *Pf*Trx^{SSS} titrated in US buffer (n=2), and F) reduced *Pf*Trx^{CSC} titrated in US buffer containing 1 mM TCEP (n=2). Representative measurements out of different test series and the mean ΔH (± SE) of the respective measurements are depicted.

In the dissociation experiments performed (Figure 33), the titrant (protein or coupled proteins) was titrated to US buffer with and without 1 mM TCEP. In the latter, the second interaction partner (TCEP) is not limited and is therefore able to reduce the same amount of titrant in every single injection step. Therefore, the arising isotherms are approximately equal in every titration step, and the curve for reaction enthalpy obtains no sigmoidal shape. This is also the reason why these dissociation experiments are not able to provide information about association constants (slope of the curve at the inflection point), dissociation constants (inverse of association constant), and stoichiometry of the binding partners (molar ratio at the inflection point) but can generate enthalpy values. These enthalpy values (ΔH) reflect the change in

internal energy of the respective chemical reactions (area under the isotherm), where the first titration step provides the most representative Δ*H*. In Figure 35, representative raw data and dissociation isotherms of all performed dissociation experiments and their controls are shown. The titration of coupled *Pf*Prx1a wt and *Pf*Trx^{CSC} in 1 mM TCEP buffer (A) generated a significantly higher enthalpy value (Δ*H* = -46.26 ± 0.93) than the titration of coupled *Pf*Prx1a wt and *Pf*Trx^{SSS} in 1 mM TCEP buffer (B) (Δ*H* = -5.66 ± 0.31). The Δ*H* for the latter is therefore caused by a change in internal energy of the reduction of the disulfide bridge of the artificially oxidized Prx (Prx-TNB) shown in Figure 35 C. A titration of the stated couples in US buffer (D and E) and the titration of reduced *Pf*Trx^{CSC} generate no heat changes at all (F).

4.3 Kinetic characterization of the human thioredoxin glutathione reductase

4.3.1 Heterologous overexpression and purification of hTGR and hTGR^{U642C}

Within this thesis, the heterologous overexpression and purification of hTGR were optimized. The construct was cloned in pET28 and co-transformed with pSelABC (containing *SelA*, *B*, and *C* genes for proper Sec incorporation) in competent BL21 cells to obtain the soluble, pure protein with a concentration of ~2 mg/mL out of 1 L *E. coli* culture. The same protocols, without adding Na_2SeO_3 at the time of induction, were used for the Sec→Cys mutant. Figure 34 shows a representative elution profile of hTGR wild type (74.1 kDa) and a Western blot of hTGR wild type using anti-His_6 antibodies.

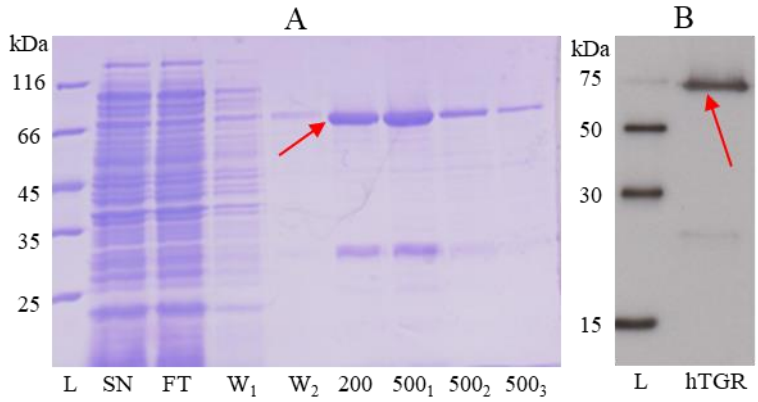

Figure 34: Purification of hTGR wild type. A) Coomassie stained elution profile of hTGR wild type on a 12 % SDS PAGE, B) Western blot confirmation of His_6-tagged hTGR. M: protein ladder, SN: supernatant, FT: flow through, W_1: 20 mM imidazole, W_2: 30 mM imidazole, 200-500: fraction eluted with 200-500 mM imidazole. Red arrows indicate hTGR.

In the Coomassie-stained SDS-PAGE, a prominent band at ~30 kDa could be observed, which was not removable via size exclusion chromatography or by adding 1 mM DTT, 1 M NaCl, 1 mM guanidine hydrochloride, or 1 M NaCl + 20 mM DTT performed in the master's thesis of Eva König [203] in parallel to this thesis. Mass spectrometry (MS) analysis identified the additional protein band as a degradation product of hTGR (see Supplementary Table 1 for the corresponding MS data).

The protocols for heterologous overexpression and purification of all Sec-containing hTGR mutants (hTGR$^{151-643}$, hTGR^{H78A}, hTGR^{C133S}, hTGR^{D134A}, and hTGR$^{C133S/D134A}$) were identical

to the protocol developed for the wild type enzyme (see Chapters 3.2.2.2 and 3.3.2.2). Due to this, the isolated Grx domain and the TrxR domain were overexpressed and purified successfully (see Figure 35).

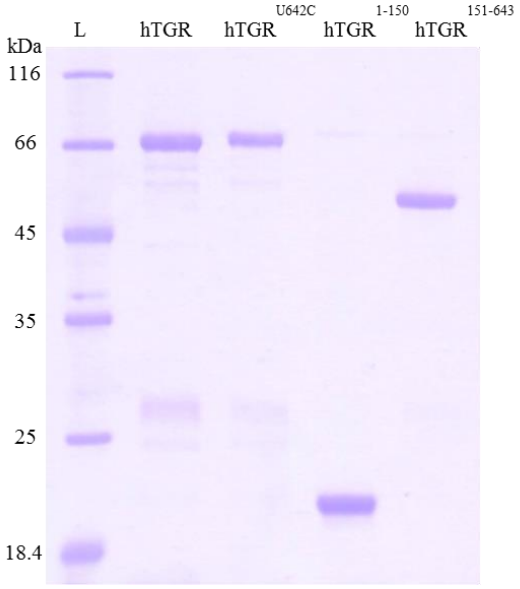

Figure 35: Protein profile of purified recombinant hTGRs and their isolated domains. Purified recombinant wild type hTGR, the Sec→Cys mutant $hTGR^{U642C}$, the isolated Grx domain $hTGR^{1-150}$ and TrxR domain $hTGR^{151-643}$ after SDS gel electrophoresis and staining with Coomassie Brilliant Blue.

In order to identify the oligomerization behavior of hTGR wild type, size exclusion chromatography was performed in US buffer, pH 7.2, characterizing hTGR as a dimer with an elution peak at about 75 mL, which corresponds to approximately 180 kDa (Figure 36).

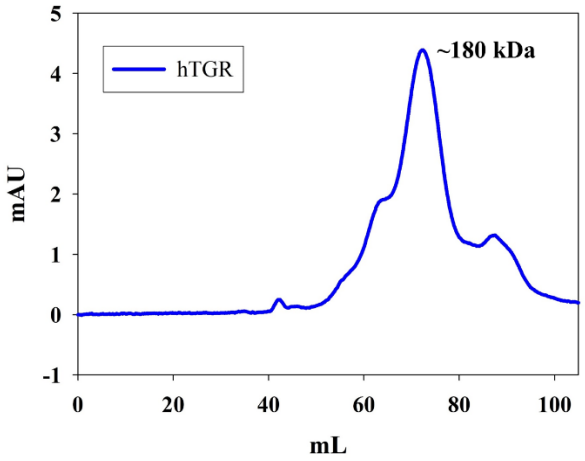

Figure 36: Oligomerization behavior of hTGR wild type. Representative size-exclusion chromatogram of hTGR after His_6-tag purification.

4.3.2 Absorption titration spectrum for hTGR

The EH_2 species (two electron reduced enzyme) of hTGR has a wavelength absorption centered at around 540 nm due to a thiolate-flavin charge transfer complex. Figure 37 demonstrates the titration of hTGR with NADPH, indicating a conversion of E_{ox} to EH_2 at 540 nm. At this

wavelength the absorbance rises with increasing NADPH concentrations, used for reduction of hTGR, and falls via oxidation with hTrx, whereas the absorption at 463 nm decreases during reduction and increases during oxidation. Therefore, a functional active thiolate-flavin charge transfer complex was confirmed within hTGR, even though the enzyme seems to be not fully saturated with the prosthetic group (Figure 37).

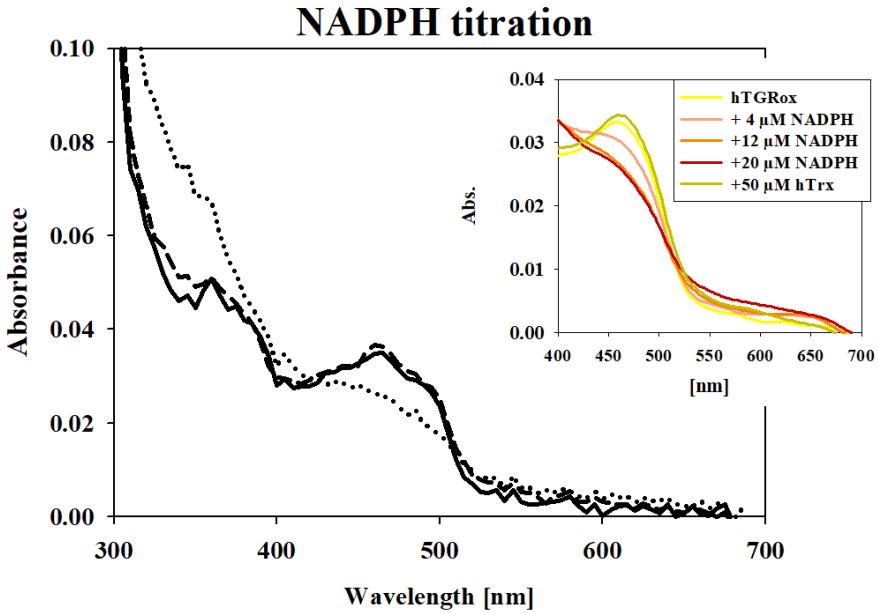

Figure 37: **NADPH titration of hTGR wild type.** Spectrum between 300 and 700 nm represent 20 µM oxidized hTGR (—), enzyme after reduction with 20 µM NADPH (•••), and reoxidized enzyme with 50 µM hTrx (---). The insert shows exponentially smoothed data (polynomial degree = 1) of the reduction of 20 µM recombinant hTGR wild type with 4, 12, and 20 µM NADPH followed by reoxidation of the enzyme with 50 µM hTrx. Resulting spectra were monitored after each titration step. A representative titration spectrum between 400 and 700 nm, where the characteristic changes (decrease at 463 nm and increase at 540 nm upon reduction) become evident, is shown. Reduction of 20 µM hTGR with 4, 12, and 20 µM of NADPH occured. Rapid reaction kinetic traces were observed at 463 nm and 540 nm for the reduction of hTGR by increasing concentrations of NADPH and reoxidizing of hTGR with 50 µM of hTrx.

4.3.3 Kinetic parameters of hTGR and hTGR^{U642C}

In order to determine the specific activity and steady-state kinetic parameters of hTGR wild type and the Sec mutant hTGR^{U642C}, a thioredoxin reductase assay, DTNB assay, HEDS assay, and glutathione reductase assay were performed. For this, one substrate concentration was set to a fixed optimum and the other substrate concentration was varied. The velocity was then plotted against the concentration of the varied substrate and fitted to the Michaelis-Menten equation.

4.3.3.1 Thioredoxin reductase activity

In the TrxR assay system, hTGR^{U642C} showed a significantly decreased specific activity compared to the wild type enzyme. In hTGR^{U642C}, the K_M-value for hTrx was significantly higher than in the wt enzyme, whereas the K_M for NADPH was decreased (Figure 38). Additionally, k_{cat} values for hTrx and NADPH were lowered. Table 10 summarizes the kinetic parameters of hTGR wild type and hTGR^{U642C} in the thioredoxin reductase assay.

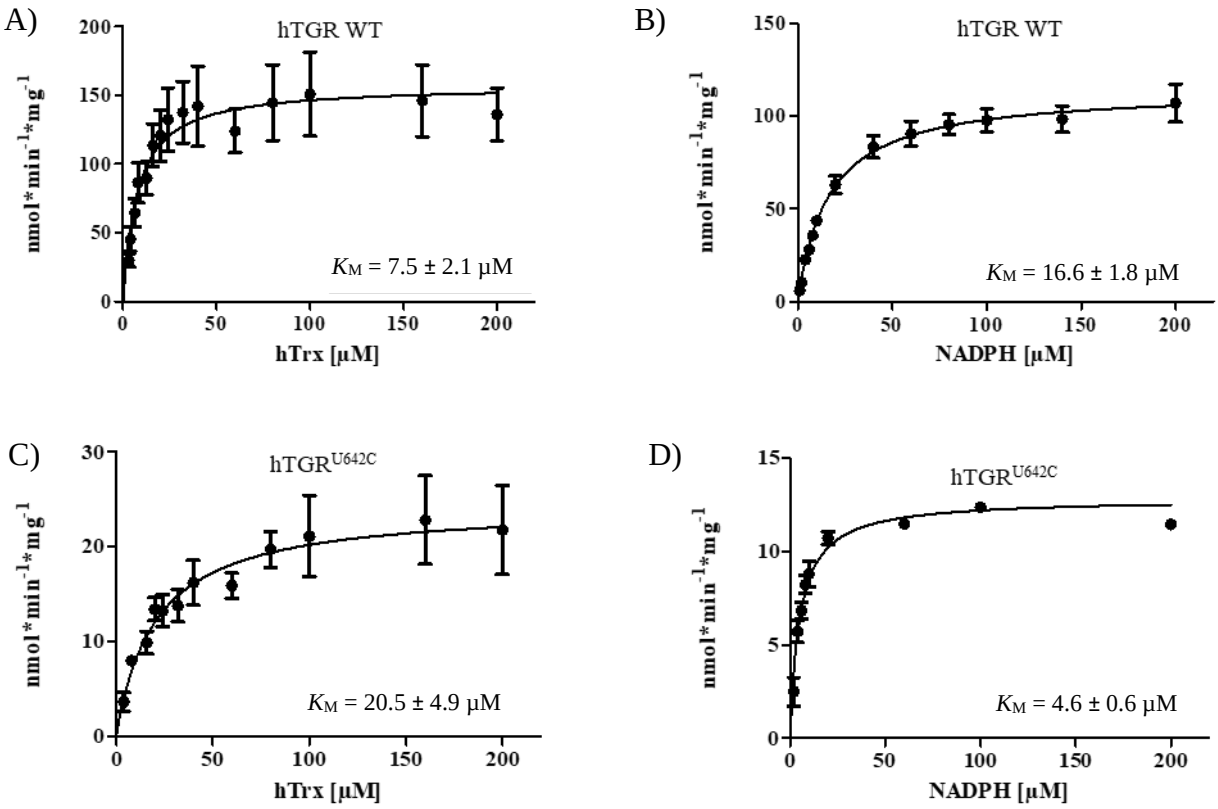

Figure 38: K_M for hTrx and NADPH in hTGR wild type and hTGR^{U642C}. A) K_M for hTrx in hTGR wild type in the presence of 100 µM NADPH. B) K_M for NADPH in hTGR wild type in the presence of 20 µM hTrx. C) K_M for hTrx in hTGR^{U642C} in the presence of 100 µM NADPH. D) K_M for NADPH in hTGR^{U642C} in the presence of 20 µM hTrx. Measurements were performed in at least three independent experiments.

Table 10: Kinetic parameters of hTGR wild type and hTGR^{U642C} in the TrxR assay.

	hTGR	*hTGR^{U642C}*
Specific activity [nmol*min^{-1}*mg^{-1}]	94.7 ± 10.6	12.5 ± 0.5***
K_M for hTrx [µM]	7.5 ± 2.1	20.5 ± 4.9***
K_M for NADPH [µM]	16.6 ± 1.8	5.1 ± 0.6***
k_{cat} for hTrx [s^{-1}]	0.18 ± 0.07	0.02 ± 0.01***
k_{cat} for NADPH [s^{-1}]	0.2 ± 0.12	0.015 ± 0.001*

Values represent mean values ± SE of at least three independent experiments. The kinetic characteristics given here were determined using the TrxR assay. A student's unpaired *t*-test with a 95% confidence level was performed in order to compare means. $^{*}p<0.05$, $^{**}p<0.01$, $^{***}p<0.001$.

Kinetic parameters were also determined in the DTNB assay. Figure 39 shows representative Michaelis-Menten curves for hTGR wild type and hTGR^{U642C} in the DTNB assay.

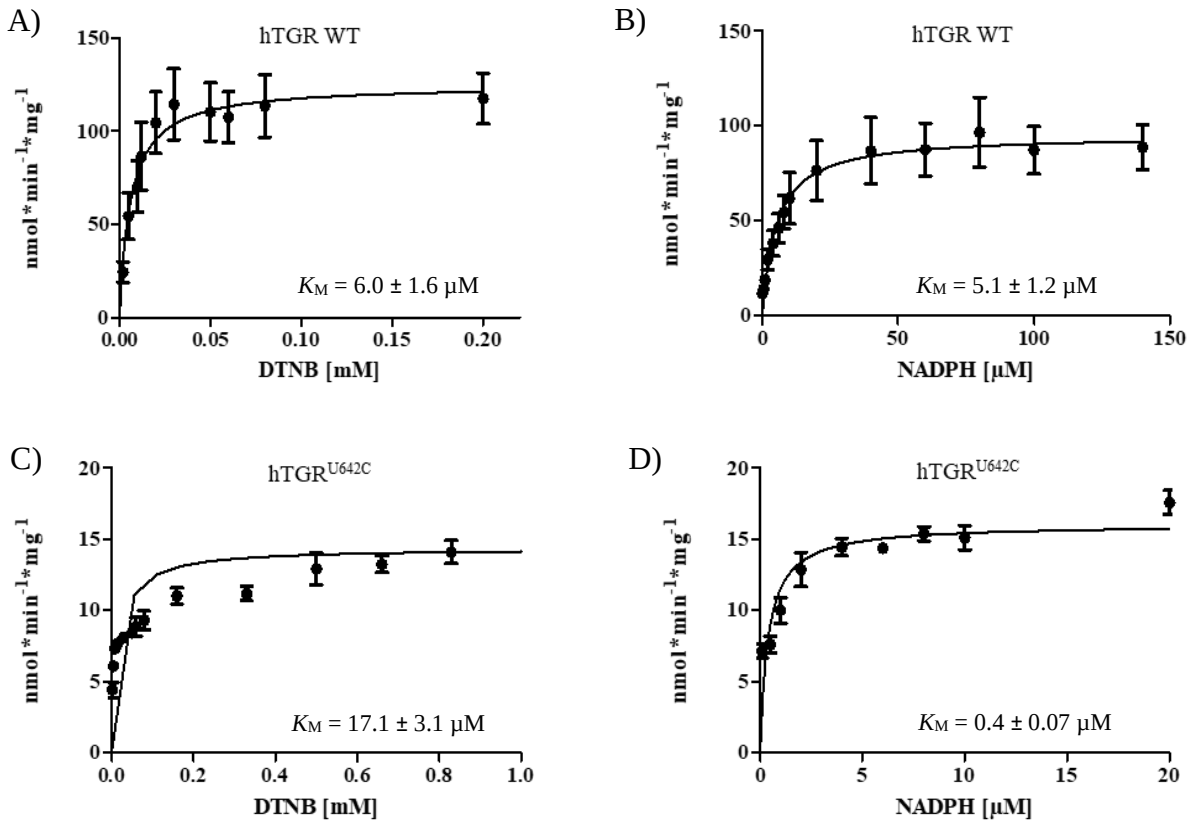

Figure 39: K_M for DTNB and NADPH in hTGR wild type and hTGR^{U642C}. A) K_M for DTNB in hTGR wild type in the presence of 200 µM NADPH. B) K_M for NADPH in hTGR wild type in the presence of 3 mM DTNB. C) K_M for DTNB in hTGR^{U642C} in the presence of 200 µM NADPH. D) K_M for NADPH in hTGR^{U642C} in the presence of 3 mM DTNB. Measurements were performed in at least five independent experiments.

Similar to the TrxR assay, hTGR^{U642C} showed a decreased specific activity in the DTNB assay compared to the wild type. The affinity of hTGR to DTNB is significantly lower than in the cysteine mutant, and the affinity of hTGR to NADPH is higher than in hTGR^{U642C}. The k_{cat} values of hTGR^{U642C} for DTNB and NADPH are reduced significantly. Table 11 summarizes the kinetic parameters of hTGR wild type and hTGR^{U642C} for their DTNB reduction properties.

Table 11: **Kinetic parameters of hTGR wild type and hTGR^{U642C} in the DTNB assay.**

	hTGR	*hTGR^{U642C}*
Specific activity [nmol*min^{-1}*mg^{-1}]	91.4 ± 15.6	14.3 ± 1.9***
K_M for DTNB [µM]	6.0 ± 1.6	17.1 ± 3.1***
K_M for NADPH [µM]	5.1 ± 1.2	0.4 ± 0.1***
k_{cat} for DTNB [s^{-1}]	0.23 ± 0.04	0.03 ± 0.004***
k_{cat} for NADPH [s^{-1}]	0.10 ± 0.04	0.02 ± 0.002**

Values represent mean values ± SE of at least five independent experiments. The kinetic characteristics given here were determined using the DTNB assay. A student's unpaired *t*-test with a 95% confidence level was performed in order to compare means. $^{*}p<0.05$, $^{**}p<0.01$, $^{***}p<0.001$.

4.3.3.2 Grx activity assay

The Grx assay describes the enzyme's ability to deglutathionylate a protein, where the protein is replaced by the substrate HEDS. In this assay, a substrate inhibition could be observed at GSH concentrations above 2 mM (shown in representative K_M curves in Figure 40) and at HEDS concentrations above 2 mM for both hTGR wild type and hTGR^{U642C}.

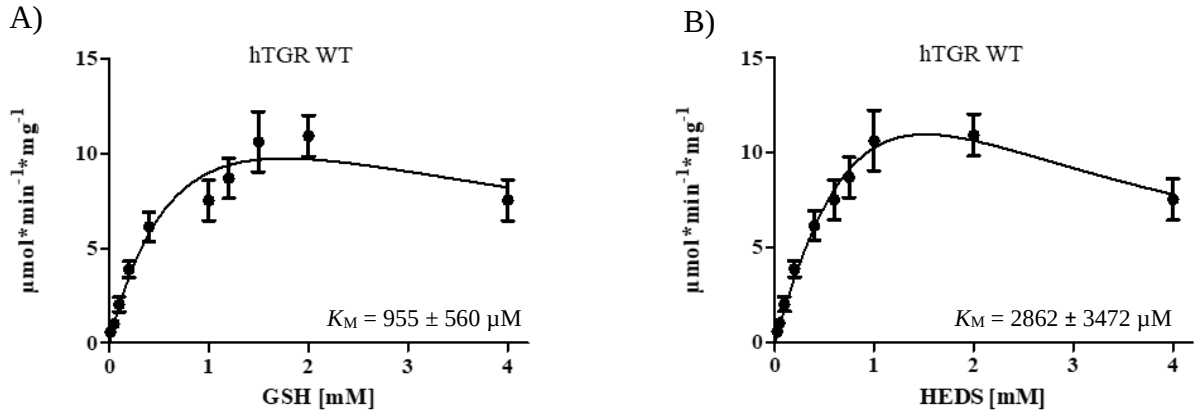

Figure 40: Substrate inhibition at hTGR with GSH and HEDS. Michaelis-Menten curves of substrate inhibition at A) [GSH] > 2 mM and B) [HEDS] > 2 mM. Measurements were performed in at least six independent experiments.

Figure 41 shows representative K_M curves of hTGR wild type and hTGR^{U642C} in the HEDS reduction assay, disregarding the reaction velocities at substrate inhibition. The steady-state kinetic parameters for NADPH were not determined since the dinucleotide is involved in the downstream reaction of hGR.

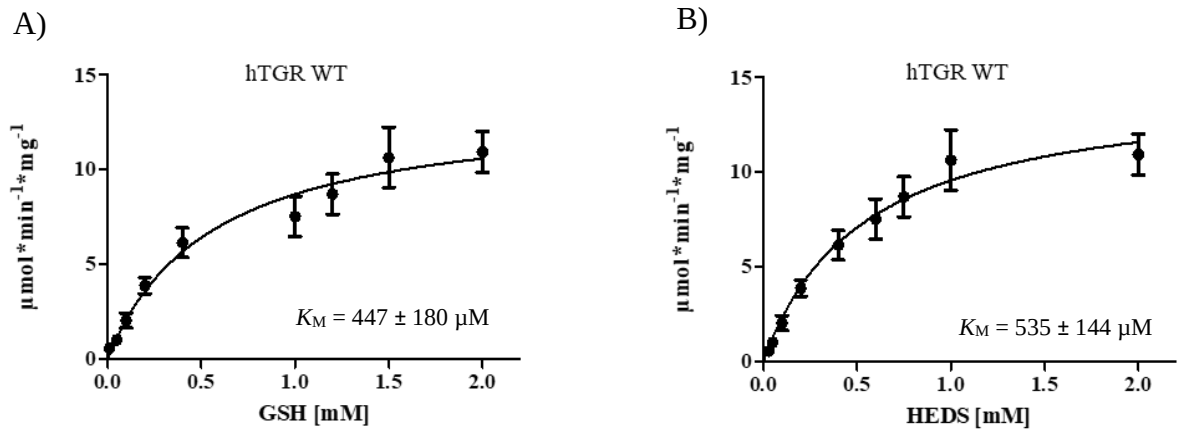

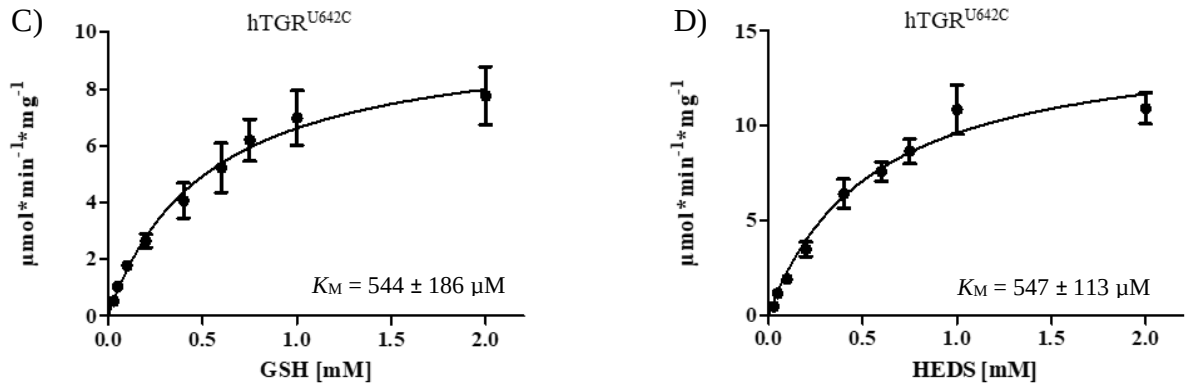

Figure 41: K_M for GSH and HEDS for the enzymes hTGR wild type and hTGR^{U642C}. A) K_M of GSH for hTGR wild type in the presence of 750 µM HEDS, 30 U/mL hGR and 100 µM NADPH. B) K_M of HEDS for hTGR wild type in the presence of 1 mM GSH, 30 U/mL hGR and 100 µM NADPH. C) K_M of GSH for hTGR^{U642C} in the presence of 750 µM HEDS, 30 U/mL hGR and 100 µM NADPH. D) K_M of HEDS for hTGR^{U642C} in the presence of 1 mM GSH, 30 U/mL hGR and 100 µM NADPH. Measurements were performed in at least six independent experiments.

The kinetic parameters for hTGR wild type and hTGR^{U642C} are presented in Table 12. No significant differences could be shown between the variants for specific activity or the K_M towards its substrates in the HEDS reduction assay. A significant increase was shown for the k_{cat} for GSH in hTGR^{U642C} with a p-value of 0.036. The HEDS reduction assay was likewise performed with the Grx domain of hTGR (hTGR$^{1-150}$), which showed a specific activity of 9.45 ± 2.2 U/mg.

Table 12: **Kinetic parameters of hTGR wild type and hTGR^{U642C} in the HEDS reduction assay.**

	hTGR	*hTGR^{U642C}*
Specific activity [µmol*min^{-1}*mg^{-1}]	7.3 ± 0.7	7.3 ± 2.3
K_M for GSH [µM]	447 ± 180	544 ± 186
K_M for HEDS [µM]	535 ± 144	547 ± 113
k_{cat} for GSH [s^{-1}]	4.77 ± 2.2	6.5 ± 1.6*
k_{cat} for HEDS [s^{-1}]	21.1 ± 1.6	20.7 ± 2.6

Values represent mean values ± SE of at least six independent experiments. The kinetic characteristics given here were determined using the HEDS assay. A student`s unpaired *t*-test with a 95% confidence level was performed in order to compare means. $^{*}p<0.05$, $^{**}p<0.01$, $^{***}p<0.001$.

To detect an unspecific reduction of the artificial substrate HEDS, a HEDS reduction assay was performed without adding GSH and hGR (modified HEDS reduction assay) to hTGR, hTGR lacking the N-terminal Grx elongation (hTGR$^{151-643}$), native hTrxR from placenta, or the recombinant hTrxR^{U498S} mutant (Table 13).

Table 13: Specific activity of hTrxR wt, hTrxR^{U498S}, hTGR$^{151-643}$, and hTGR in the mod. HEDS reduction assay.

	*Specific activity [nmol*min^{-1}*mg^{-1}]*
hTrxR wt (placenta preparation)	65 ± 13
hTrxR^{U498S}	3 ± 0.4
hTGR$^{151-643}$	2.3 ± 1.8
hTGR	3.2 ± 1.3

Values represent mean values ± SE of at least three repetitions. The kinetic characteristics given here were determined using a modified HEDS assay (without adding GSH and GR).

In the modified HEDS reduction assay all proteins were able to reduce the disulfide HEDS. All recombinant enzymes showed similar activities. Native hTrxR showed a 20% higher unspecific reduction of HEDS than the recombinant enzymes.

4.3.3.3 Glutathione reductase activity

In the glutathione reductase assay, only hTGR wild type showed a turnover of GSSG upon consumption of NADPH. Figure 42 shows representative K_M curves for GSSG and NADPH for hTGR wild type.

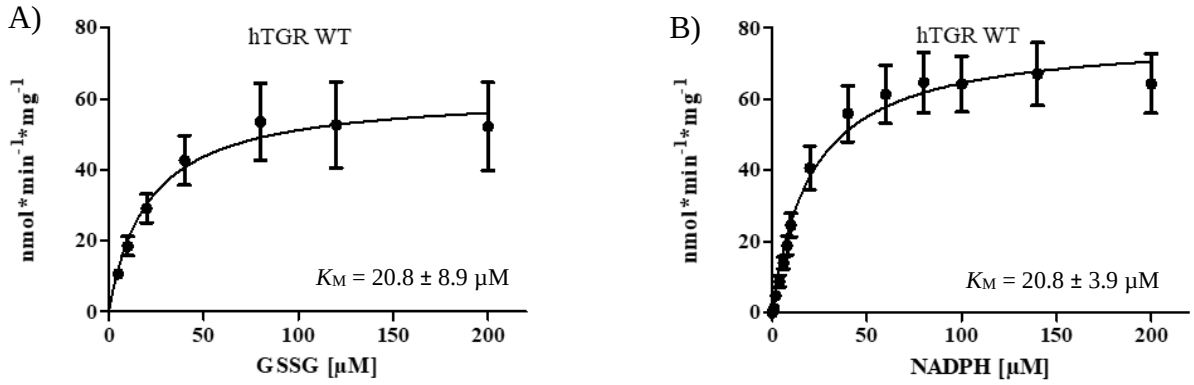

Figure 42: K_M for GSSG and NADPH for hTGR wild type. A) K_M of GSSG for hTGR wild type in the presence of 100 µM NADPH. B) K_M of NADPH for hTGR wild type in the presence of 200 µM GSSG. Measurements were performed in at least three independent experiments.

Table 14 represents the kinetic parameters of hTGR wild type in the GR assay.

Table 14: **Kinetic parameters of hTGR wild type and hTGR^{U642C} in the GR assay.**

	hTGR	*hTGR^{U642C}*
Specific activity [nmol*min^{-1}*mg^{-1}]	59.9 ± 1.6	<0.1
K_M for GSSG [µM]	20.8 ± 8.9	n.d.
K_M for NADPH [µM]	20.8 ± 3.9	n.d.

k_{cat} for GSSG [s^{-1}]	0.11 ± 0.04	n.d.
k_{cat} for NADPH [s^{-1}]	0.14 ± 0.06	n.d.

Values represent mean values ± SE of at least three independent experiments. The given kinetic characteristics were determined using the GR assay. N.d. = not detectable.

To detect GR activity dependency on the Grx-elongation, a GR assay was performed with $hTGR^{151-643}$, recombinant $hTrxR^{U498S}$ mutant, and $hTGR^{1-150}$ (Table 15). The Grx domain of hTGR ($hTGR^{1-150}$) showed no activity in the GR assay.

Table 15: Specific activity of hTrxR wt, $hTrxR^{U498S}$, $hTGR^{151-643}$, and hTGR in the GR assay.

	*Specific activity [nmol*min^{-1}*mg^{-1}]*
hTrxR (native)	n.d.
$hTrxR^{U498S}$	2.7 ± 1
$hTGR^{151-643}$	3 ± 0.9
$hTGR^{1-150}$	n.d.

Values represent mean values ± SE of at least six repetitions. Native hTrxR was purified from placenta as previously reported [204]. Since hTrxR and hGR are closely related enzymes, traces of hGR (activity) can be present in the native hTrxR sample. Therefore, GR activity was not determined for this enzyme. The given kinetic characteristics were determined using the GR assay. N.d.= not detectable.

4.3.3.4 Hysteretic behavior of the GR activity of hTGR

To identify a potential lag phase in the initial reaction velocity of hTGR in the GR assay, the full time course of NADPH oxidation was monitored over 6.5 h at increasing GSSG concentrations (100 µM – 4000 µM) and 100 µM NADPH at 340 nm. Additionally, a control containing only 100 µM GSSG and 100 µM NADPH was observed over time (Figure 43).

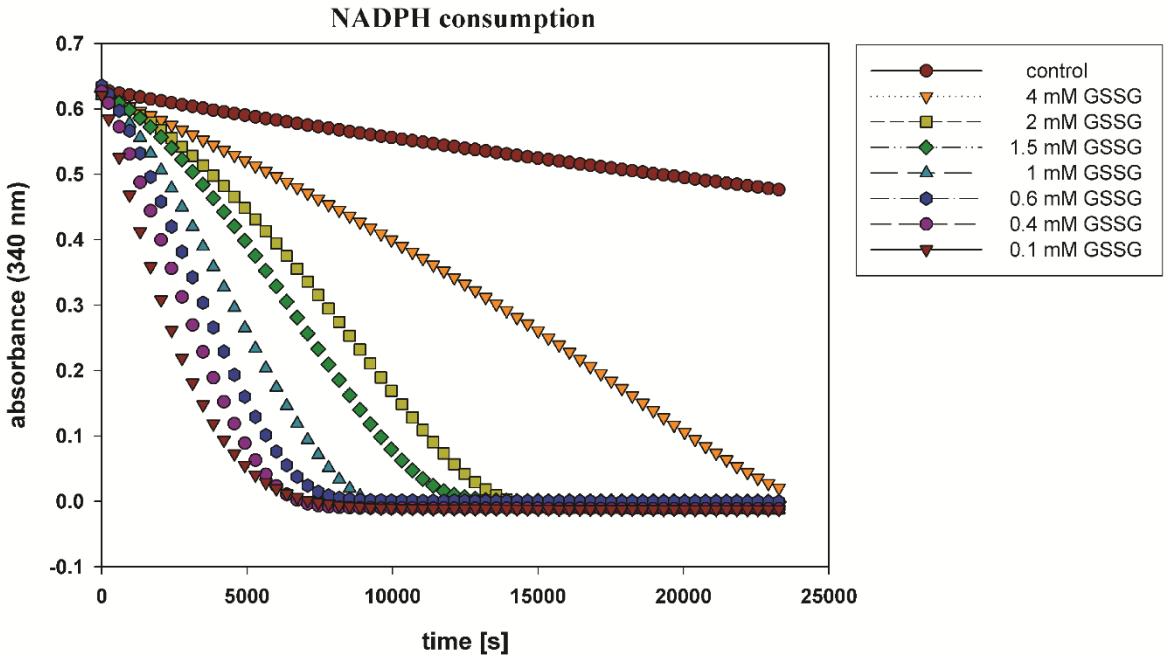

Figure 43: Full time courses of NADPH oxidation by 2 µM of hTGR in the GR assay. The decrease of absorbance was monitored at 340 nm over a time course of 6.5 h. Every third data point is shown for clarity. The experiments were carried out in triplicate with the same result. One representative dataset is shown.

Since GSSG inhibits hTGR in the GR assay at concentrations above 200 µM, the reaction velocity decreases at higher GSSG concentrations, which is visualized by flatter NADPH degradation curves. No lag phase was observed in the initial reductase activity of hTGR, and no hysteretic behavior of the enzyme during GR activity could be shown.

4.3.4 Protein-*S*-glutathionylation of hTGR

The enzyme hTGR could be glutathionylated by 5 mM of GSSG. Figure 44 shows a Western blot with anti-GSH antibody. The first lane represents the glutathionylated hTGR with DTT addition, which leads to the reduction of the covalently bound glutathione, showing no GSH detection in the Western blot. The second lane represents the glutathionylated protein without DTT addition in order to maintain the disulfide bridge between the enzyme and glutathione, resulting in a positive GSH signal.

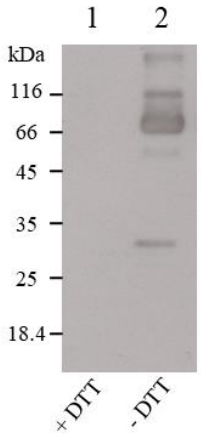

Figure 44: Western blot confirmation of *S*-glutathionylation of hTGR. Lane 1 = glutathionylated hTGR with 50 mM DTT. Lane 2 = glutathionylated hTGR without adding DTT.

The number and position of glutathionylated cysteines within hTGR could be identified via MALDI-TOF MS. MS data were obtained from three independent detections (see Supplementary Table 2). Not all cysteines located in the hTGR structure nor the Sec-containing peptide could be detected by MS analysis. Within hTGR, glutathionylated cysteines were found in triplicate at positions C93, C133, C225, and C619. Two glutathionylated cysteines were only detected in one sample each, namely C571 and C171. To analyze an activating or inhibiting influence of glutathionylation on hTGR activity, the specific activity of glutathionylated hTGR in a TrxR, DTNB, HEDS, and GR assay was measured.

Table 16: Specific activities of hTGR and glutathionylated hTGR.

	hTGR *Specific activity [nmol*min^{-1}*mg^{-1}]*	*hTGR-SG* *Specific activity [nmol*min^{-1}*mg^{-1}]*
TrxR assay	136 ± 6.9	41.6 ± 1.1***
DTNB assay	109 ± 5.1	65.8 ± 0.9***
HEDS assay	$11.46 \times 10^3 \pm 1.35 \times 10^3$	$1.26 \times 10^3 \pm 0.540 \times 10^3$***
GR assay	69.9 ± 5.8	39.9 ± 7***

Values represent mean values ± SE of at least three independent experiments with at least two replications. The kinetic characteristics given here were determined using the standard assay. A student's unpaired *t*-test with a 95% confidence level was performed in order to compare means. $^{*}p<0.05$, $^{**}p<0.01$, $^{***}p<0.001$.

Table 16 represents the specific activities under standard assay conditions in the three implemented enzyme assay systems with hTGR wild type and glutathionylated hTGR wild type. As shown here, a glutathionylation of this protein decreases the enzyme's ability to reduce thioredoxin, DTNB, oxidized glutathione, and the glutathionylated substrate HEDS.

5 DISCUSSION

5.1 Plasmodium falciparum peroxiredoxins

Over the last years research on Prxs expanded rapidly [205]. After their initial discovery in human erythrocytes [206, 207] Prxs were later described as redox-active proteins [208] present in all kingdoms of life. Prxs are cysteine-dependent peroxidases and were shown to act as sensor transducers [61]. Prxs are also found in protozoal parasites such as *Toxoplasma*, *Trypanosoma*, *Leishmania*, and *Plasmodium*. During infection, these protozoans have a high demand for reducing equivalents for enhanced metabolic rate and DNA synthesis caused by stage-dependent high proliferation rates. In addition, these parasites are challenged by the host`s immune system [209]. As a result, redox-based drug development strategies [210, 211] with a focus on peroxiredoxin networks are of major interest. A detailed knowledge of the mechanistical properties of Prxs and their redox network clusters is of utmost importance to gain further insights into the biochemistry of the parasites and to overcome the consequences of their severe impact on global health and economy.

5.1.1 Pull-down assay with 2-Cys *Pf*Prxs

In previous studies several affinity chromatography approaches based on active site cysteine mutants as bait proteins have been conducted with Trx [84, 212-216], Grx [84, 217], and Plrx [84] from *P. falciparum* and other organisms. Sturm *et al.* identified 33 putative interacting proteins for Trx, Grx, and Plrx from whole cell *Plasmodium falciparum* parasite lysate via mass spectrometry [84] using the same pull-down protocol as in this thesis. The this study, the authors identified the redox interactome (based on Trx, Grx, and Plrx) of malarial parasites and demonstrated that redoxins are highly involved in various metabolic pathways and, in part, are even required to balance metabolic fluxes [84]. In that study, as well as in others, Prxs were found to interact with Trx via an intermolecular disulfide bond, which confirmed the mechanism of the catalytic cycle of Prx reduction by Trx. The interactome of Prxs has hardly been explored so far. However, first studies suggest Prxs to "transfer oxidizing equivalents" via a mixed disulfide to downstream signaling proteins, meaning that an oxidized protein A can receive an electron from a second protein B while transferring the oxidation signal (disulfide or sulfenic acid formation) from A to B. These identified targeted proteins seem to react only slowly with hydrogen peroxide although their activities are dependent on Cys oxidation [218-220]. To identify proteins interacting with Prxs via a transient disulfide bond, we employed the principle of mixed disulfide fishing [217] to plasmodial 2-Cys peroxiredoxins.

To our knowledge a pull-down assay using Prx as bait and cell lysate as prey has never been previously reported. For this, wild types and active site Cys mutants of plasmodial 2-Cys Prxs were generated and immobilized on Sepharose beads via amine coupling. These proteins were incubated with parasite lysate and intensively washed with buffer. Covalently bound proteins were eluted with dithiothreitol and interacting proteins were identified by MS. Although the immobilized peroxiredoxins in this pull-down experiment were kept in a reduced state until incubation with parasite lysate, it can`t be excluded that the immobilized Prxs which are very prone to oxidation, were present as a mixture of reduced and oxidized proteins during protein-protein interaction. This implies that in our experimental setup the Prxs can act both, as reducers and oxidizers of putative interacting proteins. Possible reducing and oxidizing pathways of 2-Cys Prxs are explained in detail in the following.

Figure 45 A shows steps of peroxidation and resolution of the common catalytic cycle of atypical 2-Cys Prxs. Here, the fully reduced Prx is oxidized (step 1) by hydroperoxide substrates at the reactive peroxidatic Cys, resulting in sulfenic acid formation at the C_P. In the next step (2), the resolving Cys forms an intramolecular disulfide bond with the C_P by releasing H_2O. This disulfide bond can be resolved by redoxins (not shown).

Resolving Cys mutants (see Figures 45 B & C) can theoretically act as oxidizers or as reducers. C_R mutants are still highly reactive towards hydroperoxide substrates (Figure 45 B). Here, a sulfenic acid formation is triggered in the same way as in wild type Prxs (step 1). A following disulfide bond formation with the resolving Cys is however not possible, since the C_R has been mutated (to serin). The identification of proteins interacting with the remaining peroxidatic Cys supports the notion that in the next step (step 2) downstream regulatory signaling or messaging proteins can receive the oxidizing equivalents from the oxidized Prx by building a mixed disulfide intermediate. In case the 2-Cys Prx resolving Cys mutant is not oxidized by hydroperoxide substrates (Figure 45 C) the highly reactive reduced peroxidatic Cys might be able to reduce oxidized interacting proteins (step 1) by building a mixed-disulfide with the targeted protein (TP). Afterwards, these disulfide bonds might be resolved by reduced redoxins such as Trx *in vivo*, thereby releasing the reduced Prx and TP.

The same can in principle be postulated for peroxidatic Cys mutants (Figures 45 D & E). When C_P mutants are acting as transducers of oxidizing signals, the Prxs are oxidized by hydroperoxide substrates at the still remaining resolving Cys (step 1 in Figure 45 D). The formed sulfenic acid at the C_R (HOS_R) might then be able to transmit the oxidizing signal to downstream interacting proteins by building a disulfide intermediate. C_P mutants acting as reducers are not oxidized by hydroperoxide substrates but reduce oxidized targeted proteins by mixed-disulfide formation (Figure 45 E, step 1). As it was also true for C_R mutants this disulfide bond could be resolved by downstream redoxins *in vivo*. It should be noted here, that it cannot be excluded that the oxidized protein (Figures 45 C & E), which might be reduced by Prx, could also possess a disulfide bridge as a signal of oxidation rather than a sulfenic acid (not shown in the figure).

To correct for putative proteins binding to other cysteines of the Prxs, the respective *Pf*Prx wt was initially used as a control, assuming that a potential disulfide-bonded intermediate can be formed and would be released subsequently due to the present resolving cysteine. However, when evaluating our data, a huge number of proteins that had been exclusively bound to the Prx wt in all three independent experiments was identified. Our hypothesis explaining these interesting data is given at the end of Chapter 5.1.1.

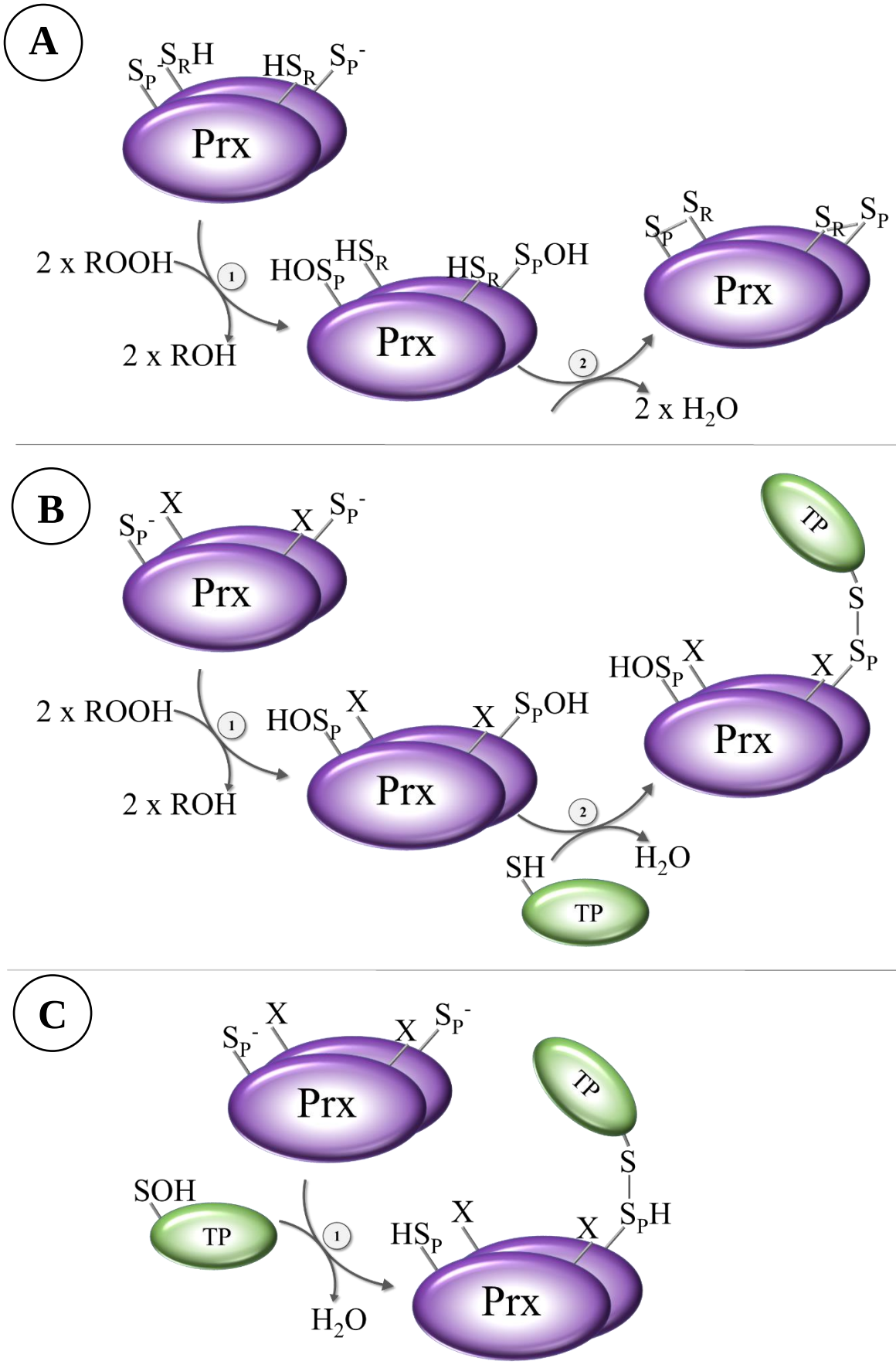
A
Prx
2 x ROOH
2 x ROH
Prx
2 x H2O
Prx
B
Prx
2 x ROOH
2 x ROH
Prx
TP
SH
TP
H2O
Prx
C
Prx
SOH
TP
H2O
TP
Prx

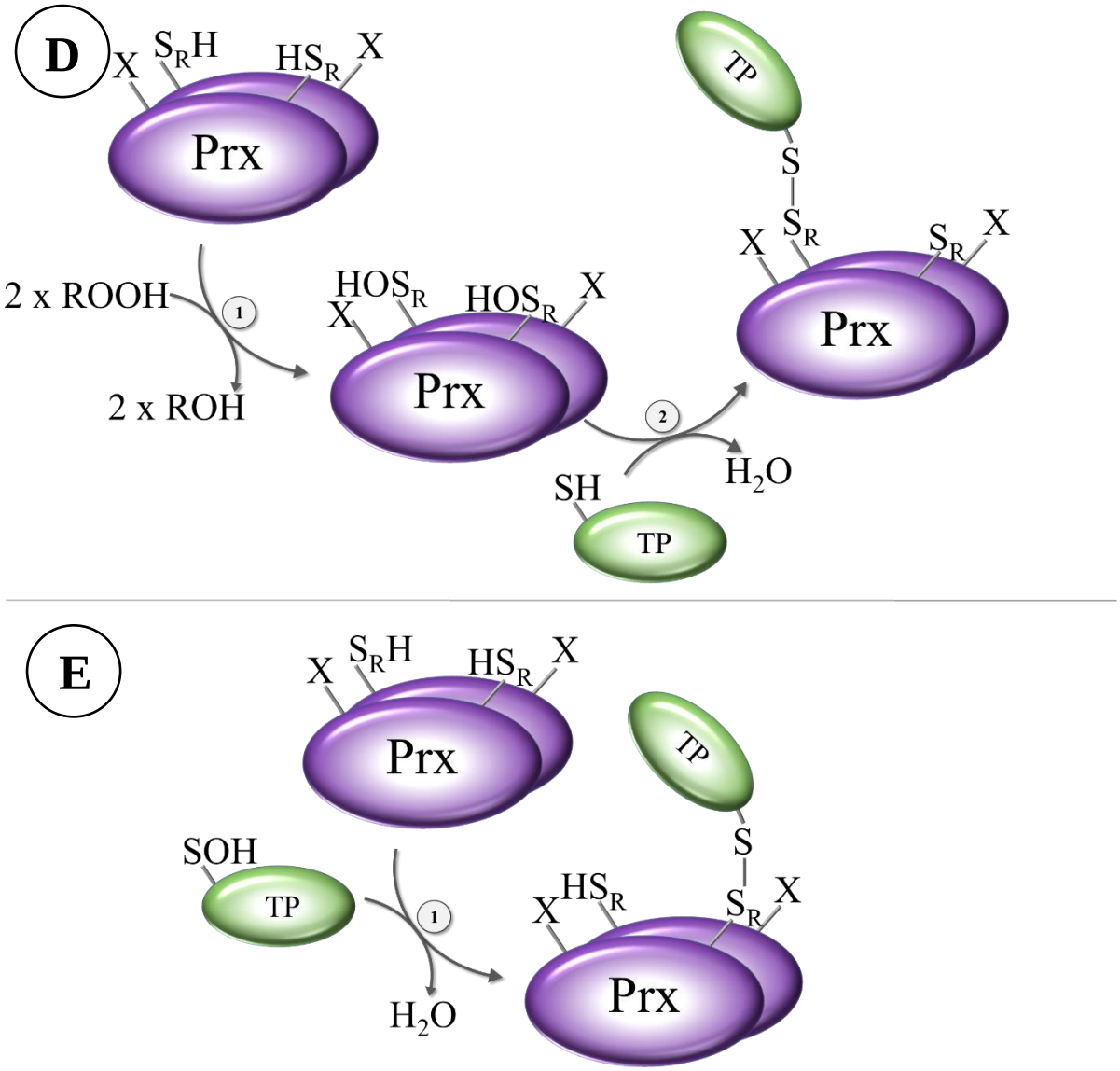

Figure 45: Proposed mechanisms of reduction and oxidation of targeted proteins via 2-Cys Prxs mutants. A) The first two steps of peroxidation and resolution of the common catalytic cycle of atypical 2-Cys Prx are shown: 1) peroxidation and 2) resolution with disulfide formation are presented. B & C represent the proposed mechanisms of transmitting oxidizing or reducing equivalents via Prx resolving Cys mutants. D & E represent the proposed mechanisms of transmitting oxidizing or reducing equivalents via Prx peroxidatic Cys mutants. For further details, please see text above.

5.1.1.1 Identification of proteins interacting with *Pf*Prx1a

In this pull-down assay, proteins from trophozoite stage *P. falciparum* cell lysate were identified that potentially interact with wild type and Cys mutants of the cytosolic *Pf*Prx1a. Captured proteins were found to be implemented in various metabolic pathways such as carbohydrate metabolism, protein folding, the translational machinery, *S*-adenosylmethionine metabolism, signal transduction, and others (clustered and summarized in Table 17). With the described method, we were able to identify 288 different putative interacting proteins for *Pf*Prx1a wt and its active site mutants (Figure 46 A). Since *Pf*Prx1a is located in the cytosol, we also evaluated our data after excluding proteins that only occur in other organelles. With this limitation, a number of 127 proteins interacting with *Pf*Prx1a and its mutants could be identified (Figure 46 B). Venn diagrams in Figure 46 demonstrate the overall amount of proteins captured exclusively by *Pf*Prx1a wild type, the C_P mutant *Pf*Prx1a^{C50S}, the C_R mutant

*Pf*Prx1a^{C170S}, or the double active site mutant *Pf*Prx1a$^{C50S/C170S}$. Furthermore, the overlap between these groups is shown. For data interpretation, only proteins that occurred in two or three independent experiments out of the triplicates were taken into account.

In our experiment, we found 91 proteins interacting with *Pf*Prx1a wild type and 70 proteins interacting with *Pf*Prx1a^{C50S} exclusively. Additionally, 68 proteins were identified interacting with *Pf*Prx1a wild type and the C_P mutant *Pf*Prx1a^{C50S} (Figure 46 A). Proteins captured with the double mutant *Pf*Prx1a$^{C50S/C170S}$ might reflect interacting partners that were caught with the remaining Cys at position C74 of *Pf*Prx1a. This C74 is located too far away from the active site cysteines of *Pf*Prx1a but was shown to be potentially able to interact with *Pf*Trx 1 (see Chapter 5.1.3.1). These results are indicating a potential role of this C74 in redox reactions in *Pf*. A very similar pattern can be recognized in the Venn diagram depicting only identified cytosolic interacting proteins (Figure 46 B). Here, most of the identified proteins were captured with *Pf*Prx1a wild type and the C_P mutant *Pf*Prx1a^{C50S} as well (37 and 21, respectively, and an overlap of 33 proteins). In general, a smaller number of proteins were identified interacting with the resolving Cys mutant *Pf*Prx1a^{C170S}. Therefore, the C_R of *Pf*Prx1a might be involved much more strongly in protein-protein interactions as the C_P (see Figures 45 D & E). This might implicate that the C_P in *Pf*Prx1a could be specialized in ROOH recognition and once the C_P is hyperoxidized the C_R could interact with proteins via a disulfide bond to transfer oxidizing or reducing equivalents (see Figures 48 C & E) or to protect the targeted protein against hyperoxidation.

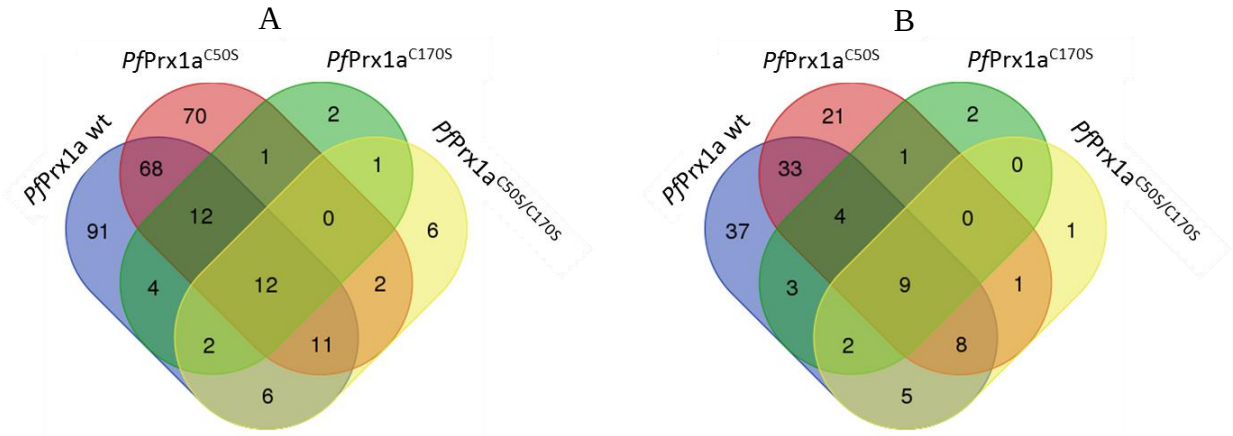

Figure 46: Venn diagrams of the number of proteins found in pull-down assay with *Pf*Prx1a. A) Total number of proteins putatively interacting via disulfides bridges with *Pf*Prx1a, *Pf*Prx1a^{C170S}, *Pf*Prx1a^{C50S}, or *Pf*Prx1a$^{C50S/C170S}$. B) Number of cytosolic proteins putatively interacting via disulfides bridges with *Pf*Prx1a, *Pf*Prx1a^{C170S}, *Pf*Prx1a^{C50S}, or *Pf*Prx1a$^{C50S/C170S}$.

Functional implications of proteins interacting with *Pf*Prx1a

Many proteins captured with *Pf*Prx1a in this study – representing potential interacting partners – have already been reported to be redox modulated in other organisms. For example, 40S ribosomal protein S23 and 40S ribosomal protein S21 (RPS21) from *Schizosaccharomyces pombe* were found to be oxidized in a thiol-labeling approach to characterize the disulfide proteome of fission yeast [221]. Lysine-tRNA ligase (KRS1) was characterized to be peroxide sensitive in *Saccharomyces cerevisiae* by the quantitative redox proteomic OxICAT method (ICAT: isotope-coded affinity tag) [222]. Moreover, heat shock protein 40 from mice (DnaJb5) was shown to be redox regulated by Trx1. DnaJb5, reduced by Trx1, is able to form a complex

with class II histone deacetylases 4 (HDAC4) via intramolecular disulfide bonds in order to hinder HDAC4 nuclear export and with this to inhibit cardiac hypertrophy after ROS-generated hypertrophic stimuli [223]. Investigated in Parkinson's disease patients, cysteine oxidation was identified in ubiquitin carboxyl-terminal hydrolase, a deubiquitinating enzyme [224], and the ubiquitin proteasome system itself can be altered with cysteine modifications such as disulfide formation, *S*-nitrosylation, and *S*-glutathionylation [225, 226]. Protein phosphatase 2C (PP2C) from *Arabidopsis thaliana* (ABI1) was significantly inactivated when challenged with hydrogen peroxide via specific cysteine oxidation [227]. The translation initiation factor 4E (eIF4E) was reported to form intramolecular disulfide bridges in order to impede a proper translation as shown in wheat [228, 229]. Protein disulfide isomerase (PDI) is a dithiol–disulfide oxidoreductase chaperone from the thioredoxin superfamily formed by four thioredoxin domains with a redox catalytic WCGHC motif and a thioredoxin fold structure, which is able to maintain disulfides and reconstruct un/misfolded proteins [230, 231]. Along with other proteins linked to protein folding, the redox-dependent heat shock protein 70 (Hsp70) was captured within this work. Hsp70 had already been identified to interact with Trx and Grx in plants [212, 216, 217, 232-234], depicting its redox linkage. Enolase, the enzyme that catalyzes the conversion of 2-phospho-D-glycerate to phosphoenolpyruvate in the penultimate step of glycolysis, was shown to be inhibited by Adriamycin, a ROS releasing potent anticancer drug in humans [235]. Furthermore, enolases of *Arabidopsis thaliana* and *Mesernbryanthemum tallinum* were reported to be redox regulated by a cytosolic Trx system at their disulfide bond between C313 and C339 [236]. Since *Pf* enolase was captured in this pull-down assay, regulation in *Plasmodium falciparum* is likewise conceivable. A redox regulation of *S*-adenosyl-L-homocysteine hydrolase depending on Grx [217] and Trx [84] has also been previously reported. Based on already published data from other working groups and the appearance of these redox-regulated proteins in the underlying experiment, similar redox regulation in *Plasmodium falciparum* can be assumed. Moreover, it can be deduced that Prxs in *Plasmodium* and potentially in other eukaryotic cells have a higher functional and redox-regulating implication than it was expected before and *Plasmodium* could serve here as a model organism for eukaryotic cells. In this context, one should mention that plasmodial L-lactate dehydrogenase, heat shock protein 70, disulfide isomerase, and *S*-adenosyl-L-homocysteine hydrolase were captured in the pull-down experiment with Trx, Grx, and Plrx by Sturm *et al*. [84], suggesting an interplay or synergy between Prx, the respective redoxin, and the effector protein.

Table 17: Functional clustering of the proteins interacting with *Pf*Prx1a.

Functional cluster	***Captured proteins***
***Pf*Prx1a wild type**	
Transcription/translation	40S ribosomal protein S23, 40S ribosomal protein S15A, 40S ribosomal protein S3A, eukaryotic initiation factor, translation initiation factor IF-2, nascent polypeptide-associated complex alpha chain, eukaryotic translation initiation factor 3 subunit 5, 40S ribosomal protein S18, 60S ribosomal protein L35ae, 40S ribosomal protein S21 (RPS21), eukaryotic translation initiation factor 3 subunit 8, eukaryotic translation initiation factor 3 subunit 10, glutamine-tRNA ligase, lysine-tRNA ligase (KRS1), 60S ribosomal protein L17, eukaryotic translation initiation factor 2 gamma subunit, 60S ribosomal protein L14
Protein degradation	26S proteasome regulatory subunit RPN11, 26S protease regulatory subunit 7, 26S protease regulatory subunit 10B, 26S protease regulatory subunit 8, 26S protease regulatory subunit 4, ubiquitin carboxyl-terminal hydrolase, proteasome regulatory protein
Protein folding	Heat shock protein 40, endoplasmin
Protein transport	Ras-related protein Rab-2 (RAB2), karyopherin alpha (KARalpha)
S-adenosylmethionine metabolism	*S*-adenosylmethionine decarboxylase/ornithine decarboxylase
Carbohydrate metabolism	Phosphoglycerate mutase
Signal transduction	Casein kinase 1 (CK1), protein phosphatase 2C (PP2C)
Others	Carbamoyl phosphate synthetase (cpsSII), acyl-CoA synthetase (ACS11), small GTP-binding protein sar1 (SAR1), serine repeat antigen 5 (SERA5)
***Pf*Prx1a^{C50S}**	
Transcription/translation	RNA pseudouridylate synthase, eukaryotic translation initiation factor 3 37.28 kDa subunit, serine-tRNA ligase, 60S ribosomal protein L11a, 40S ribosomal protein S10, 60S ribosomal protein L22, box C/D snoRNP rRNA 2'-O-methylation factor, U4/U6.U5 tri-snRNP-associated protein 2, alanine-tRNA ligase, glycine-tRNA ligase, histidine-tRNA ligase
Protein degradation	Proteasome subunit alpha type-4, ubiquitin domain-containing protein DSK2, 26S proteasome regulatory subunit RPN10, proteasome subunit alpha type-5, RING zinc finger protein
Protein folding	Peptidyl-prolyl cis-trans isomerase (CYP19B)
Protein transport	Protein transport protein SEC31, exportin-1, protein transport protein SEC13

***Pf*Prx1a^{C170S}**	
Transcription/translation	60S ribosomal protein L23
Carbohydrate metabolism	Deoxyribose-phosphate aldolase
***Pf*Prx1a$^{C50S/C170S}$**	
Transcription/translation	Elongation factor 1-beta (EF-1beta)
***Pf*Prx1a wild type, *Pf*Prx1a^{C50S}**	
Transcription/translation	60S ribosomal protein P0 (PfP0), elongation factor 1-gamma, 60S ribosomal protein L6-2, 60S acidic ribosomal protein P2 (PfP2), 40S ribosomal protein S4, 60S acidic ribosomal protein P1, translation initiation factor 4E (eIF4E), asparagine-tRNA ligase, 40S ribosomal protein S5, 60S ribosomal protein L3 (RPL3), 40S ribosomal protein S3
Protein degradation	26S proteasome AAA-ATPase subunit RPT3, suppressor of kinetochore protein 1, ubiquitin carboxyl-terminal hydrolase 2
Protein folding	Heat shock protein 70 (HSP70-3), heat shock protein 70 (HSP70-2), protein disulfide isomerase (PDI-11)
Carbohydrate metabolism	Phosphoribosylpyrophosphate synthetase, enolase (ENO), fructose-bisphosphate aldolase, L-lactate dehydrogenase (LDH), phosphoglycerate kinase
S-adenosylmethionine metabolism	*S*-adenosyl-L-homocysteine hydrolase (SAHH), phosphoethanolamine N-methyltransferase (PMT)
Energy metabolism	Adenylate kinase (AK1)
Others	Casein kinase 2, alpha subunit, 1-cys peroxiredoxins, dihydropteroate synthetase (DHPS), erythrocyte membrane-associated antigen, purine nucleoside phosphorylase (PNP), dolichyl-phosphate-mannose protein mannosyltransferase
***Pf*Prx1a wild type, *Pf*Prx1a^{C170S}**	
Transcription/translation	40S ribosomal protein S7, 60S ribosomal protein L5
Purine metabolism	Inosine-5'-monophosphate dehydrogenase

5.1.1.2 Identification of proteins interacting with *Pf*Prx1m

In mitochondria, oxidative post-translational modifications (Ox-PTMs) are linked to mitochondrial dysfunctions and clinicopathological consequences such as heart failure, acute neuronal trauma, peripheral diseases, and chronic neurodegenerative diseases [237, 238]. With the used approach, we were able to identify 20 mitochondrial proteins, which are potentially interacting with *Pf*Prx1m and its active site mutants. Figure 47 shows Venn diagrams that demonstrate the overall number of proteins exclusively captured by *Pf*Prx1m wild type, the C_P mutant *Pf*Prx1m^{C67S}, the C_R mutant *Pf*Prx1m^{C187S}, and *Pf*Prx1m$^{C67S/C187S}$. Furthermore, the overlap between these groups is shown. Figure 47 B shows the results for mitochondrial proteins only. Data interpretation only considers proteins that occurred in two or three independent experiments out of the respective triplicates. Proteins that are captured with the double active site mutant *Pf*Prx1m$^{C67S/C187S}$ are potentially interacting via a disulfide bridge between the targeted proteins and non-active site cysteines of *Pf*Prx1m (C54, C55, or C152) which seems to be not relevant in the mitochondrion (Figure 47 B). Using *Pf*Prx1m wild type as bait, we could identify one interacting mitochondrial protein (Figure 47 B). This interaction might follow the proposed mechanism of reduction and/or oxidation of targeted proteins illustrated in Figure 48. Both mitochondrial proteins that were captured using the C_P mutant *Pf*Prx1m^{C67S} (Figure 47 B and Table 18) might potentially interact via the redox mechanism depicted in Figures 45 D & E.

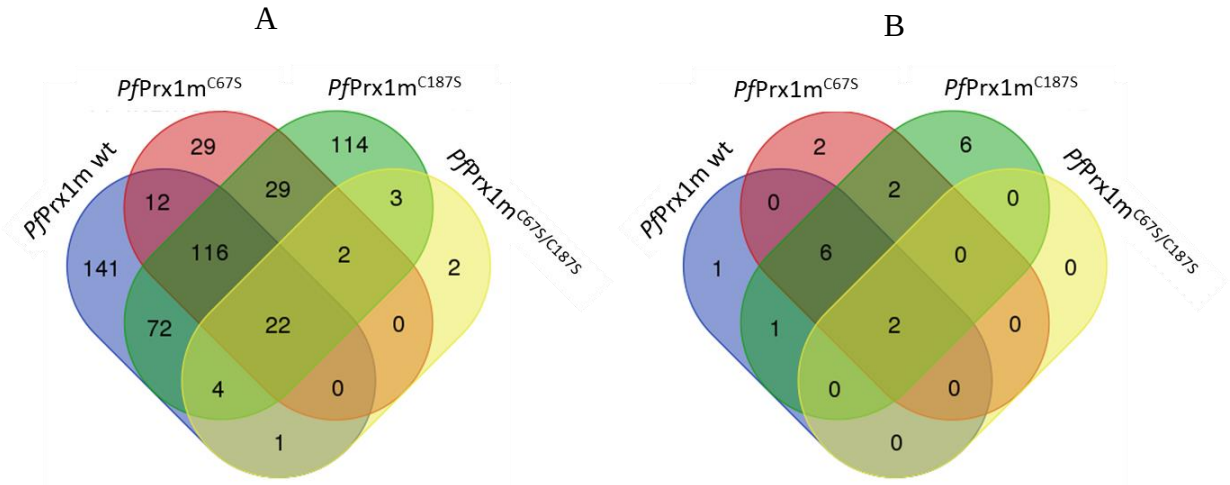

Figure 47: Venn diagrams of number of proteins found in pull-down assay with *Pf*Prx1m. A) Total number of proteins putatively interacting via disulfides bridges with *Pf*Prx1m, *Pf*Prx1m^{C187S}, *Pf*Prx1m^{C67S}, or *Pf*Prx1m$^{C67S/C187S}$. B) Number of cytosolic proteins putatively interacting via disulfides bridges with *Pf*Prx1m, *Pf*Prx1m^{C187S}, *Pf*Prx1m^{C67S}, or *Pf*Prx1m$^{C67S/C187S}$.

Functional implications of proteins interacting with *Pf*Prx1m

Identified proteins interacting with *Pf*Prx1m are involved in lipid metabolism, protein folding, redox control, and energy metabolism (clustered and summarized in Table 18). All target protein candidates contain a minimum of one cysteine inside their protein sequence, facilitating the intermolecular disulfide with *Pf*Prx1m in the conducted experiment. The respective metabolic function of the captured proteins is presented in Table 18. Some of the captured proteins have already been described to be redox modulated in humans by other authors, and will be described in the following. Human diacylglycerol kinase (DGK) reduces the activity of the diacylglycerol (DAG) protein kinase C (PKC), an enzyme involved in the pathomechanism

of diabetic nephropathy. It could be shown that antioxidants such as d-α-tocopherol and probucol are able to restore the strong glucose-induced decrease in DGK activity, and additionally that H_2O_2 mediates a downregulation of DGK activity, proving a redox-dependent regulation of DGK [239]. Since the implemented pull-down assay revealed DGK as a potential interacting partner for *Pf*Prx1m, a maintenance function of the peroxiredoxin seems to be the logical interpretation. Cellular ATP is produced by the electron transport chain in combination with the F_1F_O-ATP synthase [240]. The latter shows a high number of Ox-PTMs at cysteines of the α- and γ-subunits [241-244], which were found to be negatively correlated with conformational changes and ATP synthase hydrolytic activity (summarized in [237]). Since the aforementioned proteins could be captured with *Pf*Prx1m in triplicate and have already been reported to be redox regulated in other organisms, we conclude that a similar redox regulation of these proteins might exist in *Plasmodium falciparum*.

Table 18: Proteins interacting with *Pf*Prx1m.

Functional cluster	***Captured protein***
***Pf*Prx1m wild type**	
Lipid metabolism	Diacylglycerol kinase
***Pf*Prx1m^{C76S}**	
Protein folding	GrpE protein homolog, mitochondrial
others	Sortilin
***Pf*Prx1m^{C187S}**	
Redox metabolism	Ferrodoxin reductase-like protein, superoxide dismutase [Fe] (FeSOD), glutathione S-transferase, glutathione reductase
Energy metabolism	ATP synthase subunit beta, mitochondrial
Translation	Mitochondrial acidic protein MAM33
***Pf*Prx1m wild type, *Pf*Prx1m^{C187S}**	
Others	Acyl-CoA synthetase (ACS10)

In conclusion, the Prx pull-down assays using *Pf*Prxs as bait proteins provided new insights into Prx-mediated redox reactions in eukaryotic cells and many new candidate targets for protein-protein interaction with Prxs. The proposed mechanisms that might facilitate the transduction of reducing and oxidizing equivalents in wild type 2-Cys Prxs are depicted in Figure 48 and is explained in the following.

Reduced 2-Cys Prx wild type might reduce an oxidized target protein with its peroxidatic Cys (Figure 48 A, step 1) by forming a transient mixed disulfide with the TP. In the next step, the resolving Cys of Prx might resolve this disulfide bond and the reduced TP would be released (step 2). This step 2 could also be replaced by the reduction of the disulfide bond via Trx. In Chapter 5.1.3.1 of this thesis, it is clearly shown that *Pf*Trx attacks disulfide bridges when introduced at the peroxidatic Cys (in *Pf*Prx1a). In our experiments, using resolving Cys mutants, the former transient mixed disulfide between Prx and the targeted protein cannot be resolved since the resolving Cys is mutated (to serin). The TP is therefore “trapped” and was eluted by the reducing agent DTT in our approach.

Proteins caught with the peroxidatic Cys mutants of Prx in our experiments might reflect a second mechanism for target protein reduction (Figure 48 B). In this proposed mechanism, the reduced 2-Cys Prx is hyperoxidized to sulfinic acid by hydroperoxides at the peroxidatic Cys (step 1). The still reduced thiolate of the resolving Cys in Prx might then reduce oxidized TP by building a mixed-disulfide between the resolving Cys (step 2) and the TP which might be reduced by redoxins (not shown). This mechanism is rather likely since we caught more TPs with C_P mutants.

An oxidation/hyperoxidation of 2-Cys Prxs could theoretically also lead to a sulfenic acid formation at the resolving Cys of Prx (Figure 48 C, step 1). In this scenario, the oxidized resolving Cys of Prx might form a mixed disulfide with a former reduced target protein. This complex could serve (i) as a transmitted signal of an oxidizing environment to alter the properties of the targeted protein and/or (ii) could be resolved via downstream reduced redoxins. The fact that Trx is able to attack a disulfide bridge when introduced at the resolving Cys in 2-Cys Prxs (*Pf*Prx1m) was clearly shown in this thesis with an SPR-based approach (see Chapter 5.1.3.1). Another result that supports this hypotheses (Figures 48 B & C) is the high number of proteins captured with C_P mutants of the cytosolic *Pf*Prx1a.

A second mechanism of protein oxidation could start again with an oxidation of the 2-Cys Prx. Here, the active site Cys thiols might be oxidized both to sulfenic acid and the oxidized peroxidatic Cys might oxidize a reduced target protein via mixed-disulfide formation (not shown). However, since the simultaneous formation of sulfenic acid at both active site Cys in 2-Cys Prxs has not yet been described in literature, and since we caught only a few proteins with the *Pf*Prx1a resolving Cys mutant this mechanism seems to be unlikely/less abundant.

Since mutations can lead to consequences on protein-protein interface structures and thereby also to changes in binding affinities [245], proteins caught exclusively with wild type proteins or their active site mutants may reflect these individual alterations when binding the respective captured proteins.

Native Prxs have a high abundance inside the cell and are present in the parasite's cell lysate. Therefore, native Prxs in the used cell lysate might be able to capture a majority of interacting proteins so that the overall protein amount caught with the respective recombinant and immobilized Prxs was generally low. Many bound proteins interacting with the respective *Pf*Prx and its mutants were found, and some of those are not located in the same cell organelle as where the respective Prx occurs. This could reflect an unspecific recognition of substrate proteins due to loose complementary physio-chemical interactions between the partners. Additionally, these observed interactions can be stated as physiologically non-specific, but the proteins captured could be speculated to represent interaction partners of Prxs in other compartments [246].

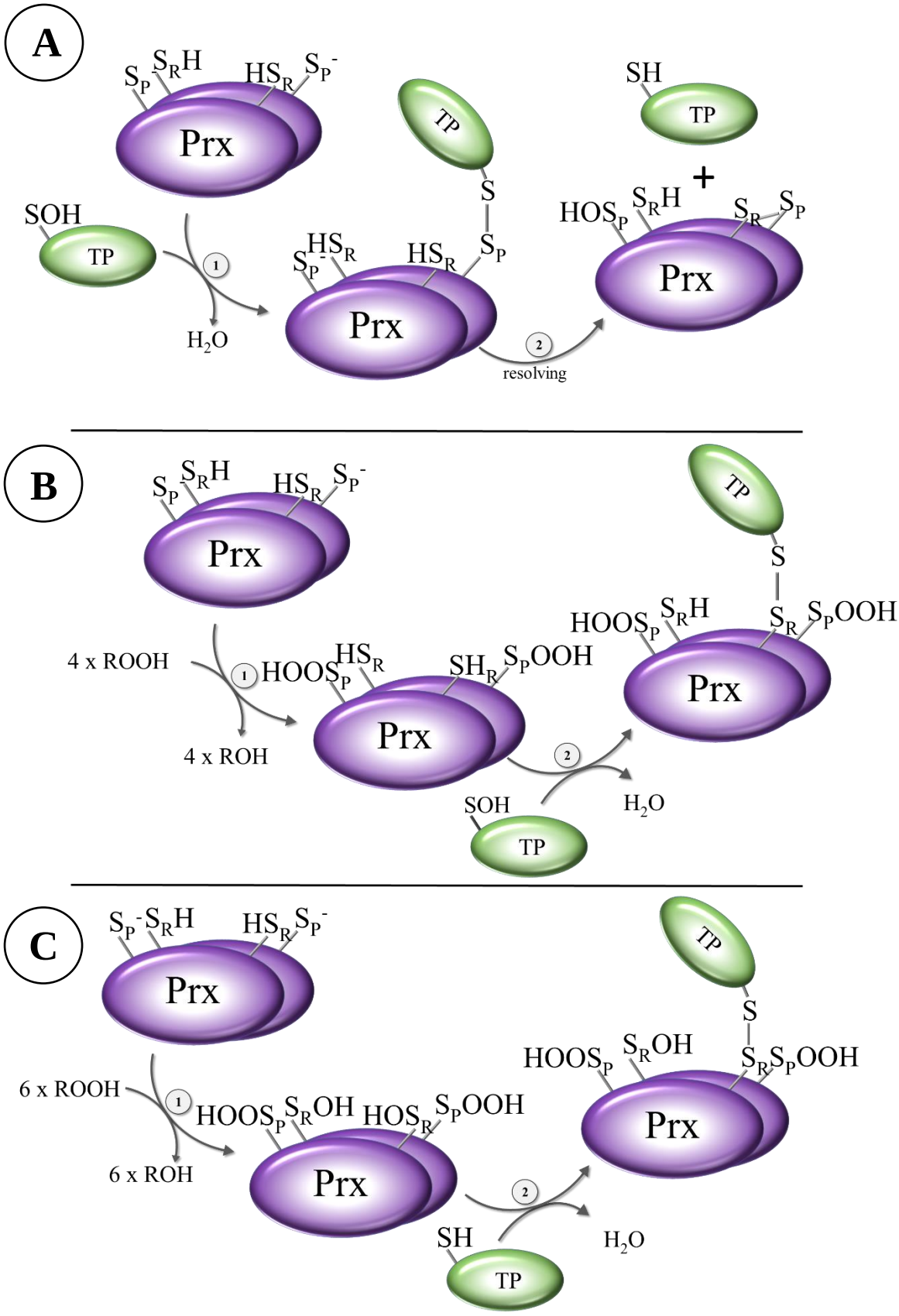

Figure 48: Proposed mechanisms of reduction and oxidation of targeted proteins via 2-Cys Prx wild type. A) Reduction of oxidized targeted proteins (TP) via the Prx peroxidatic Cys: 1) reduction of the oxidized TP via the peroxidatic Cys of Prx and 2) resolving of the mixed disulfide via the resolving Cys of Prx. B) Reduction of oxidized TP via the Prx resolving Cys: 1) oxidation of the 2-Cys Prx and 2) reduction of oxidized TP via the resolving Cys of Prx. C) Oxidation of reduced TP via the oxidized resolving Cys of Prx: 1) oxidation/hyperoxidation of Prx and 2) oxidation of the reduced TP via the resolving Cys of Prx.

In their role as nature's predominant peroxidases Prxs reduce H_2O_2, organic hydroperoxides (ROOH), and peroxynitrite ($ONOO^-$) [32] but have so far not been reported to reduce oxidized proteins. Within their catalytic cycle Prxs reduce a peroxide with the peroxidatic cysteine (C_P), converting the former thiolate of the C_P into a sulfenic acid followed by a disulfide bond formation triggered by the resolving cysteine of Prx (Figure 47 A). In this thesis, we hypothesize a potential additional function of Prx as a protein, which is able to reduce other interacting proteins based on the same catalytic mechanism with a bound sulfenic acid in proteins as a substrate. In addition, we identified potential interacting proteins in the sensor transducer cascade of plasmodial 2-Cys Prxs. In the applied pull-down assay, based on the principle of mixed disulfide fishing [84, 217], 2-Cys Prxs and their mutants lacking their resolving or peroxidatic cysteines were used to identify those potential interacting partners. Based on our hypothesis, proteins caught with C_P mutants are recipients of an oxidizing signal formed via oxidation of the remaining resolving cysteine of the 2-Cys Prx. Since the reactivity of Prxs to H_2O_2 is five to seven orders of magnitude higher than the one of other target proteins (TP) without a peroxidatic cysteine [247], and since Prxs are much more abundant than TPs, the targeted protein itself cannot outcompete with Prxs for H_2O_2. In an oxidizing environment, the C_P is prone to hyperoxidation and is thereby blocked for the resolving capacity of the C_R. The now "free" C_R can be further oxidized and could act henceforth as a signal transducer of the upstream oxidizing signal to proteins that are less prone to oxidation (Figure 48 C). It is therefore assumed that oxidized Prxs are able to selectively transfer the oxidation signal to downstream regulatory proteins through specific protein-protein interactions (PPI) and thiol-disulfide exchange reactions [58, 248] (Figures 48 A & B). This assumption is supported by the investigations of Turner-Ivey *et al*. [249] and Sobotta *et al*. [218]. The peroxidatic cysteine of Prdx1 was found to orchestrate the redox signaling to MAPK phosphatases (MKP-1 and/or MKP-5) in the senescence signaling of a tumor suppressive mechanism in breast epithelial cells [249]. Sobotta *et al*. evidenced a redox relay connecting human Prx2 with the transcription factor STAT3, where hPrx2 was found to be oxidized at the C_P (C51) at low levels of H_2O_2 and subsequently oxidized STAT3 via a mechanism involving disulfide rearrangement [218]. All these findings substantiate the role of 2-Cys *Pf*Prxs as signal transducers and the identification of interacting proteins from parasite's cell lysate.

To verify the protein-protein interaction partners identified in this thesis as biologically relevant, further experiments should be conducted, including cloning, expression, and purification of identified, interacting proteins; verifying the PPI (e.g. with surface plasmon resonance spectroscopy, isothermal titration calorimetry, microscale thermophoresis, or *in vivo* yeast or bacterial two-hybrid screenings); enzyme kinetic studies; co-crystallization; and x-ray crystallographic analyses. Nevertheless, when working with tagged recombinant target proteins, the fact that captured proteins interacting *in vivo* might not interact *in vitro* due to steric variations in the target protein or the absence of PTMs owing to the expression system should be taken into account.

5.1.2 pK_a determination of the active site cysteine of *Pf*Prxs

The peroxidatic cysteine in peroxiredoxins acts as a nucleophile in attacking hydrogen peroxide. Since a thiol group has a pK_a value of about 8.3 – 8.5 [250, 251], it is generally accepted that the peroxidatic cysteine present in a Prx has to exhibit a lower pK_a in order to act as a stronger nucleophile in its thiolate form. In this thesis the pK_a of the peroxidatic cysteine of the plasmodial Prx1a and $PrxQ^{1\text{-}164}$ could be determined to be 6.16 ± 0.1 and 6.57 ± 0.2, respectively, which demonstrates 'activation' to a nucleophile for a higher reactivity towards the peroxide substrate due to interactions with the microenvironment. The pK_a values of the

Prxs determined reflect a higher reactivity for peroxide reduction than a free cysteine but are more likely moderate compared to pK_a values detected for peroxidatic cysteines from other proteins and species. For human peroxiredoxin 2 the pK_a of the C_P was suggested to range between 5-6 [252]. Using the HRP competition assay based on the same protocol as the assay used in this thesis, Ogusucu *et al*. determined the pK_a of the peroxidatic cysteine of thioredoxin peroxidase I (TsaI) and II (TsaII) of *Saccharomyces cerevisiae*, to be 5.4 and 6.3, respectively. Although signal reading was performed with a stopped-flow spectrophotometer, results were very similar to others performed with slower devices. Interestingly the authors could demonstrate a difference of 1 unit pK_a value between these peroxidases, which share 86% identity in amino acid sequence [186]. The pK_a of the bacterial AhpC of *Salmonella typhimurium* was also determined with the HRP competition assay and was stated to be 5.84 [253], and the pK_a of AhpE of *Mycobacterium tuberculosis* found to be 5.2 [254]. In this thesis a second order rate constant of 1.6×10^8 M^{-1} sec^{-1} for *Pf*Prx1a, 2.8×10^7 M^{-1} sec^{-1} for *Pf*Prx5, and 2.2×10^6 M^{-1} sec^{-1} for *Pf*Prx$Q^{1\text{-}164}$ could be determined using H_2O_2 as substrate in the HRP competition assay. The catalytic efficiency of these proteins is very similar to those described in literature (4×10^7 M^{-1} sec^{-1} for AhpC of *Salmonella typhimurium* [255], 1×10^7 M^{-1} sec^{-1} for TsaI and II of *Saccharomyces cerevisiae* [186], 3.4×10^4 M^{-1} sec^{-1} for PrxQ of *Xylella fastidiosa* [256], and $7 \pm 3 \times 10^7$ M^{-1} sec^{-1} for human Prx5 [257]).

5.1.3 Protein-protein interaction analysis of *Pf*Prxs using SPR spectroscopy

Surface plasmon resonance spectroscopy represents a label-free approach to characterize biomolecular interactions in real time and is generally used in drug discovery research, quality control, and process development. In SPR-based research, most publications address biomedical applications with interactions of antibody-based therapeutics [258, 259], high throughput screenings [260, 261], proteomics [262-264], and cell-based detections [265-267]. In this thesis, SPR spectroscopy was shown to be able to provide deeper insights into the catalytic mechanism of electron transfer reactions on a molecular level. Using the Prx-Trx interaction as example, the method was able to reveal the regioselectivity of *Pf*Trx recognizing disulfide bonds of oxidized Prxs. This newly designed protocol for PPI analysis between Prxs and their interacting redoxins might contribute to the continuously growing area of SPR applications.

In SPR-based research, the term “binding” is generally used as soon as an attachment occurs to the surface when a sample passes the ligand. When interpreting a binding event with a wild type couple of Prx and a redoxin, it is not possible to evaluate, out of the arising sensogram, whether this interaction is based on strong chemical bonds, e.g. covalent bonds and coordinated bonds, or weak interactions such as hydrogen bonds and van der Waals forces. Since an intermolecular disulfide bond is formed in the recycling step of the catalytic cycle of the Prxs, mutations in the resolving cysteine of the redoxins can visualize this transient state under physiological conditions. A covalent bond between Trx and Prx is characterized by an increased response during the association phase. Here the Trx remains on the Prx during the dissociation phase and can only be released by a reducing agent (TCEP) in a setup, which resolves the disulfide bond between Prx and Trx.

Depending on the combination of mutants, it is possible to identify the interacting cysteines in the recycling process of Prx. During the interaction of *Pf*Prx wild type and *Pf*Trx wild type, the former reduced analyte (*Pf*Trx) reduces the oxidized ligand (*Pf*Prx). Since the reduced Trx is faced with the oxidized Prx on the surface, a reduction of Prx is directly induced, releasing a reduced Prx. The reduced Prx is no longer the substrate of the reduced Trx. Because this

reaction is very fast, recognizing a binding between wild type Prx and wild type Trx in the resulting sensograms is nearly impossible. In the first 0.5 sec of association a very low binding was observed, visualizing the interaction of reduced Trx with oxidized Prx. After this time point, the amount of oxidized Prx diminishes rapidly due to reduction by Trx. As a result, reduced Trx no longer recognizes its substrate because of the modification in the redox state of the ligand, leading to a decreasing response up to the baseline level during the 30 seconds of association phase. The same is true for Prx wt interactions with Trx^{CCS} mutants since the active site cysteine in the Trx is not altered. Trx mutants such as Trx^{SSS}, which lack all their cysteines, still bind to Prx due to weak interactions between the oxidized ligand and the analyte. Even when it is not possible to build a covalent bond (a mixed disulfide) between Prx and Trx, the Trx still recognizes its substrate (the oxidized Prx) but is not able to attack the oxidized cysteine of Prx. This recognition process was monitored via an increasing response in the sensogram and a decrease in the dissociation phase up to the baseline level. In our experiments, it was shown that Trx only recognizes disulfide bridges in the Prx substrate. Reduced Prx was not recognized. To identify a specific resolution of the disulfide bridge inside the Prx, which can exclusively been formed within the Prx wild type, an artificial disulfide bond with DTNB as an oxidation signal was introduced into the wild type and single active site mutations of the Prxs [84], building an *S*-TNB^- mixed disulfide. Since the target signal for the reduced Trx is a disulfide bond and not a sulfenic acid, this approach can be used to design an artificial disulfide bond in the absence of a peroxidatic cysteine. DTNB-oxidized *Pf*$Prx1a^{C74A/C170S}$ was recognized by reduced *Pf*$Trx1^{CSC}$, leading to an increase in response units during the association phase. The Trx mutant remained on the ligand during the dissociation phase, proving a covalent binding between the attacking cysteine of the Trx and the peroxidatic cysteine of the peroxiredoxin, which can only be resolved by TCEP.

Reduced *Pf*$Prx1a^{C74A/C170S}$ was recognized by reduced *Pf*$Trx1^{CSC}$ as well. During the dissociation phase, the response decreased down to baseline level, demonstrating a non-covalent reversible interaction. *Pf*$Prx1a^{C74A/C170S}$, which was oxidized with H_2O_2 instead of DTNB, was recognized by *Pf*$Trx1^{CSC}$, but no covalent binding could be observed. These results indicate selective attacking of disulfide bridges at the active site cysteines of Prx by the Trx. Palde and Carroll could also show the preference of S-S bonds over sulfenic acids in target recognition of *Ec*Trx, which is stated to be an entropy-driven mechanism. The authors proposed the lower entropy of oxidized targets that show conformational changes to be the preferred target conformation. A transition from the low-entropy conformer to the reduced high-entropy native form was shown to lead to decreased target recognition by Trx [268], confirming our observations with *Pf*Prx wild type and *Pf*Trx wild type. Although a TNB-mixed disulfide only partially mimics the oxidized wild type protein [269], the DTNB-oxidized Prx is a much better mimic for the native catalysis of Prxs of *Plasmodium*. Since all 2-Cys *Pf*Prxs are typical Prxs, building an intermolecular disulfide bond with a second 2-Cys *Pf*Prx monomer, and 1-Cys *Pf*Prxs are transitorily glutathionylated in the resolving mechanism with GSH and GST, representing a temporary mixed disulfide bond in the resolution process of oxidized 1-Cys *Pf*Prxs, the "bulkiness" of bonded TNB presents a preferred simulation of the native conditions of a recognition target for Trx [269].

*Pf*Prx5 and *Pf*PrxQ were both reported to be *Pf*Grx-dependent peroxidases, but they also accept *Pf*Trx as an electron donor [77, 108, 270]. Surprisingly, in the conducted SPR-based approach, no covalent interaction between *Pf*Grx and *Pf*Prx5 or *Pf*Grx and *Pf*PrxQ could be demonstrated, which was unexpected. These findings are, however supported by the study of Sturm *et al.* who did not find covalent interaction of *Pf*Grx and the mentioned Prxs in a *Pf*Grx pull-down assay either [84]. These results need to be studied in further detail.

During the catalysis of peroxide reduction, Prxs undergo local conformational changes at their active sites. The reduced Prx is in a fully folded (FF), substrate-ready conformation [42], and oxidation rotates its C_P outwards in a locally unfolded (LU), partially unwound conformation where the C_P and C_R are connected via a disulfide bond [271, 272]. Due to this, investigations revealed a successive transition of these conformations from the FF to the FF_{like} state, which describes a decoiling of the α2 helix in the still reduced enzyme. The transient FF_{like} conformation converts to a LU_{like} and finally to the LU conformation stabilized at the disulfide-bonded active site [273] (Figure 49). Since FF_{like} and LU_{like} conformations were observed in a reduced Prx, both conformations seem to be present in some reduced Prx isoforms. Additionally, conformational changes due to oxidizing processes inside Prxs were reported in already crystallized Prxs (*Xc*PrxQ from *Xanthomonas campestris*), presenting key shifts in active site residues but minimal changes between the thiolate and sulfonate forms of the C_P. In this study, the authors mentioned a potentially different behavior of other Prx isoforms due to their separation by billions of years of evolution, which could vary in how they locally unfold, for example [274]. Furthermore, the conformational alterations of a TNB-oxidized C_P should be explored in more detail in order to unravel whether a conjugation with TNB also promotes local unfolding or not.

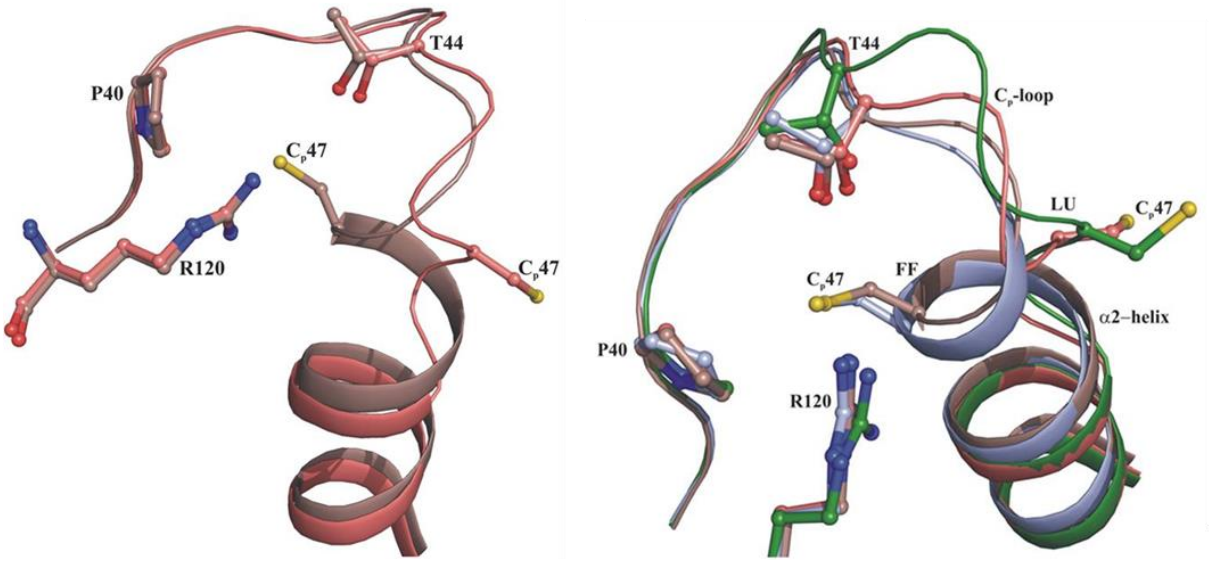

Figure 49: Comparison of FF and LU states from *Ec*AhpC$^{1-186}$-YFSKHN crystal structures. A) Superposition of two different active sites, the FF_{like}-(brown) and LU_{like} state (salmon) observed in the reduced state (PDB code 5B8B). B) The oxidized (green) and reduced (salmon) active sites observed in EcAhpC$^{1-186}$-YFSKHN structures (PDB code 5B8A) are compared to the reduced StAhpC (light blue) FF active site (PDB code 4MA9). The intermediate FF_{like} (brown) and LU_{like} (salmon) conformations represent the transition state from the FF to the LU state. Taken from [273].

5.1.3.1 Protein interaction analysis with 2-Cys *Pf*Prxs

For SPR analysis, *Pf*Prx and *Pf*Trx wild types and active site cysteine mutants were generated. In our approach, respective peroxiredoxins were immobilized via amine coupling on CM5 chips and used as ligands. Redoxins like Trx and Grx were used as analytes. Reduced ligands were incubated with DTNB in a conditioning cycle introducing an artificial mixed disulfide with TNB at the active site cysteines of the respective Prxs. After oxidation with DTNB, the ligands were incubated with reduced analytes. Reduced Trx were shown to resolve the mixed disulfide of Prx-TNB complex. By combinations of Cys mutation of Prx and Trx, it was shown that this disulfide bond recognition and resolving is regioselective.

*Pf*Trx1 possesses three Cys, were C30 is described as an attacking Cys and C33 as a resolving Cys [275]. The impact of the third Trx Cys (C43) has not been described so far. In our experiment, attacking Cys mutants of Trx were not able to bind the oxidized Prxs, whereas resolving Cys mutants of Trx were able to attack the mixed disulfide bond via a disulfide-dithiol exchange reaction. The emerging Prx-Trx mixed disulfide complex could not been resolved due to the absence of the resolving Cys in Trx^{CSC}. The usually transient mixed disulfide complex was "trapped" and therefore non-transient, which was visualized by a stable plateau in response units in the SPR system. As it was expected based on the common catalytic mechanism of Prx recycling, SPR analysis could demonstrate that *Pf*Trx reduces a mixed disulfide between *Pf*Prx1a and TNB with its C30 attacking Cys.

We also showed that Trx favors particular disulfide bonds of Prx-TNB complexes introduced at Prx active site cysteine residues. Via the underlying SPR approach, we could show that the C30 of Trx can reduce the mixed disulfide of *Pf*Prx1a and TNB when the oxidation signal is introduced at position C50 and/or C74 in *Pf*Prx1a. This conclusion was confirmed with electrophoretic mobility shift assays, with *Pf*Prx1a wt, *Pf*$Prx1a^{C170S}$, and *Pf*$Prx1a^{C50S/C74A}$ interacting with *Pf*Trx^{CSC} (Figure 30 & 31). C74 of *Pf*Prx1a is however, not suggested to be involved in the catalytic cycle since it is too far away from the active site. C74 might however be involved in oxidation signaling, and a mixed-disulfide at that position could potentially be reduced by Trx (Figure 50 A) which was clearly shown by our SPR-based approach using *Pf*$Prx1a^{C50S/C170A}$. Here, the active site cysteines were mutated to serin and the remaining C74 was still able to interact via a disulfide bond with the attacking Cys of *Pf*Trx 1. In *Pf*Prx1m, we could show that the favored cysteine for the attacking cysteine of *Pf*Trx is the resolving cysteine C187 (Figure 50 B). Similar results have been obtained with the structurally related yeast Ahp1 [276]. These two 2-Cys Prxs already demonstrate the fact that Trx target recognition is a highly individual process and can not be generalized.

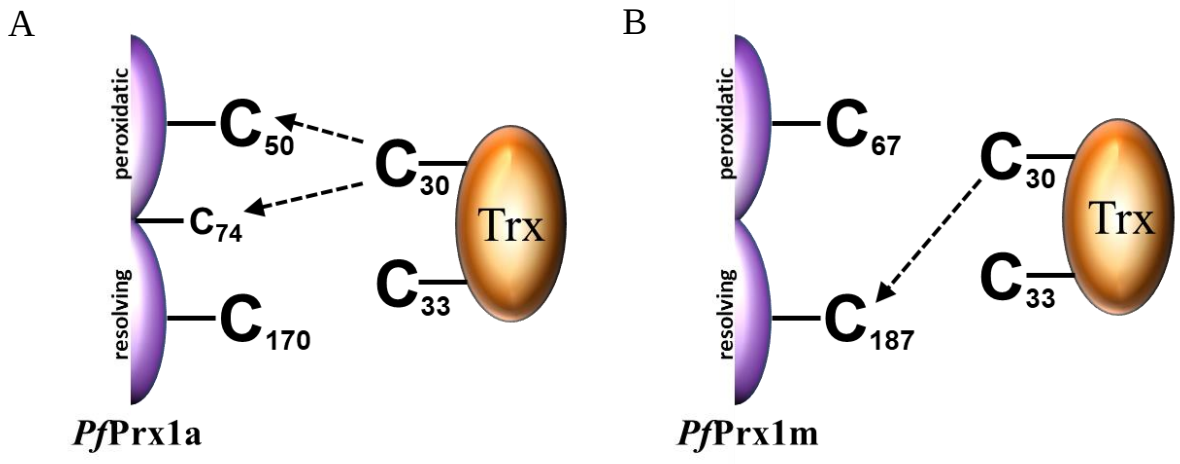

Figure 50: Cysteine preference in the recycling process of 2-Cys *Pf*Prxs with Trx. A) Interacting cysteines in *Pf*Prx1a and *Pf*Trx. B) Interacting cysteines in *Pf*Prx1m and *Pf*Trx.

5.1.3.2 Protein interaction analysis with 1-Cys *Pf*Prxs

Resolving the artificially introduced disulfide bridge at the peroxidatic cysteine of *Pf*Prx5 (Cys117) was shown to be achieved by C30 of *Pf*Trx, as expected as well. Surprisingly, in addition to that, *Pf*Trx was able to target the more C-terminally located C143 (Figure 51 A). This finding substantiates the suggestion of other authors that C143 of *Pf*Prx5 might be involved

in redox-dependent signal transduction due to glutathionylation signals or might act as a slow-acting resolving cysteine for (accidentally) formed disulfide bonds between *Pf*Prx5 and other proteins [103]. The mixed Prx-TNB disulfide bond could therefore mimic a disulfide bond to glutathione or an intermolecular disulfide bond to a protein.

For *Pf*Prx6 it was not possible to ultimately identify the cysteines targeted by *Pf*Trx. Since a covalent binding between the attacking cysteine of *Pf*Trx and the wild type but also with the C_P mutant of *Pf*Prx6 was proven, an alternative cysteine seems to be the favored cysteine for attacking via Trx. As shown in arsenate reductase from *Staphylococcus aureus*, an intricate cascading disulfide switch mechanism inside the protein, to form an accessible disulfide for thioredoxin, could be a possible explanation [277]. Since *Pf*Prx6 contains seven additional cysteines next to the C_P, the identification of the targeted cysteine(s) with Cys→Ser single and/or multiple mutations was not terminated within this thesis.

*Pf*PrxQ$^{1\text{-}164}$ possesses only two Cys (C56 and C103). Via SPR it was clearly shown that the recycling process of the disulfide group within *Pf*PrxQ$^{1\text{-}164}$ starts at position C56 and the attacking Cys of *Pf*Trx is also C30 (Figure 51 B). When C103, the second cysteine in *Pf*PrxQ$^{1\text{-}164}$ is oxidized with DTNB, the resolving Cys mutant of *Pf*Trx is able to build up the Prx-Trx mixed disulfide complex.

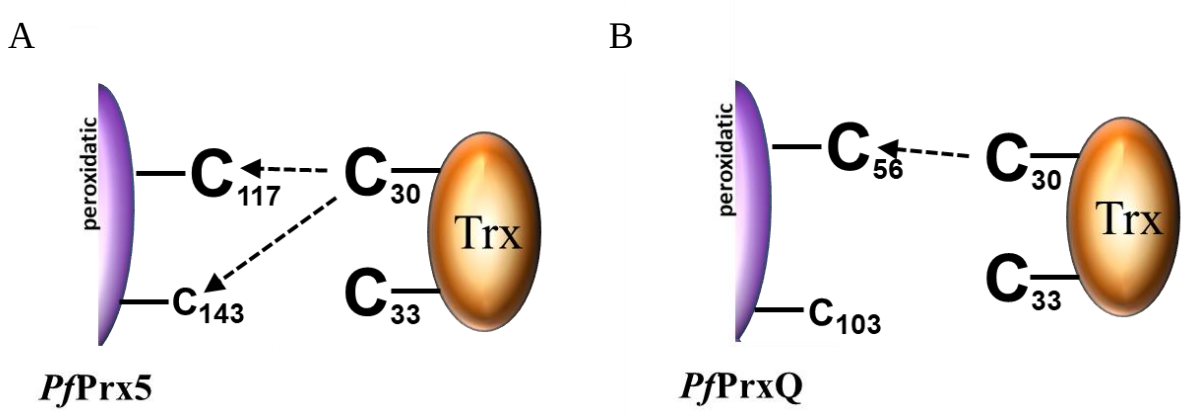

Figure 51: Cysteine preference in the recycling process of 1-Cys *Pf*Prxs with Trx. A) Interacting cysteines in *Pf*Prx5 and *Pf*Trx. B) Interacting cysteines in *Pf*PrxQ and *Pf*Trx.

The conducted experiments demonstrate a regioselectivity of specific cysteines in disulfide bond recognition and resolving of plasmodial peroxiredoxins by thioredoxin 1. It was shown that Trx preferentially binds to selected cysteines of the Prxs. Additionally, the previous concept that describes the C30 of *Pf*Trx1 as the attacking Cys [82] could be confirmed. The targeted cysteines differ between *Pf*Prxs inside the malaria parasite, strengthening the specificity of this recognition process, which may be further complicated by diverse thioredoxin-mixed disulfide complex formations.

Alternative methods for PPI analysis

Already existing methods to evaluate interacting cysteines show many disadvantages in comparison with this SPR-based approach. Enzyme assays with site-directed mutations are not always feasible due to catalytically inactive mutants. For example the peroxidase assay, used for determining peroxiredoxin activity, which includes TrxR, Trx, and NADPH as a backup reaction to maintain the reduced state of Prx, cannot be conducted with active site mutants of

thioredoxin. In that assay, a persisting covalent binding between Prx and Trx would lead to the same readout as a Prx or Trx with no activity at all. A complex formation between Prx and Trx with preincubation and complex confirmation via gel filtration requires large quantities of proteins and can provide only semiquantitative data. To identify interacting partners via disulfide bonds, a pull-down assay also requires large protein quantities and is semiquantitative, and non-covalent binding events are very difficult to detect. Co-crystallization represents a very time consuming and static possibility to detect those interactions and is not able to deliver any affinity constants. The process of cross-linking would alter the molecules involved and would give no information about affinities as well, and the detection of interacting partners with fluorescence resonance energy transfer (FRET) involves fluorophores as labels. In summary, in our new SPR-based method for the identification of interacting cysteines of Prx and Trx, several samples can be studied in parallel with a direct readout of data, and covalent, non-covalent, and no binding/interaction can be clearly distinguished and described quantitatively. This enables an elucidation of mechanism in molecular detail, can be studied in real time and label free, is very fast, and requires low quantities of protein.

To investigate the suitability of other approaches for answering our leading question, MST and ITC were performed with selected, representative interacting proteins. As shown in Figure 33, a discrimination between a covalent binding and a non-covalent interaction was not feasible with MST. The SPR data set and the mobility band shift assays demonstrated an incomplete binding of the interacting partners, under the experimental conditions chosen. Therefore, the assay solution is not composed of 100% covalently bound proteins. In principle, a distinction between covalent and non-covalent PPI with MST is possible. When all proteins in the sample are covalently bound, the emerging dose-response curve would be steeper and would also develop a ‘knee’, and a covalent binding could be estimated (personal communication with Dr. Sven-Andreas Freibert, Philipps University Marburg after consultation with NanoTemper Technologies GmbH). Since, however, our coupling samples were only partially covalently bound, purification (with fast protein liquid chromatography) would be necessary to extract the bound complexes. In that case, the leading question of whether covalent binding exists or not would already be answered and MST would be redundant. Additionally, MST proteins, which are only stable in Tris buffer, cannot be used since labeling the protein would also label the small amine Tris. An intervention in the reaction, or in our case, an addition of a reducing agent to the running system is not possible. Additionally, MST does not provide information regarding K_{on} and K_{off}, especially because the reaction between the interacting partners has already taken place when the measurement starts.

In ITC experiments, one protein can be titrated against another protein (association experiment), or a protein mixture can be titrated into a buffer (dissociation experiment) to evaluate the resulting binding or dissociation isotherms. To fathom whether our experimental approach can be realized with ITC as well, initial association experiments were conducted, leading to irreproducible isotherms with weak data readouts since the sensitivity of the ITC seems to be insufficient for our approach or the coupling reaction is to slow. The transition to dissociation experiments and the extension of coupling time then led to significant differences in dissociation behaviors of the chosen interacting partners, as well as high reproducibility and a strong data readout. In the experiments, a discrimination of a reduction-induced dissociation of a disulfide-bridged interaction couple and a dissociation of interacting proteins, where no S-S bond is involved, is clearly deducible. Here, the reduction of a disulfide-coupled Prx-Trx couple (*Pf*Prx1a wt + *Pf*Trx^{CSC}) requires significantly more energy under reductive dissociation than the reduction of a Prx-TNB couple or the non-covalently interacting couple *Pf*Prx1a wt + *Pf*Trx^{SSS} (Figure 33).

However, an intervention to the running system at a later time point with a reducing buffer, for example, is not possible either, once the reaction has started. Additionally, ITC requires large amounts of protein to generate sufficient heat changes in order to obtain valid and reproducible isotherms, and measurements of more than one analyte in parallel are not possible and are therefore more time consuming than our SPR-based method. Furthermore, in MST and ITC a discrimination of covalent and non-covalent interactions is only achievable via direct comparison of the data generated for wild type and mutants, since a concrete parameter (e.g. the stabile and visible plateau of RU in the SPR-based approach) is missing.

In conclusion, our SPR-based method for identifying interacting cysteines of Prx and Trx provides particular advantages to the existing methods due to a real-time, label-free method, which is very fast and requires low quantities of protein. Proteins that cannot be produced in high amounts or are not stable at higher concentrations can be used as well. Furthermore, in SPR, proteins can be reutilized after regeneration with buffer or, when necessary, with a reducing agent. In doing so, the immobilized proteins can be used for multiple binding analysis. Several samples can be studied in parallel with a direct readout of data, and covalent, non-covalent, and missing bindings/interactions can be clearly distinguished and described quantitatively, which enables an elucidation of mechanistic details. Due to this, this SPR-based method may also serve as a good prediction tool for co-crystallization partnerships of interacting and coupled proteins. The SPR-based method for detecting binding events of PPI in redox-regulated proteins on a molecular level therefore presents an alternative method (with particular advantages) to ITC, the current gold standard for label-free quantitative measurements of biomolecular interactions.

5.2 Human thioredoxin glutathione reductase

5.2.1 Heterologous overexpression and purification of hTGR

The rare amino acid selenocysteine is ubiquitous in all three domains of life - eukarya, bacteria, and archaea [278, 279] - and is incorporated via the genetic machinery by a unique codon (UGA). This codon has a dual function as a STOP signal for protein synthesis and as a signal for selenocysteine incorporation [280], using a stem-loop structure in the *m*RNA (SECIS element) [281, 282]. Utilizing the SECIS element as a marker, 25 selenoproteins could be identified within the human genome [283]. Since the Sec-inserting machineries of prokaryotes and eukaryotes differ in position, sequence, and structure of the SECIS element [284], recombinant expression of mammalian selenocysteine-containing proteins in bacteria are extremely difficult [285]. Nevertheless, in this thesis, we were able to recombinantly produce full length selenocysteine-containing hTGR by fusing its open reading frame with a SECIS element of the bacterial selenoprotein formate dehydrogenase H and co-expressing it with the *selA, selB,* and *selC* genes as reported previously for rat and human thioredoxin reductases [286, 287]. After different vectors, competent cells, and culture media were tested, the publication of Bar-Noy, suggesting a supplementation of sulfur in the form of L-methionine and L-cystine to decrease non-specific selenium incorporation into the protein and the supplementation of a vitamin mixture consisting of riboflavin, niacin, and pyridoxine at the time of induction [163], contributed to the successful expression of a soluble and active protein. The percentage of selenocysteine incorporation into the overexpressed protein has so far not been quantifiable, neither via MALDI-TOF MS (due to poor flight qualities of the Sec-containing peptides) nor via ICP-MS (due to a lower deviation of the detection limit). We therefore have to assume that the protein was likely a mixture of full-length and truncated Sec-containing and Sec-free molecules. Since hTGR needs FAD as a prosthetic group in order to evolve catalytic activity,

an increase in the FAD incorporation rate was attempted by adding FAD to the hTGR at different time points (in culture media before and after induction, in the purification process, and to the already purified protein) in the master's thesis of Eva König [203], however, without increasing the specific activity. Nevertheless, an incorporation of FAD, albeit without saturation, was verified with the typical absorption titration spectrum with NADPH which demonstrated a functional active thiolate-flavin charge transfer complex inside hTGR (Chapter 4.3.2).

5.2.2 Kinetic characterization of hTGR and hTGR^{U642C}

The selenocysteine protein hTGR concatenates the most powerful redox-regulating systems inside the cell: the thioredoxin and the glutathione systems. As mentioned before, the hTGR has an unusually wide substrate range by reducing thioredoxin and oxidized glutathione and also facilitating the deglutathionylation of the artificial substrate HEDS. The hTrxR domain of hTGR catalyzes the NADPH-dependent reduction of oxidized Trx ($Trx(S)_2$) in several distinct reaction steps, including the transfer of electrons from NADPH to FAD and from FAD to the N-terminal active site cysteines. The flexible C-terminal end of another subunit acts subsequently as an electron shuttle between the N-terminal active site in the TrxR domain and the Trx [78, 128, 288]. Native human TrxR from placenta was shown to have a K_M value of 88 µM and a k_{cat} of 33 sec^{-1} in the DTNB assay, but showed no GR activity, which was surprising since substrate recognition sites of hGR for GSSG are conserved in hTrxR and the same cofactors are responsible for electron transport. This non-existent GR activity was hypothesized to be a C-terminal extension of 16 amino acids [289], but other authors could disprove this concept with hTrxR mutants that lack this C-terminal tail and only showed weak GR activity (25 mU/mg) [290] compared to the wild type hGR (200 U/mg) [291-293]. The hTGR involves a TrxR module with an N-terminal elongation composed of a monothiol glutaredoxin domain [146, 294]. Based on the assembly of hTGR, naming the enzyme thioredoxin glutathione reductase does not seem to be reasonable but was indeed the right choice since hTGR shows distinct GR activity. In *Schistosoma mansoni* and other platyhelminths, TrxR and GR are absent as independent entities and only appear as a combined enzyme in the TGR form [120, 141], which is also applicable to *Taenia solium* [143], illustrating the parasite's redox system as a bottleneck dependent on TGR [295]. TGR from the helminth *Schistosoma japonicum* (*Sj*TGR) shares about 55% similarity to the human TGR and was kinetically described by Song *et al.* [296] and Han *et al.* [297]. Song *et al.* expressed the *Sj*TGR in the presence of ^{75}Se, pSUABC, and selenate and reported selenocysteine incorporation but no incorporation rate. Han *et al.* did not include any beneficial additives or a helper plasmid for Sec incorporation and could measure a TrxR activity using the DTNB assay, which was 5.13 U/mg compared to Sun *et al*. They reported a TrxR activity in the DTNB assay of 8.1 U/mg, which leads to the suggestion of a low Sec incorporation rate in the TGR of Han *et al.*. TGR from *Schistosoma mansoni* (*Sm*TGR) is 91% identical to *Sj*TGR and was likewise expressed as *Sj*TGR. Kinetic analysis of *Sm*TGR could show similar results in kinetic parameters [295]. At this point, I would like to mention that Kuntz *et al*. did a kinetic comparison of *Sm*TGR and human TGR, but the cited paper for hTGR was conducted on mouse TGR. TGR of the parasite *Taenia solium* cysticerci, which is involved in neurocysticercosis, occurs in two isoforms: cytosolic (c*Ts*TGR) and mitochondrial TGR (m*Ts*TGR). Isolated native c*Ts*TGR and m*Ts*TGR show kinetic properties in the DTNB assay that are similar to *Schistosoma* TGRs. The specific activity in the TrxR assay of both enzymes is lower than that in *Sm* and *Sj*TGR and especially in c*Ts*TGR, which had a specific activity in this assay that was four orders of magnitude lower. GR activity was also in the same range but with a lower K_M, and the HEDS assay revealed a significant difference in Grx activity

between the *Ts* isoforms [143]. Kinetic characterizations on mammalian TGR have so far been exclusively conducted on mouse TGR. Sun *et al*. [118], expressing mouse TGR at conditions very similar to this study, were able to reach a Sec incorporation rate of 10% by working with an enzyme mixture that consisted of wild type proteins and truncated proteins without Sec incorporation. Enzymatic studies of this mouse TGR revealed how important Sec is for TrxR and GR activity, whereas Cys only partially compensates for the replaced Sec. The authors also claimed that Grx activity depended on Sec, but the underlying HEDS assay was performed without GSH. As a consequence, the detected activity could be caused by TrxR or GR activity reducing the disulfide HEDS with NADPH as an electron donor, which would also lead to a weak readout, but in fact it is not the traditional HEDS assay for Grx activity measurements. A similar result with native hTrxR (from placenta) [204], $hTrxR^{U498C}$ [290], $hTGR^{151\text{-}643}$, and hTGR wild type could be shown in this thesis (Table 18). This result also explains the influence of Sec in this cut back assay since both TrxR and GR activities depend on Sec. The significant difference in HEDS activity between native hTrxR and recombinant $hTrxR^{U498S}$ strengthens the Sec dependency of this TrxR-based phenomenon. In a HEDS assay containing GSH, performed by the same authors, Grx activity did not depend on Sec, which was demonstrated on Sec→Cys, Sec→Ser, and Sec→Stop mutants. Additionally, the authors characterized the isolated Grx domain of mice TGR in the HEDS assay, detecting even higher specific activity there than in the entire TGR, which substantiates Sec independence of the Grx activity inside the TGR. Furthermore, adding human Grx2 (dithiol) and the Grx domain of rat liver TGR (monothiol) to the GR assay of rat TrxR and TGR led to an increase in GR activity [118]. This finding is also contestable since mammalian TrxRs are able to reduce oxidized dithiol Grx [298] and covalently dimerized monothiol Grxs [147, 299, 300] by using electrons from NADPH, which would also lead to an increase in GR assay read-outs but is in fact an activity based on TrxR and dependent on the concentration of Grx as demonstrated in the experiment. It was not reported whether the added Grxs were reduced prior to this experiment or if the Grx reduction due to TrxR was subtracted as a background reaction. In this thesis, the kinetic properties of human TGR were characterized for the first time. In the DTNB assay, the human homolog showed less specific activity in DTNB and NADPH turnover but a higher affinity to DTNB than other TGRs. The specific activity of hTGR in the TrxR assay was slightly lower than that of *Sj*TGR, *Sm*TGR, and m*Ts*TGR but was higher than that of c*Ts*TGR and mouse TGR. The specific activity in the GR assay was also slightly lower but higher than that in mouse TGR. Additionally, the HEDS assay showed similar results for hTGR compared to the parasitic TGRs but was significantly higher than that in mouse TGR. Although Sec incorporation was not detectable, a significant difference in activity could be shown in the TrxR and GR activities of hTGR of the full-length and truncated Sec→Cys mutant enzyme. The results suggest Sec dependency in the TrxR and GR activity but Sec independence in the HEDS activity (Table 19). It should be mentioned that the kinetic parameters determined can vary depending on the Sec incorporation and FAD saturation rates of the selenoproteins.

Table 19: Comparison of kinetic activities of TGRs from different species. Kinetic parameters of *S. japonicum*, *S. mansoni*, *M. musculus*, and both cytosolic and mitochondrial *Taenia solium* cysticerci are compared to human TGR. Enzymatic assays were performed as mentioned in Materials and Methods. All assays are based on the same or very similar protocols for TrxR, GR, and HEDS assays, varying slightly due to individual adaptations for the respective enzymes. N. d. = not detectable

	Schistosoma japonicum [296]		*Schistosoma mansoni* [295]		Mouse [118]		Mouse Sec → Cys mutant [118]		*Taenia solium* cysticerci (cytosolic) [143]		*Taenia solium* cysticerci (mitochondrial) [143]		**Human**		**Human Sec → Cys mutant**	
	Specific activity [µmol * min^{-1} * mg^{-1}]															
TrxR activity (Trx)	3.3		2.2		0.040		0.008		0.0002		1.02		**0.10**		**0.02**	
TrxR activity (DTNB)	8.1		10.2		0.174		0.123		2.14		10.1		**0.14**		**0.02**	
HEDS activity	12.1		9.9		0.413		0.348		3.05		131		**11.5**		**11.6**	
GR activity	2.2		7.2		0.023		0.004		0.98		1.3		**0.07**		**n. d.**	
	K_M (µM)	k_{cat} (s^{-1})	K_M (µM)	k_{cat} (s^{-1})	K_M (µM)	k_{cat} (s^{-1})	K_M (µM)	k_{cat} (s^{-1})	K_M (µM)	k_{cat} (s^{-1})	K_M (µM)	k_{cat} (s^{-1})	K_M (µM)	k_{cat} (s^{-1})	K_M (µM)	k_{cat} (s^{-1})
TrxR assay																
Trx	3	4.78	6.4	30	-	-	-	-	67	0.35	-	-	**7.5**	**0.2**	**20.5**	**0.02**
NADPH	-	-	-	-	-	-	-	-	-	-	-	-	**16.6**	**0.2**	**5.1**	**0.02**
DTNB assay																
DTNB	145	8.2	114	16	-	-	-	-	88	1.85	45	12.6	**6.0**	**0.2**	**17.1**	**0.03**
NADPH	21	10.9	13.7	20.1	-	-	-	-	48	1.64	1.6	12.6	**5.1**	**0.1**	**0.4**	**0.02**
HEDS assay																
GSH	1698	15.8	248	20.1	-	-	-	-	-	-	-	-	**447**	**4.8**	**544**	**6.5**
HEDS	2792	8.7	1867	17.8	-	-	-	-	184	5.13	410	163	**535**	**21.1**	**547**	**20.7**
GR assay																
GSSG	49	5.35	71	21.7	-	-	-	-	6.3	0.96	4	1.6	**20.8**	**0.11**	**n. d.**	**n. d.**
NADPH	83	4.87	-	-	-	-	-	-	-	-	-	-	**20.8**	**0.14**	**n. d.**	**n. d.**

5.2.3 Proposed catalytic reaction mechanism of hTGR

The catalytic mechanism of the TGR is not yet fully understood and is subject to ongoing mechanistic theories. Dimeric hTGR is composed of two identical subunits with two domains each (TrxR and Grx domains) (Figure 52), probably arranged in a head-to-tail manner as in other TGRs [122]. According to the catalytic mechanism of TrxR, reducing equivalents obtained from NADPH are transported to the prosthetic group FAD and to the adjacent dithiol/disulfide redox center (C203/C208) and further to the cysteine/selenocysteine pair of the second subunit (C641´/U642´) to reduce oxidized Trx, DTNB, and GSSG [130, 204, 301-303]. In contrast to parasitic TGRs, where the additional cysteine pair of the dithiol Grx domain is likewise dependent on the flexible C-terminal arm by obtaining reducing equivalents from the cysteine/selenocysteine pair, the human TGR contains a monothiol Grx domain. Huang *et al*. proposed two potential mechanisms of deglutathionylation reactions inside the Grx domain catalyzed by a dithiol Grx. After the first Cys residue is glutathionylated, resulting in a mixed disulfide, the first mechanism includes resolving the glutathionylated cysteine with high concentrations of GSH (monothiol mechanism) and the second suggests the second cysteine to act as a resolving cysteine in order to break the GrxS-SG intermediate by building a disulfide with the first cysteine and releasing GSH (dithiol mechanism). This disulfide will then be reduced by the C-terminal redox pair [304], which explains the Sec-dependency of HEDS activity in parasitic TGRs (dithiol Grx). Since human TGR contains a monothiol Grx, the second proposed mechanism for deglutathionylation processes is not conceivable for mammalian TGRs. The measured Sec independence of HEDS activity and the presence of only one redox-active cysteine in the Grx domain support the conjecture of a traditional monothiol Grx deglutathionylation mechanism inside hTGR. Additionally, TGR has GR activity that is thought to be facilitated due to its Grx domain [122, 141] by the second cysteine stabilizing the thiolate anion on the first cysteine inside the Grx domain via a hydrogen bond, which was also possible with Ser mutants of the second Cys. Stabilized as an anion, the first Cys is able to start the nucleophilic attack on GSSG. The resulting mixed disulfide between the Grx domain and GSH_I can be resolved by electron pairs from the C-terminal arm [304]. Furthermore, in NMR studies of the monothiol Grx domain of *Mus musculus* TGR, a significant overlap between the GSH and GSSG binding sites has been postulated [159]. In conclusion, the N-terminal Cys in the Grx domain of the TGR is able to bind both glutathionylated proteins (or glutathionylated HEDS) and GSSG [303].

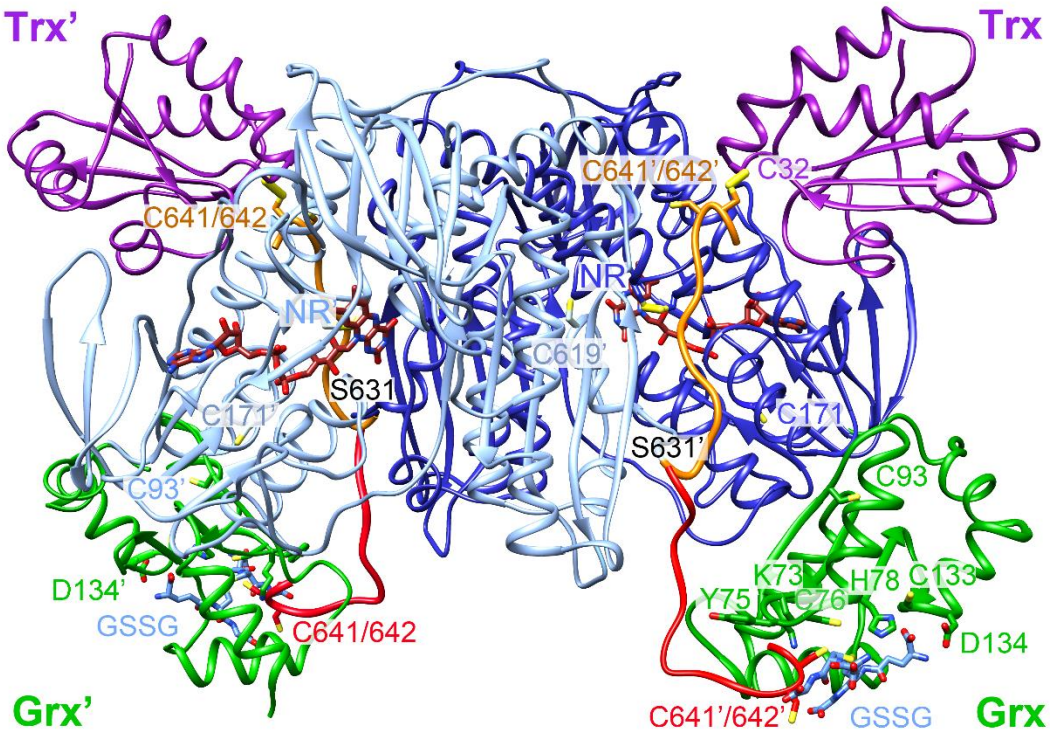

Figure 52: Model of the hTGR dimer in complex with bound Trx and GSSG. HTrx1 (purple) and hTGR are shown in ribbon representation. The two subunits of the TrxR moiety are colored dark blue and light blue and the Grx moieties are shown in green. The flexible C-terminal loop (632- 642) is colored orange or red depending whether it interacts with Trx or Grx, respectively. FAD (brown), GSSG (steel blue) and some relevant hTGR residues are shown in sticks. The NADPH dependent redox centers are marked with NR (C203, C208), the C-terminal with C641/642 and the Grx active site cysteine is labeled with C76. The rotation center of the swinging C-terminal arm is indicated by S631. Modeling was performed using the crystal structures of 3qfa (hTrxR+hTrx; TrxR-part:seq_id = 75%) [129], 3h8q (human; Grx-domain:, A51-E151) and 2x8h (*sm*TR; TrxR-part seq_id = 55%) [305] as templates [306]. The structural superposition of the models and the known structures has been done with Coot [307]; Phenix was used for the refinement of the complete model and all figures have been prepared with Chimera [308].

However, in our study, none of the four generated GSH binding site mutants showed drastic changes in GR activity when compared to wild type hTGR (C133S: 0.07 U/mg; H78A: 0.03 U/mg; D134A: 0.05 U/mg; C133S/D134A: 0.14 U/mg; wild type hTGR: 0.07 U/mg; given are mean values of two independent experiments, which differed by less than 10%) [303]. Therefore, although the GR activity of TGR clearly depends on the Grx domain – be it monothiol or dithiol (Table 14 & 15) [122, 141] – the residues involved in GSH binding seem to contribute only partially to GSSG binding. The crystal structures of *Co*Grx with bound GSH (4tr0) and with bound GSSG (4tr1) [309] showed that oxidized GSH (GSSG), composed of two GSH molecules (GSH_I and GSH_{II}), is mainly bound by GSH_I to the enzyme. Interestingly, the comparison of the highly conserved GSH binding pocket of *Co*Grx, hTGR, mice TGR, and *Sm*TGR showed more similarity between the mammalian TGRs and *Co*Grx than with bacterial TGR [303]. In *Sm*TGR, the GSH γ-glutamyl moiety interacts with Asp84, which is replaced by a glycine in *Co*Grx (G65), hTGR (G132), and mouse TGR (G104); instead the interacting asparagine residues are Asp67, Asp134, and Asp106, respectively. Ser85 in *Sm*TGR is substituted by a cysteine and Thr27 by a tyrosine residue in *Clostridium oremlandii*, humans, and mice. Therefore, we modelled the GSH and GSSG binding to the Grx domain of hTGR according to the *Co*Grx crystal structures (Figure 52) [303]. GSH_I has a large number of interactions with Grx in contrast to GSH_{II}, which is bound very loosely and is only stabilized with one hydrogen bond to the main chain of Tyr11 and van der Waals interactions with the

side chains of Pro13 and Tyr11 (corresponding to Tyr75 in hTGR). The position of GSH_I differs only slightly between the two mentioned structures; however, upon GSSG binding, Grx markedly changes its conformation - mainly in the region aa 10-14 (NY**C**PY), corresponding to aa 74-78 (SY**C**PH) in hTGR, to aa 46-50 (SY**C**PH) in mouse TGR, and to aa 26-30 (TT**C**PY) in *Sm*TGR [303]. Furthermore, the side chain of the first tyrosine residue (Tyr75 in hTGR) moves outwards and interacts with the second GSH moiety (GSH_{II}). Based on our considerations, this is a central mechanistic turning point in catalysis since the movement of the tyrosine opens the access for the reducing C-terminal arm to the oxidizing disulfide. We hypothesize that in case of the GR reaction of hTGR this could be either the bound GSSG molecule itself or a nascent mixed disulfide between Cys76 and GSH_I. As long as only GSH is bound, the side chain of Tyr75 (hTGR) blocks this access, and the GSH glycine moiety interacts per two strong hydrogen interactions with the side chains of Tyr75 and Lys73 (Figure 53) [303]. These interactions are not present when GSSG is bound, which allows the positively charged Lys73 to stabilize the negatively charged C-terminal arm, thus enabling the reduction process of substrates. In our model, only the last 10 residues of the C-terminal arm have to oscillate towards the active site of Grx, and notably the last 4 residues (GCUG) keep the same conformation as seen in the hTrxR-Trx complex structure (Figure 52). We therefore propose that GSH and GSSG binding in hTGR depend on the intracellular [GSH]/[GSSG] ratio. At low GSSG concentrations and high GSH concentrations, the Grx domain is able to act independently to deglutathionylate specific interaction partners conjugated with GSH. The high GSH concentration would then help resolve the Cys-SG mixed disulfide as mentioned before, which could be verified with the $hTGR^{1-150}$ (Grx domain) in the HEDS assay. At high GSSG concentrations (and low GSH concentrations) (GR assay), GSSG binds to the Grx domain and is directly or indirectly (via a mixed disulfide with Cys76) reduced by the flexible arm [303]. In both cases, the NADPH-reduced, Cys-Sec-containing arm will deliver the electrons required for GSH release [303], in accordance to the reaction model proposed by Sun *et al*. [118, 119].

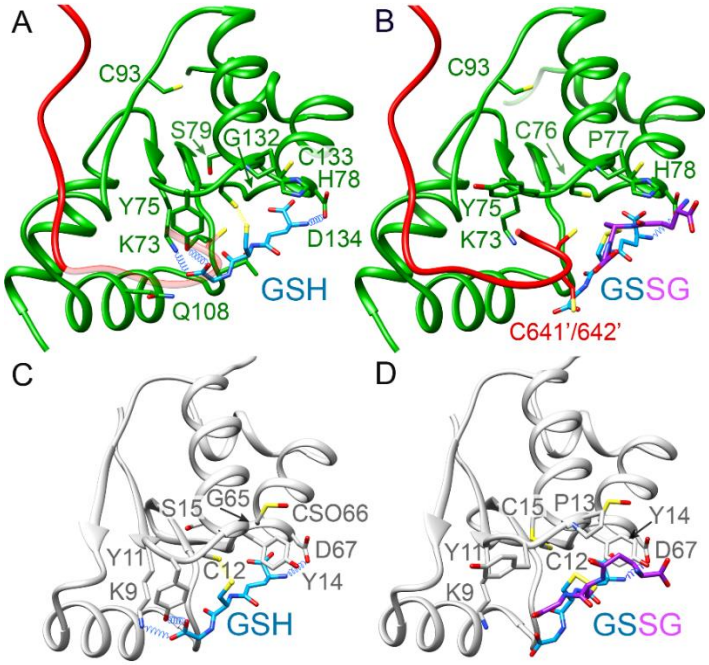

Figure 53: Structural model of GSH (A) and GSSG (B) binding to the monothiol Grx domain of hTGR, according to the Grx crystal structures from the bacterium *Clostridium oremlandii* with bound GSH (C, 4tr0) or with bound GSSG (D, 4tr1). GSH, GSSG, and Grx residues involved in substrate binding are shown as sticks; for clarity hTGR residues are marked in A or B. GSSG is composed of two molecules GSH1 (blue) and GSH2 (light purple). Hydrogen bonds to GSH are shown with blue springs. In A and B the Grx ribbon is colored green and the C-terminal arm of the TrxR-domain red; in A the access for the arm is blocked by Y75, marked by a transparent representation.

5.2.4 *S*-glutathionylation of hTGR

Protein-*S*-glutathionylation is an established modification of reactive cysteines in the context of PTM, which is site specific and reversible. This modification was reported to inhibit [310-312] or activate [313, 314] proteins, sometimes both, depending on the cysteines involved inside the protein [315]. For the TGR homolog from the platyhelmith *Echinococcus granulosus*, glutathionylation on specific cysteines has already been reported in connection with a hysteretic behavior of the enzyme (see Chapters 4.3.3.4 and 4.3.4). The authors could detect glutathionylation sites at position C88 and C354 and intramolecular disulfide formations in cysteines belonging to the Grx active site and TGR CxxxxC catalytic redox center when the protein was glutathionylated [141, 142]. The authors did not conduct an inhibitory or activating effect on TGR activity. Cysteine 88 of *E. granulosus* is located in a motif conserved in human TGR and corresponds to the C171 of hTGR. [315]. Five mM of GSSG could glutathionylate the enzyme hTGR (Figure 44). The inhibiting influence of glutathionylation on the enzyme's activity in the TrxR, DTNB, HEDS, and GR assays is shown in Table 16. All specific activities are significantly inhibited in this manner. The glutathionylated protein showed 30% less activity in the TrxR assay, 60% less in the DTNB assay, 11% less in the HEDS assay, and 57% less in the GR assay than the non-modified enzyme. Although peptides that contain the active site cysteines of hTGR were undetectable via mass spectrometry, it could be proved that hTGR can be glutathionylated at different cysteines. The glutathionylated protein showed significant inhibitions in its kinetic efficiency towards Trx, DTNB, GSSG, and HEDS. Cysteine 571 and 171 are both buried in the hTGR structure and were found once to be glutathionylated in triplicate. Cysteines that are modified by glutathione in all three repetitions are C93, C133, and C619. Glutathionylation at C93 in hTGR could hinder the flexibility of the C-terminal arm, which would lead to an inhibition of all Sec-dependent activities (TrxR and GR activity). Moreover, the modification at C619 could lead to restricted electron transport from the C-terminal arm to the redox-active sites. The cysteine at position 133 is located in the immediate vicinity of Grx's active site (also described in Brandstaedter *et al.*). Therefore, HEDS activity might be impaired via glutathionylation at this residue. Since mass spectrometry data did not include the active site cysteines of hTGR, no information about the glutathionylation status of these cysteines is available so far, and modification at these redox-active centers is possible as well. Active site glutathionylation here would lead to direct inhibition of the respective enzyme activities, but this remains speculative. Human thioredoxin glutathione reductase catalyzes the reduction of GSSG and exhibits deglutathionylation properties, raising the question of whether hTGR glutathionylation itself takes place *in vivo* under physiological conditions.

5.2.5 Hysteretic behavior of hTGR

In several TGR homologs, a hysteretic behavior was reported when GSSG was used as a substrate in high concentrations [141-143, 189, 316, 317] but was not reported to appear in *Schistosoma* or any mammalian TGRs. Some authors explained the hysteretic behavior as strong, temporary substrate inhibition of GSSG that an increase in enzyme concentration could reverse [143], and others suggested that the lag phase depended on the Grx domain of TGR [316]. Since mutants of the C-terminal Cys in the Grx domain were reported to be able to abolish GR hysteresis [304, 318], implicating a disulfide intermediate between GSSG and the C-terminal Cys residue [189], which unfortunately could not be found in the Grx domain or catalytic redox center of TGR [141]. Additionally, in all hysteretic TGRs found so far, the inhibitory influence of GSSG has been reported to be reversible and temporary. Nonetheless, in this thesis it was shown that hTGR does not exhibit hysteretic behavior at high GSSG

concentrations in the GR assay under tested conditions. Although a glutathionylation could be verified, which has a significant influence on any kinetic activities of hTGR, and substrate inhibition at GSSG concentrations above 200 µM occured, these inhibiting modifications were not temporary. In the full time course of the GR assay, no lag phase due to a reduced initial reaction velocity at high GSSG concentrations was monitored (Figure 43). The inhibiting effect of high GSSG concentrations was illustrated as a persisting influence on the enzyme. Hysteretic behavior therefore seems not to be a common feature of all TGRs, even when some cysteine residues that are glutathionylated are highly conserved. Parasitic and helminthic TGRs contain a dithiol Grx domain instead of the monothiol Grx domain in mammalian TGRs, which could suggest that this second cysteine in the N-terminal elongation is involved in the manifestation of this unusual kinetic behavior [303].

In this thesis, recombinant hTGR was kinetically characterized, interacting with its substrates NADPH, GSSG, Trx, and HEDS. To determine the pK_a of the active site cysteines of the respective catalytic domains, functional assays could be conducted in future analyses with the isolated Grx and TrxR domains at varying pH values, revealing the reactivity of the active site Cys. Furthermore, the influence of additional posttranslational modifications such as nitrosylation could be studied in more detail, and crystallization (and co-crystallization) trials might give a deeper insight into the structure and kinetic mechanisms. To gather the full spectrum of kinetic parameters of the fully FAD-saturated hTGR and to obtain a sample consisting of pure Sec-containing enzyme, an isolation of hTGR from human testes could be a useful tool. As shown for other NADPH dependent and Sec-rich proteins, a chloroform-1-butanol extraction followed by acetone precipitation and DEAE cellulose chromatography, 2′,5′-ADP-Sepharose 4B affinity chromatography as well as an add-on fast protein liquid chromatography could lead to the native protein [204]. Due to this, interaction partners might be identified with mutants of the recombinant enzyme using testes cell lysate as a pool of interacting proteins. Additionally, cell culture experiments in human cancer cells lines and cross-linking as well as immunoprecipitation could also identify potentially interacting proteins. Once interacting proteins are identified, the biochemical relevance of hTGR as a hybrid enzyme of two independently existing and highly active enzymes could be illustrated, and inhibition studies could outline a potential medical impact of hTGR.

REFERENCES

1. Martindale JL & Holbrook NJ (**2002**) Cellular response to oxidative stress: Signaling for suicide and survival. ***J Cell Physiol*** 192, 1-15.

2. Ray PD, Huang BW & Tsuji Y (**2012**) Reactive oxygen species (ROS) homeostasis and redox regulation in cellular signaling. ***Cell Signal*** 24, 981-990.

3. Stohs SJ & Bagchi D (**1995**) Oxidative mechanisms in the toxicity of metal ions. ***Free Radical Bio Med*** 18, 321-336.

4. Dzaugis ME, Spivack AJ, D'Hondt S (**2015**) A quantitative model of water radiolysis and chemical production rates near radionuclide-containing solids. ***Radiat Phys Chem*** 115, 127-134.

5. Yamauchi R (**1997**) Vitamin E: Mechanism of its antioxidant activity. ***Food Sci Technol Int Tokyo*** 3, 301-309.

6. White E, Shannon JS, Patterson RE (**1997**) Relationship between vitamin and calcium supplement use and colon cancer. ***Cancer Epidem Biomar*** 6, 769-774.

7. Meister A, Anderson ME (**1983**) Glutathione. ***Annu Rev Biochem*** 52, 711-760.

8. Masella R, Di Benedetto R, Vari R, Filesi C, Giovannini C (**2005**) Novel mechanisms of natural antioxidant compounds in biological systems: Involvement of glutathione and glutathione-related enzymes. ***J Nutr Biochem*** 16, 577-586.

9. Pompella A, Visvikis A, Paolicchi A, De Tata V, Casini AF (**2003**) The changing faces of glutathione, a cellular protagonist. ***Biochem Pharmacol*** 66, 1499-1503.

10. Birben E, Sahiner UM, Sackesen C, Erzurum S, Kalayci O (**2012**) Oxidative Stress and Antioxidant Defense. ***World Allergy Organ J*** 5, 9-19.

11. Girotti AW (**1985**) Mechanisms of lipid peroxidation. ***J Free Radic Biol Med*** 1, 87-95.

12. Dean RT, Roberts CR, Jessup W (**1985**) Fragmentation of extracellular and intracellular polypeptides by free radicals. ***Prog Clin Biol Res*** 180, 341-350.

13. Yang J, Carroll KS, Liebler DC (**2016**) The expanding landscape of the thiol redox proteome. ***Mol Cell Proteomics*** 15, 1-11.

14. Jones DP, Sies H (**2015**) The redox code. ***Antioxid Redox Signal*** 23, 734-746.

15. Belcastro E, Gaucher C, Corti A, Leroy P, Lartaud I, Pompella A (**2017**) Regulation of protein function by *S*-nitrosation and *S*-glutathionylation: processes and targets in cardiovascular pathophysiology. ***Biol Chem*** 398, 1267-1293.

16. Miseta A, Csutora P (**2000**) Relationship between the occurrence of cysteine in proteins and the complexity of organisms. ***Mol Biol Evol*** 17, 1232-1239.

17. Deponte M, Lillig CH (**2015**) Enzymatic control of cysteinyl thiol switches in proteins. ***Biol Chem*** 396, 401-413.

18. Deponte M (**2013**) Glutathione catalysis and the reaction mechanisms of glutathione-dependent enzymes. ***Biochim Ciophys Acta*** 1830, 3217-3266.

19. Kojer K, Riemer J (**2014**) Balancing oxidative protein folding: the influences of reducing pathways on disulfide bond formation. ***Biochim Ciophys Acta*** 1844, 1383-1390.

20. Hogg PJ (**2003**) Disulfide bonds as switches for protein function. ***Trends Biochem Sci*** 28, 210-214.

21. Wiita AP, Perez-Jimenez R, Walther KA, Grater F, Berne BJ, Holmgren A, Sanchez-Ruiz JM, Fernandez JM (**2007**) Probing the chemistry of thioredoxin catalysis with force. ***Nature*** 450, 124-127.

22. Roos G, Foloppe N, Van Laer K, Wyns L, Nilsson L, Geerlings P, Messens J (**2009**) How Thioredoxin dissociates its mixed disulfide. ***Plos Comput Biol*** 5**,** e1000461.

23. Nelson JW, Creighton TE (**1994**) Reactivity and ionization of the active-site cysteine residues of Dsba, a protein required for disulfide bond formation *in vivo*. ***Biochemistry*** 33, 5974-5983.

24. Forman HJ, Maiorino M, Ursini F (**2010**) Signaling functions of reactive oxygen species. ***Biochemistry*** 49, 835-842.

25. Marino SM, Gladyshev VN (**2010**) Structural analysis of cysteine *S*-nitrosylation: a modified acid-based motif and the emerging role of trans-nitrosylation. ***J Mol Biol*** 395, 844-859.

26. Allison WS (**1976**) Formation and reactions of sulfenic acids in proteins. ***Accounts Chem Res*** 9, 293-299.

27. Conway ME, Poole LB, Hutson SM (**2004**) Roles for cysteine residues in the regulatory CXXC motif of human mitochondrial branched chain aminotransferase enzyme. ***Biochemistry*** 43, 7356-7364.

28. Stewart EJ, Aslund F, Beckwith J (**1998**) Disulfide bond formation in the *Escherichia coli* cytoplasm: an in vivo role reversal for the thioredoxins. ***Embo J*** 17, 5543-5550.

29. Brigelius-Flohe R, Flohe L (**2011**) Basic principles and emerging concepts in the redox control of transcription factors. ***Antioxid Redox Signal*** 15, 2335-2381.

30. Delaunay A, Pflieger D, Barrault MB, Vinh J, Toledano MB (**2002**) A thiol peroxidase is an H_2O_2 receptor and redox-transducer in gene activation. ***Cell*** 111, 471-481.

31. Wood ZA, Schroder E, Harris JR, Poole LB (**2003**) Structure, mechanism and regulation of peroxiredoxins. ***Trends Biochem Sci*** 28, 32-40.

32. Perkins A, Poole LB, Karplus PA (**2014**) Tuning of peroxiredoxin catalysis for various physiological roles. ***Biochemistry*** 53, 7693-7705.

33. Wen ST, VanEtten RA (**1997**) The PAG gene product, a stress-induced protein with antioxidant properties, is an Abl SH3-binding protein and a physiological inhibitor of c-Abl tyrosine kinase activity. ***Gene Dev*** 11, 2456-2467.

34. Neumann CA, Krause DS, Carman CV, Das S, Dubey DP, Abraham JL, Bronson RT, Fujiwara Y, Orkin SH, Van Etten RA (**2003**) Essential role for the peroxiredoxin Prdx1 in erythrocyte antioxidant defence and tumour suppression. ***Nature*** 424, 561-565.

35. Shau HY, Gupta RK, Golub SH (**1993**) Identification of a natural killer enhancing factor (Nkef) from human erythroid cells. ***Cell Immunol*** 147, 1-11.

36. Rhee SG, Woo HA (**2011**) Multiple functions of peroxiredoxins: peroxidases, sensors and regulators of the intracellular messenger H_2O_2, and protein chaperones. ***Antioxid Redox Signal*** 15, 781-794.

37. Prosperi MT, Ferbus D, Karczinski I, Goubin G (**1993**) A human cDNA corresponding to a gene overexpressed during cell proliferation encodes a product sharing homology with amoebic and bacterial proteins. ***J Biol Chem*** 268, 11050-11056.

38. Diet A, Abbas K, Bouton C, Guillon B, Tomasello F, Fourquet S, Toledano MB, Drapier JC (**2007**) Regulation of peroxiredoxins by nitric oxide in immunostimulated macrophages. ***J Biol Chem*** 282, 36199-36205.

39. Ishii T, Yamada M, Sato H, Matsue M, Taketani S, Nakayama K, Sugita Y, Bannai S (**1993**) Cloning and characterization of a 23 kDa stress-induced mouse peritoneal macrophage protein. ***J Biol Chem*** 268, 18633-18636.

40. Day AM, Brown JD, Taylor SR, Rand JD, Morgan BA, Veal EA (**2012**) Inactivation of a peroxiredoxin by hydrogen peroxide is critical for thioredoxin-mediated repair of oxidized proteins and cell survival. ***Mol Cell*** 45, 398-408.

41. Karplus PA, Poole LB (**2012**) Peroxiredoxins as molecular triage agents, sacrificing themselves to enhance cell survival during a peroxide attack. ***Mol Cell*** 45, 275-278.

42. Wood ZA, Poole LB, Karplus PA (**2003**) Peroxiredoxin evolution and the regulation of hydrogen peroxide signaling. ***Science*** 300, 650-653.

43. World Health Organization (**2011**) Working to overcome the global impact of neglected tropical diseases. Geneva, Switzerland.

44. Perkins A, Nelson KJ, Parsonage D, Poole LB, Karplus PA (**2015**) Peroxiredoxins: guardians against oxidative stress and modulators of peroxide signaling. ***Trends Biochem Sci*** 40, 435-445.

45. Nelson KJ, Knutson ST, Soito L, Klomsiri C, Poole LB, Fetrow JS (**2011**) Analysis of the peroxiredoxin family: Using active-site structure and sequence information for global classification and residue analysis. ***Proteins*** 79, 947-964.

46. Knoops B, Loumaye E, van der Eecken V (**2007**) Evolution of the peroxiredoxins. Taxonomy, homology and characterization. ***Subcell Biochem*** 44, 27-40.

47. Rhee SG, Woo HA, Kil IS, Bae SH (**2012**) Peroxiredoxin functions as a peroxidase and a regulator and sensor of local peroxides. ***J Biol Chem*** 287, 4403-4410.

48. Karplus PA, Hall A (**2007**) Structural survey of the peroxiredoxins. ***Subcell Biochem*** 44, 41-60.

49. Choi J, Choi S, Chon JK, Choi J, Cha MK, Kim IH & Shin W (**2005**) Crystal structure of the C107S/C112S mutant of yeast nuclear 2-Cys peroxiredoxin. ***Proteins*** 61, 1146-1149.

50. Lowther WT, Haynes AC (**2011**) Reduction of cysteine sulfinic acid in eukaryotic, typical 2-Cys reroxiredoxins by sulfiredoxin. ***Antioxid Redox Signal*** 15, 99-109.

51. Saccoccia F, Di Micco P, Boumis G, Brunori M, Koutris I, Miele AE, Morea V, Sriratana P, Williams DL, Bellelli A (**2012**) Moonlighting by different stressors: crystal structure of the chaperone species of a 2-Cys ceroxiredoxin. ***Structure*** 20, 429-439.

52. Konig J, Galliardt H, Jutte P, Schaper S, Dittmann L, Dietz KJ (**2013**) The conformational bases for the two functionalities of 2-cysteine peroxiredoxins as peroxidase and chaperone. ***J Exp Bot*** 64, 3483-3497.

53. Chae HZ, Oubrahim H, Park JW, Rhee SG, Chock PB (**2012**) Protein glutathionylation in the regulation of peroxiredoxins: a family of thiol-specific peroxidases that function as antioxidants, molecular chaperones, and signal modulators. ***Antioxid Redox Signal*** 16, 506-523.

54. Rhee SG, Woo HA, Kil IS, Bae SH (**2012**) Peroxiredoxin functions as a peroxidase and a regulator and sensor of local peroxides. ***J Biol Chem*** 287, 4403-4410.

55. Seo JH, Lim JC, Lee DY, Kim KS, Piszczek G, Nam HW, Kim YS, Ahn T, Yun CH, Kim K (**2009**) Novel protective mechanism against irreversible hyperoxidation of peroxiredoxin N-alpha-terminal acetylation of human peroxiredoxin II. ***J Biol Chem*** 284, 13455-13465.

56. Koo KH, Lee S, Jeong SY, Kim ET, Kim HJ, Kim K, Song K & Chae HZ (**2002**) Regulation of thioredoxin peroxidase activity by C-terminal truncation. ***Arch Biochem Biophys*** 397, 312-318.

57. Poole LB (**2007**) The catalytic mechanism of peroxiredoxins. ***Subcell Biochem*** 44, 61-81.

58. Netto LES, de Oliveira MA, Tairum CA & Neto JFD (**2016**) Conferring specificity in redox pathways by enzymatic thiol/disulfide exchange reactions. ***Free Radic Res*** 50, 206-245.

59. Saitoh M, Nishitoh H, Fujii M, Takeda K, Tobiume K, Sawada Y, Kawabata M, Miyazono K & Ichijo H (**1998**) Mammalian thioredoxin is a direct inhibitor of apoptosis signal-regulating kinase (ASK) 1. ***Embo J*** 17, 2596-2606.

60. Hayashi T, Ueno Y & Okamoto T (**1993**) Oxidoreductive regulation of nuclear factor-kappa-B - Involvement of a cellular reducing catalyst thioredoxin. ***J Biol Chem*** 268, 11380-11388.

61. Netto LE & Antunes F (**2016**) The roles of peroxiredoxin and thioredoxin in hydrogen peroxide sensing and in signal transduction. ***Mol Cells*** 39, 65-71.

62. Organization WH (**2015**) World Malaria Report 2015, Geneva, Switzerland.

63. Cox FEG (**2010**) History of the discovery of the malaria parasites and their vectors. ***Parasit Vectors*** 3, 3:5.

64. Organisation WH (**2008**) World Malaria Report 2008, Geneva, Switzerland.

65. Lucius R, Loose-Frank B (**2008**) Biologie von Parasiten. In. Springer-Verlag, Berlin Heidelberg.

66. Garcia-Basteiro AL, Bassat Q & Alonso PL (**2012**) Approaching the target: the path towards an effective malaria vaccine. ***Mediterr J Hematol Infect Dis*** 4, e2012015.

67. Percario S, Moreira DR, Gomes BAQ, Ferreira MES, Goncalves ACM, Laurindo PSOC, Vilhena TC, Dolabela MF, Green MD (**2012**) Oxidative stress in malaria. ***Int J Mol Sci*** 13, 16346-16372.

68. Wink DA, Hines HB, Cheng RYS, Switzer CH, Flores-Santana W, Vitek MP, Ridnour LA, Colton CA (**2011**) Nitric oxide and redox mechanisms in the immune response. ***J Leukocyte Biol*** 89, 873-891.

69. Becker K, Tilley L, Vennerstrom JL, Roberts D, Rogerson S, Ginsburg H (**2004**) Oxidative stress in malaria parasite-infected erythrocytes: host-parasite interactions. ***Int J Parasitol*** 34, 163-189.

70. Loria P, Miller S, Foley M, Tilley L (**1999**) Inhibition of the peroxidative degradation of haem as the basis of action of chloroquine and other quinoline antimalarials. ***Biochem J*** 339, 363-370.

71. Egan TJ, Combrinck JM, Egan J, Hearne GR, Marques HM, Ntenteni S, Sewell BT, Smith PJ, Taylor D, van Schalkwyk DA (**2002**) Fate of haem iron in the malaria parasite *Plasmodium falciparum.* ***Biochem J*** 365, 343-347.

72. Rahlfs S, Schirmer RH, Becker K (**2002**) The thioredoxin system of *Plasmodium falciparum* and other parasites. ***Cell Mol Life Sci*** 59, 1024-1041.

73. Becker K, Rahlfs S, Nickel C, Schirmer RH (**2003**) Glutathione - Functions and metabolism in the malarial parasite *Plasmodium falciparum*. ***Biol Chem*** 384, 551-566.

74. Sztajer H, Gamain B, Aumann KD, Slomianny C, Becker K, Brigelius-Flohe R, Flohe L (**2001**) The putative glutathione peroxidase gene of *Plasmodium falciparum* codes for a thioredoxin peroxidase. ***J Biol Chem*** 276, 7397-7403.

75. Jortzik E, Becker K (**2012**) Thioredoxin and glutathione systems in *Plasmodium falciparum*. ***Int J Med Microbiol*** 302, 187-194.

76. Kehr S, Sturm N, Rahlfs S, Przyborski JM, Becker K (**2010**) Compartmentation of redox metabolism in malaria parasites. ***PLoS Pathog*** 6, e1001242.

77. Nickel C, Rahlfs S, Deponte M, Koncarevic S, Becker K (**2006**) Thioredoxin networks in the malarial parasite *Plasmodium falciparum*. ***Antioxid Redox Signal*** 8, 1227-1239.

78. Williams CH, Arscott LD, Muller S, Lennon BW, Ludwig ML, Wang PF, Veine DM, Becker K, Schirmer RH (**2000**) Thioredoxin reductase - Two modes of catalysis have evolved. ***Eur J Biochem*** 267, 6110-6117.

79. Krnajski Z, Gilberger TW, Walter RD, Cowman AF, Muller S (**2002**) Thioredoxin reductase is essential for the survival of *Plasmodium falciparum* erythrocytic stages. ***J Biol Chem*** 277, 25970-25975.

80. Martin JL (**1995**) Thioredoxin - a fold for all reasons. ***Structure*** 3, 245-250.

81. Berndt C, Lillig CH, Holmgren A (**2008**) Thioredoxins and glutaredoxins as facilitators of protein folding. ***Biochim Biophys Acta*** 1783, 641-650.

82. Krnajski Z, Gilberger TW, Walter RD, Muller S (**2001**) The malaria parasite *Plasmodium falciparum* possesses a functional thioredoxin system. ***Mol Biochem Parasitol*** 112, 219-228.

83. Kanzok SM, Schirmer RH, Turbachova I, Iozef R, Becker K (**2000**) The thioredoxin system of the malaria parasite *Plasmodium falciparum* - Glutathione reduction revisited. ***J Biol Chem*** 275, 40180-40186.

84. Sturm N, Jortzik E, Mailu BM, Koncarevic S, Deponte M, Forchhammer K, Rahlfs S, Becker K (**2009**) Identification of proteins targeted by the thioredoxin superfamily in *Plasmodium falciparum*. ***PLoS Pathog*** 5, e1000383.

85. Kehr S, Jortzik E, Delahunty C, Yates JR, Rahlfs S, Becker K (**2011**) Protein *S*-glutathionylation in malaria parasites. ***Antioxid Redox Signal*** 15, 2855-2865.

86. Becker K, Kanzok SM, Iozef R, Fischer M, Schirmer RH, Rahlfs S (**2003**) Plasmoredoxin, a novel redox-active protein unique for malarial parasites. ***Eur J Biochem*** 270, 1057-1064.

87. Harding JJ, Blakytny R, Ganea E (**1996**) Glutathione in disease. ***Biochem Soc Trans*** 24, 881-884.

88. Patzewitz EM, Wong EH, Muller S (**2012**) Dissecting the role of glutathione biosynthesis in *Plasmodium falciparum*. ***Mol Microbiol*** 83, 304-318.

89. Sarma GN, Savvides SN, Becker K, Schirmer M, Schirmer RH, Karplus PA (**2003**) Glutathione reductase of the malarial parasite *Plasmodium falciparum*: Crystal structure and inhibitor development. ***J Mol Biol*** 328, 893-907.

90. Pastrana-Mena R, Dinglasan RR, Franke-Fayard B, Vega-Rodriguez J, Fuentes-Caraballo M, Baerga-Ortiz A, Coppens I, Jacobs-Lorena M, Janse CJ, Serrano AE (**2010**) Glutathione reductase-null malaria parasites have normal blood stage growth but arrest during development in the mosquito. ***J Biol Chem*** 285, 27045-27056.

91. Buchholz K, Schirmer RH, Eubel JK, Akoachere MB, Dandekar T, Becker K, Gromer S (**2008**) Interactions of methylene blue with human disulfide reductases and their orthologues from *Plasmodium falciparum*. ***Antimicrob Agents Chemother*** 52, 183-191.

92. Stroher E, Millar AH (**2012**) The biological roles of glutaredoxins. ***Biochem J*** 446, 333-348.

93. Rahlfs S, Fischer M, Becker K (**2001**) *Plasmodium falciparum* possesses a classical glutaredoxin and a second, glutaredoxin-like protein with a PICOT homology domain. ***J Biol Chem*** 276, 37133-37140.

94. Koncarevic S, Rohrbach P, Deponte M, Krohne G, Prieto JH, Yates J, Rahlfs S, Becker K (**2009**) The malarial parasite *Plasmodium falciparum* imports the human protein peroxiredoxin 2 for peroxide detoxification. ***Proc Natl Acad Sci U S A*** 106, 13323-13328.

95. Muller S (**2004**) Redox and antioxidant systems of the malaria parasite *Plasmodium falciparum*. ***Mol Microbiol*** 53, 1291-1305.

96. Akerman SE, Muller S (**2003**) 2-Cys peroxiredoxin PfTrx-Px1 is involved in the antioxidant defence of *Plasmodium falciparum*. ***Mol Biochem Parasitol*** 130, 75-81.

97. Rahlfs S, Becker K (**2001**) Thioredoxin peroxidases of the malarial parasite *Plasmodium falciparum*. ***Eur J Biochem*** 268, 1404-1409.

98. Nickel C, Trujillo M, Rahlfs S, Deponte M, Radi R, Becker K (**2005**) *Plasmodium falciparum* 2-Cys peroxiredoxin reacts with plasmoredoxin and peroxynitrite. ***Biol Chem*** 386, 1129-1136.

99. Kimura R, Komaki-Yasuda K, Kawazu S, Kano S (**2013**) 2-Cys peroxiredoxin of *Plasmodium falciparum* is involved in resistance to heat stress of the parasite. ***Parasitol Int*** 62, 137-143.

100. Yano K, Komaki-Yasuda K, Tsuboi T, Torii M, Kana S, Kawazu S (**2006**) 2-Cys peroxiredoxin TPx-1 is involved in gametocyte development in *Plasmodium berghei*. ***Mol Biochem Parasitol*** 148, 44-51.

101. Yano K, Otsuki H, Arai M, Komaki-Yasuda K, Tsuboi T, Torii M, Kano S, Kawazu SI (**2008**) Disruption of the *Plasmodium berghei* 2-Cys peroxiredoxin TPx-1 gene hinders the sporozoite development in the vector mosquito. ***Mol Biochem Parasitol*** 159, 142-145.

102. Boucher IW, McMillan PJ, Gabrielsen M, Akerman SE, Brannigan JA, Schnick C, Brzozowski AM, Wilkinson AJ, Muller S (**2006**) Structural and biochemical characterization of a mitochondrial peroxiredoxin from *Plasmodium falciparum*. ***Mol Microbiol*** 61, 948-959.

103. Djuika CF, Fiedler S, Schnolzer M, Sanchez C, Lanzer M, Deponte M (**2013**) *Plasmodium falciparum* antioxidant protein as a model enzyme for a special class of glutaredoxin/glutathione-dependent peroxiredoxins. ***Biochim Biophys Acta*** 1830, 4073-4090.

104. Sarma GN, Nickel C, Rahlfs S, Fischer M, Becker K, Karplus PA (**2005**) Crystal structure of a novel *Plasmodium falciparum* 1-Cys peroxiredoxin. ***J Mol Biol*** 346, 1021-1034.

105. Kawazu S, Tsuji N, Hatabu T, Kawai S, Matsumoto Y, Kano S (**2000**) Molecular cloning and characterization of a peroxiredoxin from the human malaria parasite *Plasmodium falciparum*. ***Mol Biochem Parasitol*** 109, 165-169.

106. Krnajski Z, Walter RD, Muller S (**2001**) Isolation and functional analysis of two thioredoxin peroxidases (peroxiredoxins) from *Plasmodium falciparum*. ***Mol Biochem Parasitol*** 113, 303-308.

107. Kawazu S, Ikenoue N, Takemae H, Komaki-Yasuda K, Kano S (**2005**) Roles of 1-Cys peroxiredoxin in haem detoxification in the human malaria parasite *Plasmodium falciparum*. ***Febs J*** 272, 1784-1791.

108. Richard D, Bartfai R, Volz J, Ralph SA, Muller S, Stunnenberg HG, Cowman AF (**2011**) A genome-wide chromatin-associated nuclear peroxiredoxin from the malaria parasite *Plasmodium falciparum*. ***J Biol Chem*** 286, 11746-11755.

109. Syed SH, Goutte-Gattat D, Becker N, Meyer S, Shukla MS, Hayes JJ, Everaers R, Angelov D, Bednar J, Dimitrov S (**2010**) Single-base resolution mapping of H1-nucleosome interactions and 3D organization of the nucleosome. ***Proc Natl Acad Sci U S A*** 107, 9620-9625.

110. Kehr S, Sturm N, Rahlfs S, Przyborski JM, Becker K (**2010**) Compartmentation of redox metabolism in malaria parasites. ***PLoS Pathog*** 6, e1001242.

111. Angelucci F, Miele AE, Ardini M, Boumis G, Saccoccia F, Bellelli A (**2016**) Typical 2-Cys peroxiredoxins in human parasites: Several physiological roles for a potential chemotherapy target. ***Mol Biochem Parasitol*** 206, 2-12.

112. Carey KL, Westwood NJ, Mitchison TJ, Ward GE (**2004**) A small-molecule approach to studying invasive mechanisms of *Toxoplasma gondii*. ***Proc Natl Acad Sci U S A*** 101, 7433-7438.

113. Haraldsen JD, Liu G, Botting CH, Walton JGA, Storm J, Phalen TJ, Kwok LY, Soldati-Favre D, Heintz NH, Muller S (**2009**) Identification of conoidin A as a covalent inhibitor of peroxiredoxin II. ***Org Biomol Chem*** 7, 3040-3048.

114. Brindisi M, Brogi S, Relitti N, Vallone A, Butini S, Gemma S, Novellino E, Colotti G, Angiulli G, Di Chiaro F, *et al*. (**2015**) Structure-based discovery of the first non-covalent inhibitors of *Leishmania major* tryparedoxin peroxidase by high throughput docking. ***Sci Rep*** 5, 9705.

115. Su D, Novoselov SV, Sun QA, Moustafa ME, Zhou Y, Oko R, Hatfield DL, Gladyshev VN (**2005**) Mammalian selenoprotein thioredoxin-glutathione reductase. Roles in disulfide bond formation and sperm maturation. ***J Biol Chem*** 280, 26491-26498.

116. Jakupoglu C, Przemeck GKH, Schneider M, Moreno SG, Mayr N, Hatzopoulos AK, de Angelis MH, Wurst W, Bornkamm GW, Brielmeier M, *et al.* (**2005**) Cytoplasmic thioredoxin reductase is essential for embryogenesis but dispensable for cardiac development. ***Mol Cell Biol*** 25, 1980-1988.

117. Conrad M, Jakupoglu C, Moreno SG, Lippl S, Banjac A, Schneider M, Beck H, Hatzopoulos AK, Just U, Sinowatz F, *et al*. (**2004**) Essential role for mitochondrial thioredoxin reductase in hematopoiesis, heart development, and heart function. ***Mol Cell Biol*** 24, 9414-9423.

118. Sun QA, Su D, Novoselov SV, Carlson BA, Hatfield DL, Gladyshev VN (**2005**) Reaction mechanism and regulation of mammalian thioredoxin/glutathione reductase. ***Biochemistry*** 44, 14528-14537.

119. Sun QA, Kirnarsky L, Sherman S, Gladyshev VN (**2001**) Selenoprotein oxidoreductase with specificity for thioredoxin and glutathione systems. ***Proc Natl Acad Sci U S A*** 98, 3673-3678.

120. Alger HM, Williams DL (**2002**) The disulfide redox system of *Schistosoma mansoni* and the importance of a multifunctional enzyme, thioredoxin glutathione reductase. ***Mol Biochem Parasitol*** 121, 129-139.

121. Agorio A, Chalar C, Cardozo S, Salinas G (**2003**) Alternative mRNAs arising from trans-splicing code for mitochondrial and cytosolic variants of *Echinococcus granulosus* thioredoxin glutathione reductase. ***J Biol Chem*** 278, 12920-12928.

122. Angelucci F, Miele AE, Boumis G, Dimastrogiovanni D, Brunori M, Bellelli A (**2008**) Glutathione reductase and thioredoxin reductase at the crossroad: the structure of *Schistosoma mansoni* thioredoxin glutathione reductase. ***Proteins*** 72, 936-945.

123. Ljungdahl LG, Andreesen JR (**1975**) Tungsten, a component of active formate dehydrogenase from *Clostridium thermoaceticum*. ***FEBS Lett*** 54, 279-282.

124. Turner DC, Stadtman TC (**1973**) Purification of protein components of the clostridial glycine reductase system and characterization of protein A as a selenoprotein. ***Arch Biochem Biophys*** 154, 366-381.

125. Byun BJ, Kang YK (**2011**) Conformational preferences and pK(a) value of selenocysteine residue. ***Biopolymers*** 95, 345-353.

126. Roy G, Sarma BK, Phadnis PP, Mugesh G (**2005**) Selenium-containing enzymes in mammals: Chemical perspectives. ***J Chem Sci*** 117, 287-303.

127. Lu J, Holmgren A (**2009**) Selenoproteins. ***J Biol Chem*** 284, 723-727.

128. Zhong L, Arner ES, Holmgren A (**2000**) Structure and mechanism of mammalian thioredoxin reductase: the active site is a redox-active selenolthiol/selenenylsulfide formed from the conserved cysteine-selenocysteine sequence. ***Proc Natl Acad Sci U S A*** 97, 5854-5859.

129. Fritz-Wolf K, Kehr S, Stumpf M, Rahlfs S, Becker K (**2011**) Crystal structure of the human thioredoxin reductase-thioredoxin complex. ***Nat Commun*** 2, 383.

130. Arscott LD, Gromer S, Schirmer RH, Becker K, Williams CH, Jr. (**1997**) The mechanism of thioredoxin reductase from human placenta is similar to the mechanisms of lipoamide dehydrogenase and glutathione reductase and is distinct from the mechanism of thioredoxin reductase from *Escherichia coli*. ***Proc Natl Acad Sci U S A*** 94, 3621-3626.

131. Becker K, Gromer S, Schirmer RH, Muller S (**2000**) Thioredoxin reductase as a pathophysiological factor and drug target. ***Eur J Biochem*** 267, 6118-6125.

132. Gromer S, Urig S, Becker K (**2004**) The thioredoxin system-from science to clinic. ***Med Res Rev*** 24, 40-89.

133. Ahmadi R, Urig S, Hartmann M, Helmke BM, Koncarevic S, Allenberger B, Kienhoefer C, Neher M, Steiner HH, Unterberg A, *et al*. (**2006**) Antiglioma activity of 2,2 ': 6 ',2 "-terpyridineplatinum(II) complexes in a rat model - Effects on cellular redox metabolism. ***Free Radical Bio Med*** 40, 763-778.

134. Bradshaw TD, Matthews CS, Cookson J, Chew EH, Shah M, Bailey K, Monks A, Harris E, Westwell AD, Wells G, *et al*. (**2005**) Elucidation of thioredoxin as a molecular target for antitumor quinols. ***Cancer Res*** 65, 3911-3919.

135. Engman L, Al-Maharik N, McNaughton M, Birmingham A, Powis G (**2003**) Thioredoxin reductase and cancer cell growth inhibition by organotellurium antioxidants. ***Anti-Cancer Drug*** 14, 153-161.

136. Schirmer RH, Schulz GE, Untuchtgrau R (**1983**) On the geometry of leukocyte NADPH-oxidase, a membrane flavoenzyme - Inferences from the structure of glutathione-reductase. ***FEBS Lett*** 154, 1-4.

137. Thieme R, Pai EF, Schirmer RH, Schulz GE (**1981**) 3-Dimensional structure of glutathione-reductase at 2 a resolution. ***J Mol Biol*** 152, 763-782.

138. Pai EF & Schulz GE (**1983**) The catalytic mechanism of glutathione-reductase as derived from X-ray-diffraction analyses of reaction intermediates. ***J Biol Chem*** 258, 1752-1757.

139. Savvides SN, Karplus PA (**1996**) Kinetics and crystallographic analysis of human glutathione reductase in complex with a xanthene inhibitor. ***J Biol Chem*** 271, 8101-8107.

140. Berkholz DS, Faber HR, Savvides SN, Karplus PA (**2008**) Catalytic cycle of human glutathione reductase near 1 A resolution. ***J Mol Biol*** 382, 371-384.

141. Bonilla M, Denicola A, Novoselov SV, Turanov AA, Protasio A, Izmendi D, Gladyshev VN, Salinas G (**2008**) Platyhelminth mitochondrial and cytosolic redox homeostasis is controlled by a single thioredoxin glutathione reductase and dependent on selenium and glutathione. ***J Biol Chem*** 283, 17898-17907.

142. Guevara-Flores A, Pardo JP, Rendon JL (**2011**) Hysteresis in thioredoxin-glutathione reductase (TGR) from the adult stage of the liver fluke *Fasciola hepatica*. ***Parasitol Int*** 60, 156-160.

143. Plancarte A, Nava G (**2015**) Purification and kinetic analysis of cytosolic and mitochondrial thioredoxin glutathione reductase extracted from *Taenia solium* cysticerci. ***Exp Parasitol*** 149, 65-73.

144. Tan SX, Greetham D, Raeth S, Grant CM, Dawes IW, Perrone GG (**2010**) The thioredoxin-thioredoxin reductase system can function *in vivo* as an alternative system to reduce oxidized glutathione in *Saccharomyces cerevisiae*. ***J Biol Chem*** 285, 6118-6126.

145. Muller EG (**1996**) A glutathione reductase mutant of yeast accumulates high levels of oxidized glutathione and requires thioredoxin for growth. ***Mol Biol Cell*** 7, 1805-1813.

146. Fernandes AP, Holmgren A (**2004**) Glutaredoxins: Glutathione-dependent redox enzymes with functions far beyond a simple thioredoxin backup system. ***Antioxid Redox Signal*** 6, 63-74.

147. Mesecke N, Mittler S, Eckers E, Herrmann JM, Deponte M (**2008**) Two novel monothiol glutaredoxins from *Saccharomyces cerevisiae* provide further insight into iron-sulfur

cluster binding, oligomerization, and enzymatic activity of glutaredoxins. ***Biochemistry*** 47, 1452-1463.

148. Comini MA, Rettig J, Dirdjaja N, Hanschmann EM, Berndt C, Krauth-Siegel RL (**2008**) Monothiol glutaredoxin-1 is an essential iron-sulfur protein in the mitochondrion of African trypanosomes. ***J Biol Chem*** 283, 27785-27798.

149. Kelley JJ, Caputo TM, Eaton SF, Laue TM, Bushweller JH (**1997**) Comparison of backbone dynamics of reduced and oxidized *Escherichia coli* glutaredoxin-1 using N-15 NMR relaxation measurements. ***Biochemistry*** 36, 5029-5044.

150. Johansson C, Kavanagh KL, Gileadi O, Oppermann U (**2007**) Reversible sequestration of active site cysteines in a 2Fe-2S-bridged dimer provides a mechanism for glutaredoxin 2 regulation in human mitochondria. ***J Biol Chem*** 282, 3077-3082.

151. Iwema T, Picciocchi A, Traore DAK, Ferrer JL, Chauvat F, Jacquamet L (**2009**) Structural basis for delivery of the intact [Fe2S2] cluster by monothiol glutaredoxin. ***Biochemistry*** 48, 6041-6043.

152. Johansson C, Roos AK, Montano SJ, Sengupta R, Filippakopoulos P, Guo K, von Delft F, Holmgrent A, Oppermann U, Kavanagh KL (**2011**) The crystal structure of human GLRX5: iron-sulfur cluster co-ordination, tetrameric assembly and monomer activity. ***Biochem J*** 433, 303-311.

153. Kalinina EV, Chernov NN, Novichkova MD (**2014**) Role of glutathione, glutathione transferase, and glutaredoxin in regulation of redox-dependent processes. ***Biochemistry (Moscow)*** 79, 1562-1583.

154. Sun QA, Wu Y, Zappacosta F, Jeang KT, Lee BJ, Hatfield DL, Gladyshev VN (**1999**) Redox regulation of cell signaling by selenocysteine in mammalian thioredoxin reductases. ***J Biol Chem*** 274, 24522-24530.

155. Su D, Novoselov SV, Sun QA, Moustafa ME, Zhou Y, Oko R, Hatfield DL, Gladyshev VN (**2005**) Mammalian selenoprotein thioredoxin-glutathione reductase - Roles in disulfide bond formation and sperm maturation. ***J Biol Chem*** 280, 26491-26498.

156. Gerashchenko MV, Su D, Gladyshev VN (**2010**) CUG Start codon generates thioredoxin/glutathione reductase isoforms in mouse testes. ***J Biol Chem*** 285, 4595-4602.

157. Kawai H, Ota T, Suzuki F, Tatsuka M (**2000**) Molecular cloning of mouse thioredoxin reductases. ***Gene*** 242, 321-330.

158. Bondareva AA, Capecchi MR, Iverson SV, Li Y, Lopez NI, Lucas O, Merrill GF, Prigge JR, Siders AM, Wakamiya M, *et al*. (**2007**) Effects of thioredoxin reductase-1 deletion on embryogenesis and transcriptome. ***Free Radical Bio Med*** 43, 911-923.

159. Dobrovolska O, Shumilina E, Gladyshev VN, Dikiy A (**2012**) Structural analysis of glutaredoxin domain of *Mus musculus* thioredoxin glutathione reductase. ***PLoS One*** 7, e52914.

160. Sanger F, Air GM, Barrell BG, Brown NL, Coulson AR, Fiddes JC, Hutchison CA, Slocombe PM & Smith M (**1977**) Nucleotide-sequence of bacteriophage ΦX174 DNA. ***Nature*** 265, 687-695.

161. Su D, Li YH & Gladyshev VN (**2005**) Selenocysteine insertion directed by the 3'-UTR SECIS element in *Escherichia coli*. ***Nucleic Acids Res*** 33, 2486-2492.

162. Cosloy SD & Oishi M (**1973**) Nature of transformation process in *Escherichia coli* K12. ***Mol Gen Genet*** 124, 1-10.

163. Bar-Noy S, Gorlatov SN & Stadtman TC (**2001**) Overexpression of wild type and SeCys/Cys mutant of human thioredoxin reductase in *E. coli*: the role of selenocysteine in the catalytic activity. ***Free Radic Biol Med*** 30, 51-61.

164. Porath J, Carlsson J, Olsson I, Belfrage G (**1975)** Metal chelate affinity chromatography, a new approach to protein fractionation. ***Nature*** 258, 598-599.

165. Laemmli UK (**1970**) Cleavage of structural proteins during the assembly of the head of bacteriophage T4. ***Nature*** 227, 680-685.

166. Bradford MM (**1976**) A rapid and sensitive method for the quantitation of microgram quantities of protein utilizing the principle of protein-dye binding. ***Anal Biochem*** 72, 248-254.

167. Towbin H, Staehelin T, Gordon J (**1979**) Electrophoretic transfer of proteins from polyacrylamide gels to nitrocellulose sheets: procedure and some applications. ***Proc Natl Acad Sci U S A*** 76, 4350-4354.

168. Xu T, Venable JD, Park SK, Cociorva D, Lu B, Liao L, Wohlschlegel J, Hewel J, Yates JR (**2006**) ProLuCID, a fast and sensitive tandem mass spectra-based protein identification program. ***Mol Cell Proteomics*** 5, S174-S174.

169. Tabb DL, McDonald WH, Yates JR, 3rd (**2002**) DTASelect and Contrast: tools for assembling and comparing protein identifications from shotgun proteomics. ***J Proteome Res*** 1, 21-26.

170. Cociorva D, D LT, Yates JR (**2007**) Validation of tandem mass spectrometry database search results using DTASelect. ***Curr Protoc Bioinformatics*** Chapter 13, Unit 13-14.

171. McDonald WH, Tabb DL, Sadygov RG, MacCoss MJ, Venable J, Graumann J, Johnson JR, Cociorva D, Yates JR, 3rd (**2004**) MS1, MS2, and SQT-three unified, compact, and easily parsed file formats for the storage of shotgun proteomic spectra and identifications. ***Rapid Commun Mass Spectrom*** 18, 2162-2168.

172. Peng J, Elias JE, Thoreen CC, Licklider LJ, Gygi SP (**2003**) Evaluation of multidimensional chromatography coupled with tandem mass spectrometry (LC/LC-MS/MS) for large-scale protein analysis: the yeast proteome. ***J Proteome Res*** 2, 43-50.

173. Wang LH, Delahunty C, Fritz-Wolf K, Rahlfs S, Prieto JH, Yates JR, Becker K (**2015**) Characterization of the 26S proteasome network in *Plasmodium falciparum*. ***Sci Rep*** 5, 17818.

174. Mirabella FM (**1985**) Internal-reflection spectroscopy. ***Appl Spectrosc Rev*** 21, 45-178.

175. Kretschmann E, Raether H (**1968**) Radiative decay of non radiative surface plasmons excited by light. ***Z Naturforsch*** 23, 2135-2136.

176. Healthcare G (**2001**) Technology Note 1 Surface plasmon resonance. In. GE Healthcare.

177. Guo X (**2012**) Surface plasmon resonance based biosensor technique: a review. ***J Biophotonics*** 5, 483-501.

178. Cooper MA (**2002**) Optical biosensors in drug discovery. ***Nat Rev Drug Discov*** 1, 515-528.

179. Duhr S, Braun D (**2006**) Why molecules move along a temperature gradient. ***Proc Natl Acad Sci U S A*** 103, 19678-19682.

180. Wienken CJ, Baaske P, Rothbauer U, Braun D, Duhr S (**2010**) Protein-binding assays in biological liquids using microscale thermophoresis. ***Nat Commun*** 1, 100.

181. Reineck P, Wienken CJ, Braun D (**2010**) Thermophoresis of single stranded DNA. ***Electrophoresis*** 31, 279-286.

182. Seidel SAI, Dijkman PM, Lea WA, van den Bogaart G, Jerabek-Willemsen M, Lazic A, Joseph JS, Srinivasan P, Baaske P, Simeonov A, *et al.* (**2013**) Microscale thermophoresis quantifies biomolecular interactions under previously challenging conditions. ***Methods*** 59, 301-315.

183. Liu YN, Liu N, Ma XH, Li XL, Ma J, Li Y, Zhou ZJ, Gao ZX (**2015**) Highly specific detection of thrombin using an aptamer-based suspension array and the interaction analysis via microscale thermophoresis. ***Analyst*** 140, 2762-2770.

184. Heerklotz H, Seelig J (**2000**) Titration calorimetry of surfactant-membrane partitioning and membrane solubilization. ***Biochim Biophys Acta*** 1508, 69-85.

185. Hegyi GKJ, Kovács M, Málnási-Csizmadia A, Nyitray L, Pál G, Radnai L, Reményi A, Venekei I (**2013**) Introduction to practical biochemistry. In. Eötvös Loránd University.

186. Ogusucu R, Rettori D, Munhoz DC, Netto LES, Augusto O (**2007**) Reactions of yeast thioredoxin peroxidases I and II with hydrogen peroxide and peroxynitrite: Rate constants by competitive kinetics. ***Free Radical Bio Med*** 42, 326-334.

187. Nelson KJ, Parsonage D (2011) Measurement of peroxiredoxin activity. ***Curr Protoc Toxicol*** Chapter 7, Unit7-10.

188. Dolman D, Newell, GA, Thurlow, MD, Dunford, HB (**1975**) A kinetic study of the reaction of horseradish peroxidase with hydrogen peroxide. ***Can J Biochem*** 53, 495-501.

189. Williams DL, Bonilla M, Gladyshev VN, Salinas G (**2013**) Thioredoxin glutathione reductase-dependent redox networks in platyhelminth parasites. ***Antioxid Redox Signal*** 19, 735-745.

190. Ellman GL (**1959**) Tissue sulfhydryl groups. ***Arch Biochem Biophys*** 82, 70-77.

191. Bushweller JH, Aslund F, Wuthrich K, Holmgren A (**1992**) Structural and functional characterization of the mutant *Escherichia coli* glutaredoxin (C14S) and its mixed disulfide with glutathione. ***Biochemistry*** 31, 9288-9293.

192. Gravina SA, Mieyal JJ (**1993**) Thioltransferase is a specific glutathionyl mixed disulfide oxidoreductase. ***Biochemistry*** 32, 3368-3376.

193. Nagai S, Black S (**1968**) A thiol-disulfide transhydrogenase from yeast. ***J Biol Chem*** 243, 1942-1947.

194. Carlberg I, Mannervik B (**1985**) Glutathione-Reductase. ***Methods in Enzymol*** 113, 484-490.

195. Trager W, Jensen JB (**1976**) Human malaria parasites in continuous culture. ***Science*** 193, 673-675.

196. Lambros C, Vanderberg JP (**1979**) Synchronization of *Plasmodium falciparum* erythrocytic stages in culture. ***J Parasitol*** 65, 418-420.

197. Koncarevic S, Bogumil R, Becker K (**2007**) SELDI-TOF-MS analysis of chloroquine resistant and sensitive *Plasmodium falciparum* strains. ***Proteomics*** 7, 711-721.

198. Dessau MA, Modis Y (**2011**) Protein crystallization for X-ray crystallography. ***J Vis Exp*** 47, pii: 2285.

199. Chayen NE (**1999**) Recent advances in methodology for the crystallization of biological macromolecules. ***J Cryst Growth*** 198, 649-655.

200. McPherson A (**2004**) Introduction to protein crystallization. ***Methods*** 34, 254-265.

201. Pauli K (**2015**) Conformational changes and redox-dependent functions of peroxiredoxins in *Plasmodium falciparum*. Master thesis, Justus-Liebig-University, Giessen.

202. Kabsch W (**2010**) XDS. ***Acta Crystallogr D Biol Crystallogr*** 66, 125-132.

203. König E (**2015**) Characterization of the human selenoprotein thioredoxin glutathione reductase. Master thesis, Justus-Liebig-University, Giessen.

204. Gromer S, Arscott LD, Williams CH, Jr., Schirmer RH, Becker K (**1998**) Human placenta thioredoxin reductase. Isolation of the selenoenzyme, steady state kinetics, and inhibition by therapeutic gold compounds. ***J Biol Chem*** 273, 20096-20101.

205. Flohè L, Harris R (**2007**) History of the peroxiredoxins and topical perspectives. In ***Peroxiredoxin Systems*** 44, 1-25. Springer, New York.

206. Harris JR (**1968**) Release of a macromolecular protein component from human erythrocyte ghosts. ***Biochim Biophys Acta*** 150, 534-537.

207. Harris JR (**1969**) Some negative contrast staining features of a protein from erythrocyte ghosts. ***J Mol Biol*** 46, 329-335.

208. Chae HZ, Robison K, Poole LB, Church G, Storz G, Rhee SG (**1994**) Cloning and sequencing of thiol-specific antioxidant from mammalian brain - alkyl hydroperoxide reductase and thiol-specific antioxidant define a large family of antioxidant enzymes. ***Proc Natl Acad Sci U S A*** 91, 7017-7021.

209. Gostner JM, Becker K, Fuchs D & Sucher R (**2013**) Redox regulation of the immune response. ***Redox Rep*** 18, 88-94.

210. Deponte M, Rahlfs S, Becker K (**2007**) Peroxiredoxin system of protozoal parasites. In *Peroxiredoxin Systems* 44, 219-229. Springer, New York.

211. Gretes MC, Poole LB, Karplus PA (**2012**) Peroxiredoxins in parasites. ***Antioxid Redox Signal*** 17, 608-633.

212. Balmer Y, Koller A, del Val G, Manieri W, Schurmann P, Buchanan BB (**2003**) Proteomics gives insight into the regulatory function of chloroplast thioredoxins. ***Proc Natl Acad Sci U S A*** 100, 370-375.

213. Motohashi K, Kondoh A, Stumpp MT, Hisabori T (**2001**) Comprehensive survey of proteins targeted by chloroplast thioredoxin. ***Proc Natl Acad Sci U S A*** 98, 11224-11229.

214. Hisabori T, Hara S, Fujii T, Yamazaki D, Hosoya-Matsuda N, Motohashi K (**2005**) Thioredoxin affinity chromatography: a useful method for further understanding the thioredoxin network. ***J Exp Bot*** 56, 1463-1468.

215. Hosoya-Matsuda N, Motohashi K, Yoshimura H, Nozaki A, Inoue K, Ohmori M, Hisabori T (**2005**) Anti-oxidative stress system in cyanobacteria - Significance of type II peroxiredoxin and the role of 1-Cys peroxiredoxin in *Synechocystis* sp strain PCC 6803. ***J Biol Chem*** 280, 840-846.

216. Yamazaki D, Motohashi K, Kasama T, Hara Y, Hisabori T (**2004**) Target proteins of the cytosolic thioredoxins in *Arabidopsis thaliana*. ***Plant Cell Physiol*** 45, 18-27.

217. Rouhier N, Villarejo A, Srivastava M, Gelhaye E, Keech O, Droux M, Finkemeier I, Samuelsson G, Dietz KJ, Jacquot JP, *et al*. (**2005**) Identification of plant glutaredoxin targets. ***Antioxid Redox Signal*** 7, 919-929.

218. Sobotta MC, Liou W, Stocker S, Talwar D, Oehler M, Ruppert T, Scharf AND, Dick TP (**2015**) Peroxiredoxin-2 and STAT3 form a redox relay for H_2O_2 signaling. ***Nat Chem Biol*** 11, 64-70.

219. Jarvis RM, Hughes SM & Ledgerwood EC (**2012**) Peroxiredoxin 1 functions as a signal peroxidase to receive, transduce, and transmit peroxide signals in mammalian cells. ***Free Radical Bio Med*** 53, 1522-1530.

220. Yan Y, Sabharwal P, Rao M & Sockanathan S (**2009**) The antioxidant enzyme Prdx1 controls neuronal differentiation by thiol-redox-dependent activation of GDE2. ***Cell*** 138, 1209-1221.

221. Garcia-Santamarina S, Boronat S, Espadas G, Ayte J, Molina H, Hidalgo E (**2011**) The oxidized thiol proteome in fission yeast – Optimization of an ICAT-based method to identify H_2O_2-oxidized proteins. ***J Proteomics*** 74, 2476-2486.

222. Brandes N, Reichmann D, Tienson H, Leichere LI, Jakob U (**2011**) Using quantitative redox proteomics to dissect the yeast redoxome. ***J Biol Chem*** 286, 41893-41903.

223. Ago T, Liu T, Zhai P, Chen W, Li H, Molkentin JD, Vatner SF, Sadoshima J (**2008**) A redox-dependent pathway for regulating class II HDACs and cardiac hypertrophy. ***Cell*** 133, 978-993.

224. Choi J, Levey AI, Weintraub ST, Rees HD, Gearing M, Chin LS & Li L (**2004**) Oxidative modifications and down-regulation of ubiquitin carboxyl-terminal hydrolase L1 associated with idiopathic Parkinson's and Alzheimer's diseases. ***J Biol Chem*** 279, 13256-13264.

225. Jahngen-Hodge J, Obin MS, Gong X, Shang F, Nowell TR, Gong JX, Abasi H, Blumberg J, Taylor A (**1997**) Regulation of ubiquitin-conjugating enzymes by glutathione following oxidative stress. ***J Biol Chem*** 272, 28218-28226.

226. Yao DD, Gu ZZ, Nakamura T, Shi ZQ, Ma YL, Gaston B, Palmer LA, Rockenstein EM, Zhang ZH, Masliah E, *et al*. (**2004**) Nitrosative stress linked to sporadic Parkinson's disease: *S*-nitrosylation of parkin regulates its E3 ubiquitin ligase activity. ***Proc Natl Acad Sci U S A*** 101, 13969-13969.

227. Meinhard M, Grill E (**2001**) Hydrogen peroxide is a regulator of ABI1, a protein phosphatase 2C from *Arabidopsis*. ***FEBS Lett*** 508, 443-446.

228. Monzingo AF, Dhaliwal S, Dutt-Chaudhuri A, Lyon A, Sadow JH, Hoffman DW, Robertus JD, Browning KS (**2007**) The structure of eukaryotic translation initiation factor-4E from wheat reveals a novel disulfide bond. ***Plant Physiol*** 143, 1504-1518.

229. O'Brien JP, Mayberry LK, Murphy PA, Browning KS, Brodbelt JS (**2013**) Evaluating the conformation and binding interface of Cap-binding proteins and complexes via ultraviolet photodissociation mass spectrometry. ***J Proteome Res*** 12, 5867-5877.

230. Laurindo FR, Pescatore LA, Fernandes DdeD (**2012**) Protein disulfide isomerase in redox cell signaling and homeostasis. ***Free Radical Bio Med*** 52, 1954-1969.

231. Uehara T, Nakamura T, Yao D, Shi ZQ, Gu Z, Ma Y, Masliah E, Nomura Y, Lipton SA (**2006**) *S*-nitrosylated protein-disulphide isomerase links protein misfolding to neurodegeneration. ***Nature*** 441, 513-517.

232. Lemaire SD, Guillon B, Le Marèchal P, Keryer E, Miginiac-Maslow M, Decottignies P (**2004**) New thioredoxin targets in the unicellular photosynthetic eukaryote *Chlamydomonas reinhardtii*. ***Proc Natl Acad Sci U S A*** 101, 7475-7480.

233. Lindahl M, Florencio FJ (**2003**) Thioredoxin-linked processes in cyanobacteria are as numerous as in chloroplasts, but targets are different. ***Proc Natl Acad Sci U S A*** 100, 16107-16112.

234. Wong JH, Cal N, Balmer Y, Tanaka CK, Vensel WH, Hurkman WJ, Buchanan BB (**2004**) Thioredoxin targets of developing wheat seeds identified by complementary proteomic approaches. ***Phytochemistry*** 65, 1629-1640.

235. Chen YM, Daosukho C, Opii WO, Turner DM, Pierce WM, Klein JB, Vore M, Butterfield DA, Clair DKS (**2006**) Redox proteomic identification of oxidized cardiac proteins in Adriamycin-treated mice. ***Free Radical Bio Med*** 41, 1470-1477.

236. Anderson LE, Li AD, Stevens FJ (**1998**) The enolases of ice plant and *Arabidopsis* contain a potential disulphide and are redox sensitive. ***Phytochemistry*** 47, 707-713.

237. Wang SB, Murray CI, Chung HS, Van Eyk JE (**2013**) Redox-regulation of mitochondrial ATP synthase. ***Trends Cardiovas Med*** 23, 14-18.

238. Caito SW, Aschner M (**2015**) Mitochondrial redox dysfunction and environmental exposures. ***Antioxid Redox Signal*** 23, 578-595.

239. Atsumi H, Kitada M, Kanasaki K, Koya D (**2011**) Reversal of redox-dependent inhibition of diacylglycerol kinase by antioxidants in mesangial cells exposed to high glucose. ***Mol Med Rep*** 4, 923-927.

240. Boyer PD (**1997**) The ATP synthase - A splendid molecular machine. ***Annu Rev Biochem*** 66, 717-749.

241. Kane LA, Van Eyk JE (**2009**) Post-translational modifications of ATP synthase in the heart: biology and function. ***J Bioenerg Biomembr*** 41, 145-150.

242. Sun J, Morgan M, Shen RF, Steenbergen C, Murphy E (**2007**) Preconditioning results in *S*-nitrosylation of proteins involved in regulation of mitochondrial energetics and calcium transport. ***Circ Res*** 101, 1155-1163.

243. Wang SB, Foster DB, Rucker J, O'Rourke B, Kass DA, Van Eyk JE (**2011**) Redox regulation of mitochondrial ATP synthase: Implications for cardiac resynchronization therapy. ***Circ Res*** 109, 750-757.

244. Bald D, Noji H, Yoshida M, Hirono-Hara Y, Hisabori T (**2001**) Redox regulation of the rotation of F-1-ATP synthase. ***J Biol Chem*** 276, 39505-39507.

245. Winterbourn CC, Hampton MB (**2008**) Thiol chemistry and specificity in redox signaling. ***Free Radical Bio Med*** 45, 549-561.

246. Gutsche M, Sobotta MC, Wabnitz GH, Ballikaya S, Meyer AJ, Samstag Y, Dick TP (**2009**) Proximity-based protein thiol oxidation by H_2O_2-scavenging peroxidases. ***J Biol Chem*** 284, 31532-31540.

247. Turner-Ivey B, Manevich Y, Schulte J, Kistner-Griffin E, Jezierska-Drutel A, Liu Y, Neumann CA (**2013**) Role for Prdx1 as a specific sensor in redox-regulated senescence in breast cancer. ***Oncogene*** 32, 5302-5314.

248. Brender JR, Zhang Y (**2015**) Predicting the effect of mutations on protein-protein binding interactions through structure-based interface profiles. ***Plos Comput Biol*** 11.

249. Cerveau D, Kraut A, Stotz HU, Mueller MJ, Coute Y, Rey P (**2016**) Characterization of the *Arabidopsis thaliana* 2-Cys peroxiredoxin interactome. ***Plant Sci*** 252, 30-41.

250. Krekel F, Samland AK, Macheroux P, Amrhein N & Evans JNS (**2000**) Determination of the pK(a) value of C115 in MurA (UDP-N-acetylglucosamine enolpyruvyltransferase) from *Enterobacter cloacae*. ***Biochemistry*** 39, 12671-12677.

251. Tajc SG, Tolbert BS, Basavappa R & Miller BL (**2004**) Direct determination of thiol pK(a) by isothermal titration microcalorimetry. ***J Am Chem Soc*** 126, 10508-10509.

252. Peskin AV, Low FM, Paton LN, Maghzal GJ, Hampton MB, Winterbourn CC (**2007**) The high reactivity of peroxiredoxin 2 with H_2O_2 is not reflected in its reaction with other oxidants and thiol reagents. ***J Biol Chem*** 282, 11885-11892.

253. Nelson KJ, Parsonage D, Hall A, Karplus PA, Poole LB (**2008**) Cysteine pK(a) values for the bacterial peroxiredoxin AhpC. ***Biochemistry*** 47, 12860-12868.

254. Hugo M, Turell L, Manta B, Botti H, Monteiro G, Netto LES, Alvarez B, Radi R, Trujillo M (**2009**) Thiol and sulfenic acid oxidation of AhpE, the one-cysteine peroxiredoxin from *Mycobacterium tuberculosis*: kinetics, acidity constants, and conformational dynamics. ***Biochemistry*** 48, 9416-9426.

255. Parsonage D, Youngblood DS, Sarma GN, Wood ZA, Karplus PA, Poole LB (**2005**) Analysis of the link between enzymatic activity and oligomeric state in AhpC, a bacterial peroxiredoxin. ***Biochemistry*** 44, 10583-10592.

256. Horta BB, de Oliveira MA, Discola KF, Cussiol JRR, Netto LES (**2010**) Structural and biochemical characterization of peroxiredoxin Q beta from *Xylella fastidiosa*: catalytic mechanism and high reactivity. ***J Biol Chem*** 285, 16051-16065.

257. Trujillo M, Clippe A, Manta B, Ferrer-Sueta G, Smeets A, Declercq JP, Knoops B, Radi R (**2007**) Pre-steady state kinetic characterization of human peroxiredoxin 5: Taking advantage of Trp84 fluorescence increase upon oxidation. ***Arch Biochem Biophys*** 467, 95-106.

258. Santora LC, Kaymakcalan Z, Sakorafas P, Krull IS, Grant K (**2001**) Characterization of noncovalent complexes of recombinant human monoclonal antibody and antigen using cation exchange, size exclusion chromatography, and BIAcore. ***Anal Biochem*** 299, 119-129.

259. Abdiche YN, Yeung YA, Chaparro-Riggers J, Barman I, Strop P, Chin SM, Pham A, Bolton G, McDonough D, Lindquist K, *et al*. (**2015**) The neonatal Fc receptor (FcRn) binds independently to both sites of the IgG homodimer with identical affinity. ***MAbs*** 7, 331-343.

260. Smith EA, Corn RM (**2003**) Surface plasmon resonance imaging as a tool to monitor biomolecular interactions in an array based format. ***Appl Spectrosc*** 57, 320a-332a.

261. Jung SO, Ro HS, Kho BH, Shin YB, Kim MG, Chung BH (**2005**) Surface plasmon resonance imaging-based protein arrays for high-throughput screening of protein-protein interaction inhibitors. ***Proteomics*** 5, 4427-4431.

262. Li YA, Wark AW, Lee HJ, Corn RM (**2006**) Single-nucleotide polymorphism genotyping by nanoparticle-enhanced surface plasmon resonance imaging measurements of surface ligation reactions. ***Anal Chem*** 78, 3158-3164.

263. Wang YC, Zhu X, Wu MH, Xia N, Wang JX, Zhou FM (**2009**) Simultaneous and label-free determination of wild-type and mutant p53 at a single surface plasmon resonance chip preimmobilized with consensus DNA and monoclonal antibody. ***Anal Chem*** 81, 8441-8446.

264. Uludag Y, Tothill IE (**2012**) Cancer biomarker detection in serum samples using surface plasmon resonance and quartz crystal microbalance sensors with nanoparticle signal amplification. ***Anal Chem*** 84, 5898-5904.

265. Yanase Y, Suzuki H, Tsutsui T, Hiragun T, Kameyoshi Y, Hide M (**2007**) The SPR signal in living cells reflects changes other than the area of adhesion and the formation of cell constructions. ***Biosens Bioelectron*** 22, 1081-1086.

266. Hide M, Tsutsui T, Sato H, Nishimura T, Morimoto K, Yamamoto S, Yoshizato K (**2002**) Real-time analysis of ligand-induced cell surface and intracellular reactions of living mast cells using a surface plasmon resonance-based biosensor. ***Anal Biochem*** 302, 28-37.

267. Nguyen HH, Park J, Kang S, Kim M (**2015**) surface plasmon resonance: a versatile technique for biosensor applications. ***Sensors*** (Basel) 15, 10481-10510.

268. Palde PB, Carroll KS (**2015**) A universal entropy-driven mechanism for thioredoxin-target recognition. ***Proc Natl Acad Sci U S A*** 112, 7960-7965.

269. Jönsson TJ, Ellis HR, Poole LB (**2007**) Cysteine reactivity and thiol-disulfide interchange pathways in AhpF and AhpC of the bacterial alkyl hydroperoxide reductase system. ***Biochemistry*** 46, 5709-5721.

270. Djuika CF, Fiedler S, Schnolzer M, Sanchez C, Lanzer M, Deponte M (**2013**) *Plasmodium falciparum* antioxidant protein as a model enzyme for a special class of glutaredoxin/glutathione-dependent peroxiredoxins. ***Biochim Biophys Acta*** 1830, 4073-4090.

271. Wood ZA, Poole LB, Hantgan RR, Karplus PA (**2002**) Dimers to doughnuts: Redox-sensitive oligomerization of 2-cysteine peroxiredoxins. ***Biochemistry*** 41, 5493-5504.

272. Dip PV, Kamariah N, Manimekalai MSS, Nartey W, Balakrishna AM, Eisenhaber F, Eisenhaber B, Gruber G (**2014**) Structure, mechanism and ensemble formation of the alkylhydroperoxide reductase subunits AhpC and AhpF from *Escherichia coli*. ***Acta Crystallogr D*** 70, 2848-2862.

273. Kamariah N, Sek MF, Eisenhaber B, Eisenhaber F, Gruber G (**2016**) Transition steps in peroxide reduction and a molecular switch for peroxide robustness of prokaryotic peroxiredoxins. ***Sci Rep*** (UK) 6, Artn 37610.

274. Perkins A, Parsonage D, Nelson KJ, Ogba OM, Cheong PHY, Poole LB, Karplus PA (**2016**) Peroxiredoxin catalysis at atomic resolution. ***Structure*** 24, 1668-1678.

275. Holmgren A (**1995**) Thioredoxin structure and mechanism - conformational-changes on oxidation of the active-site sulfhydryls to a disulfide. ***Structure*** 3, 239-243.

276. Lian FM, Yu J, Ma XX, Yu XJ, Chen YX, Zhou CZ (**2012**) Structural snapshots of yeast alkyl hydroperoxide reductase Ahp1 peroxiredoxin reveal a novel two-cysteine mechanism of electron transfer to eliminate reactive oxygen species. ***J Biol Chem*** 287, 17077-17087.

277. Messens J, Van Molle I, Vanhaesebrouck P, Limbourg M, Van Belle K, Wahni K, Martins JC, Loris R, Wyns L (**2004**) How thioredoxin can reduce a buried disulphide bond. ***J Mol Biol*** 339, 527-537.

278. Gladyshev VN, Kryukov GV (**2001**) Evolution of selenocysteine-containing proteins: Significance of identification and functional characterization of selenoproteins. ***Biofactors*** 14, 87-92.

279. Rother M, Resch A, Wilting R, Bock A (**2001**) Selenoprotein synthesis in archaea. ***Biofactors*** **1**4, 75-83.

280. Chambers I, Frampton J, Goldfarb P, Affara N, Mcbain W, Harrison PR (**1986**) The structure of the mouse glutathione-peroxidase gene - the selenocysteine in the active-site is encoded by the termination codon, TGA. ***Embo J*** 5, 1221-1227.

281. Heider J, Baron C, Bock A (**1992**) Coding from a distance - dissection of the messenger-RNA determinants required for the incorporation of selenocysteine into protein. ***Embo J*** 11, 3759-3766.

282. Tujebajeva RM, Copeland PR, Xu XM, Carlson BA, Harney JW, Driscoll DM, Hatfield DL, Berry MJ (2000) Decoding apparatus for eukaryotic selenocysteine insertion. ***Embo Rep*** 1, 158-163.

283. Kryukov GV, Castellano S, Novoselov SV, Lobanov AV, Zehtab O, Guigo R, Gladyshev VN (**2003**) Characterization of mammalian selenoproteomes. ***Science*** 300, 1439-1443.

284. Krol A (**2002**) Evolutionarily different RNA motifs and RNA-protein complexes to achieve selenoprotein synthesis. ***Biochimie*** 84, 765-774.

285. Hondal RJ (**2005**) Incorporation of selenocysteine into proteins using peptide ligation. ***Protein Pept Lett*** 12, 757-764.

286. Arner ESJ, Sarioglu H, Lottspeich F, Holmgren A, Bock A (**1999**) High-level expression in *Escherichia coli* of selenocysteine-containing rat thioredoxin reductase utilizing gene fusions with engineered bacterial-type SECIS elements and co-expression with the *selA*, *selB* and *selC* genes. ***J Mol Biol*** 292, 1003-1016.

287. Bar-Noy S, Gorlatov SN, Stadtman TC (**2001**) Overexpression of wild type and SeCys/Cys mutant of human thioredoxin reductase in *E. coli*: the role of selenocysteine in the catalytic activity. ***Free Radical Bio Med*** 30, 51-61.

288. Gromer S, Wissing J, Behne D, Ashman K, Schirmer RH, Flohe L, Becker K (**1998**) A hypothesis on the catalytic mechanism of the selenoenzyme thioredoxin reductase. ***Biochem J*** 332, 591-592.

289. Sandalova T, Zhong LW, Lindqvist Y, Holmgren A, Schneider G (**2001**) Three-dimensional structure of a mammalian thioredoxin reductase: implications for mechanism and evolution of a selenocysteine-dependent enzyme. ***Proc Natl Acad Sci U S A*** 98, 9533-9538.

290. Urig S, Lieske J, Fritz-Wolf K, Irmler A, Becker K (**2006**) Truncated mutants of human thioredoxin reductase 1 do not exhibit glutathione reductase activity. ***FEBS Lett*** 580, 3595-3600.

291. Krohne-Ehrich G, Schirmer RH, Untucht-Grau R (**1977**) Glutathione reductase from human erythrocytes. Isolation of enzyme and sequence-analysis of redox-active peptide. ***Eu J Biochem*** 80, 65-71.

292. Wong KK, Vanoni MA, Blanchard JS (**1988**) Glutathione-reductase: solvent equilibrium and kinetic isotope effects. ***Biochemistry*** 27, 7091-7096.

293. Jacob J, Schirmer RH, Gromer S (**2005**) The conserved histidine 106 of large thioredoxin reductases is likely to have a structural role but not a base catalyst function. ***FEBS Lett*** 579, 745-748.

294. Arner ES (**2009**) Focus on mammalian thioredoxin reductases - important selenoproteins with versatile functions. ***Biochim Biophys Acta*** 1790, 495-526.

295. Kuntz AN, Davioud-Charvet E, Sayed AA, Califf LL, Dessolin J, Arner ES, Williams DL (**2007**) Thioredoxin glutathione reductase from *Schistosoma mansoni*: an essential parasite enzyme and a key drug target. ***PLoS Med*** 4, e206.

296. Song L, Li J, Xie S, Qian C, Wang J, Zhang W, Yin X, Hua Z, Yu C (**2012**) Thioredoxin glutathione reductase as a novel drug target: evidence from *Schistosoma japonicum*. ***PLoS One*** 7, e31456.

297. Han Y, Zhang M, Hong Y, Zhu Z, Li D, Li X, Fu Z, Lin J (**2012**) Characterization of thioredoxin glutathione reductase in *Schiotosoma japonicum*. ***Parasitol Int*** 61, 475-480.

298. Johansson C, Lillig CH, Holmgren A (**2004**) Human mitochondrial glutaredoxin reduces *S*-glutathionylated proteins with high affinity accepting electrons from either glutathione or thioredoxin reductase. ***J Biol Chem*** 279, 7537-7543.

299. Fernandes AP, Fladvad M, Berndt C, Andresen C, Lillig CH, Neubauer P, Sunnerhagen M, Holmgren A, Vlamis-Gardikas A (**2005**) A novel monothiol glutaredoxin (Grx4) from *Escherichia coli* can serve as a substrate for thioredoxin reductase. ***J Biol Chem*** 280, 24544-24552.

300. Tamarit J, Belli G, Cabiscol E, Herrero E, Ros J (**2003**) Biochemical characterization of yeast mitochondrial Grx5 monothiol glutaredoxin. ***J Biol Chem*** 278, 25745-25751.

301. Wang PF, Arscott LD, Gilberger TW, Muller S, Williams CH (**1999**) Thioredoxin reductase from *Plasmodium falciparum*: Evidence for interaction between the C-terminal cysteine residues and the active site disulfide-dithiol. ***Biochemistry*** 38, 3187-3196.

302. Zhong LW, Holmgren A (**2000**) Essential role of selenium in the catalytic activities of mammalian thioredoxin reductase revealed by characterization of recombinant enzymes with selenocysteine mutations. ***J Biol Chem*** 275, 18121-18128.

303. Brandstaedter C, Fritz-Wolf K, Weder S, Fischer M, Hecker B, Rahlfs S & Becker K (**2018**) Kinetic characterization of wild-type and mutant human thioredoxin glutathione reductase defines its reaction and regulatory mechanisms. ***FEBS J*** 285, 542-558.

304. Huang HH, Day L, Cass CL, Ballou DP, Williams CH, Williams DL (**2011**) Investigations of the catalytic mechanism of thioredoxin glutathione reductase from *Schistosoma mansoni*. ***Biochemistry*** 50, 5870-5882.

305. Angelucci F, Dimastrogiovanni D, Boumis G, Brunori M, Miele AE, Saccoccia F, Bellelli A (**2010**) Mapping the catalytic cycle of *Schistosoma mansoni* thioredoxin glutathione reductase by X-ray crystallography. ***J Biol Chem*** 285, 32557-32567.

306. Arnold K, Bordoli L, Kopp J, Schwede T (**2006**) The SWISS-MODEL workspace: a web-based environment for protein structure homology modelling. ***Bioinformatics*** 22, 195-201.

307. Emsley P, Lohkamp B, Scott WG, Cowtan K (**2010**) Features and development of Coot. ***Acta Crystallogr D*** 66, 486-501.

308. Pettersen EF, Goddard TD, Huang CC, Couch GS, Greenblatt DM, Meng EC, Ferrin TE (**2004**) UCSF chimera - A visualization system for exploratory research and analysis. ***J Comput Chem*** 25, 1605-1612.

309. Lee EH, Kim HY, Hwang KY (**2014**) The GSH- and GSSG-bound structures of glutaredoxin from *Clostridium oremlandii*. ***Arch Biochem Biophys*** 564, 20-25.

310. Mohr S, Hallak H, de Boitte A, Lapetina EG, Brune B (**1999**) Nitric oxide induced *S*-glutathionylation and inactivation of glyceraldehyde-3-phosphate dehydrogenase. ***J Biol Chem*** 274, 9427-9430.

311. Kim HS, Ullevig SL, Zamora D, Lee CF, Asmis R (**2012**) Redox regulation of MAPK phosphatase 1 controls monocyte migration and macrophage recruitment. ***Proc Natl Acad Sci U S A*** 109, E2803-E2812.

312. Sun R, Eriksson S & Wang LY (**2012**) Oxidative stress induced *S*-glutathionylation and proteolytic degradation of mitochondrial thymidine kinase 2. ***J Biol Chem*** 287, 24304-24312.

313. Lock JT, Sinkins WG, Schilling WP (**2012**) Protein *S*-glutathionylation enhances Ca^{2+}-induced Ca^{2+} release via the IP_3 receptor in cultured aortic endothelial cells. ***J Physiol*** London 590, 3431-3447.

314. Kil IS, Shin SW, Park JW (**2012**) *S*-glutathionylation regulates GTP-binding of Rac2. ***Biochem Biophys Res Commun*** 425, 892-896.

315. Cabiscol E, Levine RL (**1996**) The phosphatase activity of carbonic anhydrase III is reversibly regulated by glutathiolation. ***Proc Natl Acad Sci U S A*** 93, 4170-4174.

316. Rendon JL, del Arenal IP, Guevara-Flores A, Uribe A, Plancarte A, Mendoza-Hernandez G (**2004**) Purification, characterization and kinetic properties of the multifunctional thioredoxin-glutathione reductase from *Taenia crassiceps* metacestode (cysticerci). ***Mol Biochem Parasitol*** 133, 61-69.

317. Guevara-Flores A, Del Arenal, I.P., Mendoza-Hernandez, G., Pardo, J.P., Flores-Herrera, O., Rendon, J.L. (**2010**) Mitochondrial thioredoxin-glutathione reductase from larval *Taenia crassiceps* (cysticerci). ***J Parasitol Res***, pii:719856.

318. Bonilla M, Denicola A, Marino SM, Gladyshev VN, Salinas G (**2011**) Linked thioredoxin-glutathione systems in platyhelminth parasites alternative pathways for glutathione reduction and deglutathionylation. ***J Biol Chem*** 286, 4959-4967.

SUPPLEMENTS

Supplementary Table 1. Mass spectrometry analysis of proteolytic hTGR band. Recombinant hTGR was analyzed on SDS-PAGE and stained with Coomassie. The appearing band at ~30 kDa was subjected to in-gel tryptic digestion and analyzed by MALDI-TOF analysis in duplicate with a sequence coverage between 17.2 – 18.1%. Here, the detected peptides of the additional appearing band belong to the N-terminal, C-terminal and central parts of the enzyme.

RESIDUE NUMBER[1]	SEQUENCE	THEORETICAL PEPTIDE MASS (M/Z)[2]
4-13	SPPQSPGPGK	951.458
14-21	AGDAPNRR	856.478
40-47	LSSPGPSR	800.377
40-52	LSSPGPSRSSEAR	1330.711
58-65	HLVGLIER	936.557
107-118	VQEVLSEITNQK	1387.753
119-127	TVPNIFVNK	1031.614
366-379	SILLRGFDQEMAEK	1652.815
380-390	VGSYMEQHGVK	1234.660
501-508	LFGASLEK	864.438
579-601	VIGFHILGPNAGEVTQGFAAAMK	2344.130

1 Amino acid residues of human thioredoxin glutathione reductase (according to Uniprot-HUMAN: Q86VQ6).

2 Theoretical peptide masses were obtained using the sequence editor of BioTools V3.2 (Bruker Daltonics, Bremen).

Supplementary Table 2. Mass spectrometry analysis of glutathionylated hTGR. Recombinant hTGR was incubated with 5 mM GSSG and analyzed on non-reducing SDS-PAGE and stained with Coomassie. The protein band at ~70 kDa was subjected to in-gel tryptic digestion and analyzed by MALDI-TOF analysis in triplicate with a sequence coverage between 61.4 – 66.1%. Peptides containing modifications by glutathione and the frequency of this modification are listed (n) and cysteines are marked in light grey.

RESIDUE NUMBER[1]	SEQUENCE	THEORETICAL PEPTIDE MASS (M/Z)[2]	GLUTATHIONYLATION	N[3]
4-13	SPPQSPGPGK	951.4821		
14-21	AGDAPNRR	856.4985		
30-37	VLSPPGRR	881.4663		
40-47	LSSPGPSR	800.3956		
48-56	SSEAREELR	1076.524		
57-65	RHLVGLIER	1092.6333		
58-65	HLVGLIER	936.5533		
82-106	VKELFSSLGVECNVLELDQVDDGAR	3040.4779	Cys 93	2
84-106	ELFSSLGVECNVLELDQVDDGAR	2813.3055	Cys 93	3
107-118	VQEVLSEITNQK	1387.7522		
119-127	TVPNIFVNK	1031.5932		
128-147	VHVGGCDQTFQAYQSGLLQK	2484.1831	Cys 133	3
148-173	LLQEDLAYDYDLIIIGGGSGGLSCAK	2989.4728	Cys 171	1
182-211	VMVLDFVVPSPQGTSWGLGGTCVN VGCIPK	3060.4666		
213-228	LMHQAALLGQALCDSR	2031.9450	Cys 225	3
213-229	LMHQAALLGQALCDSRK	2160.0311	Cys 225	3
229-239	KFGWEYNQQVR	1454.7272		

230-239	FGWEYNQQVR	1326.6286		
240-247	HNWETMTK	1046.4875		
248-261	AIQNHISSLNWGYR	1658.8235		
248-265	AIQNHISSLNWGYRLSLR	2128.0983		
266-283	EKAVAYVNSYGEFVEHHK	2107.0494		
268-283	AVAYVNSYGEFVEHHK	1849.8854		
290-310	KGQETYYTAAQFVIATGERPR	2386.2353		
311-318	YLGIQGDK	893.4591		
371-379	GFDQEMAEK	1054.4453		
380-390	VGSYMEQHGVK	1234.6085		
394-405	KFIPVMVQQLEK	1459.8388		
395-405	FIPVMVQQLEK	1331.7388		
417-437	STEGTETIEGVYNTVLLAIGR	2223.1676		
460-495	IPVNDVEQTNVPYVYAVGDILEDKPE LTPVAIQSGK	3910.9837		
501-508	LFGASLEK	864.4799		
534-540	AIEVYKK	850.4706		
540-560	KENLEIYHTLFWPLEWTVAGR	2602.3404		
541-560	ENLEIYHTLFWPLEWTVAGR	2474.2320		
561-568	ENNTCYAK	942.4049		
569-573	IICNK	895.4576	Cys 571	1
569-578	IICNKFDHDR	1260.6316		
569-578	IICNKFDHDR	1260.6176		
579-601	VIGFHILGPNAGEVTQGFAAAMK	2328.2331		
607-630	QLLDDTIGIHPTCGEVFTTLEITK	2949.4607	Cys 619	3
631-639	SSGLDITQK	948.5016		

1 Amino acid residues of human thioredoxin glutathione reductase (according to Uniprot-HUMAN; Q86VQ6).

2 Theoretical peptide masses were obtained using the sequence editor of BioTools V3.2 (Bruker Daltonics, Bremen).

3 Number of positive glutathionylation sites in the triplicate.

***Pf*Prx1a** (PlasmoDB: PF14_0368, PF3D7_1438900)

Sequence Length: 588 bp

```
   1 - ATGGCATCATATGTAGGAAGAGAAGCTCCTTATTTTAAGGCTGAAGCAGTTTTTGCAGAT - 60
   1 - M  A  S  Y  V  G  R  E  A  P  Y  F  K  A  E  A  V  F  A  D   - 20

  61 - AACACATTTGGAGAAGTAAATTTGCATGATTTTATTGGAAAGAAATATGTATTATTATAT - 120
  21 - N  T  F  G  E  V  N  L  H  D  F  I  G  K  K  Y  V  L  L  Y   - 40

 121 - TTTTATCCATTAGATTTTACGTTTGTATGTCCATCTGAAATCATTGCATTAGATAAGGCT - 180
  41 - F  Y  P  L  D  F  T  F  V  C  P  S  E  I  I  A  L  D  K  A   - 60

 181 - CTTGATGCATTTAAGGAAAGAAATGTTGAATTAATAGGCTGTAGTGTGGATAGTAAATAT - 240
  61 - L  D  A  F  K  E  R  N  V  E  L  I  G  C  S  V  D  S  K  Y   - 80

 241 - ACTCATTTGGCATGGAAAAAAACACCATTAACTAAAGGAGGTATAGGAAATATCCAACAT - 300
  81 - T  H  L  A  W  K  K  T  P  L  T  K  G  G  I  G  N  I  Q  H   - 100

 301 - ACATTAATATCTGATATTACTAAAAGTATATCAAGAAGTTATAATGTGTTGTTTGGTGAT - 360
 101 - T  L  I  S  D  I  T  K  S  I  S  R  S  Y  N  V  L  F  G  D   - 120

 361 - AGTGTATCATTAAGAGCATTTGTATTAATCGACAAGCAAGGTGTTGTTCAACATTTACTT - 420
 121 - S  V  S  L  R  A  F  V  L  I  D  K  Q  G  V  V  Q  H  L  L   - 140

 421 - GTTAATAATTTAGCTATTGGTAGATCAGTTGAGGAAGTCTTAAGAATTATTGATGCTGTA - 480
 141 - V  N  N  L  A  I  G  R  S  V  E  E  V  L  R  I  I  D  A  V   - 160

 481 - CAACACCACGAACAACATGGAGATGTTTGCCCAGCAAACTGGAAAAAGGGAAAGGTAGCC - 540
 161 - Q  H  H  E  Q  H  G  D  V  C  P  A  N  W  K  K  G  K  V  A   - 180

 541 - ATGAAACCATCAGAAGAAGGTGTTAGTGAATATTTATCAAAGTTGTAA - 588
 181 - M  K  P  S  E  E  G  V  S  E  Y  L  S  K  L  *  X - 200
```

***Pf*Prx1m** (PlasmoDB: PFL0725w, PF3D7_1215000)

Sequence Length: 651 bp

```
   1 - ATGTTTTTAAAAAAACTGTGCAGGAGCAATTTTTTCGGGAATTCAAGAAGATCCTTTTCG - 60
   1 - M  F  L  K  K  L  C  R  S  N  F  F  G  N  S  R  R  S  F  S   - 20

  61 - CTAGTGACAAAGAAGGCTTATAATTTCACAGCTCAAGGATTAAATAAAAATAATGAAATA - 120
  21 - L  V  T  K  K  A  Y  N  F  T  A  Q  G  L  N  K  N  N  E  I   - 40

 121 - ATAAATGTTGACCTTTCCTCTTTTATAGGTCAGAAATACTGTTGTTTGTTATTTTATCCA - 180
  41 - I  N  V  D  L  S  S  F  I  G  Q  K  Y  C  C  L  L  F  Y  P   - 60

 181 - TTAAACTATACCTTCGTATGTCCAACAGAAATAATTGAATTTAATAAGCATATAAAAGAT - 240
  61 - L  N  Y  T  F  V  C  P  T  E  I  I  E  F  N  K  H  I  K  D   - 80

 241 - TTTGAAAATAAAAATGTAGAGTTATTAGGTATATCCGTAGATTCAGTATATAGTCATTTG - 300
  81 - F  E  N  K  N  V  E  L  L  G  I  S  V  D  S  V  Y  S  H  L   - 100

 301 - GCATGGAAAAATATGCCTATTGAAAAAGGAGGAATTGGAAATGTGGAATTTACTTTAGTA - 360
 101 - A  W  K  N  M  P  I  E  K  G  G  I  G  N  V  E  F  T  L  V   - 120

 361 - TCAGATATAAATAAAGACATTTCTAAAAATTATAATGTACTTTATGATAATTCTTTTGCT - 420
 121 - S  D  I  N  K  D  I  S  K  N  Y  N  V  L  Y  D  N  S  F  A   - 140
```

```
421 - TTAAGAGGTTTATTTATTATTGATAAAAATGGATGTGTAAGACATCAAACCGTTAATGAT - 480
141 - L  R  G  L  F  I  I  D  K  N  G  C  V  R  H  Q  T  V  N  D  - 160

481 - TTACCAATAGGTAGAAATGTACAGGAAGTTTTAAGAACTATAGATTCAATTATTCATGTA - 540
161 - L  P  I  G  R  N  V  Q  E  V  L  R  T  I  D  S  I  I  H  V  - 180

541 - GATACAAGTGGAGAAGTTTGTCCAATCAACTGGAAAAAGGGACAAAAAGCATTCAAACCA - 600
181 - D  T  S  G  E  V  C  P  I  N  W  K  K  G  Q  K  A  F  K  P  - 200

601 - ACTACCGAATCGTTAATAGATTATATGAATAATGCAAATAAAAATGTATAA - 651
201 - T  T  E  S  L  I  D  Y  M  N  N  A  N  K  N  V  *  X - 220
```

***Pf*Prx5** (PfAOP; PlasmoDB: PF3D7_0729200)

Sequence Length: 723 bp

```
  1 - ATGAGAATGAGAAGAACAATACTAATATTTACTGTTATATTAATACCTCTTACTTTTTGT - 60
  1 - M  R  M  R  R  T  I  L  I  F  T  V  I  L  I  P  L  T  F  C  - 20

 61 - TTTAAAAATGCTTTAATTAAGCATTCTATTAATATAGTATCCAAGCGAGGAAACTCGAAG - 120
 21 - F  K  N  A  L  I  K  H  S  I  N  I  V  S  K  R  G  N  S  K  - 40

121 - AATCGGTTTTCCCAAAAAGTTTATGAATCCAAAAATATAGATTTGGAAAATGATATAAAA - 180
 41 - N  R  F  S  Q  K  V  Y  E  S  K  N  I  D  L  E  N  D  I  K  - 60

181 - GAAAATGATCTTATTCCTAACGTGAAAGTTATGATTGACGTAAGAAATATGAACAACATA - 240
 61 - E  N  D  L  I  P  N  V  K  V  M  I  D  V  R  N  M  N  N  I  - 80

241 - TCTGATACCGATGGGAGCCCAAACGATTTTACTTCAATAGATACACATGAATTATTTAAT - 300
 81 - S  D  T  D  G  S  P  N  D  F  T  S  I  D  T  H  E  L  F  N  - 100

301 - AACAAAAAGATTTTATTAATCAGTTTACCTGGGGCATTTACGCCTACTTGCAGTACAAAA - 360
101 - N  K  K  I  L  L  I  S  L  P  G  A  F  T  P  T  C  S  T  K  - 120

361 - ATGATACCAGGATATGAAGAAGAATATGATTATTTTATAAAAGAGAATAATTTTGATGAC - 420
121 - M  I  P  G  Y  E  E  E  Y  D  Y  F  I  K  E  N  N  F  D  D  - 140

421 - ATTTATTGTATTACTAATAATGATATATATGTATTAAAGAGTTGGTTTAAAAGTATGGAT - 480
141 - I  Y  C  I  T  N  N  D  I  Y  V  L  K  S  W  F  K  S  M  D  - 160

481 - ATAAAAAAAATAAAATATATAAGTGATGGTAATAGTTCATTTACAGAAAGTATGAATATG - 540
161 - I  K  K  I  K  Y  I  S  D  G  N  S  S  F  T  E  S  M  N  M  - 180

541 - TTAGTAGACAAATCTAATTTTTTTATGGGAATGAGACCTTGGAGATTTGTTGCTATTGTT - 600
181 - L  V  D  K  S  N  F  F  M  G  M  R  P  W  R  F  V  A  I  V  - 200

601 - GAAAATAATATTTTGGTTAAAATGTTTCAAGAAAAAGATAAACAACATAATATTCAAACA - 660
201 - E  N  N  I  L  V  K  M  F  Q  E  K  D  K  Q  H  N  I  Q  T  - 220

661 - GACCCATATGATATATCAACTGTCAATAATGTAAAAGAGTTTTTAAAAAATAATCAGTTA - 720
221 - D  P  Y  D  I  S  T  V  N  N  V  K  E  F  L  K  N  N  Q  L  - 240

721 - TAA - 723
241 - *  X - 260
```

***Pf*Prx6** (1-cys peroxiredoxin (1-CysPxn); PlasmoDB: PF3D7_0802200; PF08_0131)

Sequence Length: 663 bp

```
   1 - ATGGCTTACCATTTAGGAGCTACTTTTCCAAACTTTACTGCTACTGCTTCTAATGTAGAT - 60
   1 - M  A  Y  H  L  G  A  T  F  P  N  F  T  A  T  A  S  N  V  D   - 20

  61 - GGAGTTTTTGACTTTTATAAATATGTAGGAGATAATTGGGCTATTTTATTTAGTCACCCA - 120
  21 - G  V  F  D  F  Y  K  Y  V  G  D  N  W  A  I  L  F  S  H  P   - 40

 121 - CATGATTTTACTCCCGTTTGTACCACTGAACTTGCTGAATTTGGTAAAATGCATGAAGAA - 180
  41 - H  D  F  T  P  V  C  T  T  E  L  A  E  F  G  K  M  H  E  E   - 60

 181 - TTTTTAAAACTCAACTGCAAATTAATAGGATTTAGCTGTAACTCCAAAGAATCTCACGAT - 240
  61 - F  L  K  L  N  C  K  L  I  G  F  S  C  N  S  K  E  S  H  D   - 80

 241 - CAATGGATTGAAGATATAAAATTTTACGGAAACCTAGATAAGTGGGATATTCCTATGGTT - 300
  81 - Q  W  I  E  D  I  K  F  Y  G  N  L  D  K  W  D  I  P  M  V   - 100

 301 - TGTGATGAATCCAGAGAATTAGCTAACCAATTAAAAATTATGGATGAAAAAGAAAAAGAT - 360
 101 - C  D  E  S  R  E  L  A  N  Q  L  K  I  M  D  E  K  E  K  D   - 120

 361 - ATTAAAGGACTTCCATTAACTTGTAGATGTGTTTTCTTTATTTCTCCAGATAAAAAAGTC - 420
 121 - I  K  G  L  P  L  T  C  R  C  V  F  F  I  S  P  D  K  K  V   - 140

 421 - AAAGCAACCGTTCTTTATCCAGCCACAACAGGAAGAAATTCTCAAGAAATTCTTAGAGTT - 480
 141 - K  A  T  V  L  Y  P  A  T  T  G  R  N  S  Q  E  I  L  R  V   - 160

 481 - CTTAAATCCTTACAACTTACAAACACACACCCTGTTGCTACTCCTGTTAATTGGAAAGAA - 540
 161 - L  K  S  L  Q  L  T  N  T  H  P  V  A  T  P  V  N  W  K  E   - 180

 541 - GGAGACAAATGCTGTATCTTACCATCTGTTGATAATGCAGACCTTCCAAAACTTTTTAAA - 600
 181 - G  D  K  C  C  I  L  P  S  V  D  N  A  D  L  P  K  L  F  K   - 200

 601 - AATGAAGTAAAAAAAATTGGATGTACCATCCCAAAAGGCATATTTAAGATTTGTTCAAATG - 660
 201 - N  E  V  K  K  L  D  V  P  S  Q  K  A  Y  L  R  F  V  Q  M   - 220

 661 - TAA - 663
 221 - *  X - 240
```

***Pf*PrxQ** (PlasmoDB: PF3D7_1027300)

Sequence Length: 1182 bp

```
   1 - ATGGCTCAATTAGCAGAAAATACTGTATTAGATGAAAGCATTCAAAAAGTTGAAGTCTTA - 60
   1 - M  A  Q  L  A  E  N  T  V  L  D  E  S  I  Q  K  V  E  V  L   - 20

  61 - AATCATAATGGAGAGACAACAAGTTTTTATAATGAAGTCGAAAAACATAAAGAGAACAAC - 120
  21 - N  H  N  G  E  T  T  S  F  Y  N  E  V  E  K  H  K  E  N  N   - 40

 121 - GAAGGTATTGTAGTTTTTACATACCCAAAGGCAAATACCCCAGGATGTACAAAACAAGCC - 180
  41 - E  G  I  V  V  F  T  Y  P  K  A  N  T  P  G  C  T  K  Q  A   - 60

 181 - GAATTATTTAAAGAAAAACATGAAGAATTTGTAAATAACAAATATGTTGTTTATGGTTTG - 240
  61 - E  L  F  K  E  K  H  E  E  F  V  N  N  K  Y  V  V  Y  G  L   - 80

 241 - TCTGCAGATACTGCTGAGGACCAACTCAAATGGAAAGAAAAGCTAGAACTTCCTTACGAA - 300
  81 - S  A  D  T  A  E  D  Q  L  K  W  K  E  K  L  E  L  P  Y  E   - 100
```

```
301 - TTATTATGCGATGTAGACAAGAATTTATTGAAACTTTTAGGTTTGACCAACGAAGAAGAT - 360
101 - L  L  C  D  V  D  K  N  L  L  K  L  L  G  L  T  N  E  E  D  - 120

361 - AAAACCATAAGATCCCACCTTGTTCTTAAGAACGATTTTACGGTTTCTTATGTAAAAAAG - 420
121 - K  T  I  R  S  H  L  V  L  K  N  D  F  T  V  S  Y  V  K  K  - 140

421 - AGCGTATCCCCAGGAAAGTCAGCAACCCAAGTTTTAAACTTTCTTGTGAATGGTGACGAT - 480
141 - S  V  S  P  G  K  S  A  T  Q  V  L  N  F  L  V  N  G  D  D  - 160

481 - GGAGGTGATGGAAACGAAGAAGAAGAAAATGAAGAAAATAATAATAATGAAGATAAGGAT - 540
161 - G  G  D  G  N  E  E  E  E  N  E  E  N  N  N  N  E  D  K  D  - 180

541 - AATAACGAAAATGATGAAGAAGGTGATGTCCAAGGAGAAGGAGAAGGTGAAGGTGAAGGT - 600
181 - N  N  E  N  D  E  E  G  D  V  Q  G  E  G  E  G  E  G  E  G  - 200

601 - GATGAAGAGAAAACAGCAGACACCGATAAAGAAAAACCAAAGAAATCATCCACCAGCACA - 660
201 - D  E  E  K  T  A  D  T  D  K  E  K  P  K  K  S  S  T  S  T  - 220

661 - CAAAAGAAAAAAGGTAGTGTTAGTAGTACTATTTCTAAAAAGTCCGTAAAAAAAAGTAAC - 720
221 - Q  K  K  K  G  S  V  S  S  T  I  S  K  K  S  V  K  K  S  N  - 240

721 - AAAGTTGTTAAAAAAAATGTTAAAGTAAAAAAAGAAATAAAAAAAAAAACAAATAAAAAA - 780
241 - K  V  V  K  K  N  V  K  V  K  K  E  I  K  K  K  T  N  K  K  - 260

781 - GCTGATAACAAAAAAGGAAAAAATGTGAACAACAAACTTATGAAAAGCAATGCTAAAGGT - 840
261 - A  D  N  K  K  G  K  N  V  N  N  K  L  M  K  S  N  A  K  G  - 280

841 - GCTAACAAAAAAGGTGGAAAAAAAAATAGTGTTGTTAAAAAAGAAGACAACAAAAAAAAA - 900
281 - A  N  K  K  G  G  K  K  N  S  V  V  K  K  E  D  N  K  K  K  - 300

901 - GGAAAAAATAATAAGAAGAAAAATAAAAATCAAAACTTAAAAGATTTAAAGAAAAAAAAT - 960
301 - G  K  N  N  K  K  K  N  K  N  Q  N  L  K  D  L  K  K  K  N  - 320

961 - GTGAAATCAGGAAAAGGAAGCGTCTCCTCATCAAACAAAAAATTACCTAAAGGATTAAAG - 1020
321 - V  K  S  G  K  G  S  V  S  S  S  N  K  K  L  P  K  G  L  K  - 340

1021 - AATGCTGCCAAAAAAGCTGGAAAAAAAATTGACAAAAAAAAAGAACAAGCCAACAAAAAA - 1080
341 - N  A  A  K  K  A  G  K  K  I  D  K  K  K  E  Q  A  N  K  K  - 360

1081 - AATAACAATAACAAAAATAAAAATAAAAATAAAAATCTATCCAAAGGAAATAATATGAAA - 1140
361 - N  N  N  N  K  N  K  N  K  N  K  N  L  S  K  G  N  N  M  K  - 380

1141 - CATAACAAAAAACCAGCCAAAAAAGTGGTAAAGAAAAAGTAA - 1182
381 - H  N  K  K  P  A  K  K  V  V  K  K  K  *  X - 400
```

hTGR (UniProtKB: Q86VQ6)

Sequence Length: 1932 bp

```
   1 - CTGGAGCGGTCGCCGCCGCAGTCGCCCGGGCCGGGAAAGGCGGGCGATGCCCCCAACCGC - 60
   1 - M  E  R  S  P  P  Q  S  P  G  P  G  K  A  G  D  A  P  N  R   - 20

  61 - CGCTCGGGCCATGTCCGAGGGGCGCGCGTGTTGTCGCCGCCGGGGCGCCGTGCCCGCCTG - 120
  21 - R  S  G  H  V  R  G  A  R  V  L  S  P  P  G  R  R  A  R  L   - 40

 121 - TCGTCCCCCGGGCCCAGCCGCTCGTCCGAGGCCCGCGAGGAGCTGCGCCGCCACCTCGTG - 180
  41 - S  S  P  G  P  S  R  S  S  E  A  R  E  E  L  R  R  H  L  V   - 60

 181 - GGCCTCATCGAGCGCAGCCGGGTGGTGATCTTCAGCAAGAGCTACTGTCCCCATAGTACT - 240
  61 - G  L  I  E  R  S  R  V  V  I  F  S  K  S  Y  C  P  H  S  T   - 80

 241 - CGGGTGAAAGAACTCTTTTCTTCTTTGGGAGTCGAATGTAATGTCTTGGAACTTGATCAA - 300
  81 - R  V  K  E  L  F  S  S  L  G  V  E  C  N  V  L  E  L  D  Q   - 100

 301 - GTTGATGATGGGGCCAGGGTTCAAGAAGTGCTGTCAGAAATCACTAATCAGAAAACTGTG - 360
 101 - V  D  D  G  A  R  V  Q  E  V  L  S  E  I  T  N  Q  K  T  V   - 120

 361 - CCCAATATTTTCGTGAATAAAGTGCATGTAGGTGGATGTGACCAAACTTTCCAGGCATAT - 420
 121 - P  N  I  F  V  N  K  V  H  V  G  G  C  D  Q  T  F  Q  A  Y   - 140

 421 - CAGAGTGGTTTGTTACAGAAGCTCCTTCAGGAAGATTTGGCATATGATTATGATCTCATC - 480
 141 - Q  S  G  L  L  Q  K  L  L  Q  E  D  L  A  Y  D  Y  D  L  I   - 160

 481 - ATCATCGGTGGTGGTTCTGGAGGCCTTTCATGTGCGAAGGAAGCTGCCATTTTGGGAAAG - 540
 161 - I  I  G  G  G  S  G  G  L  S  C  A  K  E  A  A  I  L  G  K   - 180

 541 - AAAGTTATGGTGCTAGACTTTGTTGTCCCGTCACCTCAGGGCACATCCTGGGGTCTTGGT - 600
 181 - K  V  M  V  L  D  F  V  V  P  S  P  Q  G  T  S  W  G  L  G   - 200

 601 - GGCACTTGTGTAAATGTAGGTTGTATTCCTAAGAAATTGATGCATCAGGCTGCCCTTTTG - 660
 201 - G  T  C  V  N  V  G  C  I  P  K  K  L  M  H  Q  A  A  L  L   - 220

 661 - GGGCAGGCATTATGTGACTCAAGGAAATTTGGCTGGGAATATAATCAACAAGTGAGGCAC - 720
 221 - G  Q  A  L  C  D  S  R  K  F  G  W  E  Y  N  Q  Q  V  R  H   - 240

 721 - AACTGGGAGACAATGACAAAAGCGATTCAGAACCACATCAGCTCTCTAAACTGGGGCTAC - 780
 241 - N  W  E  T  M  T  K  A  I  Q  N  H  I  S  S  L  N  W  G  Y   - 260

 781 - AGGTTGTCTCTGAGGGAAAAGGCTGTGGCCTATGTCAATTCCTATGGAGAATTTGTTGAA - 840
 261 - R  L  S  L  R  E  K  A  V  A  Y  V  N  S  Y  G  E  F  V  E   - 280

 841 - CATCATAAAATAAAGGCAACCAATAAAAAAGGACAGGAGACTTATTATACTGCTGCACAG - 900
 281 - H  H  K  I  K  A  T  N  K  K  G  Q  E  T  Y  Y  T  A  A  Q   - 300

 901 - TTTGTCATAGCAACGGGTGAAAGGCCACGGTATTTAGGAATCCAAGGAGATAAAGAATAC - 960
 301 - F  V  I  A  T  G  E  R  P  R  Y  L  G  I  Q  G  D  K  E  Y   - 320

 961 - TGTATTACTAGTGATGACCTTTTTTCTCTGCCTTATTGCCCTGGCAAAACATTAGTGGTG -1020
 321 - C  I  T  S  D  D  L  F  S  L  P  Y  C  P  G  K  T  L  V  V   - 340

1021 - GGTGCCTCTTATGTTGCCCTGGAGTGTGCAGGGTTTCTGGCTGGCTTTGGCCTAGATGTC -1080
 341 - G  A  S  Y  V  A  L  E  C  A  G  F  L  A  G  F  G  L  D  V   - 360

1081 - ACAGTTATGGTACGCTCAATCCTTCTCCGTGGCTTCGACCAAGAAATGGCAGAAAAAGTG -1140
 361 - T  V  M  V  R  S  I  L  L  R  G  F  D  Q  E  M  A  E  K  V   - 380
```

```
1141 - GGTTCCTACATGGAGCAGCATGGTGTGAAGTTCCTACGGAAATTCATACCTGTGATGGTT -1200
 381 - G  S  Y  M  E  Q  H  G  V  K  F  L  R  K  F  I  P  V  M  V   - 400

1201 - CAACAGTTGGAGAAAGGTTCACCTGGAAAGCTGAAAGTGTTGGCTAAATCCACTGAAGGA -1260
 401 - Q  Q  L  E  K  G  S  P  G  K  L  K  V  L  A  K  S  T  E  G   - 420

1261 - ACAGAAACAATTGAAGGAGTCTATAACACAGTTTTGTTAGCTATTGGTCGTGACTCCTGT -1320
 421 - T  E  T  I  E  G  V  Y  N  T  V  L  L  A  I  G  R  D  S  C   - 440

1321 - ACAAGGAAAATAGGCTTGGAGAAGATTGGTGTCAAAATTAATGAGAAGAGTGGAAAAATA -1380
 441 - T  R  K  I  G  L  E  K  I  G  V  K  I  N  E  K  S  G  K  I   - 460

1381 - CCTGTAAATGATGTGGAACAGACCAATGTGCCATATGTCTATGCTGTTGGTGATATTTTG -1440
 461 - P  V  N  D  V  E  Q  T  N  V  P  Y  V  Y  A  V  G  D  I  L   - 480

1441 - GAGGATAAGCCAGAGCTCACTCCTGTCGCCATACAGTCAGGCAAGCTGCTAGCTCAGAGA -1500
 481 - E  D  K  P  E  L  T  P  V  A  I  Q  S  G  K  L  L  A  Q  R   - 500

1501 - CTTTTTGGGGCCTCTTTAGAAAAGTGTGATTATATTAATGTTCCGACTACAGTGTTTACT -1560
 501 - L  F  G  A  S  L  E  K  C  D  Y  I  N  V  P  T  T  V  F  T   - 520

1561 - CCTCTGGAGTATGGTTGCTGTGGATTATCTGAAGAGAAAGCTATTGAAGTATATAAAAAA -1620
 521 - P  L  E  Y  G  C  C  G  L  S  E  E  K  A  I  E  V  Y  K  K   - 540

1621 - GAGAATCTAGAAATATATCATACTTTGTTCTGGCCTCTTGAATGGACAGTAGCTGGCAGA -1680
 541 - E  N  L  E  I  Y  H  T  L  F  W  P  L  E  W  T  V  A  G  R   - 560

1681 - GAGAACAACACTTGTTATGCAAAGATAATCTGCAATAAATTCGACCATGATCGGGTGATA -1740
 561 - E  N  N  T  C  Y  A  K  I  I  C  N  K  F  D  H  D  R  V  I   - 580

1741 - GGATTTCATATTCTTGGACCAAACGCCGGTGAGGTTACCCAAGGATTTGCAGCTGCAATG -1800
 581 - G  F  H  I  L  G  P  N  A  G  E  V  T  Q  G  F  A  A  A  M   - 600

1801 - AAATGTGGGCTCACAAAACAGCTACTTGATGACACCATTGGAATTCACCCCACATGTGGG -1860
 601 - K  C  G  L  T  K  Q  L  L  D  D  T  I  G  I  H  P  T  C  G   - 620

1861 - GAGGTGTTCACGACTTTGGAAATCACAAAGTCGTCAGGACTAGACATCACTCAGAAAGGC -1920
 621 - E  V  F  T  T  L  E  I  T  K  S  S  G  L  D  I  T  Q  K  G   - 640

1921 - TGCTGAGGCTAG - 1932
 641 - C  U  G  *  X - 643
```